Research Report 2014-01
Civil & Natural Resources Engineering

UNIVERSITY OF CANTERBURY
Te Whare Wānanga o Waitaha
CHRISTCHURCH NEW ZEALAND

DEVELOPMENT AND EVALUATION OF CPT-V_S CORRELATION FOR CANTERBURY NEW ZEALAND SOILS OF THE SHALLOW CHRISTCHURCH AND SPRINGSTON FORMATIONS

Christopher R. McGann
Brendon A. Bradley
Misko Cubrinovski
Merrick L. Taylor
Liam M. Wotherspoon

ISSN 1172-9511

UC ENGINEERING

May 2014

DEVELOPMENT AND EVALUATION OF CPT-V_s CORRELATION FOR CANTERBURY NEW ZEALAND SOILS OF THE SHALLOW CHRISTCHURCH AND SPRINGSTON FORMATIONS

Christopher R. McGann
Brendon A. Bradley
Misko Cubrinovski
Merrick L. Taylor
Liam M. Wotherspoon

Research Report 2014-01

Department of Civil and Natural Resources Engineering
University of Canterbury
Christchurch, New Zealand

May 29, 2014

Acknowledgements

Funding for this work was provided by the New Zealand Earthquake Commission (EQC) and the Natural Hazards Research Platform (NHRP). The authors would also like to thank the Canterbury Geotechnical Database and Perry Drilling Ltd. for providing access to the data used in this study.

Executive Summary

A detailed characterization of the subsurface shear wave velocity profile for the greater Christchurch area is an essential tool to aid in identifying and understanding the physical processes resulting in the strong ground motions observed in the 2010-2011 Canterbury earthquake sequence. While in-situ measurement of shear wave velocity, V_s, is impractical on the scale necessary for a full characterization of the region, measurements made at selected sites can be used to establish a relationship between measured V_s and cone penetration test (CPT) data. When combined with the large existing local CPT data set (Canterbury Geotechnical Database, 2012), such a correlation can be used to produce the desired description of the near surface V_s profile of the Canterbury region. To this purpose, data obtained using seismic peizocone (SCPTu) devices (Robertson et al., 1986) at 86 sites located throughout the greater Christchurch area are used establish a Canterbury-specific CPT-V_s correlation. The development of this correlation includes:

- An evaluation of the characteristics of the SCPTu data set; including factors such as site surficial geology, the distributions of CPT-based measurements and relationships within the SCPTu database, and the date of the SCPTu investigations relative to major seismic events in the 2010-2011 Canterbury earthquake sequence;

- An evaluation of several existing empirical CPT-V_s correlations developed from global data sets of various soil types for suitability in describing the strength-to-stiffness relationship for the soils and site conditions found in the Canterbury region;

- A comparison of the residuals for regression models developed with the Canterbury SCPTu database using functional forms used by previous CPT-V_s correlations to determine an appropriate regression functional form for use in the Canterbury-specific model;

- An examination of the residuals for the chosen regression functional form and how these residuals vary with changing magnitude of the predictor variables, leading to the consideration for non-constant depth variance in the regression model, as well as an evaluation of the performance of the regression model with various predictor variables;

It is shown that the considered existing CPT-V_s correlations are biases towards overestimation of the in-situ shear wave velocities at the Canterbury SCPTu database sites, and it is hypothesized that the unique depositional environment of the considered soils, along with potential loss of (or reduction in) ageing effects brought about by the Canterbury earthquakes, are primarily responsible for the observed bias in the V_s predictions made using the existing CPT-V_s models. The Canterbury-specific CPT-V_s correlation developed from the SCPTu database is shown to have good performance in forward predictions using synthetic CPT profiles and in comparisons to measured in-situ V_s at the SCPTu sites.

Table of Contents

Chapter 1

INTRODUCTION

Site effects related to the influence of near-surface (< 50 m) stratigraphy strongly affect observed surficial ground motions. Seismic waves must always pass through these near-surface soil and rock layers before reaching the surface, thus site effects tend to be a systematic feature of observed ground motions at a particular location, while path and source effects, which also strongly affect surficial ground motions, can vary significantly for earthquakes originating from different sources. The systematic nature of site effects at a particular location, in combination with the ready availability of direct measurements and estimates of the characteristics and properties of the near-surface soils, indicates that local site effects can be modeled with potentially greater accuracy than source and path effects and therefore offer a potentially more efficient means with which to predict the character, and effects of, future surficial ground motions at specific sites (Bradley, 2012a; Montalva, 2010; Rodriguez-Marek et al., 2011; Bazzurro and Cornell, 2004).

The small strain shear modulus is a fundamental parameter required to evaluate the dynamic response of surficial soil deposits using seismic site response analysis. It defines the shear stress-strain response for low levels of strain ($< 10^{-4}\%$), and is typically used to define normalized relationships describing the degradation in soil shear stiffness with increasing levels of strain that are critical to nonlinear and equivalent linear site response analyses (e.g., Idriss and Seed, 1970; Darendeli, 2001). Due to this association with low levels of strain, the small strain shear modulus is highly susceptible to disturbances that are nearly unavoidable in any laboratory assessment (Stokoe II and Santamarina, 2000). In-situ measurement or estimation techniques for obtaining soil shear wave velocity, V_s, which is related to the small strain shear modulus through the linear elastic wave propagation equation, are therefore often used to obtain the low strain shear stiffness profiles necessary for dynamic site response analyses.

There are numerous techniques available for obtaining in-situ measurements of V_s, including invasive techniques that require one or more boreholes or cone penetration tests such as cross-hole and downhole techniques (Woods, 1978, 1994) and P-S suspension logging measurements (Kaneko et al., 1990); and noninvasive active-source surface wave techniques such as the spectral and multi-channel analysis of surface waves techniques (SASW and MASW, respectively) (Nazarian and Stokoe II, 1984; Park et al., 1999); and passive-source surface wave measurement techniques such as linear and microtremor array methods (Louie, 2001; Park and Miller, 2008; Tokimatsu et al., 1992; Okada, 2003). These direct measurement approaches all have specific advantages and disadvantages relative to each other, however, one general drawback that is common to these methods is the need for specialized equipment and training. Due to these requirements, such measurements are not commonly made during site characterization efforts for projects of lower relative importance. As a result, there is often a lack of site-specific V_s data for such sites and a general scarcity of direct $V_s$measurement data for use in region-wide characterization efforts such as the development of regional ground shaking hazard maps.

Near surface V_s profiles can also be obtained via empirical correlations with common geotechnical investigations such as the standard penetration test (SPT) (e.g., Ohta and Goto, 1978; Sykora and Stokoe II, 1983; Rollins et al., 1998) and the cone penetration test (CPT) (e.g., Andrus et al., 2007; Hegazy and Mayne, 2006; Robertson, 2009; Sykora and Stokoe II, 1983; Baldi et al., 1989; Mayne and Rix, 1993; Hegazy and Mayne, 1995). Such empirical correlations

are typically developed through regression analysis using a series of predictor variables from the conventional geotechnical investigations (SPT or CPT) and V_s measurements obtained through one of the previously mentioned techniques. Many of the more recent empirical correlations have been developed using data for general soil deposits (i.e., cohesive and cohesionless) from globally located sites of varying geological ages in order to obtain prediction correlations that can be applied in a general manner. Wair et al. (2012) provide a good general overview of existing SPT- and CPT-based empirical correlation efforts.

Direct measurement of V_s is preferable to indirect estimation, however, many direct measurement techniques have disadvantages that limit their use in general geotechnical practice. Surface wave analysis methods are useful in that they are non-intrusive, but they often require the solution of an ill-posed inverse problem. As a result, V_s profiles estimated using surface wave techniques often suffer from non-uniqueness of the solution (Tarantola, 2005) and from issues related to the equivalence problem (Xia et al., 1999; Louie, 2001). These issues can be manifested in the resulting profiles via decreased resolution with increasing depth, an inability to identify thin layers, and difficulties in resolving the portions of layers adjacent to large velocity contrasts (Stokoe II and Santamarina, 2000). Borehole-type measurement techniques are inherently invasive, though this in itself does not preclude their use, as invasive site characterization techniques (e.g., SPT and CPT) are common in practice. Borehole-type measurement techniques have the advantage of being able to properly resolve inclusions and anomalies that may be missed by surface-based approaches, but have the disadvantage of the increased temporal and financial expenses associated with drilling (especially for crosshole techniques, which require multiple boreholes) (Stokoe II and Santamarina, 2000), and only represent the subsurface conditions at a single point, rather than the conditions averaged along a line as in the surface wave methods. The downhole technique, of which the seismic cone penetration test (SCPT) is a specialized subset, requires only a single borehole, but can suffer from depth limits depending on the energy of the seismic wave source. The suspension logger test can be used for great depths ($>$ 100 m), and is arguably the most precise invasive measurement method currently available, but this test has limited application in soft sediments (Stokoe II and Santamarina, 2000).

A detailed characterization of the subsurface V_s profile for the greater Christchurch, New Zealand area is an essential tool to aid in identifying and understanding the physical processes resulting in the strong ground motions observed in the 2010-2011 Canterbury earthquake sequence (Cubrinovski et al., 2010; Bradley and Cubrinovski, 2011; Cubrinovski et al., 2011; Bradley, 2012a,b; Cubrinovski et al., 2011). While in-situ measurement of V_s is impractical on the scale necessary for a full characterization of the region, measurements made at selected sites can be used to establish a region-specific relationship between measured V_s and CPT data. When combined with the large ($>$ 15000 as of 1/1/2014) existing local CPT data set (Canterbury Geotechnical Database, 2012), such a correlation can be used to produce the desired description of the near surface V_s profile of the Christchurch region (Lee et al., 2014).

Data obtained using seismic piezocone (SCPTu) devices (Robertson et al., 1986) at 86 sites located throughout the greater Christchurch area are used to establish the need for a Christchurch-specific CPT-V_s correlation through an assessment of the applicability of existing CPT-V_s models developed elsewhere to describing the strength-to-stiffness relationship for the soils and site conditions found in the Christchurch region. The compiled SCPTu database is first presented, including the spatial distribution of sites, data processing, and overall database statistics. Existing CPT-V_s correlations are then described and the prediction bias when applied to the SCPTu database is examined with respect to various predictor variables. The specific nature of the soils encountered and the recent Canterbury earthquakes are considered as possibilities for the observed bias in the considered prediction models, as the examined Christchurch

sites do not display an increase in V_s with effective deposit age in line with that displayed by other existing data sets.

Following these steps related to establishing the need for a new Christchurch-specific CPT-V_s correlation, the new correlation is developed through regression analysis. The initial phase of this development focuses on the selection of an appropriate functional form for the regression analysis. The second phase involves an assessment of the quality of the regression model using the selected functional form, with particular attention given to the dependence of the model prediction and standard deviation on various predictor variables, and also direct comparison for selected profiles and for synthetic CPT profiles that represent a wide spectrum of soil conditions.

Chapter 2

CANTERBURY SCPTu DATABASE

Seismic piezocone (SCPTu) data were obtained at 86 sites in the greater Christchurch area and made available through the Canterbury Geotechnical Database (Canterbury Geotechnical Database, 2012). Figure 2.1 shows the locations of the SCPTu sites. Those sites closest to central Christchurch are in the main portion of Figure 2.1; two sites located beyond the southern boundary of this main portion (in Tai Tapu), and 14 sites located beyond the northern boundary (five in Spencerville and nine in Kaiapoi) are shown in the insets on the right-hand side. As shown in Figure 2.1, the majority of the Christchurch sites are located near the Avon River, though there are a number of sites near the Heathcote River or located away from either river system. The Spencerville sites are located along the Styx River and the Kaiapoi sites are near the banks of the Kaiapoi River and Courtenay Stream.

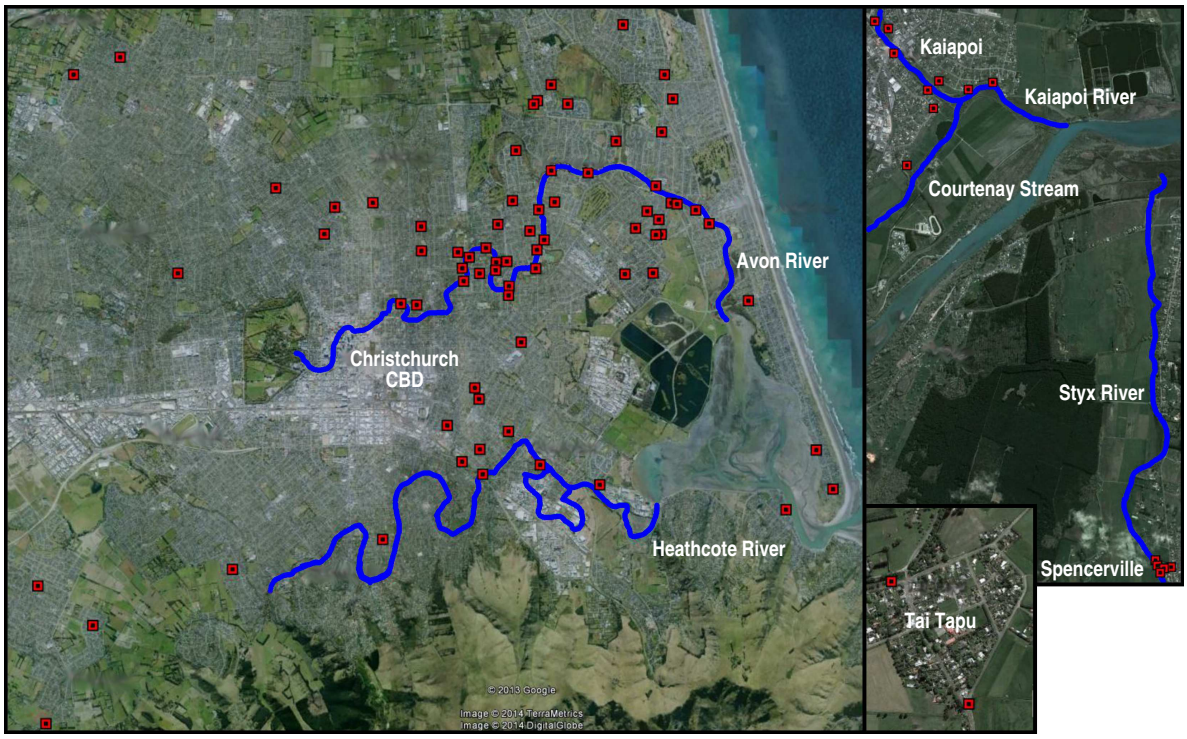

Figure 2.1: Map of Christchurch showing the 86 SCPTu site locations (Kaiapoi, Spencerville, and Tai Tapu sites inset). Some local rivers and streams are indicated for reference.

2.1 Geological Setting of SCPTu Sites

Figure 2.2 shows the centrally-located SCPTu sites with respect to the Brown and Weeber (1992) map of the surficial geologic units of the Christchurch urban area. As shown, the surficial soils at these sites are split between the beach, estuarine, lagoonal, dune, and coastal swamp deposits of the Christchurch formation (blue and grey-blue in Figure 2.2) and the fluvial channel and overbank sediment deposits of the Springston formation (yellow and yellow-grey in Figure 2.2). The sites located in Tai Tapu, Spencerville, and Kaiapoi (as well as a site in southern Halswell)

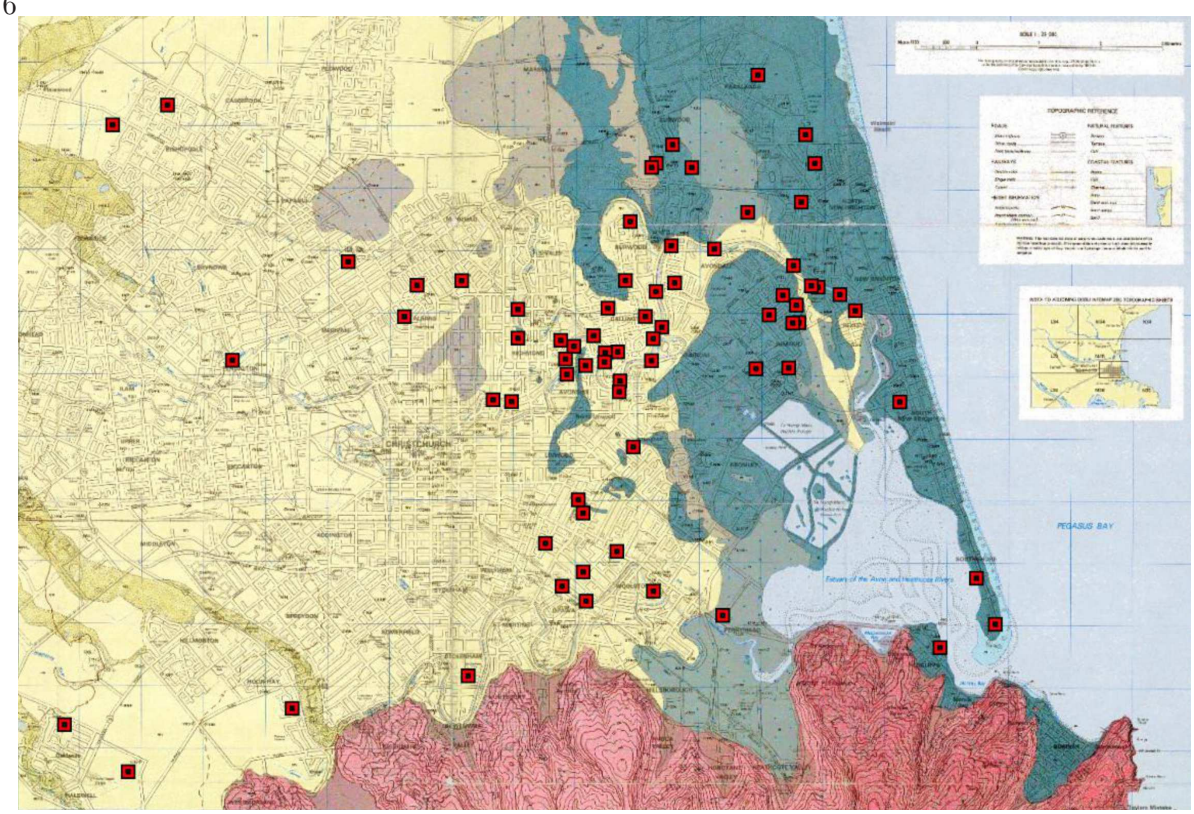

Figure 2.2: Map of Christchurch SCPTu sites indicating surficial soil deposits after Brown and Weeber (1992). Yellow regions correspond to the Springston formation, blue to the Christchurch formation, and pink to the Banks Peninsula loess and Mt. Pleasant formation.

are located outside of the bounds of the Brown and Weeber (1992) map, and are therefore not included in Figure 2.2. These sites are however located within the same surficial geologic units (Christchurch and Springston formations) as those that fit within the map boundaries. Of the 86 total SCPTu sites, there are 26 Christchurch formation sites, 56 Springston formation sites, and 4 sites located on the boundary between the formations.

The Christchurch and Springston formations that exist on the surface of the Canterbury plains date to the Holocene period (deposited $\leq$ 10,000 years before present day). The content of the Springston formation is primarily well-sorted, rounded gravel within a predominantly sand matrix with occasional silt and clay lenses. The Christchurch formation is composed primarily of blue gravel, sand, shells, sandy silt, clay, peat, and wood (Brown et al., 1995).

2.2 Data Processing

Pseudo-interval travel time measurements were made by recording seismic signals at 2 m intervals at each SCPTu site. Shear wave velocities were determined from these seismic signals using the cross-over method (Robertson et al., 1986) for sites with only pre-processed wave data available, and the cross-correlation method (Campanella and Stewart, 1992) for sites with digitized data available. Figure 2.3 shows an example of the polarized seismic wave traces that were used to determine V_s via the cross-over method, or to check the V_s returned by the cross-correlation method. The shear wave velocities determined from the available data are assumed to be constant over the full intervals between the measurements, and the midpoint depth of each interval is assumed to be the depth of the V_s data point.

For comparison between the shear wave velocity, V_s, and CPT data, the geometric mean of the CPT data are determined over the V_s measurement intervals (as the subsequently developed

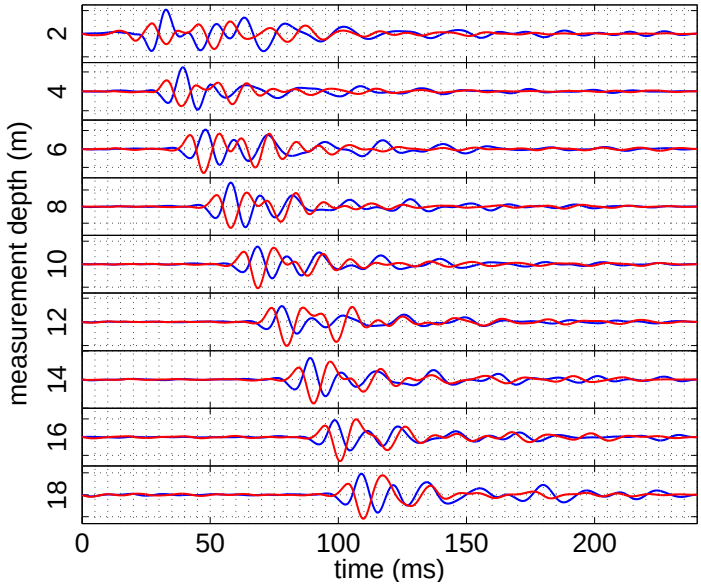

Figure 2.3: Example set of seismic wave traces for site in Canterbury SCPTu database. Red and blue lines indicate polarized pairs of waves at each measurement depth.

correlation is linear in V_s space), ultimately yielding 513 coupled pairs of V_s and CPT data. Averaging the CPT data in this manner helps to alleviate issues associated with comparing measured to CPT-correlated V_s values at locations where the smaller measurement intervals of the CPT ($\approx$ 1-2 cm) detect a localized feature that cannot be captured by the much larger V_s measurement intervals.

2.3 Distributions of Measured and Computed SCPTu Data

Figure 2.4 shows an example of the information provided by each CPT record in the database. In this work, the primary CPT data quantities considered are the cone tip resistance q_c, the frictional cone resistance f_s, the hydrostatic and penetration pore pressures, u_0 and u_2, respectively, and the I_c soil behaviour type index (Robertson and (Fear) Wride, 1998). The soil profile for this site is typical of the database; per I_c, the profile is primarily comprised of soil with the behaviour of clean to silty sand ($1.31 < I_c \leq 2.05$), with relatively small interbedded layers of silty sands to sandy silts ($2.05 < I_c \leq 2.60$), clayey silts to silty clays ($2.6 < I_c \leq 2.95$), and clays or organic soils ($I_c > 2.95$).

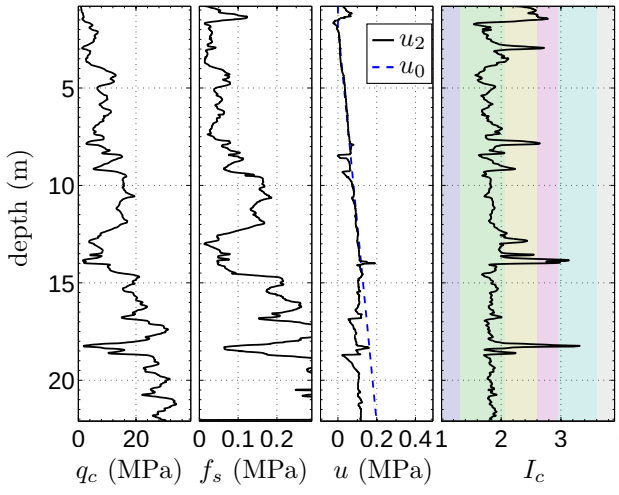

Figure 2.4: Example CPT data traces for site in Canterbury SCPTu database.

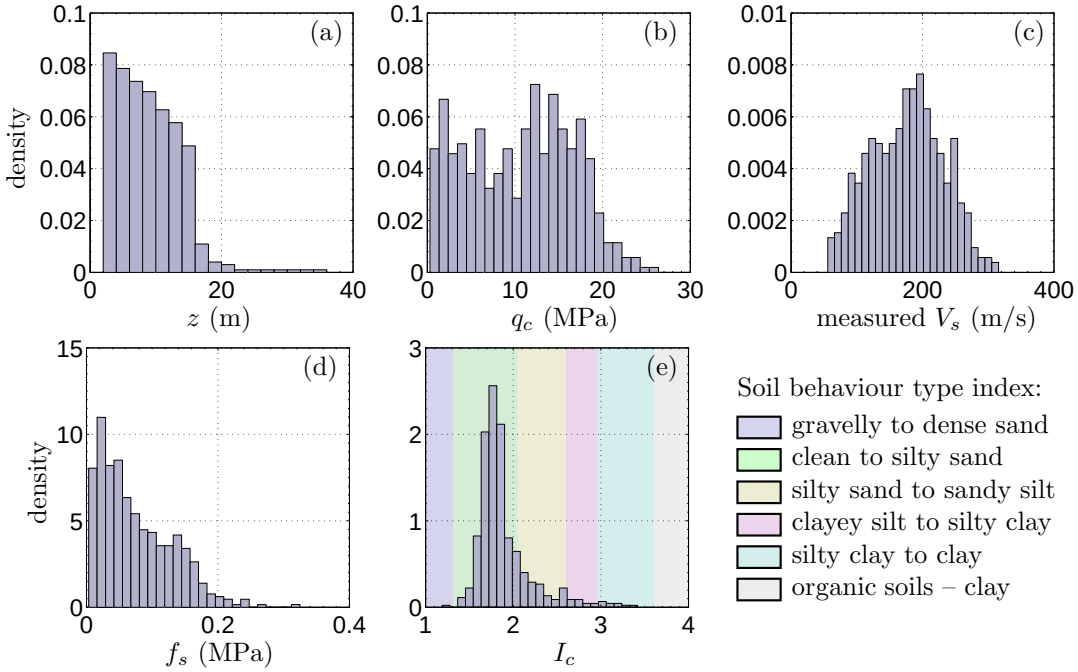

Figure 2.5: Density distributions of: (a) depth, z; (b) cone tip resistance, q_c; (c) measured shear wave velocity, V_s; (d) frictional resistance, f_s; and (e) soil behaviour type index, I_c, in SCPTu database.

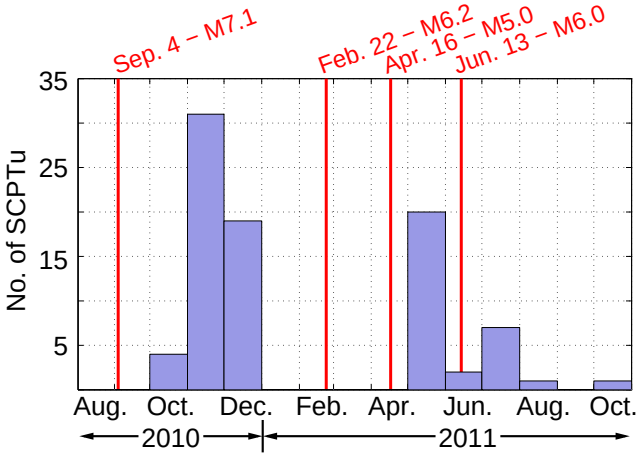

Figure 2.6: Distribution of SCPTu test dates (binned by month) with reference to dates of significant Canterbury earthquakes.

Figure 2.5 shows the distributions of interval midpoint depth, z, cone tip resistance, q_c, measured shear wave velocity, V_s, cone frictional resistance, f_s, and soil behaviour type index, I_c, for the full SCPTu database. The majority of the data is at depths less than 16 m; only a small number of sites had V_s measurements below this depth. The I_c plot of Figure 2.5 indicates that, as would be expected for soil profiles similar to that shown in Figure 2.4, the majority of the data points have I_c values in the upper half of the clean to silty sand range. The measured V_s values range from 50 m/s to a little over 300 m/s. Measured $V_s < 50$ m/s are omitted from the data set due to lack of confidence in the accuracy of these measurements.

Figure 2.6 shows the distribution of SCPTu test dates over the fifteen month period between August 2010 and October 2011. Approximately 60% of the tests in the SCPTu database were performed in the months following the 4 September 2010 M_w7.1 earthquake in areas where liquefaction occurred. These 2010 tests were part of the initial efforts to assess the viability for rebuilding in liquefaction-affected areas following the September earthquake, and are largely

located in areas of marginal to severe liquefaction vulnerability for this reason (TC3 and red zone, respectively, according to the residential land zoning categories used by the Canterbury Earthquake Recovery Authority (CERA) `http://cera.govt.nz/land-information/land-zones`). With respect to the maps of Figures 2.1 and 2.2, these 2010 tests comprise the sites in Tai Tapu, Spencerville, Kaiapoi and the western suburbs of Christchurch along with a few coastal locations and the majority of the Avon River sites. The SCPTu tests that took place after the 22 February 2011 M_w6.2 earthquake are not as concentrated in the residential red zone areas, as these regions had essentially been defined and designated for abandonment by the time of the second earthquake. The 2011 tests in the SCPTu database are all located within the Christchurch urban area, somewhat evenly divided between the Avon and Heathcote river systems.

2.4 Summary

A database of 86 SCPTu sites was compiled from subsurface explorations performed in the greater Christchurch, New Zealand area following the 2010-2011 Canterbury earthquake sequence. All of the considered sites were obtained from logs made available in the Canterbury Geotechnical Database (Canterbury Geotechnical Database, 2012). These sites are located in areas in which the surficial geologic deposits are from the Christchurch and Springston formations (Brown and Weeber, 1992). In-situ shear wave velocities were determined from pseudo-interval travel time data (spaced at 2 m intervals) using the cross-over and cross-correlation approaches. The CPT data were averaged over the V_s measurement intervals using the geometric mean to yield 513 unique pairs of CPT and V_s data for the soils of the Canterbury region.

Chapter 3

APPLICABILITY OF EXISTING CPT-V_s CORRELATIONS TO CANTERBURY SCPTu DATABASE

Substantial research has been conducted to develop and evaluate correlations between shear wave velocity, V_s, and CPT data. Such efforts can be divided into three categories based on the considered soil type: (1) correlations for cohesive soils (e.g., Mayne and Rix, 1993); (2) correlations for cohesionless soils (e.g., Sykora and Stokoe II, 1983; Baldi et al., 1989); and (3) general soil correlations that consider both cohesive and cohesionless soil sites and a predictor variable (e.g., I_c) which can account for differences in soil type (e.g., Hegazy and Mayne, 1995, 2006; Andrus et al., 2007; Robertson, 2009). Of these three categories, the general soil correlations are the most appealing as they are simpler to apply and have been shown to perform similar to soil type-specific correlations in predicting V_s for general soil profiles (Wair et al., 2012).

In this chapter, the suitability of three general soil correlations for describing the relationship between shear wave velocity and cone penetration resistance variables suggested by the SCPTu data in Canterbury is evaluated in terms of the bias between the estimated and measured shear wave velocities. It is determined that all four considered correlations are biased in predicting the V_s of Canterbury soil deposits, tending to overestimate the V_s values to varying degrees. This prediction bias demonstrates the need for the Canterbury-specific correlation between V_s and CPT data discussed in subsequent chapters.

3.1 Review of Selected CPT-V_s Correlations

Four recently developed general soil CPT-V_s correlations derived from relatively independent data sets are considered herein (Hegazy and Mayne, 2006; Andrus et al., 2007; Robertson, 2009). The CPT-V_s correlations from each work are presented in the discussion below with a brief summary of the characteristics of the underlying databases used in their development.

3.1.1 Robertson (2009) CPT-V_s Correlation

Robertson (2009) developed a CPT-V_s correlation based on a global set of 1035 pairs of V_s and CPT measurement data from predominantly Holocene and Pleistocene-age general soil sites of the form:

$$V_s = \left[10^{0.55 I_c + 1.68}\left(\frac{q_t - \sigma_{v0}}{p_a}\right)\right]^{0.5} \tag{3.1}$$

where q_t is the corrected cone tip resistance (Campanella et al., 1982), I_c is the soil behaviour type index (Robertson and (Fear) Wride, 1998), σ_{v0} is the initial vertical total stress, and p_a is atmospheric pressure. This correlation was obtained from a database of CPT soundings with a mean normalized cone tip resistance (Robertson and (Fear) Wride, 1998; Zhang et al., 2002), $Q_{tn} = 57$, and a range of $0.67 \leq Q_{tn} \leq 577$; a mean friction ratio (Robertson, 1990), $F_r = 3.13\%$, with a range of $0.15 \leq F_r \leq 13.13\%$; and a mean vertical effective stress, $\sigma'_{v0} = 190$ kPa, with a range of $19 \leq \sigma'_{vo} \leq 580$ kPa. Robertson (2009) does not detail the techniques used to measure the in-situ V_s at these sites; it is likely that various techniques were used for this purpose.

3.1.2 Hegazy and Mayne (2006) CPT-V_s Correlation

Hegazy and Mayne (2006) developed at CPT-V_{s1} correlation based on 558 data pairs taken from a combined database comprised of the 31 clay soil sites of Mayne and Rix (1993), the 30 general soil sites of Hegazy and Mayne (1995), and 12 additional general soil sites. The presented correlation was developed in terms of V_{s1}, the normalized shear wave velocity of Robertson et al. (1992). When rearranged to solve for V_s, the correlation has the form:

$$V_s = 0.0831 Q_{tn} e^{1.786 I_c} \left(\frac{\sigma'_{v0}}{p_a} \right)^{0.25} \tag{3.2}$$

where σ'_{v0} is the initial vertical effective stress, e is the natural exponent, and other terms are as previously defined. The database used to develop this correlation had a range of soil behaviour type index of $1.0 \leq I_c \leq 4.8$. The in-situ V_s measurements were made using a variety of techniques, including SCPT, downhole tests, crosshole tests, and SASW.

3.1.3 Andrus et al. (2007) CPT-V_s Correlations

Andrus et al. (2007) considered V_s and CPT measurements for general soil deposits with various geologic ages as part of a larger study of the effects of deposit age on shear wave velocity. Excluding the Tertiary-age sites considered by Andrus et al. (2007) that are not applicable to the current study, the Andrus et al. (2007) database included 185 data pairs (72 Holocene, 113 Pleistocene). Two applicable CPT-V_s correlations are presented here, one based on the Holocene-age data only, and the other based on the combined Holocene-Pleistocene database that includes a scaling factor based on the age of the particular soil deposit to which the correlation is applied. The Holocene-only correlation has the form:

$$V_s = 2.27 q_t^{0.412} I_c^{0.989} z^{0.033} \tag{3.3}$$

where z is the depth below the ground surface in metres and q_t is expressed in units of kPa. The combined Holocene-Pleistocene correlation has the form:

$$V_s = 2.62 A q_t^{0.395} I_c^{0.912} z^{0.124} \tag{3.4}$$

where A is a scaling factor that depends on soil deposit age ($A = 0.92$ for Holocene-age sites, $A = 1.12$ for Pleistocene sites) and the other terms are as defined previously.

The majority of shear wave velocity measurements in the Andrus et al. (2007) database were obtained using SCPT (14 from crosshole tests, 6 from suspension logger measurements). The CPT soundings for the Holocene sites had a range of soil behaviour type index of $1.19 \leq I_c \leq 4.0$, with all data pairs at depths $z \leq 10$ m. The Pleistocene CPT soundings had a range of soil behaviour type index of $1.16 \leq I_c \leq 3.25$, with 58 data pairs at depths $z \leq 10$ m, 52 pairs at depths $10 < z < 20$ m, and 3 pairs at depths $z \geq 20$ m. Data pairs at depths $z < 3$ m were omitted from both the Holocene and Pleistocene data sets.

3.2 Evaluation of Selected CPT-V_s Correlations

The general soil CPT-V_s correlations discussed in the previous section were applied to the 86 CPT soundings in the SCPTu database for the greater Christchurch area, and the predicted V_s profiles for each correlation compared to the measured V_s values at each site. Figure 3.1 shows a comparison between the estimated and measured V_s profiles for a typical site from the SCPTu database. As shown, the existing correlations tend to overestimate the measured V_s

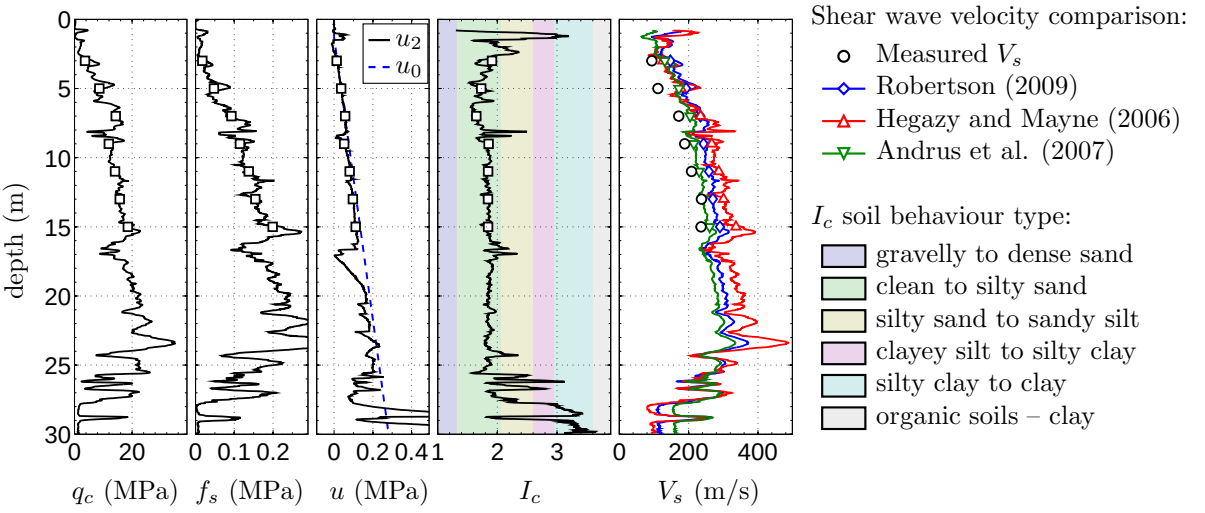

Figure 3.1: Example CPT sounding from SCPTu database with comparison of measured and estimated V_s profiles. Markers for CPT resistance and estimated V_s plots represent geometric mean over SCPTu V_s measurement intervals.

values to varying degrees, though the essential form of the V_s profile suggested by the measured values (an increase of V_s with depth) is captured reasonably well by all three correlations. The trend between the measured and estimated V_s values in Figure 3.1 is representative of the full database. Appendix A provides similar plots for the full set of 86 SCPTu sites.

In order to quantify the applicability of each existing correlation to Canterbury soil deposits, the shear wave velocity prediction bias is defined in terms of the ratio of the estimated V_s value to the measured V_s value at each data point, i.e.,

$$V_s \text{ bias} = \frac{\text{estimated } V_s}{\text{measured } V_s} \tag{3.5}$$

When defined in this manner, a V_s bias > 1.0 represents an overestimation of the measured V_s and a V_s bias < 1.0 represents an underestimation. Figures 3.2 and 3.3 summarize the general performance of the considered shear wave velocity correlations for the Canterbury SCPTu data set. The plots on the left-hand side of Figures 3.2 and 3.3 show the distribution of the bias for each correlation and provide the mean, μ, and coefficient of variation, COV, of a normal distribution fit to the residual data. The plots on the right-hand side compare the measured and estimated shear wave velocities and provide the coefficient of determination, r^2, values. The marker colour in Figures 3.2 and 3.3 correspond to I_c soil behaviour type index as indicated.

Figure 3.2 compares the performance of the two considered Andrus et al. (2007) CPT-V_s correlations Of the two, the Andrus et al. (2007) Holocene-soils correlation appears to be most applicable to the current data set. The mean bias for the Holocene-only correlation is closer to 1.0, and though the 16.8% COV for this case is larger, the Holocene-only correlation provides the more balanced overall bias, tending to overestimate the lower measured V_s values and underestimate the higher V_s values, whereas the Holocene-Pleistocene correlation tends to systematically overestimate the measured V_s values. This systematic overestimation for the combined correlation is likely due to the influence of the naturally higher in-situ V_s values for the Pleistocene-age data pairs on the regression.

The Hegazy and Mayne (2006) correlation of Figure 3.3 appears to be the least applicable to the Canterbury soils, with a mean bias $\mu = 1.22$, bias COV = 21.1%, and $r^2 = 0.70$, this correlation displays the most spread of the four estimation methods and most poorly represents the measured data. The Robertson (2009) correlation returns a narrower range of estimated V_s and a better representation of the measured V_s data, but systematically overestimates the

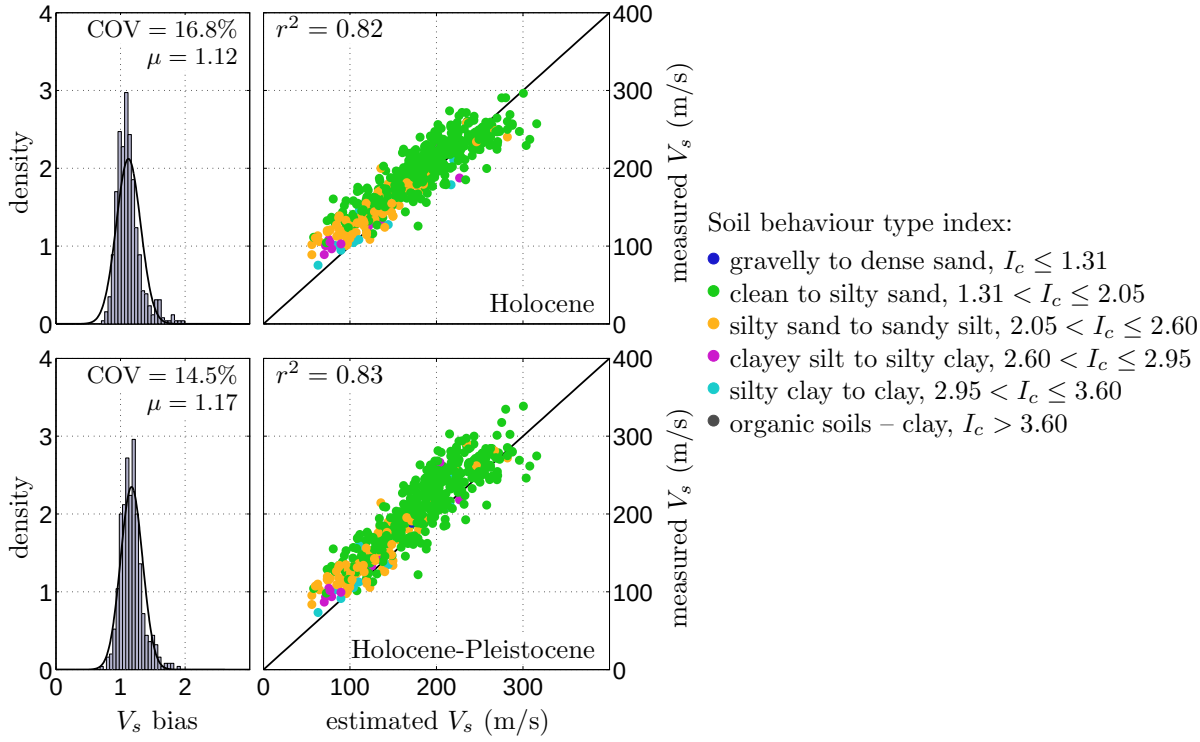

Figure 3.2: Performance of Andrus et al. (2007) CPT-V_s correlations in Canterbury soils.

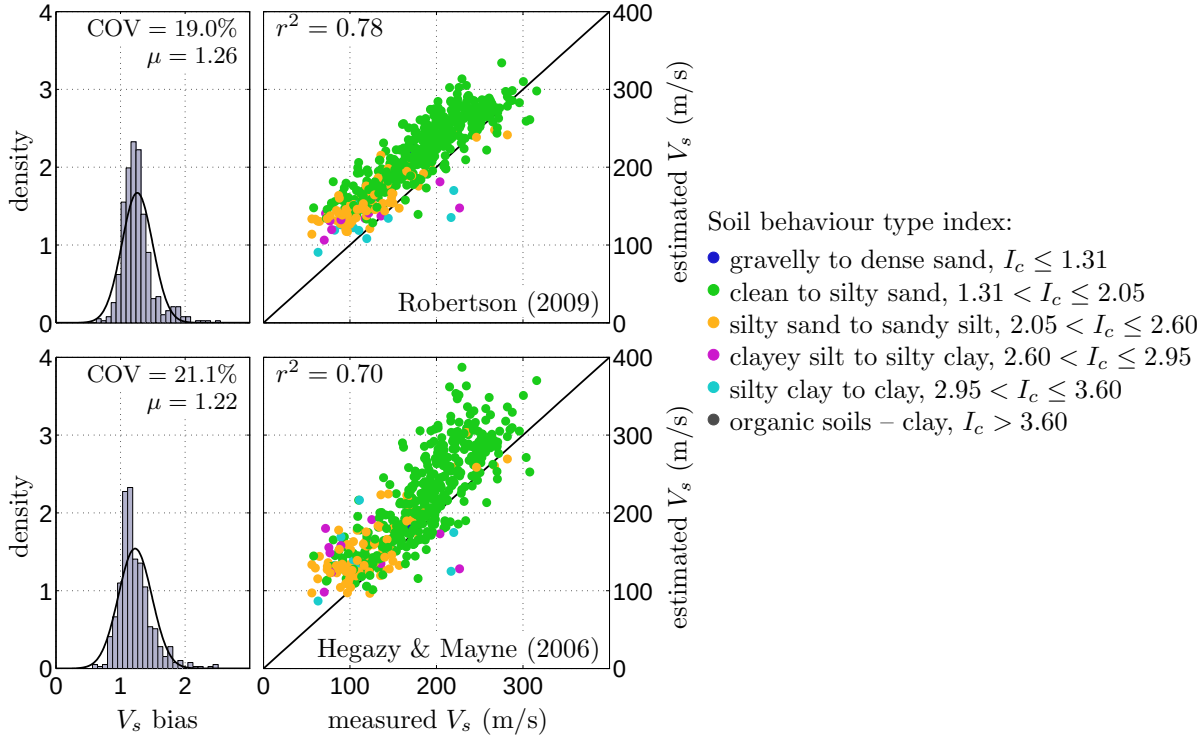

Figure 3.3: Performance of Robertson (2009) and Hegazy and Mayne (2006) CPT-V_s correlations in Canterbury soils.

measured values, leading to the largest mean bias of $\mu = 1.26$. The Holocene-only correlation of Andrus et al. (2007) appears to be more applicable to the current data set than either of the correlations shown in Figure 3.3, with the lowest mean bias, $\mu = 1.12$, a lower COV, and the highest coefficient of determination at $r^2 = 0.82$.

Figure 3.4 shows how the V_s prediction bias varies with raw cone tip resistance, q_c, cone frictional resistance, f_s, and interval midpoint depth, z, for the three indicated existing correlations (the Holocene-only correlation of Andrus et al. (2007) is used hereafter unless otherwise noted). The black lines in these plots represent the moving averages (solid line), with 95% confidence intervals (dashed lines), providing a depiction of the mean trend suggested in these plots. Determining the ranges of these CPT-based variables that display concentrations of high and low bias can aid in understanding why the correlations may or may not be applicable to the current soil deposits, and can also help determine which of these terms are important to consider in a Canterbury-specific CPT-V_s correlation.

The depth variation plots of Figure 3.4 show the most dramatic variations of the three variables considered, and indicate that the overestimation apparent in all three correlations is most prevalent at relatively shallow depths (approximately $z < 4$ m). In contrast, the intermediate range of depths ($4 \leq z \leq 20$ m) show a fairly constant average bias. There is a significant decrease in the number of measured V_s data points beyond $z \approx 20$ m; trends in the average bias for these deeper locations may be influenced by this relative lack of data. All three empirical predictions show similar concentrations of bias at the lower end of the cone resistance ranges (approximately $q_c \leq 3$ MPa and $f_s \leq 0.05$ MPa). Beyond these ranges, the average bias for both the Andrus et al. (2007) and Robertson (2009) correlations tends to decrease with increasing q_c while remaining relatively constant with increasing f_s. The Hegazy and Mayne (2006) average correlation bias tends to increase slightly with increasing q_c, and more significantly with increasing f_s. It appears from the plots of Figure 3.4 that the zones of larger bias at lower values of q_c and f_s coincide with values of $I_c > 2.0$, indicating that soils with silt or clay behaviour types may be poorly predicted.

The inability of the three correlations to represent the shallow V_s values, and the apparent concentrations of larger bias at low q_c and f_s values, may be due, in part, to extrapolation beyond the original considered data sets. For example, the Andrus et al. (2007) study explicitly omitted data with depths $z < 3$ m from the correlation database, thus, this relationship is not applicable to the full range of depths considered in the current study. Extrapolation error does however not appear to account for all of the bias apparent in the existing V_s correlations, as the ranges of CPT measurements and implied soil behaviour types indicated in each work coincide reasonably well with the current data set. The observed bias could also be due to differences between in V_s measurement techniques (SCPTu in current study, various in existing correlations), or more likely, due to the region-specific geological history of the soils involved.

Figure 3.5 shows how the bias for each correlation varies with the I_c values of the data set. The marker colours in these plots represent the magnitudes of q_c and f_s as indicated. As shown in Figure 3.5, the average bias for all three cases increases with increasing I_c for values of $I_c < 2.5$. Beyond this point the bias for the Andrus et al. (2007) and Robertson (2009) correlations tends to decrease with increasing I_c, while the bias for the Hegazy and Mayne (2006) correlation remains relatively constant with increasing I_c. The confidence interval for the Andrus et al. (2007) correlation is essentially constant for the considered I_c range, while the results for the other correlations display a clear reduction in confidence for the mean bias as I_c increases and the data points spread apart and become less frequent. As expected, the larger q_c and f_s values are concentrated in the clean-to-silty sand range of the chart, though the inclusion of these magnitudes does not reveal any significant trend in the relationship between I_c and the prediction bias not already noted from the results of Figure 3.4.

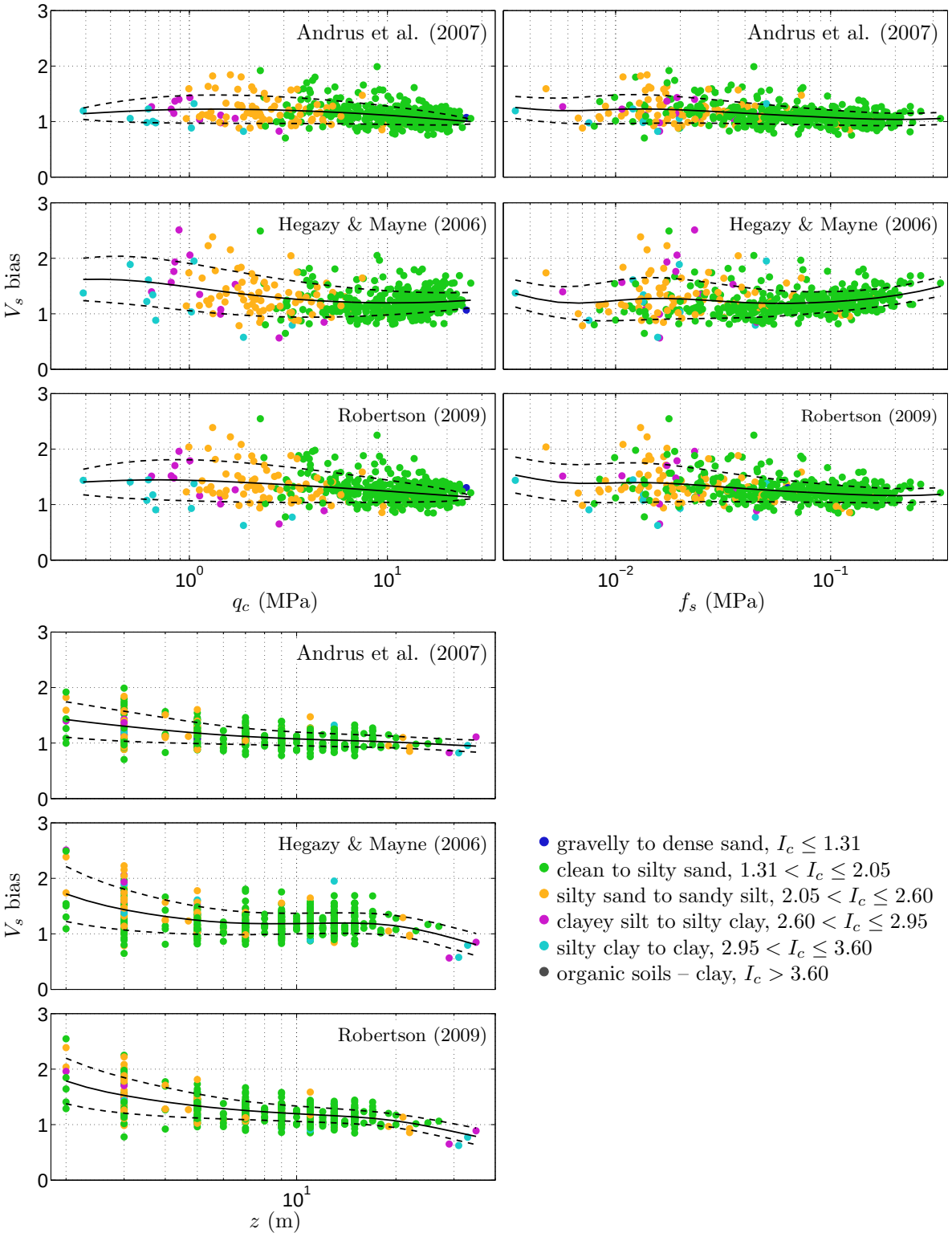

Figure 3.4: Variation of V_s bias with raw cone tip resistance, frictional resistance, and depth.

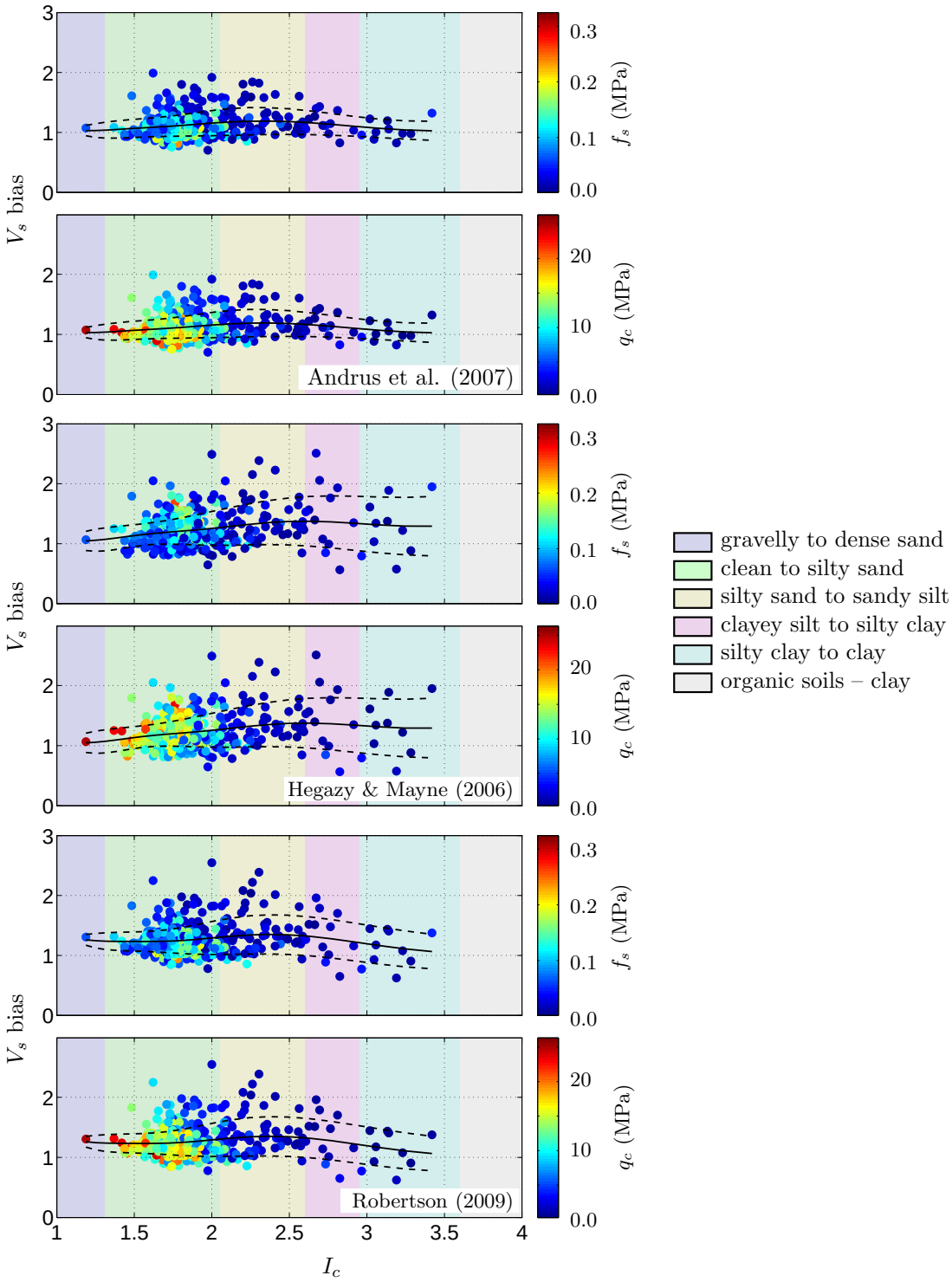

Figure 3.5: Variation of V_s bias with I_c soil behaviour type index.

3.3 Consideration for Age Effects

Another source of the bias present in the results of Figures 3.4 and 3.5 could be related to a loss or reduction of age effects (e.g., time effects on soil micro-structure, reorientation of grains due to load, creep, cementation at grain contact points) in the Canterbury soils brought about by large strains and induced pore pressures associated with the events of the 2010-2011 Canterbury earthquake sequence. Age effects generally lead to an increase in V_s over time, and it is likely that such effects were destroyed or significantly reduced at most of the sites in the SCPTu database from either the Canterbury earthquake sequence or potentially prior significant seismic events. As discussed in Chapter 2, the SCPTu records that comprise the current database were obtained during various post-earthquake site evaluation efforts used to assess the viability of rebuilding in liquefaction-affected areas, therefore many of the SCPTu sites were located in areas of moderate to severe liquefaction. A complete loss of age effects is expected for soils that liquefied and resedimented, and the concentrated bias in the examined relationships at shallow depths coincides with the soils most susceptible to these phenomena, indicating that the liquefaction associated with the earthquakes may have played a significant role in eliminating age effects in, and reducing the applicability of the existing correlations to, the Canterbury soils.

As part of a study on liquefaction resistance corrections for aged sands, Andrus et al. (2009) showed how the ratio of measured to estimated V_s increases with the apparent age of a soil deposit (time since original deposition or since intervening critical disturbance such as liquefaction) for V_s values estimated using the combined Holocene-Pleistocene CPT-V_s correlation given by Equation 3.4. The results of Andrus et al. (2009) indicate that sites with apparent ages beyond the scope considered during the development of the correlation tend to be underestimated (older deposits) or overestimated (younger deposits) on average by the CPT-V_s relationship. To evaluate the current data set in this context, the apparent age of each data pair is defined as the time since initial deposition for locations where liquefaction did not occur or the time since the most recent occurrence of liquefaction for locations that experienced liquefaction due to the 2010-2011 Canterbury earthquakes.

Original depositional ages are estimated using the minimum age with depth suggested by a chart compiled by Cubrinovski and McCahon (2011) to describe the age of soils overlying the Riccarton Gravel deposit based on radiocarbon ages of Christchurch soils reported by Brown and Weeber (1992). The time since the most recent occurrence of liquefaction is estimated as the number of days elapsed between the date of the SCPTu test and the most recent earthquake (of the four shown in Figure 2.6, 4 September 2010 and 22 February, 16 April, and 13 June 2011) for which the factor of safety against liquefaction, FS_{liq}, as computed using the method of Idriss and Boulanger (2008), indicates a high likelihood of liquefaction or significant soil fabric disturbance. To this purpose, fines content, FC, values are estimated from the I_c soil behaviour type index using the Canterbury-specific correlation developed by Robinson et al. (2013) for Avon River soil sites. Data pairs that meet the $I_c > 2.6$ and friction ratio $F_r > 1.0\%$ criteria proposed by Robertson and (Fear) Wride (1998) are excluded from this age effect study.

Figure 3.6 shows the variation of V_s bias (as defined by Equation 3.5) with FS_{liq} for the Holocene-Pleistocene CPT-V_s correlation of Andrus et al. (2007). As shown, this correlation overpredicts the in-situ V_s on average over the full range of FS_{liq} values. The background colours and accompanying FS_{liq} ranges noted in Figure 3.6 correspond to the likelihood of liquefaction classes of Taylor (2014) summarized in Table 3.1. Taylor (2014) developed these likelihood classes (Chen and Juang, 2000) based on probabilities of liquefaction, P_{liq}, computed for FS_{liq} values returned by the deterministic Idriss and Boulanger (2008) liquefaction potential evaluation method in a manner similar to that done by Ku et al. (2012) for the Robertson and (Fear) Wride (1998) liquefaction potential evaluation method.

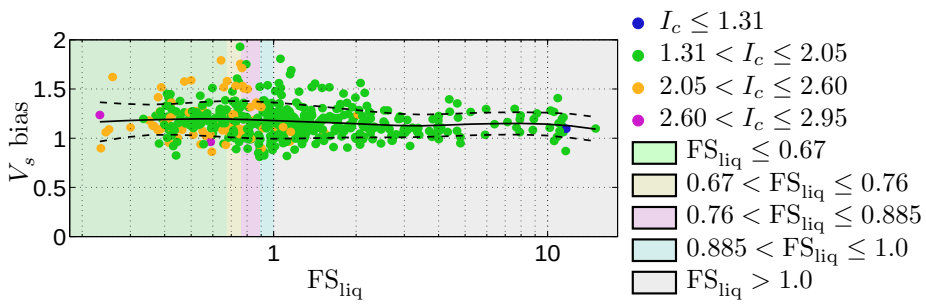

Figure 3.6: Variation of V_s bias with estimated factor of safety against liquefaction, FS_{liq}, for Andrus et al. (2007) Holocene-Pleistocene CPT-V_s correlation.

Table 3.1: Liquefaction likelihood classes based on probabilities of liquefaction computed for Idriss and Boulanger (2008) FS_{liq} values (after Chen and Juang, 2000; Taylor, 2014).

Class	Probability	Factor of Safety	Likelihood Description
5	$0.85 \leq P_{liq}$	$FS_{liq} \leq 0.67$	Almost certain to liquefy
4	$0.65 \leq P_{liq} \leq 0.85$	$0.67 \leq FS_{liq} \leq 0.76$	Very likely to liquefy
3	$0.35 \leq P_{liq} \leq 0.65$	$0.76 \leq FS_{liq} \leq 0.885$	Liquefaction and no liquefaction equally likely
2	$0.15 \leq P_{liq} \leq 0.35$	$0.885 \leq FS_{liq} \leq 1.0$	Unlikely to liquefy
1	$P_{liq} < 0.15$	$1.0 < FS_{liq}$	Almost certain not to liquefy

Figures 3.7 and 3.8 show the variation of measured to estimated V_s ratio, MEVR, for the Andrus et al. (2007) Holocene-Pleistocene CPT-V_s correlation applied to the sand data points of Andrus et al. (2009) (black markers) and the current Canterbury SCPTu database sites (coloured markers). The MEVR in this context is defined as the reciprocal of the V_s bias given in Equation 3.5. The solid black line in each plot represents the mean regression line fit to the existing data, given by Andrus et al. (2009) as:

$$\text{MEVR} = \frac{\text{measured } V_s}{\text{estimated } V_s} = 0.0820 \log_{10}(t) + 0.935 \tag{3.6}$$

where t is time. The dashed black lines show $+/-$ one standard deviation from the mean regression line. The time since critical disturbance for the current data set shown in Figure 3.7 is defined as $FS_{liq} \leq 0.885$ based on the liquefaction likelihood classes of Table 3.1, as Taylor (2014) indicates that locations with factors of safety > 0.885 are unlikely or almost certain not to liquefy for the given events. With this definition for critical disturbance, the current data set is split fairly evenly into two groupings. One containing the sites where liquefaction was deemed likely to have occurred and the apparent ages are less than one year, and one with the sites deemed undisturbed by the $FS_{liq} \leq 0.885$ criteria where the apparent ages are the original depositional ages ($\approx$ 1000-10000 years) estimated from the chart of Cubrinovski and McCahon (2011), which assumes that there have been no significant seismic events in the immediate vicinity of the region over this time period. Figure 3.8 shows the same information, but for a different definition of the time since critical disturbance for the current data set. In this case, the critical disturbance is defined as $FS_{liq} \leq 2.0$ which, per Ishihara and Yoshimine (1992), roughly corresponds with the point at which non-negligible maximum shear strains develop in sands. For this criteria, the majority of the current data set is considered to have been critically disturbed by one of the events of the Canterbury earthquake sequence, though as shown in Figure 3.8 a grouping of undisturbed data points remains.

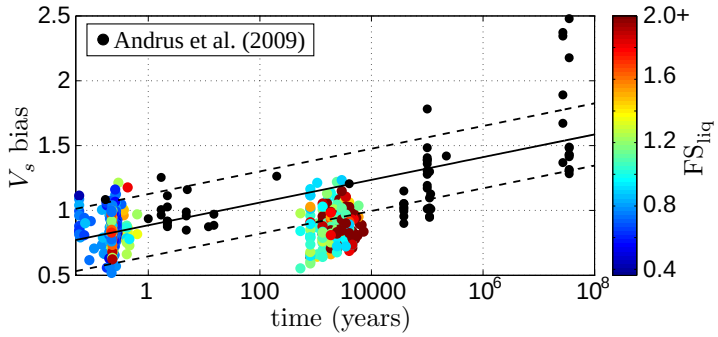

Figure 3.7: Variation of MEVR with time since critical disturbance or initial deposition, with critical disturbance defined as $FS_{liq} \leq 0.885$. Marker colour for current data set corresponds to FS_{liq} as indicated.

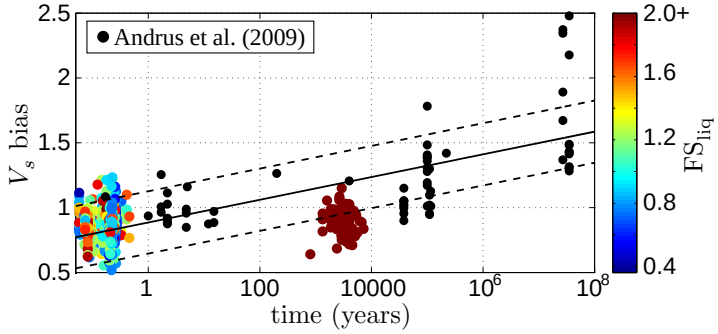

Figure 3.8: Variation of MEVR with time since critical disturbance or initial deposition, with critical disturbance defined as $FS_{liq} \leq 2.0$. Marker colour for current data set corresponds to FS_{liq} as indicated.

The results of Figures 3.7 and 3.8 show that the V_s values of the current data set, even the undisturbed locations with apparent ages similar to those used to develop the correlation, are overestimated by the Andrus et al. (2007) Holocene-Pleistocene correlation. The data points with apparent ages < 1 year appear to follow the trend suggested by the Andrus et al. (2009) data set for both considered definitions of critical disturbance, while the data points considered to be undisturbed by both the $FS_{liq} \leq 0.885$ and $FS_{liq} \leq 2.0$ criteria do not follow this trend. This marked difference between the increase in V_s with age displayed by the existing data and the lack of increase displayed by the current data suggests two possibilities:

1. All of the soils comprising the sites in Canterbury SCPTu database experienced a complete loss or significant reduction in age effects from shear strains and induced pore pressures due to the 2010-2011 earthquakes, regardless of whether liquefaction did or did not occur.

2. The depositional environment or the affects of deposit age on the strength and stiffness of these Canterbury soil sites is unique in some fundamental way. The aquifer conditions for the soils of this region could possibly have contributed to disturbances in the accumulation of age effects. Additionally, estimation of the undisturbed ages from the Cubrinovski and McCahon (2011) chart ignores any reduction or loss in age effects brought about by significant seismic events that took place in the region after original deposition but prior to the start of the historical record (about 150 years ago for New Zealand) or known historical events such as the approximately M_w5 earthquake that took place in 1870 (Gledhill et al., 2011). This uncertain effect of past seismic activity on the apparent age of soil deposits is inherent in the Andrus et al. (2009) results as well, and the assumption equality between the apparent and estimated depositional ages for soils undisturbed by known seismic events may hold true in regions of low seismicity or with a long historical record of earthquakes.

In either case, it is clear that the soils in the greater Christchurch area are poorly represented by the considered CPT-V_s correlations, and it appears that the unique depositional and post-earthquake conditions of these soils contribute significantly to this difference.

3.4 Summary

The large Canterbury-specific SCPTu data set compiled and discussed in Chapter 2 was utilized to assess the suitability of four existing CPT-V_s correlations for describing the relationship between CPT data and in-situ shear wave velocity for soil deposits in the greater Christchurch area. It was determined that all four correlations produce biased V_s estimates when applied to the CPT soundings of the database, with each existing correlation tending to overestimate the in-situ V_s to varying degrees. The Holocene-age correlation of Andrus et al. (2007) was found to be the most applicable to the soils of the Canterbury region, displaying the smallest degree of overestimation (12% on average) and the best representation of the current data. Adjustments to account for disturbances to soil ageing effects at the considered soil sites due to the events of the 2010-2011 Canterbury earthquake sequence showed that the observed bias persisted irrespective of the apparent soil age, suggesting that the considered Canterbury soils possess a unique region-specific geologic history that leads to the biased estimates returned by the existing CPT-V_s correlations. These findings suggest that the development of a Canterbury-specific correlation that captures this unique nature of the regional soils will be beneficial to future research efforts.

Chapter 4

DEVELOPMENT OF CANTERBURY-SPECIFIC CPT-V_s CORRELATION

The comparison study presented in Chapter 3 evaluated the suitability of four existing empirical models for estimating the in-situ V_s of Canterbury soils using CPT data. The existing CPT-V_s correlations were shown to be biased, generally overestimating the observed V_s with depth, thus demonstrating the need for the development of a Canterbury-specific CPT-V_s correlation through regression analysis. The first step in this development is the selection of an appropriate functional form for the regression analysis. The second step is an assessment of the quality of the regression using the selected functional form. The details of the correlation development are presented in the ensuing sections, followed by a discussion of the recommended Canterbury-specific CPT-V_s correlation determined through this process.

4.1 Evaluation of Regression Function Forms

Six distinct relations between V_s and various CPT-based variables are considered as candidate regression functions. The considered regression forms include the Andrus et al. (2007) form:

$$V_s = a{q_t}^b {I_c}^d z^e \tag{4.1}$$

where a, b, d, and e are regression coefficients, q_t is the corrected cone tip resistance (Campanella et al., 1982), I_c is the soil behaviour type index (Robertson and (Fear) Wride, 1998), and z is the depth; the Hegazy and Mayne (2006) form rearranged to solve for shear wave velocity:

$$V_s = aQ_{tn} \exp(bI_c) \left(\frac{\sigma'_{v0}}{p_a}\right)^{0.25} \tag{4.2}$$

where Q_{tn} is the normalized cone resistance (Robertson and (Fear) Wride, 1998; Zhang et al., 2002), σ'_{v0} is vertical effective stress, and p_a is atmospheric pressure; the Robertson (2009) form:

$$V_s = \left[10^{a+bI_c} \left(\frac{q_t - \sigma_{vo}}{p_a}\right)\right]^{0.5} \tag{4.3}$$

the form recommended for use in CPT-V_s regression analysis by Wair et al. (2012):

$$V_s = a{q_t}^b {f_s}^d {\sigma'_{vo}}^e \tag{4.4}$$

where f_s is the cone frictional resistance; and two hybrid forms that consider different combinations of terms from the Andrus et al. (2007) and Wair et al. (2012) forms:

$$V_s = a{q_t}^b {f_s}^d z^e \tag{4.5}$$

$$V_s = a{q_t}^b {I_c}^d {\sigma'_{vo}}^e \tag{4.6}$$

Multiple linear regression in logarithmic space is used with the Canterbury SCPTu data set for each of the six considered regression forms. Figure 4.1 shows a comparison between the measured V_s values from the database and the V_s values estimated using each considered regression form (indicated by Equation number). The plots and associated coefficients of determination, r^2,

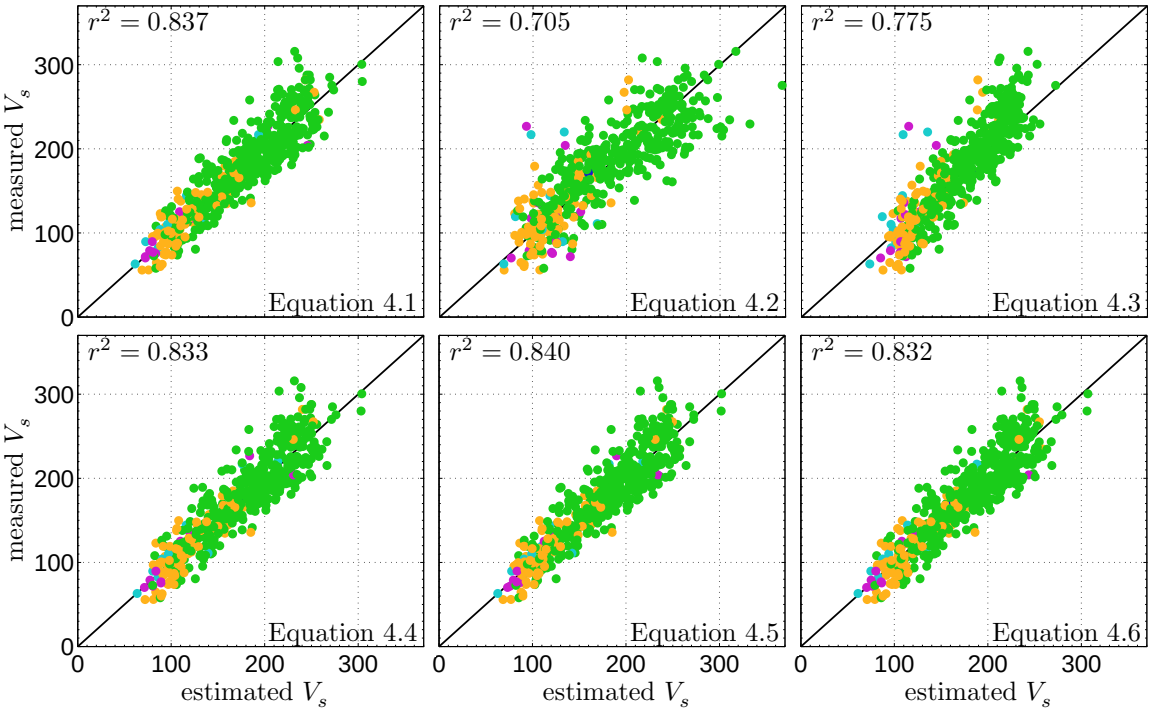

Figure 4.1: Comparison of estimated and measured V_s for indicated regression functional forms.

shown in Figure 4.1 indicate the relative compatibility of each regression form to the current data set. Based on these results, the Hegazy and Mayne (2006) and Robertson (2009) forms (Equations 4.2 and 4.3, respectively) appear to be the least applicable to the Canterbury data set, while the remaining four polynomial-based forms all provide a similar representation of the measured data.

The residuals for the fitted regression lines provide another means of evaluating the various regression forms. To this purpose, the residuals, ε, are defined as:

$$\varepsilon = \frac{\ln(y_i) - \ln(\bar{y}_i)}{s_{Y|x}} \tag{4.7}$$

where $\ln(\circ)$ is the natural logarithm function, y_i are the measured V_s values, $\bar{y}_i$ are the V_s values returned by the regression lines, and $s_{Y|x}$ is an estimate of the conditional standard deviation (Ang and Tang, 2007, pp. 306-325):

$$s_{Y|x} = \sqrt{\frac{\sum (\ln(y_i) - \ln(\bar{y}_i))^2}{n-4}} \tag{4.8}$$

where $n = 513$ is the number of data pairs included in the regression. Figure 4.2 shows how the computed residuals vary with the depth, z, of the SCPTu data set, as depth shows the largest variation in residuals of the considered CPT variables. Figures B.1–B.5 in Appendix B provide the variation of the residuals with the remaining CPT-based variables, the raw cone tip resistance, q_c, frictional resistance, f_s, depth, z, estimated V_s, and the I_c soil behaviour type index. The marker colours in Figure 4.2 represent the I_c soil behaviour type index as indicated, while the black lines represent the moving averages (solid line) with 95% confidence intervals (dashed lines) for the residuals (Wasserman, 2006).

As shown in Figure 4.2, the regression forms given by Equations 4.1, 4.4, 4.5, and 4.6, the first two of which were the forms of Andrus et al. (2007) and Wair et al. (2012), respectively, produce reasonably consistent, and nearly identical, residual distributions across the range of

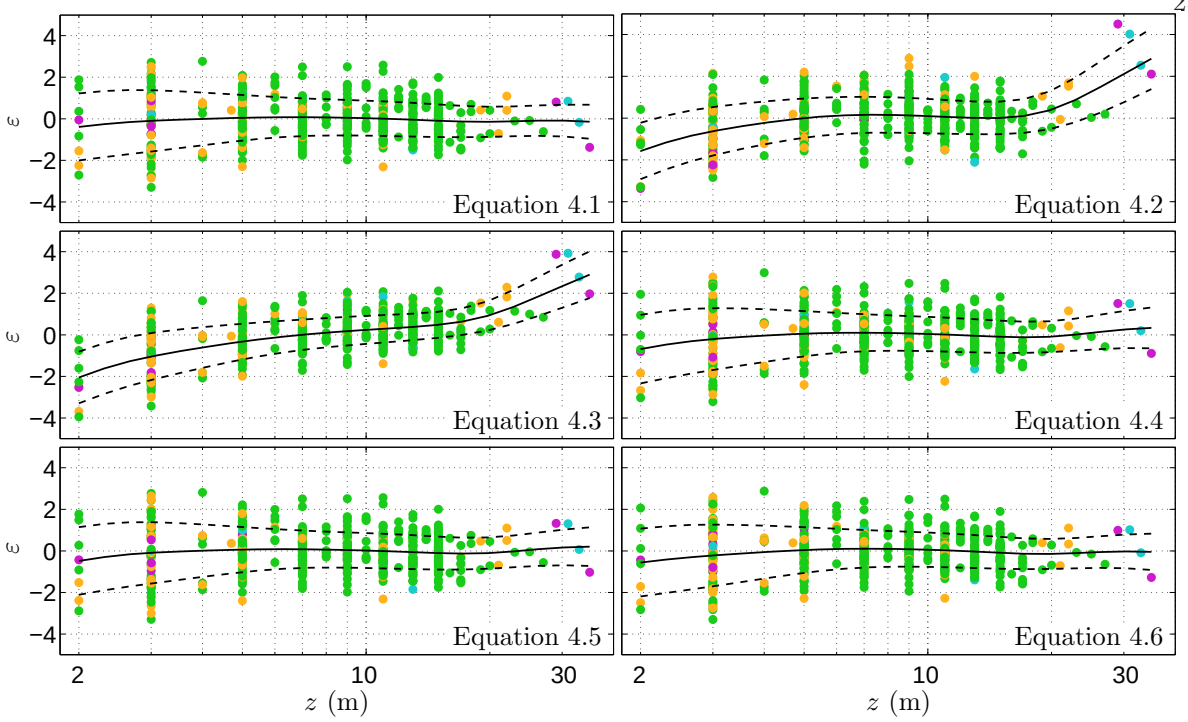

- gravelly to dense sand, $I_c \leq 1.31$
- clean to silty sand, $1.31 < I_c \leq 2.05$
- silty sand to sandy silt, $2.05 < I_c \leq 2.60$
- clayey silt to silty clay, $2.60 < I_c \leq 2.95$
- silty clay to clay, $2.95 < I_c \leq 3.60$
- organic soils – clay, $I_c > 3.60$

Figure 4.2: Variation of residuals with depth, z, for indicated regression forms.

depths in the database. Equations 4.2 and 4.3, the Hegazy and Mayne (2006) and Robertson (2009) functional forms, display regions of concentrated bias, tend to overestimate the measured data at shallow ($z < 4$ m) locations and underestimate the data at deeper locations ($z > 20$ m). Figures B.1–B.5 (not shown here) show similar trends to those of Figure 4.2; the Hegazy and Mayne (2006) and Robertson (2009) regression forms return residuals that are biased towards under- or over-prediction of the measured V_s for certain ranges of q_c, f_s, estimated V_s, and I_c, while the remaining regression forms produce residual distributions that are consistent across the considered CPT-based variable ranges.

After ruling out the Hegazy and Mayne (2006) and Robertson (2009) regression forms, the selection criteria for the most applicable functional form becomes more subtle. As shown in Figures 4.1, 4.2, and B.1–B.5, the differences between the V_s estimates provided by the four remaining regression forms (Equations 4.1, 4.4, 4.5, and 4.6) are practically negligible over the principal ranges of the data set. Given this similarity in performance, consideration for the variables included in the regression equations and how these variables affect the use of the resulting correlation becomes important. The first distinguishing characteristic between these four functional forms is the use of depth, z, or initial vertical effective stress, σ'_{v0}, as an indicator for the state of stress in the soil. From a theoretical standpoint, σ'_{v0} is preferable, however from a practical standpoint, depth may be a better choice. For a given site and CPT record, the depth is an inherently known quantity, while σ'_{v0} is typically estimated based on assumptions of soil mass density and groundwater table depth, and errors or uncertainties in estimated values for density, water table depth, and σ'_{v0} could lead to less reliable V_s predictions. This distinction is somewhat supported by the r^2 values provided in Figure 4.1, which are slightly larger for the regression forms that consider z instead of σ'_{v0}.

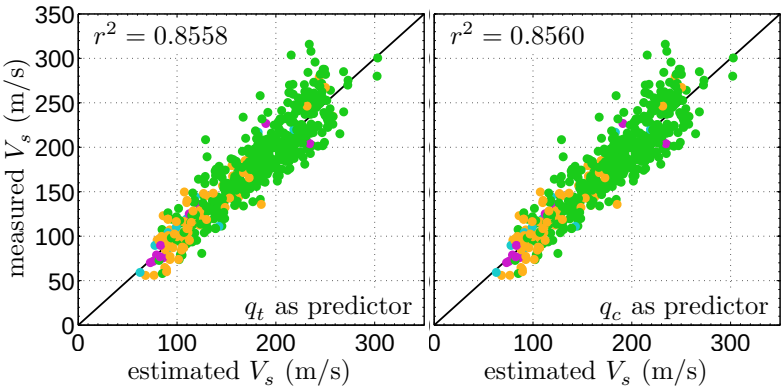

Figure 4.3: Comparison of estimated and measured V_s for regression forms that consider raw and corrected tip resistance (q_c and q_t, respectively) as indicated.

The second decision relates to the use of the cone frictional resistance, f_s, or the soil behaviour type index, I_c, as these terms are the only differences between the remaining two regression forms (Equations 4.1 and 4.5). Since each functional form appears to be equally applicable to the Canterbury data set by the measures presented here, the form given in Equation 4.5 is chosen due to its use of f_s, which is directly measured by the CPT, instead of I_c, which is a computed variable (function of q_c, f_s, and depth). While I_c is a commonly-used indicator of soil behaviour type that carries useful connotations for many geotechnical engineers, its computation requires an additional step not required by f_s and its use in the CPT-V_s correlation may lead to erroneous predictions due to various available presentations of the I_c function or soil behaviour type zones (e.g., Jefferies and Davies, 1991; Robertson and (Fear) Wride, 1998; Robertson, 2010).

It is also of interest to assess the effects of consideration for the raw cone tip resistance, q_c, instead of the corrected resistance, q_t. As shown in Figure 4.3, there is effectively zero difference in the quality of the regression when consideration is made for the raw cone resistance. The V_s values estimated using q_c as a predictor variable differ from those estimated using q_t by a maximum of 0.65%. This similarity makes sense in the context of the Canterbury SCPTu sites, which as discussed in Chapter 2 and shown in the profile plots of Appendix A, are predominantly composed of soils with I_c values in the clean to silty sand behaviour zone where pore pressure readings are typically small (i.e., $q_c \approx q_t$). Given the similarity in results shown by Figure 4.3, it is preferable to replace the q_t term in Equation 4.5 with q_c to avoid any additional uncertainties introduced into the regression through the calculation of the corrected cone resistance. Based on this evaluation, the chosen regression functional form:

$$V_s = a{q_c}^b {f_s}^d z^e \tag{4.9}$$

is based entirely on terms directly measured by the CPT (q_c, f_s, and z). These terms are the least uncertain quantities that can be considered in the regression function, and this study has shown that the quality of the regression to the considered Canterbury-specific data set is not significantly different when consideration is given to these direct terms.

4.2 Consideration for Non-Constant Conditional Variance

Figure 4.4 summarizes the performance of the regression form given by Equation 4.9 when applied to the Canterbury SCPTu database. As indicated by the moving average trend lines (solid black lines), the residuals for this correlation are relatively consistent across the considered ranges of CPT-based variables, though it is evident from the depth variation plot that there is some variance in the data set with z, as the data points are more spread out and confidence

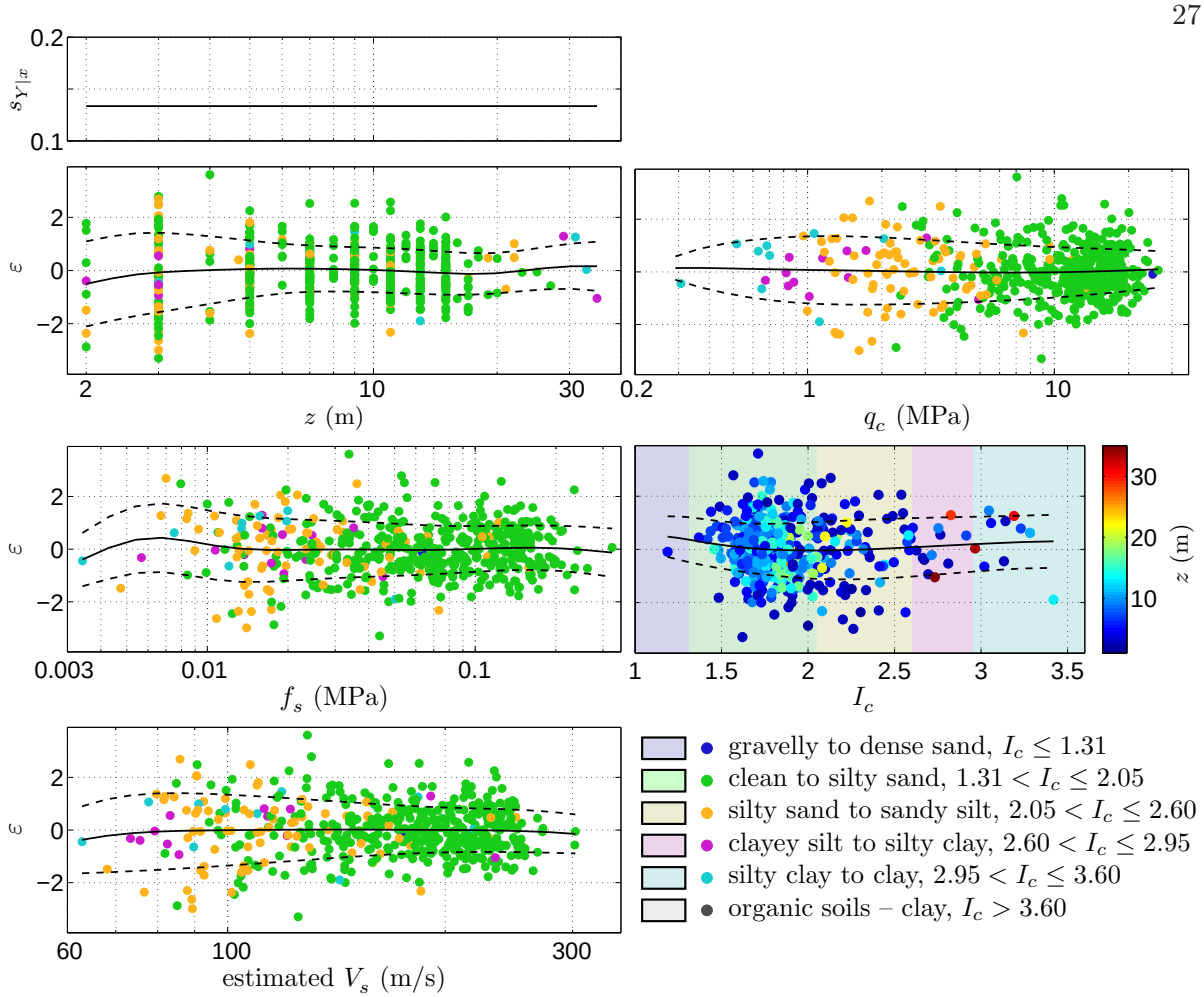

Figure 4.4: Variation of residuals with z, q_c, f_s, I_c, and estimated V_s for multiple linear regression (using functional form of Equation 4.9) with constant variance. Marker colour indicates I_c or depth, z, as noted.

intervals (dashed black lines) are wider for shallow locations. As indicated in the upper left plot of Figure 4.4, the presented results correspond to a regression analysis that considers constant conditional variance, hence constant conditional standard deviation $s_{Y|x}$, with depth. These results imply that consideration for a conditional variance that is non-constant with depth in the regression analysis could lead to an improved prediction of shear wave velocity.

Figure 4.5 presents the performance of the regression with consideration for a non-constant conditional variance that varies with depth. Based on an examination of the residuals, it was determined that the depth is the only predictor variable with which there was an apparent non-constant variance. As shown for $s_{Y|x}$ in the upper left plot of Figure 4.5, a piecewise linear variation of variance with depth was considered. The depths at which the piecewise variance function changes ($z = 5$ m and $z = 10$ m) were manually chosen based on the regression results. For the non-constant conditional variance model, the spread in the residuals evident in Figure 4.4 at shallow depths becomes less pronounced and the overall distribution of the residuals with depth becomes more consistent. Because shallow depths typically correspond with lower shear wave velocities, the non-constant variance regression analysis naturally results in a tighter distribution of residuals at the lower ranges of the estimated V_s plot. Based on visual comparison of Figures 4.4 and 4.5, the non-constant variance regression produces more consistent residual distributions for all considered CPT-based variables. Additionally, the non-constant variance model yields a smaller standard deviation for deeper locations ($z > 10$ m) than the constant variance model.

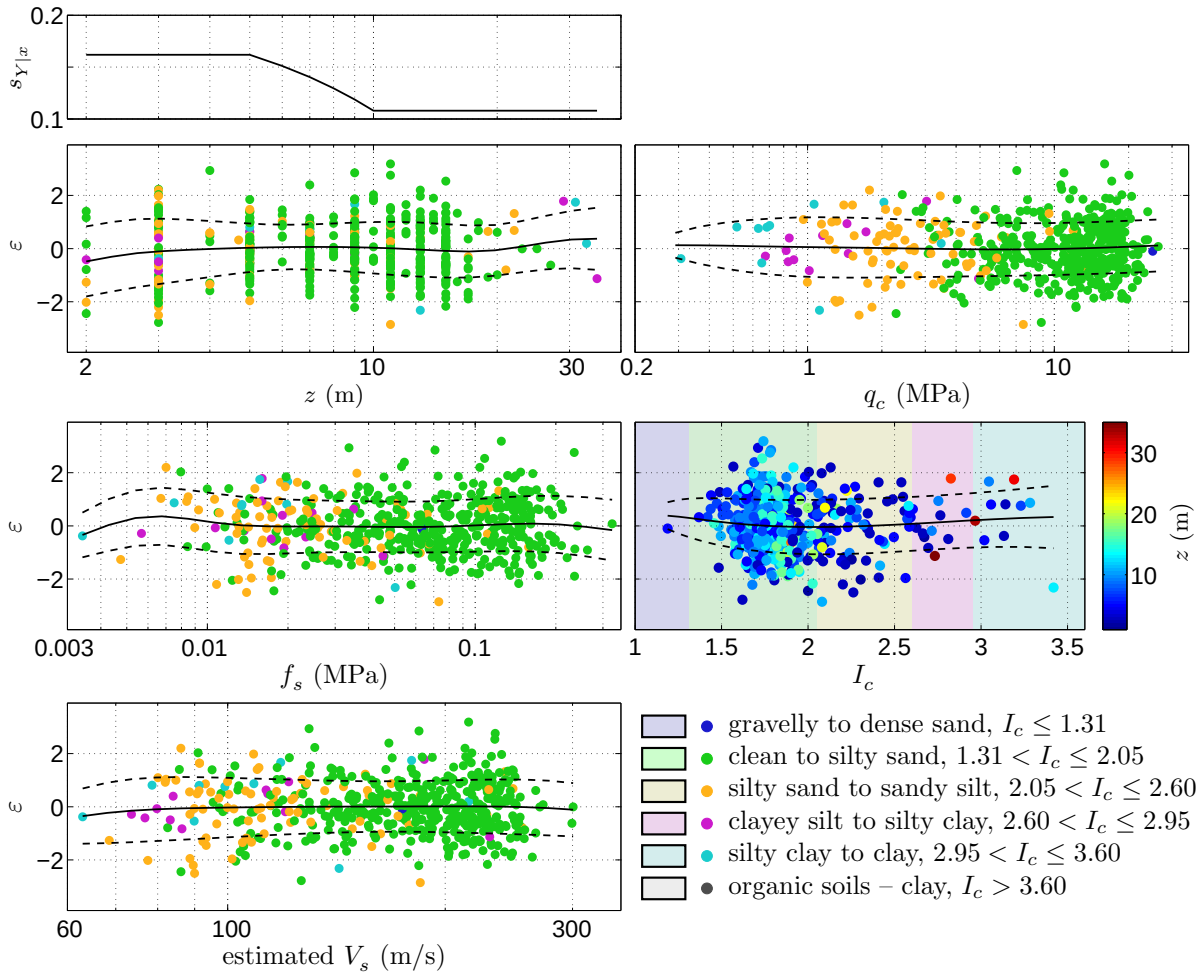

Figure 4.5: Variation of residuals with z, q_c, f_s, I_c, and estimated V_s for multiple linear regression (using functional form of Equation 4.9) with non-constant variance. Marker colour indicates I_c or depth, z, as noted.

4.3 Regression Analysis

The Canterbury-specific CPT-V_s correlation is determined from multiple linear regression in natural log space using the non-constant variance distribution and functional form (Equation 4.9) discussed in the previous sections. The recommended best-fit equation for predicting V_s from CPT data in Canterbury soils is:

$$V_s = 18.4\, {q_c}^{0.144} {f_s}^{0.0832} z^{0.278} \tag{4.10}$$

where q_c and f_s are the raw cone tip and frictional resistances, respectively, in units of kPa, z is the depth below the ground surface in metres, and V_s is the shear wave velocity in units of metres per second. The piecewise standard deviation for this regression model is given by:

$$\sigma_{\ln(V_s)} = \begin{cases} 0.162 & \text{for } z \leq 5 \text{ m} \\ 0.216 - 0.0108z & \text{for } 5 \text{ m} < z < 10 \text{ m} \\ 0.108 & \text{for } z \geq 10 \text{ m} \end{cases} \tag{4.11}$$

from which the prediction of V_s for a given percentile can be obtained as:

$$V_{s\,x} = V_{s\,50} \exp\left(z_x \sigma_{\ln(V_s)}\right) \tag{4.12}$$

where x is the desired percentile, $V_{s\,50}$ is the median prediction (given by Equation 4.10), and z_x is the standard normal variate for the xth percentile (e.g., $z_x = 0, 1$ for the 50th and 84th percentiles, respectively). As shown by the plots of Figure 4.5, the regression model of Equation 4.10 produces consistent estimates of V_s across the full ranges of depth, cone and frictional resistance, and I_c soil behaviour type represented in the database, as well as for the full range of estimated V_s values returned by the correlation.

Support for the validity of the employed regression approach is provided by Figure 4.6, which compares the cumulative probability distribution (CDF) for the analytical lognormal distribution with the CDF of the residuals, ε, for the empirical correlation (computed using Equation 4.7). The shown similarity between the empirical and theoretical cumulative distributions indicates that the data are lognormally distributed with respect to the prediction equation, providing confirmation that the normality assumption in the regression model, i.e., $\ln(V_s) = f\left(\ln(q_c), \ln(f_s), \ln(z)\right)$, is appropriate for the data set.

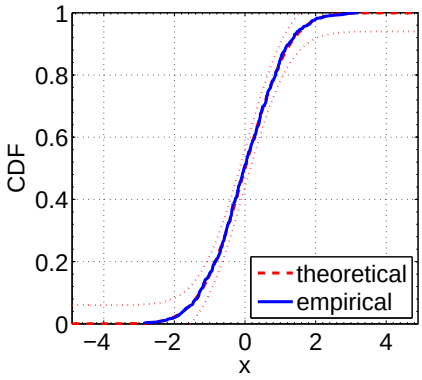

Figure 4.6: Comparison of CDFs for normalized empirical residuals with analytical lognormal distribution. Dotted lines represent Kolmogorov-Smirnov goodness-of-fit bounds for $\alpha = 0.05$.

Figure 4.7 shows the variation of the residuals with the factor of safety against liquefaction, $\mathrm{FS_{liq}}$, computed using the method of Idriss and Boulanger (2008) for each data pair as discussed in Chapter 3. The background colours in this plot correspond to the likelihood of liquefaction classes of Taylor (2014) summarized in Table 3.1, while marker colour corresponds to the soil behaviour type. When the plotted $\mathrm{FS_{liq}}$ are interpreted as an indicator of apparent soil age as done in Chapter 3, Figure 4.7 essentially indicates that the Canterbury-specific CPT-V_s correlation given by Equation 4.10 performs equally well for the full range of liquefaction histories and apparent ages in the data set.

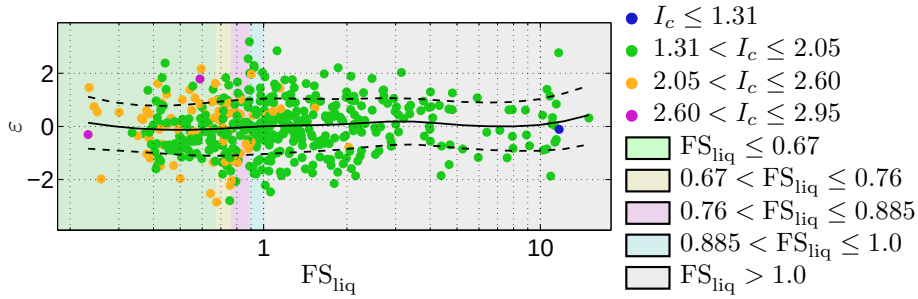

Figure 4.7: Variation of residuals with estimated factor of safety against liquefaction, $\mathrm{FS_{liq}}$, for multiple linear regression with non-constant variance. Marker colour indicates I_c and background colour indicates liquefaction likelihood class, as noted (see Table 3.1 in Chapter 3).

Figures 4.8–4.11 compare V_s profiles estimated using the Canterbury-specific CPT-V_s correlation of Equation 4.10 with the measured V_s profiles for four sites in the Canterbury SCPTu database. The central solid line in the V_s plots of Figures 4.8–4.11 defines the median estimated profile ($V_{s\,50}$), while the shaded region bounded by dashed lines indicates the shear wave velocities at +/− one standard deviation from the solid line (i.e., $V_{s\,16}$ and $V_{s\,84}$ from Equation 4.12). Appendix C provides similar plots for the full set of 86 SCPTu sites. The sites shown in Figures 4.8 through 4.11 were selected to demonstrate the ability of the current regression model to handle a variety of soil behaviour types and soil stiffness conditions. Figures 4.8 and 4.9 represent relatively stiff (higher q_c) soil sites that have the general behaviour types of a reasonably clean sand and a siltier sand, respectively. Figures 4.10 and 4.11 are representative of relatively soft (lower q_c) soil sites with the same two respective general soil behaviour types. As shown, the measured and estimated V_s profiles appear visually similar for all four site soil conditions, and the measured V_s values generally fall within one standard deviation from the median prediction for each site.

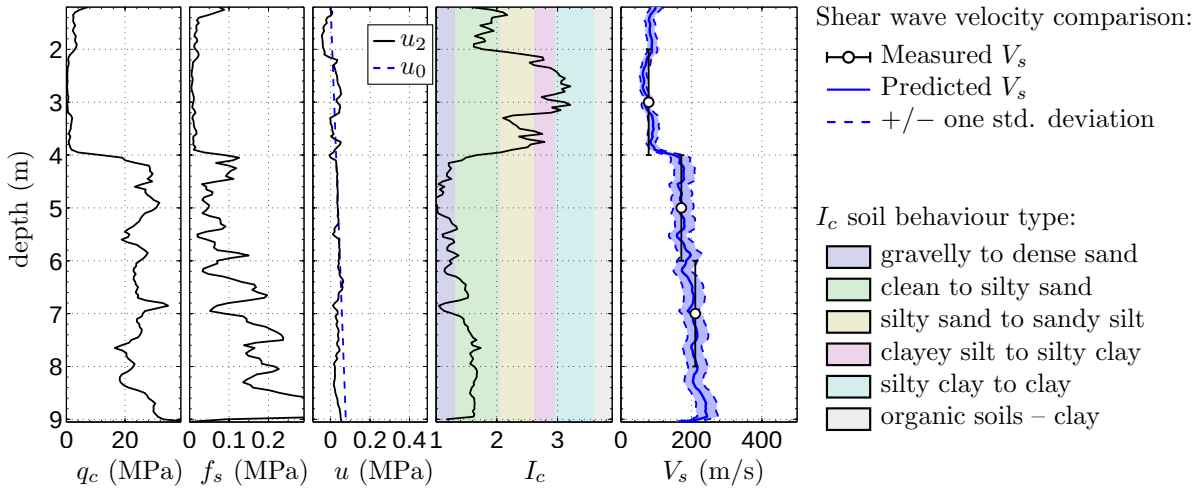

Figure 4.8: Comparison of measured V_s values with Canterbury-specific CPT-V_s estimated profile for site KAS46, representative of a clean sand (lower I_c) soil site (for $z > 4$ m) with a relatively stiff (higher q_c) response.

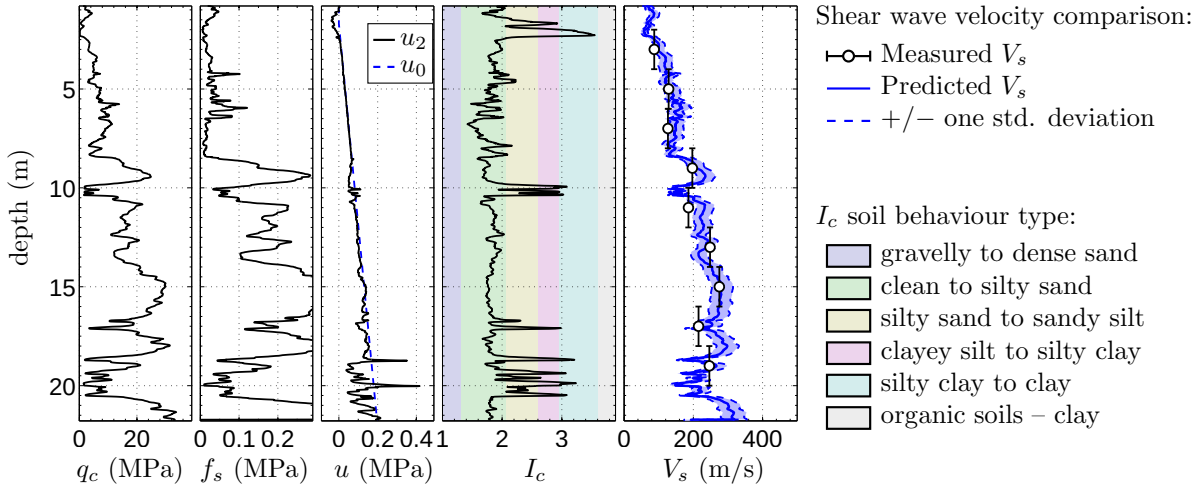

Figure 4.9: Comparison of measured V_s values with Canterbury-specific CPT-V_s estimated profile for site WAI14, representative of a silty sand (higher I_c) soil site with a relatively stiff (higher q_c) response.

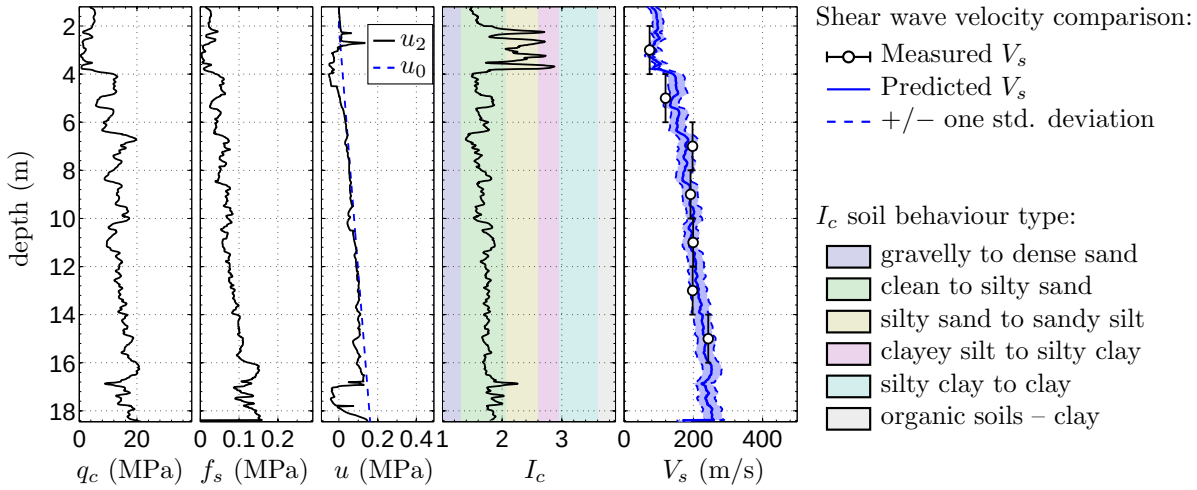

Figure 4.10: Comparison of measured V_s values with Canterbury-specific CPT-V_s estimated profile for site ARN28, representative of a sand (lower I_c) soil site (for $z > 4$ m) with a relatively soft (lower q_c) response.

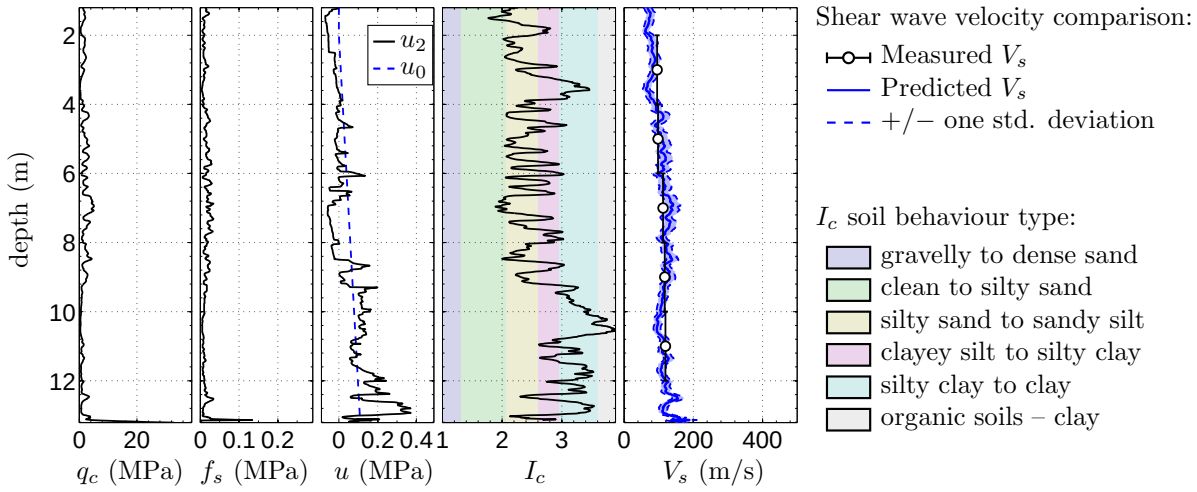

Figure 4.11: Comparison of measured V_s values with Canterbury-specific CPT-V_s estimated profile for site BDL08, representative of a siltier (higher I_c) soil site with a relatively soft (lower q_c) response.

To demonstrate and assess the performance of the Canterbury-specific CPT-V_s correlation in a purely forward prediction, as opposed to the comparisons of prediction and observation given by Figures 4.8–4.11, six synthetic CPT profiles are generated and the regression model is applied to predict V_s. These synthetic profiles are based on three I_c soil behaviour type cases: a relatively clean sand ($I_c = 1.55$), a silty sand ($I_c = 1.95$), and a sandy silt ($I_c = 2.45$). Two q_c profiles are assumed for each I_c case, one which represents a softer version of each soil behaviour type, and one which represents a stiff version. The chosen I_c and q_c values are informed by the distributions of these terms within the Canterbury SCPTu database as discussed in Chapter 2. In order to apply the regression model to these synthetic profiles, f_s values are computed from the I_c equation of Robertson and (Fear) Wride (1998) for each combination of q_c, I_c, and depth z. Figure 4.12 shows the synthetic profiles and corresponding V_s profile predictions for each considered case. The soft-soil q_c values for each I_c case are approximately equal to the smallest values possible without requiring a negative frictional resistance.

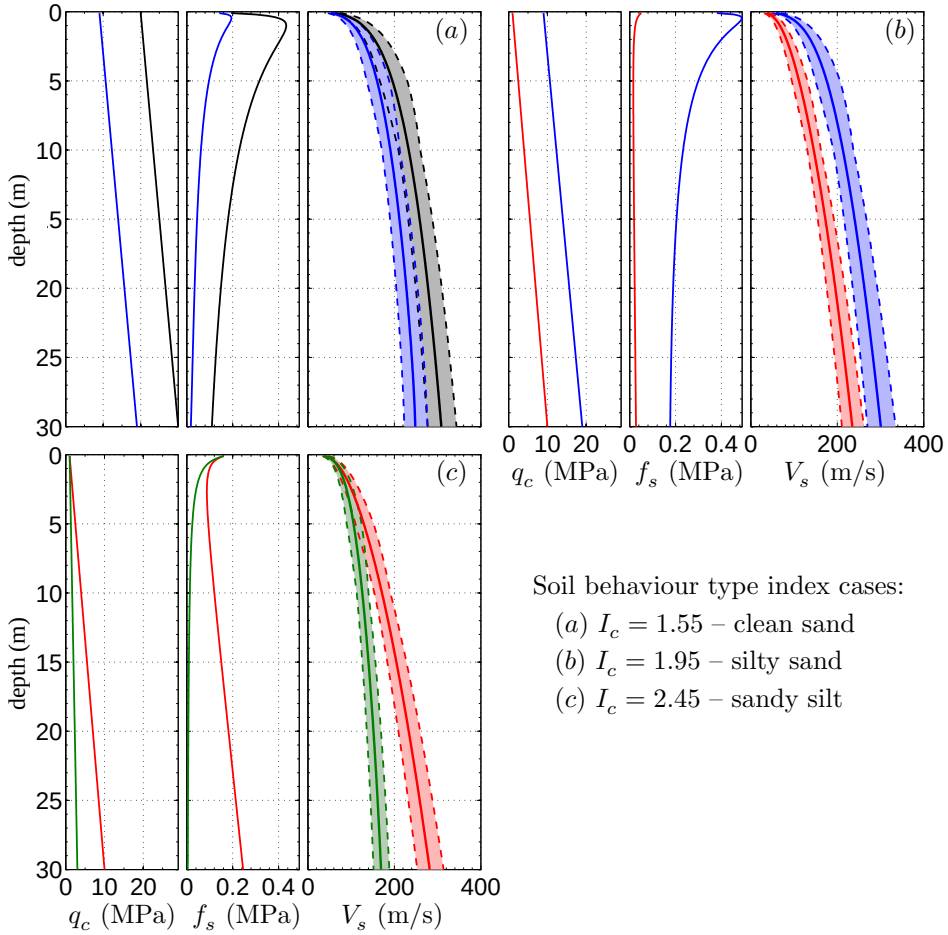

Figure 4.12: Estimated V_s profiles for synthetic CPT records representative of soft and stiff soil profiles for the three indicated I_c soil behaviour type cases. Solid lines in V_s plots are median predictions, the dashed lines indicate +/− one standard deviation from each median profile.

As shown in Figure 4.12, the V_s predictions generally appear to be appropriately sensitive to changes in the predictor variables. Increasing the soil stiffness (via an increase in q_c) for a given soil behaviour type results in higher shear wave velocities with depth. Comparison of the soft soil profiles (lower q_c), which hold a consistent relationship to I_c not reflected in the stiff profiles, across the three soil behaviour type cases shows that increasing I_c generally leads to a decrease in V_s for a given depth. Overall, the performance of the regression model is consistent with expectations in all of the considered synthetic forward prediction cases.

4.4 Summary

Multiple linear regression analysis was used to develop a CPT-V_s relationship for Canterbury, New Zealand soils of the shallow Christchurch and Springston formations. The selected regression form depends on the raw cone tip and frictional resistances measured via CPT, q_c and f_s, respectively, and the depth, z below the ground surface. The regression analysis considers non-constant variance with depth to create a correlation that returns consistent residuals with variations in depth and estimated shear wave velocity. The new CPT-V_s correlation provides a viable method to estimate V_s from CPT data that is specific to the non-gravel soils of the Canterbury region in their current post-earthquake state.

REFERENCES

Andrus, R., Hayati, H., and Mohanan, N. (2009). "Correcting liquefaction resistance for aged sands using measured to estimated velocity ratio." *Journal of Geotechnical and Geoenvironmental Engineering*, 135(6), 735–744.

Andrus, R., Mohanan, N., Piratheepan, P., Ellis, B., and Holzer, T. (2007). "Predicting shear-wave velocity from cone penetration resistance." *Proc. 4th International Conference on Earthquake Geotechnical Engineering*, Thessaloniki, Greece, June 25-28, Paper No. 1454.

Ang, A.-S. and Tang, W. (2007). *Probability Concepts in Engineering Emphasis on Applications to Civil and Environmental Engineering.* John Wiley & Sons, Inc., Hoboken, NJ, USA. 2nd Edition.

Baldi, G., Belloti, R., Ghionna, V., Jamiolkowski, M., and Lo Presti, D. (1989). "Modulus of sands from CPTs and DMTs." *Proc. 12th International Conference on Soil Mechanics and Foundation Engineering, Vol. 1*, Rio de Janeiro. 165–170.

Bazzurro, P. and Cornell, C. (2004). "Nonlinear soil-site effects in probabalistic seismic-hazard analysis." *Bulletin of the Seismological Society of America*, 94(6), 2110–2123.

Bradley, B. (2012a). "Ground motions observed in the Darfield and Christchurch earthquakes and the importance of local site response effects." *New Zealand Journal of Geology and Geophysics*, 55(3), 279–286.

Bradley, B. (2012b). "Strong ground motion characteristics observed in the 4 September 2010 Darfield, New Zealand earthquake." *Soil Dynamics and Earthquake Engineering*, 42, 32–46.

Bradley, B. and Cubrinovski, M. (2011). "Near-source strong ground motions observed in the 22 February 2011 Christchurch earthquake." *Seismological Research Letters*, 82(6), 853–865.

Brown, L., Beetham, R., Paterson, B., and Weeber, J. (1995). "Geology of Christchurch, New Zealand." *Environmental & Engineering Geoscience*, 1(4), 427–488.

Brown, L. and Weeber, J. (1992). *Geology of the Christchurch urban area.* Institute of Geological and Nuclear Sciences Ltd., Lower Hutt, New Zealand.

Campanella, R., Gillespie, D., and Robertson, P. (1982). "Pore pressures during cone penetration testing." *Proc. 2nd European Symposium on Penetration Testing, ESPOT II*, Amsterdam, May 24-27. 507–512.

Campanella, R. and Stewart, W. (1992). "Seismic cone analysis using digital signal processing for dynamic site characterization." *Canadian Geotechnical Journal*, 29(3), 477–486.

Canterbury Geotechnical Database (2012). *canterburygeotechnicaldatabase.projectorbit.com.*

Chen, C. and Juang, C. (2000). "Calibration of SPT- and CPT-based liquefaction evaluation methods." *Innovations and Applications in Geotechnical Site Characterization: Proceedings of Sessions of Geo-Denver 2000 (GSP 97)*, P. Mayne and R. Hryciw, eds., ASCE, Reston, VA. 49–64.

Cubrinovski, M., Bradley, B., Wotherspoon, L., Green, R., Bray, J., Wood, C., Pender, M., Allen, J., Bradshaw, A., Rix, G., Taylor, M., Robinson, K., Henderson, D., Giorgini, S., Ma, K., Winkley, A., Zupan, J., O'Rourke, T., DePascale, G., and Wells, D. (2011). "Geotechnical aspects of the 22 February 2011 Christchurch earthquake." *Bulletin of the New Zealand Society for Earthquake Engineering*, 44(4), 205–226.

Cubrinovski, M., Bray, J., Taylor, M., Giorgini, S., Bradley, B., Wotherspoon, L., and Zupan, J. (2011). "Soil liquefaction effects in the central business district during the February 2011 Christchurch earthquake." *Seismological Research Letters*, 82(6), 893–904.

Cubrinovski, M., Green, R., Allen, J., Ashford, S., Bowman, E., Bradley, B., Cox, B., Hutchinson, T., Kavazanjian, E., Orense, R., Pender, M., Quigley, M., and Wotherspoon, L. (2010). "Geotechnical reconnaissance of the 2010 Darfield (Canterbury) earthquake." *Bulletin of the New Zealand Society for Earthquake Engineering*, 43(4), 243–320.

Cubrinovski, M. and McCahon, I. (2011). *Foundations of Deep Alluvial Soils.* Technical Report Prepared for the Canterbury Earthquakes Royal Commission.

Darendeli, M. (2001). *Development of a new family of normalized modulus reduction and damping curves.* Ph.D. Dissertation, University of Texas, Austin, TX, USA.

Gledhill, K., Ristau, J., Reyners, M., Fry, B., and Holden, C. (2011). "The Darfield (Canterbury, New Zealand) M_w7.1 earthquake of September 2010: A preliminary seismological report." *Seimological Research Letters*, 82(3), 378–386.

Hegazy, Y. and Mayne, P. (1995). "Statistical correlations between V_s and cone penetration data for different soil types." *Proc. of CPT '95, Vol. 2*, Linköping, Sweden. Swedish Geotechnical Society, 173–178.

Hegazy, Y. and Mayne, P. (2006). "A global statistical correlation between shear wave velocity and cone penetration data." *Proc. of GeoShanghai, Site and Geomaterial Characterization (GSP 149)*, A. Puppala, D. Fratta, K. Alshibli, and S. Pamukcu, eds., ASCE, Reston, VA. 243–248.

Idriss, I. and Boulanger, R. (2008). *Soil Liquefaction During Earthquakes.* Earthquake Engineering Research Institute (EERI), MNO-12.

Idriss, I. and Seed, H. (1970). *Soil moduli and damping factors for dynamic response analysis.* Report EERC 70-10, University of California, Berkeley.

Ishihara, K. and Yoshimine, M. (1992). "Evaluation of settlements in sand deposits following liquefaction during earthquakes." *Soils and Foundations*, 32(1), 173–188.

Jefferies, M. and Davies, M. (1991). "Soil classification by the cone penetration test: Discussion." *Canadian Geotechnical Journal*, 28(1), 173–176.

Kaneko, F., Kanemori, T., and Tonouchi, K. (1990). "Low-frequency shear wave logging in unconsolidated formations for geotechnical applications." *Geophysical Applications for Geotechnical Investigations, ASTM STP 1101*, F. Paillet and W. Saunders, eds., Philadelphia, PA, USA. American Society for Testing and Materials, 79–98.

Ku, C.-S., Juang, C., Chang, C.-W., and Ching, J. (2012). "Probabalistic version of the Robertson and Wride method for liquefaction evaluation: development and application." *Canadian Geotechnical Journal*, 49(1), 27–44.

Lee, R., Bradley, B., Pettinga, J., Hughes, M., and Graves, R. (2014). "Ongoing development of a 3D seismic velocity model of Canterbury, New Zealand for broadband ground motion simulation." *New Zealand Society for Earthquake Engineering Annual Conference*, Auckland, March 21-23, Paper No. 8.

Louie, J. (2001). "Faster, better shear wave velocity to 100 meters depth from refraction microtremor arrays." *Bulletin of the Seismological Society of America*, 91(2), 347–364.

Mayne, P. and Rix, G. (1993). "$G_{\max}$–V_s relationships for clays." *Geotechnical Testing Journal*, 16(1), 54–60.

Montalva, G. (2010). *Site-Specific Seismic Hazard Analyses.* Ph.D. Dissertation, Washington State University.

Nazarian, S. and Stokoe II, K. (1984). "In-situ shear wave velocities from spectral analysis of surface wave tests." *Proc. 8th World Conference on Earthquake Engineering*, San Franciso, CA. 31–38.

Ohta, Y. and Goto, N. (1978). "Empirical shear wave velocity equations in terms of characteristic soil indexes." *Earthquake Engineering & Structural Dynamics*, 6(2), 167–187.

Okada, H. (2003). *The Microtremor Survey Method*. (K. Suto, trans.): SEG Geophysical Monograph Series No. 12, Society of Exploration Geophysicists.

Park, C. and Miller, R. (2008). "Roadside passive multichannel analysis of surface waves (MASW)." *Journal of Environmental and Engineering Geophysics*, 13(1), 1–13.

Park, C., Miller, R., and Xia, J. (1999). "Multichannel analysis of surface waves." *Geophysics*, 64(3), 800–880.

Robertson, P. (1990). "Soil classification using the cone penetration test." *Canadian Geotechnical Journal*, 27(1), 151–158.

Robertson, P. (2009). "Interpretation of cone penetration tests – a unified approach." *Canadian Geotechnical Journal*, 46(11), 1337–1355.

Robertson, P. (2010). "Soil behaviour type from the CPT: an update." *CPT '10, 2nd International Symposium on Cone Penetration Testing*, Huntington Beach, CA, May 9-11, Paper No. 2-56.

Robertson, P., Campenella, R., Gillespie, D., and Rice, A. (1986). "Seismic CPT to measure in-situ shear wave velocity." *Journal of Geotechnical Engineering*, 112(8), 791–804.

Robertson, P. and (Fear) Wride, C. (1998). "Evaluation cyclic liquefaction potential using the cone penetration test." *Canadian Geotechnical Journal*, 35(3), 442–459.

Robertson, P., Woeller, D., and Finn, W. (1992). "Seismic cone penetration test for evaluating liquefaction potential." *Canadian Geotechnical Journal*, 29(4), 686–695.

Robinson, K., Cubrinovski, M., and Bradley, B. (2013). "Sensitivity of predicted liquefaction-induced lateral displacements from the 2010 Darfield and 2011 Christchurch earthquakes." *Proc. 19th New Zealand Geotechnical Society (NZGS) Symposium*, Queenstown, New Zealand, November 20-23.

Rodriguez-Marek, A., Montalva, G., Cotton, F., and Bonilla, F. (2011). "Analysis of single-station standard deviation using the KiK-net data." *Bulletin of the Seismological Society of America*, 101, 1242–1258.

Rollins, K., Evans, M., Diehl, N., and Daily, W. (1998). "Shear modulus and damping relationships for gravels." *Journal of Geotechnical and Geoenvironmental Engineering*, 124(5), 396–405.

Stokoe II, K. and Santamarina, J. (2000). "Seismic-wave-based testing in geotechnical engineering." *Proc. of the International Conference on Geotechnical and Geological Engineering, GeoEng 2000*, Melbourne, Australia. 1490–1536.

Sykora, D. and Stokoe II, K. (1983). *Correlations of In-Situ Measurements in Sands and Shear Wave Velocity*. Geotechnical Engineering Report GR83-33, The University of Texas at Austin.

Tarantola, A. (2005). *Inverse problem theory and methods for model parameter estimation*. Society for Industrial and Applied Mathematics (SIAM), Philadelphia, PA, USA.

Taylor, M. (2014). *Assessment of Liquefaction Hazard using Effective Stress Analysis*. Ph.D. Dissertation, University of Canterbury, Christchurch, New Zealand.

Tokimatsu, K., Shinzawa, K., and Kuwayama, S. (1992). "Use of short-period microtremors for V_s profiling." *Journal of Geotechnical Engineering*, 118(10), 1544–1558.

Wair, B., DeJong, J., and Shantz, T. (2012). *Guidelines for Estimation of Shear Wave Velocity Profiles.* PEER Report No. 2012/08, Pacific Earthquake Engineering Research Center, University of California, Berkeley.

Wasserman, L. (2006). *All of Nonparametric Statistics.* Springer-Verlag New York, Inc., Secaucus, NJ, USA.

Woods, R. (1978). "Measurement of dynamic soil properties, state of the art report." *Proc. ASCE Specialty Conference on Earthquake Engineering & Soil Dynamics*, Vol. 1, California Institute of Technology, Pasadena, USA. 91–178.

Woods, R. (1994). "Borehole methods in shallow seismic exploration." *Geophysical Characterization of Sites*, R. Woods, ed., New Delhi, India. ISSMFE Technical Committee #10, 91–100.

Xia, J., Miller, R., and Park, C. (1999). "Estimation of near-surface shear-wave velocity by inversion of Rayleigh waves." *Geophysics*, 64(3), 691–700.

Zhang, G., Robertson, P., and Brachman, R. (2002). "Estimating liquefaction-induced ground settlements from CPT for level ground." *Canadian Geotechnical Journal*, 39(5), 1168–1180.

Appendix A

CANTERBURY SCPTu DATABASE SITE PROFILE SUMMARIES

The CPT tip resistance, q_c, frictional resistance, f_s, hydrostatic pore pressure, u_0, measured pore pressure, u_2, and computed I_c soil behaviour type index profiles for each site in the Canterbury SCPTu database are shown in Figures A.1–A.86. These plots include a comparison of the measured V_s profiles with those computed using the indicated empirical models. The SCPTu ID and associated Canterbury Geotechnical Database CPT number (in parentheses) are noted for each site along with the Easting-Northing site locations. The non-circular markers in the CPT measurement and estimated V_s traces represent the geometric mean of each quantity over the 2 m thick SCPTu V_s measurement intervals.

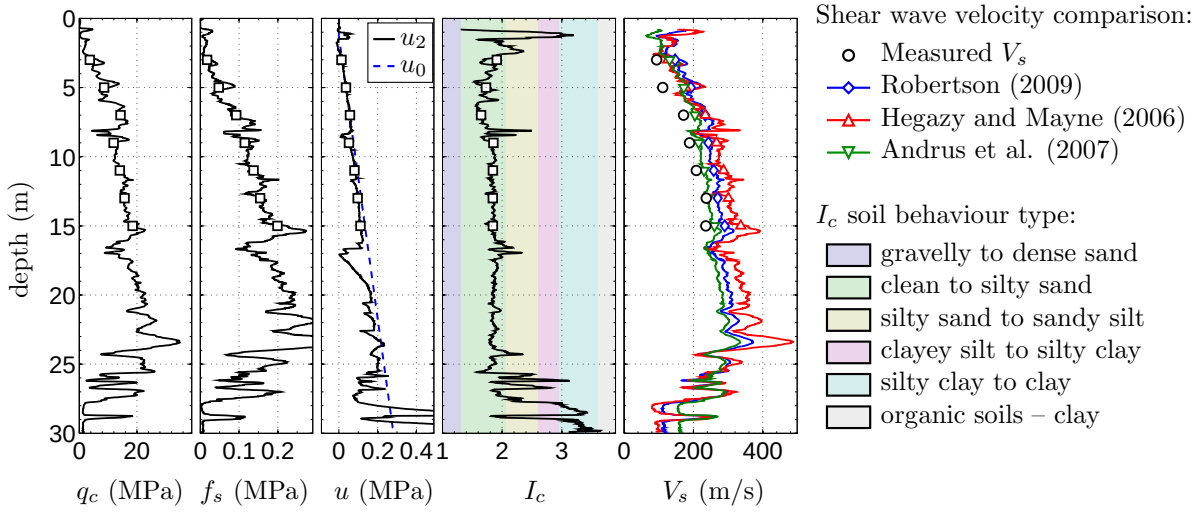

Figure A.1: SCPTu ARN03 (CPT-3) E2486512.58 N5743861.75.

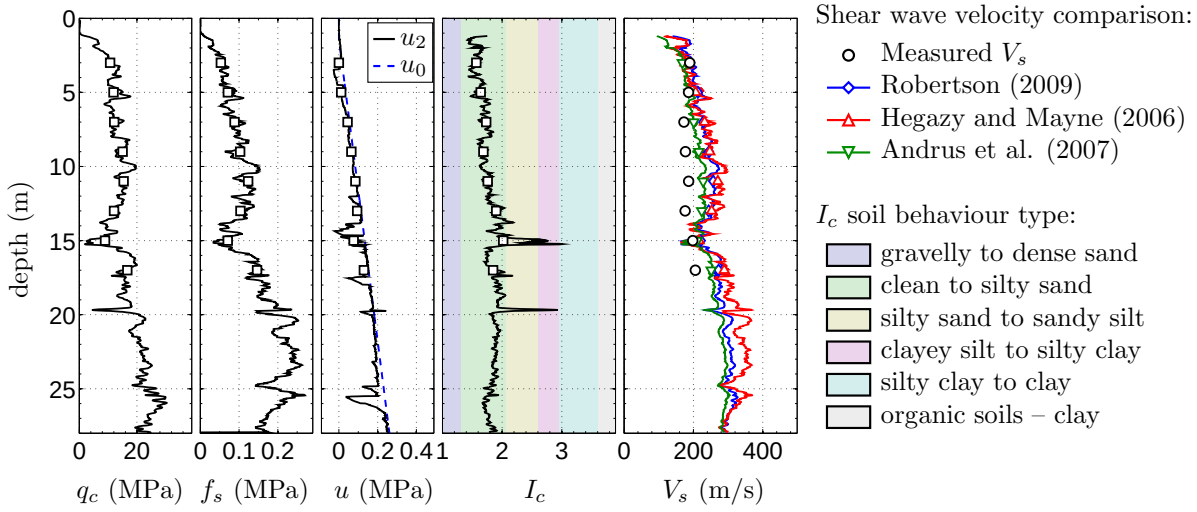

Figure A.2: SCPTu ARN09 (CPT-9) E2485920.04 N5743126.63.

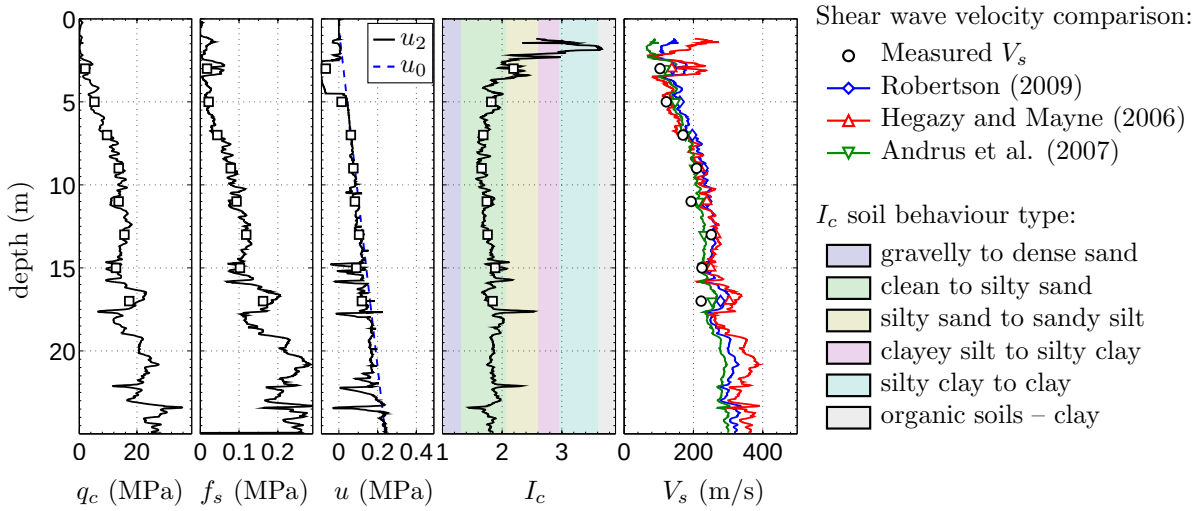

Figure A.3: SCPTu ARN19 (CPT-19) E2486449.96 N5743141.33.

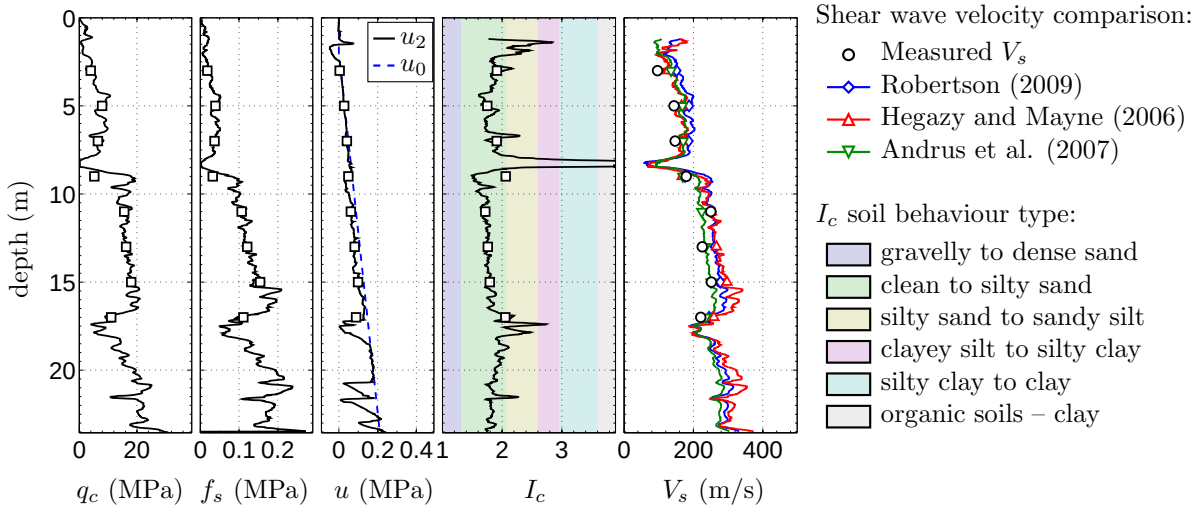

Figure A.4: SCPTu ARN25 (CPT-25) E2486613.15 N5743869.23.

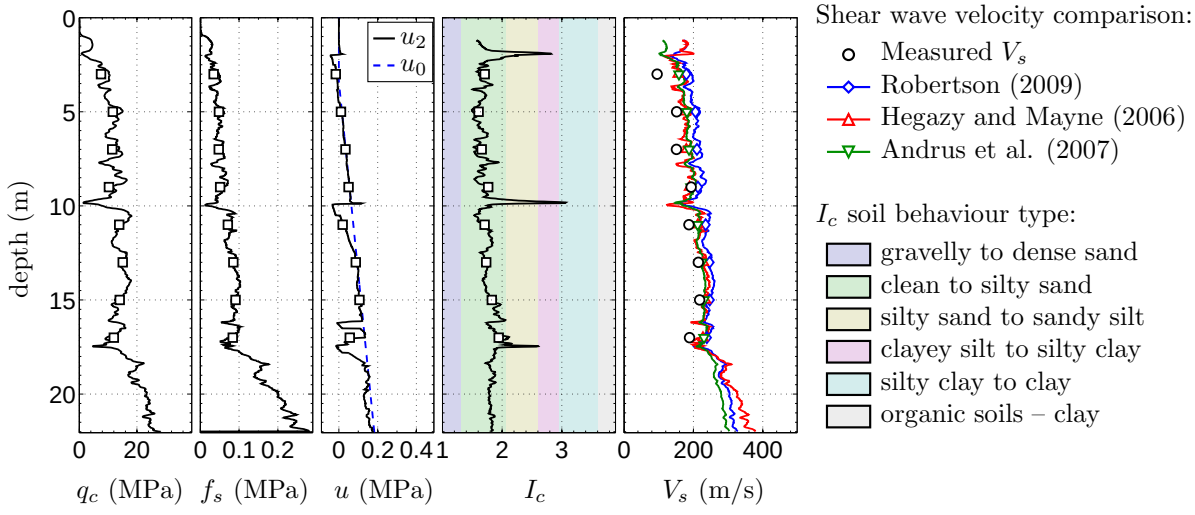

Figure A.5: SCPTu ARN27 (CPT-27) E2486130.57 N5743990.60.

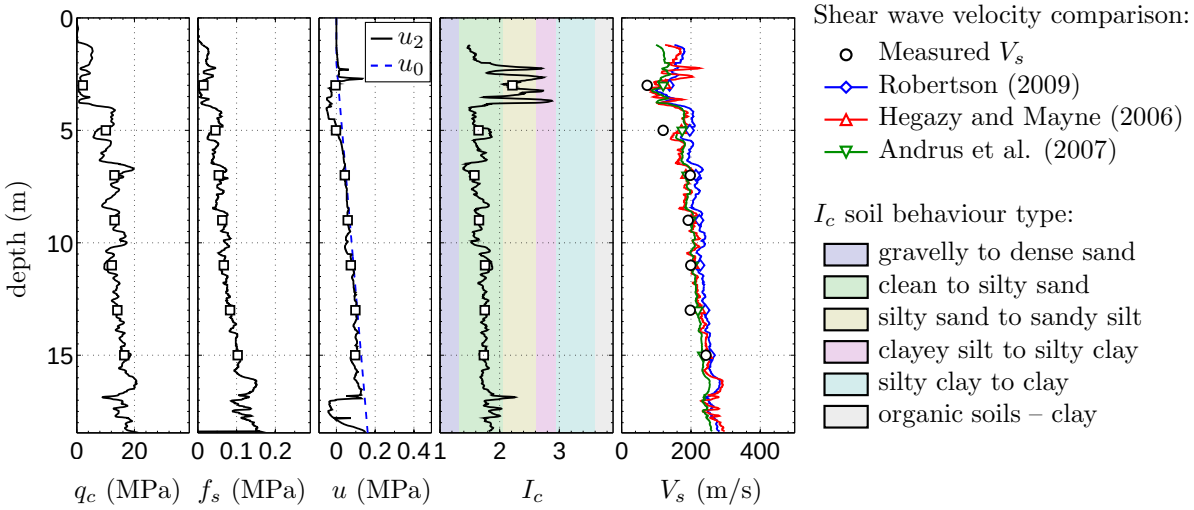

Figure A.6: SCPTu ARN28 (CPT-28) E2486352.61 N5744307.41.

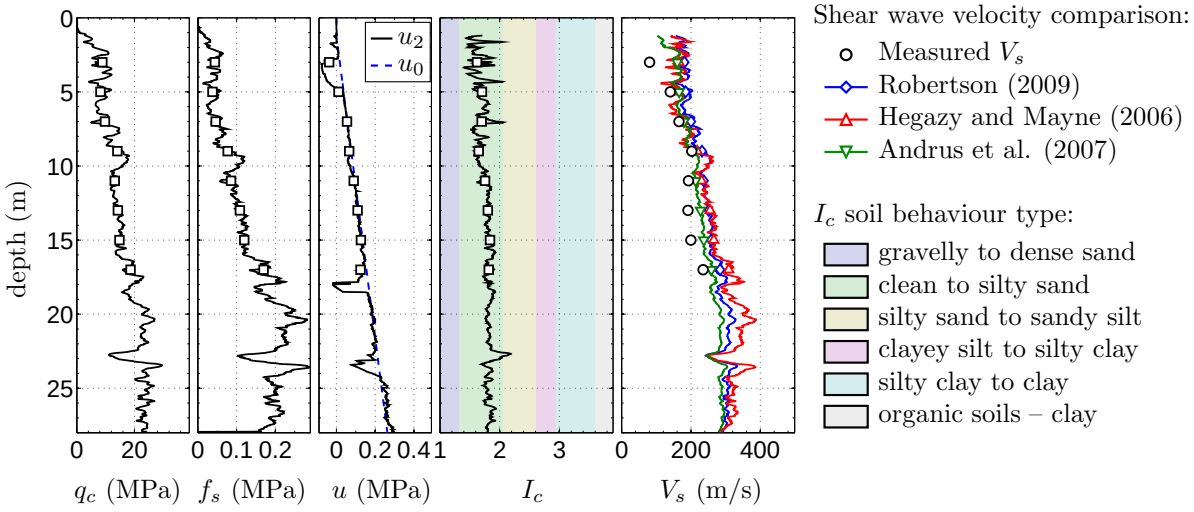

Figure A.7: SCPTu ARN29 (CPT-29) E2486571.38 N5744149.65.

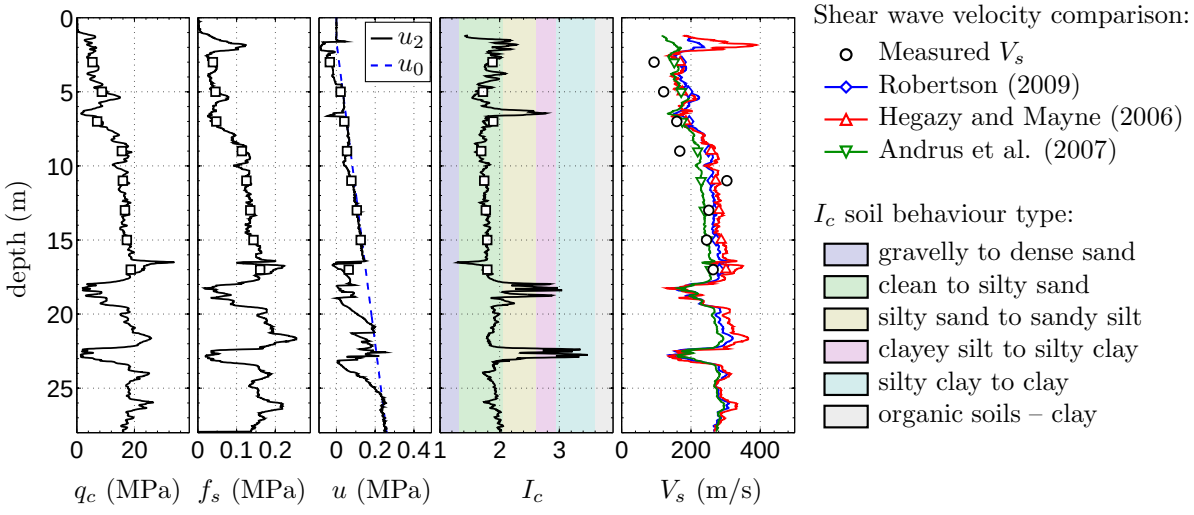

Figure A.8: SCPTu ARN34 (CPT-34) E2486810.77 N5744461.05.

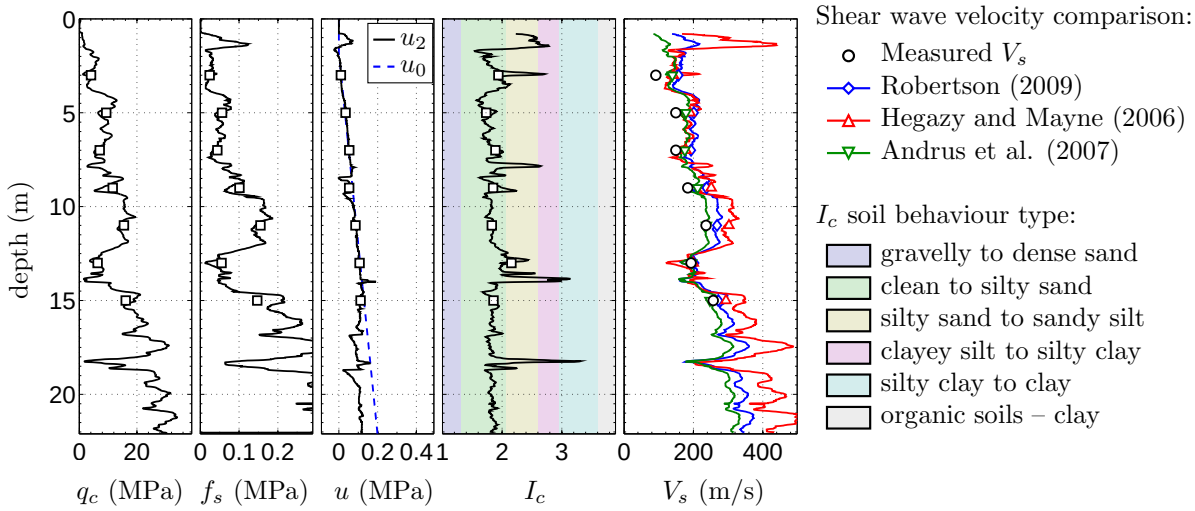

Figure A.9: SCPTu AVD02 (CPT-36) E2484604.59 N5744501.00.

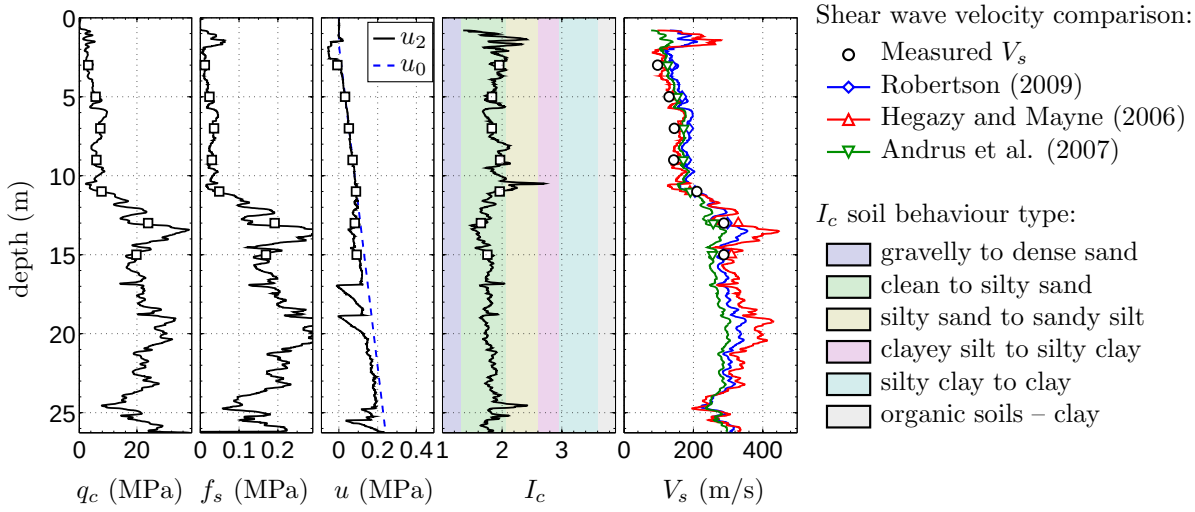

Figure A.10: SCPTu AVD09 (CPT-43) E2484547.92 N5745096.05.

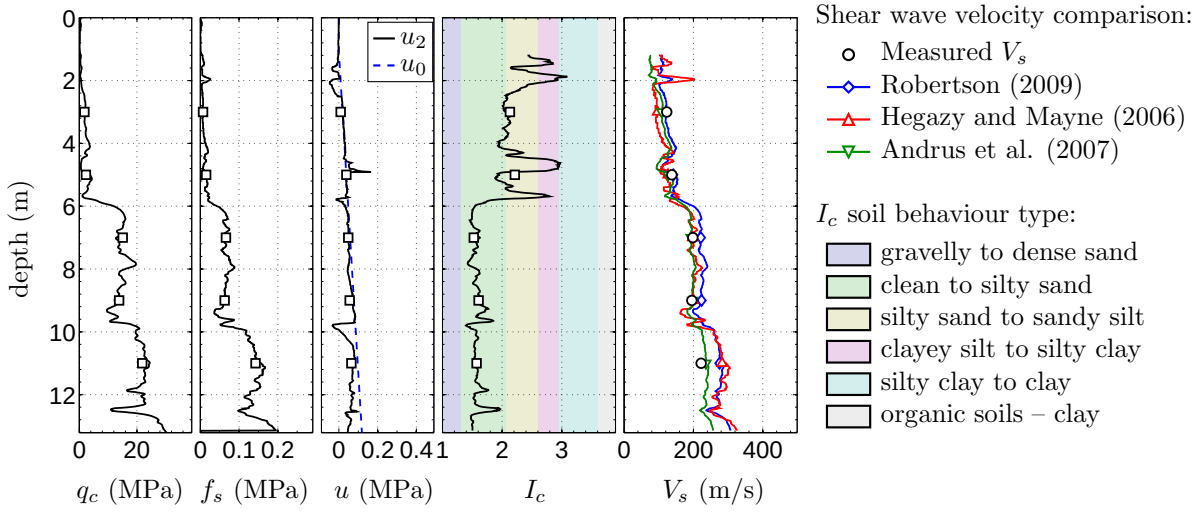

Figure A.11: SCPTu AVL03 (CPT-92) E2481679.63 N5742615.49.

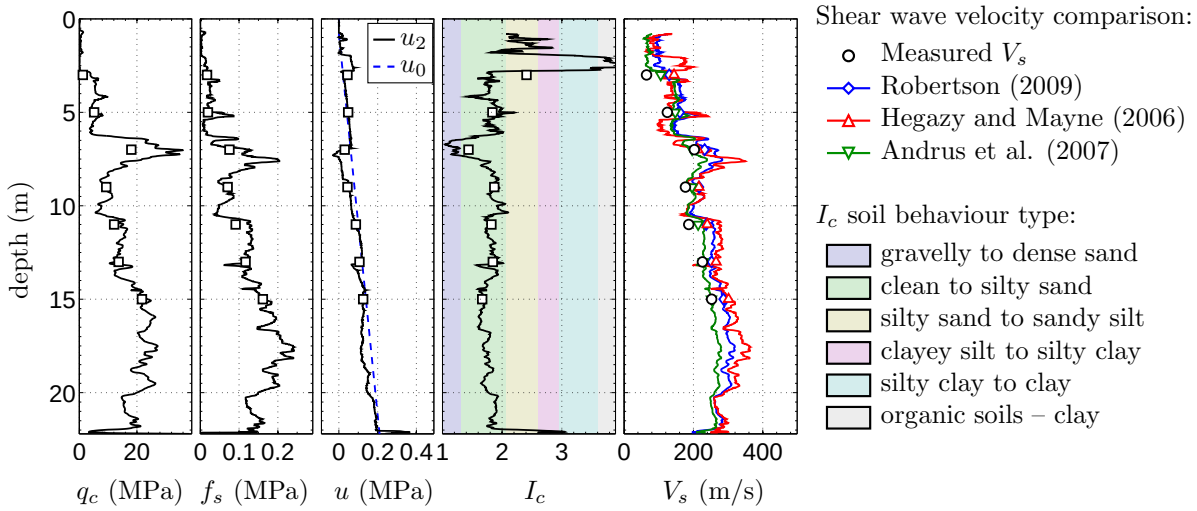

Figure A.12: SCPTu AVS14 (CPT-108) E2482869.70 N5743026.94.

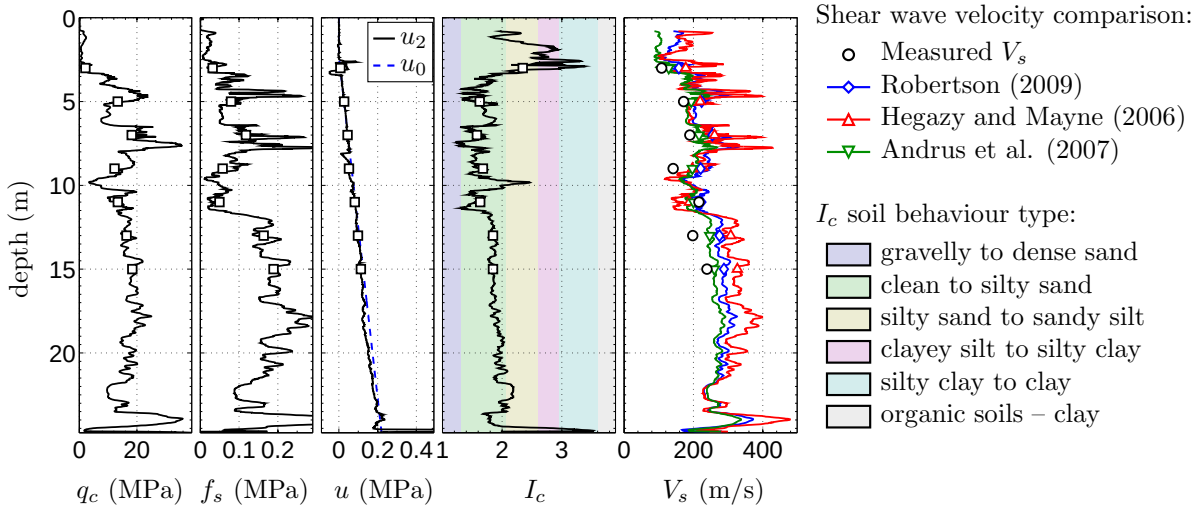

Figure A.13: SCPTu AVS16 (CPT-110) E2483172.56 N5743169.95.

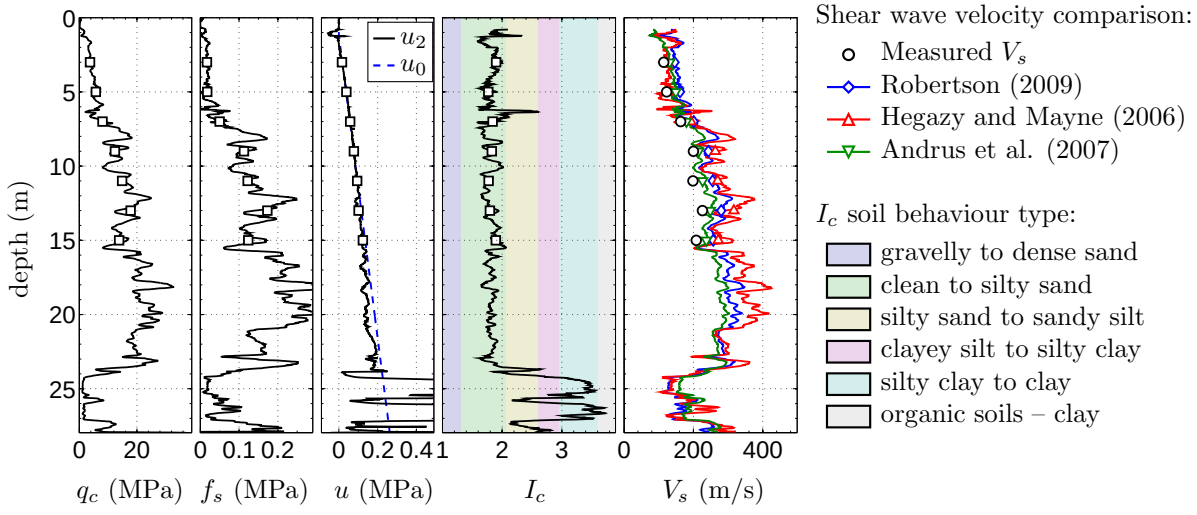

Figure A.14: SCPTu AVS21 (CPT-115) E2483488.92 N5743376.06.

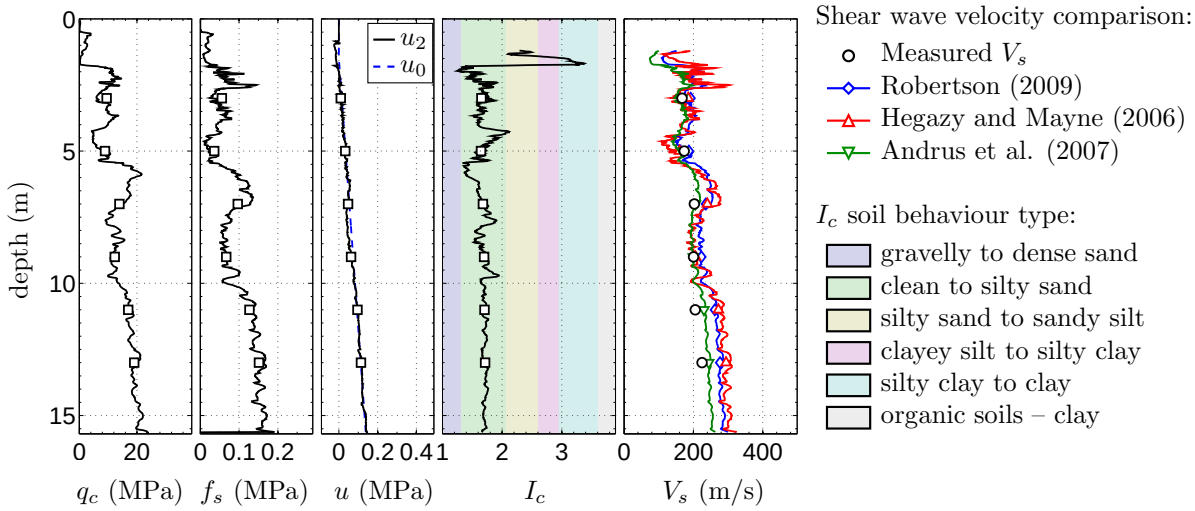

Figure A.15: SCPTu AVS22 (CPT-116) E2482981.25 N5743477.02.

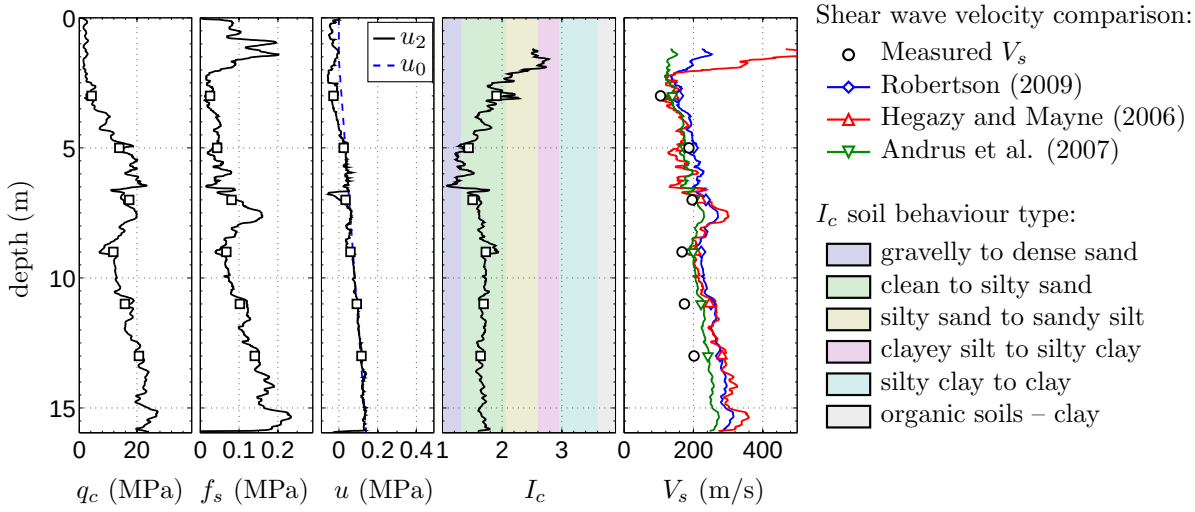

Figure A.16: SCPTu AVS49 (CPT-137) E2483716.42 N5742749.17.

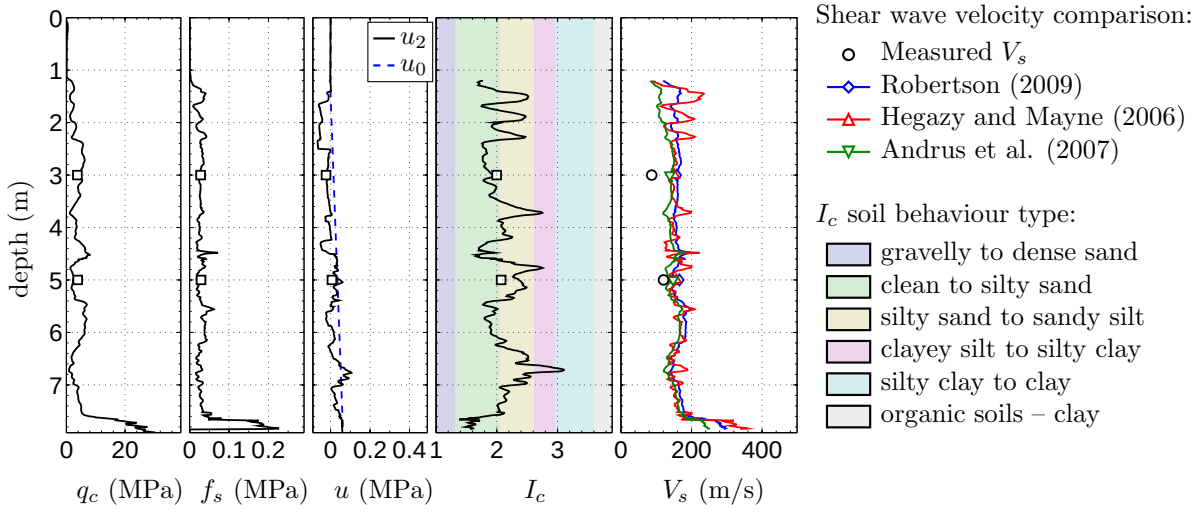

Figure A.17: SCPTu BDL03 (CPT-145) E2475526.77 N5747008.16.

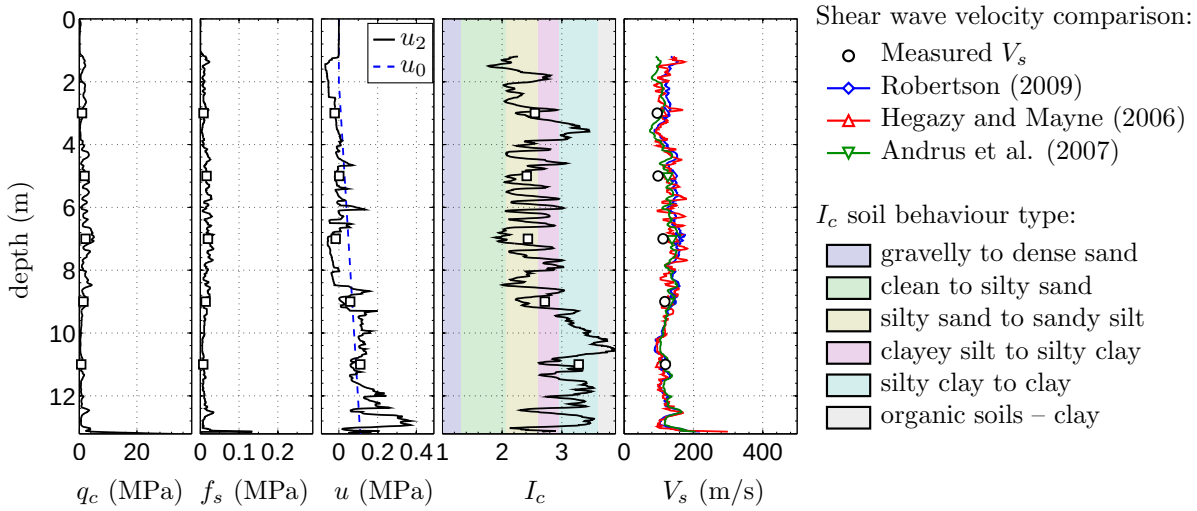

Figure A.18: SCPTu BDL08 (CPT-150) E2476410.74 N5747328.40.

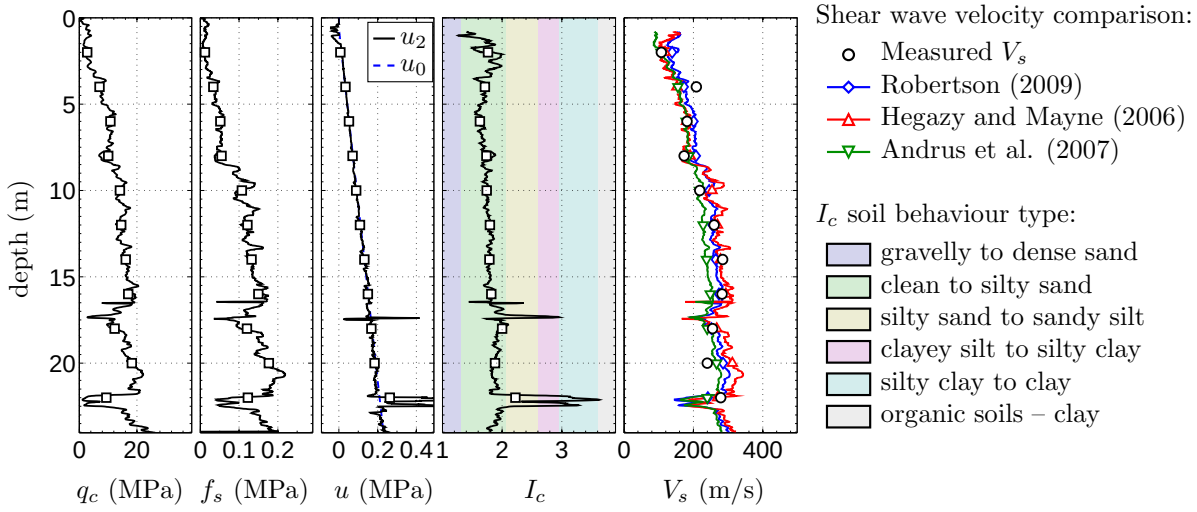

Figure A.19: SCPTu BEX15 (CPT-167) E2487522.33 N5744064.06.

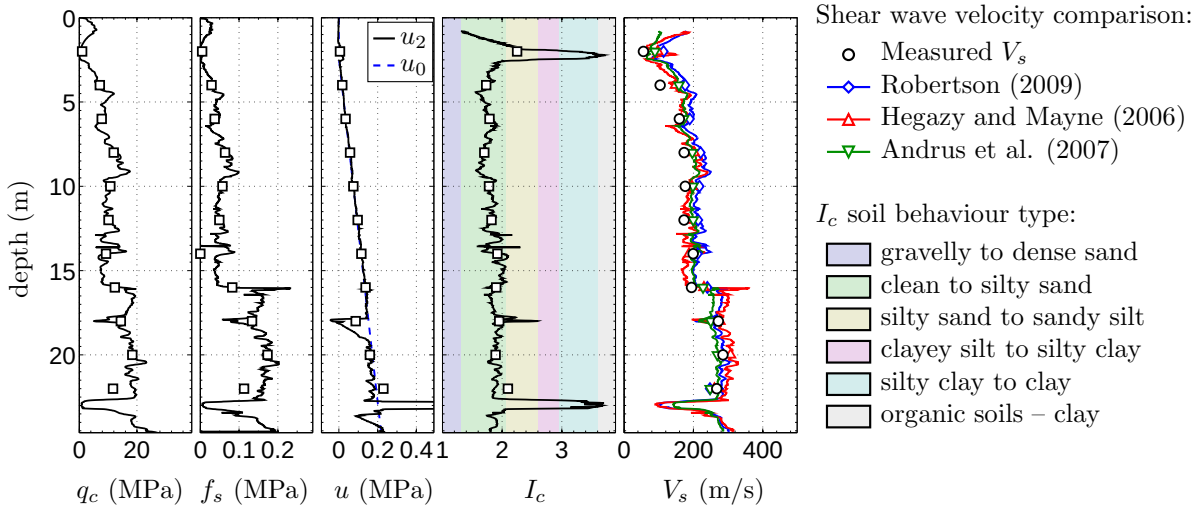

Figure A.20: SCPTu BEX17 (CPT-169) E2487273.26 N5744320.98.

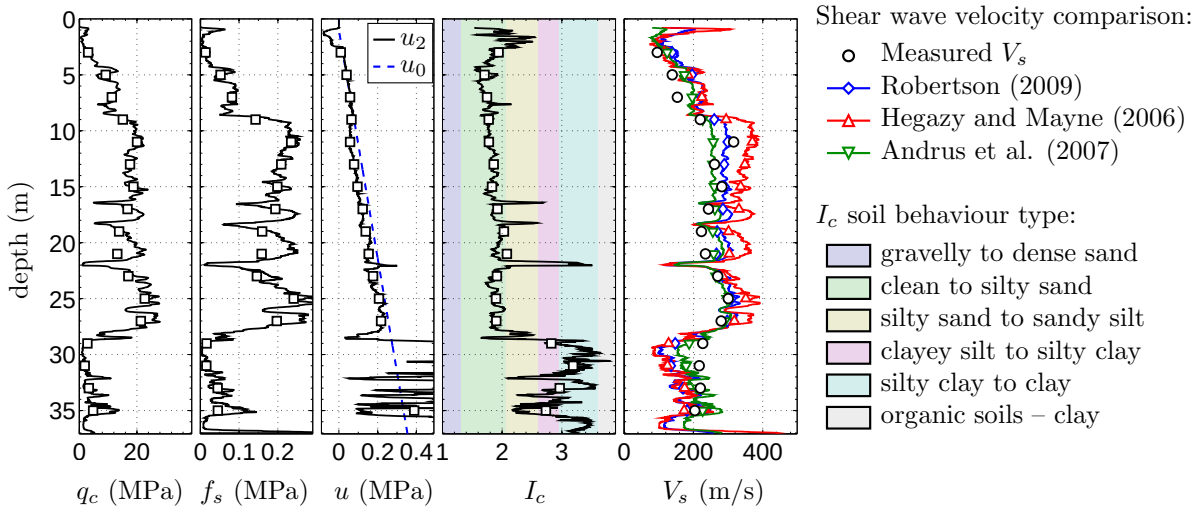

Figure A.21: SCPTu BEX19 (CPT-171) E2486919.80 N5744438.91.

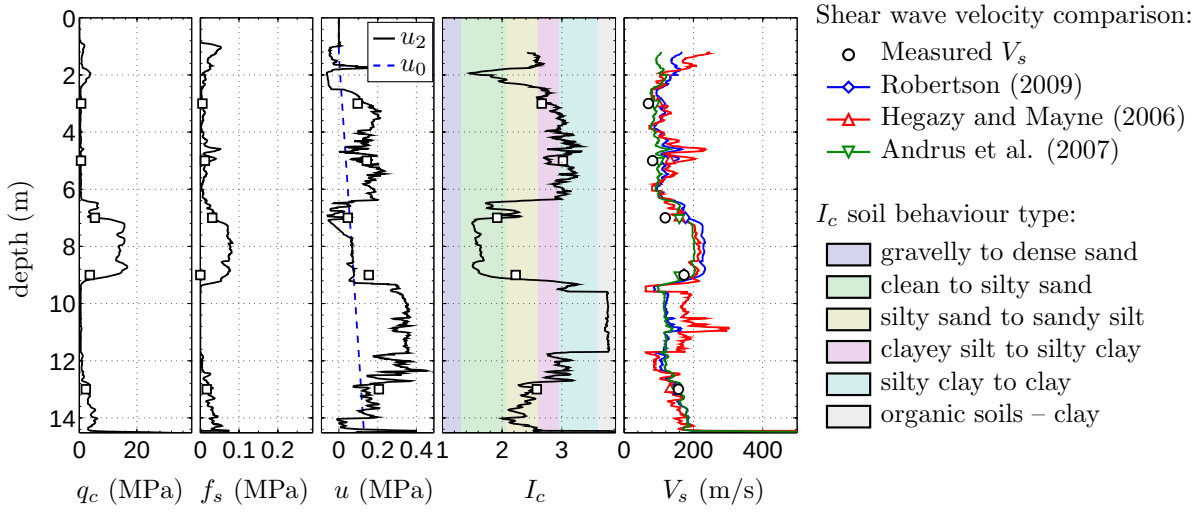

Figure A.22: SCPTu BKM12 (CPT-207) E2481292.89 N5738183.06.

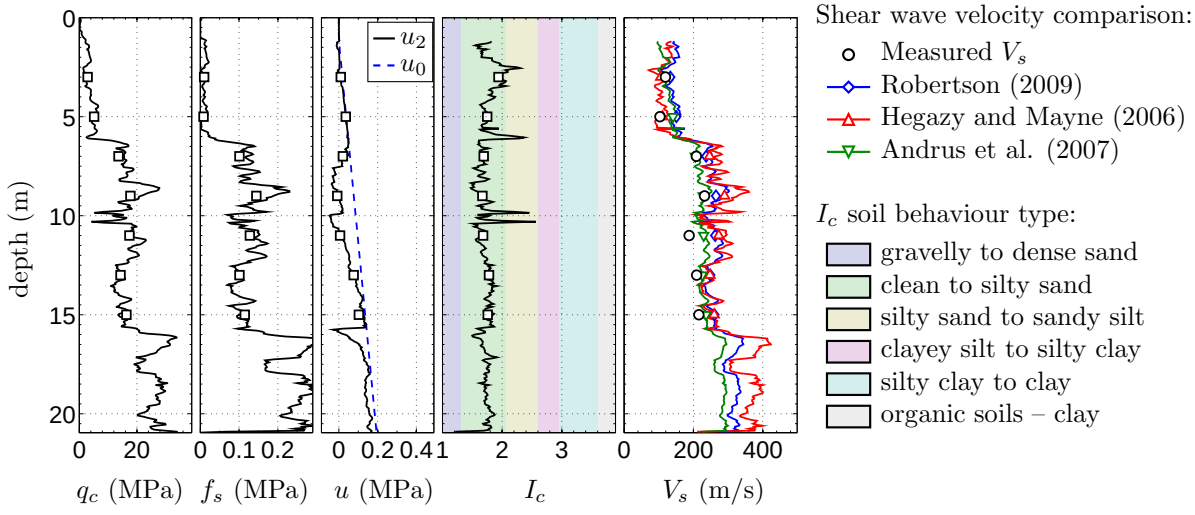

Figure A.23: SCPTu BUR30 (CPT-291) E2483884.34 N5745481.95.

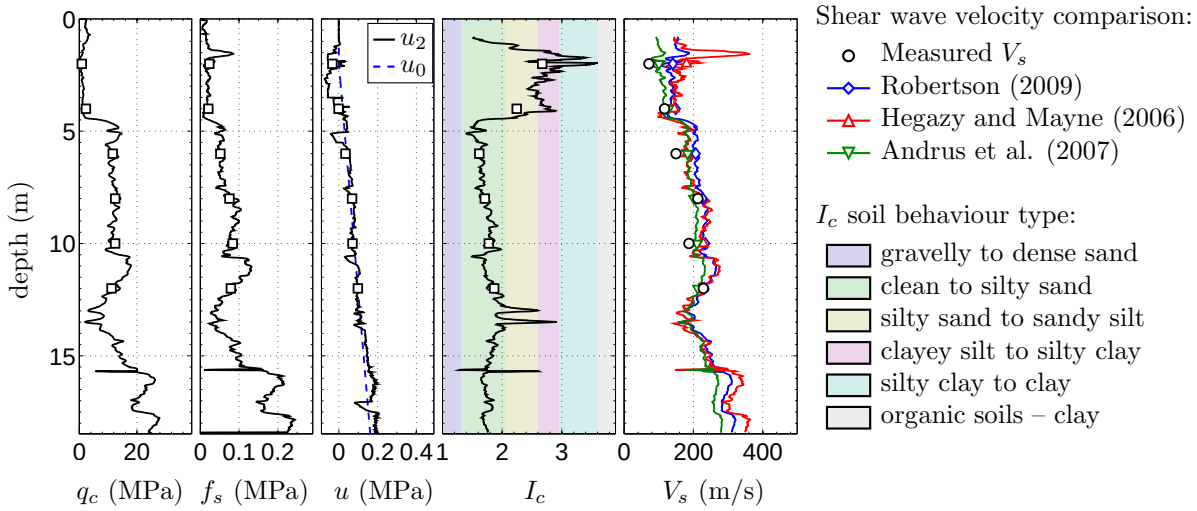

Figure A.24: SCPTu BUR36 (CPT-297) E2484228.47 N5746352.35.

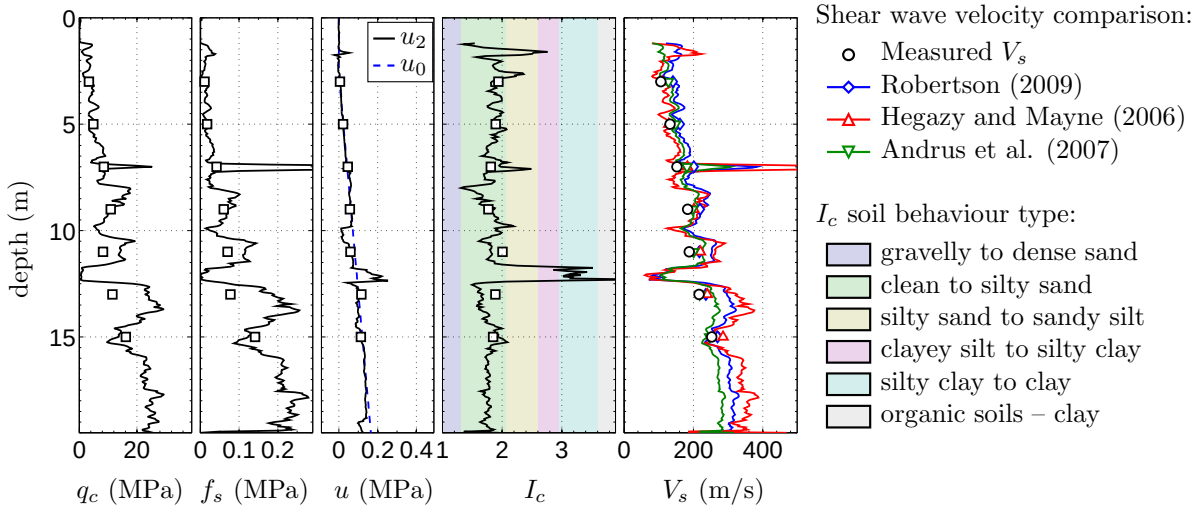

Figure A.25: SCPTu BUR40 (CPT-301) E2485244.01 N5745047.00.

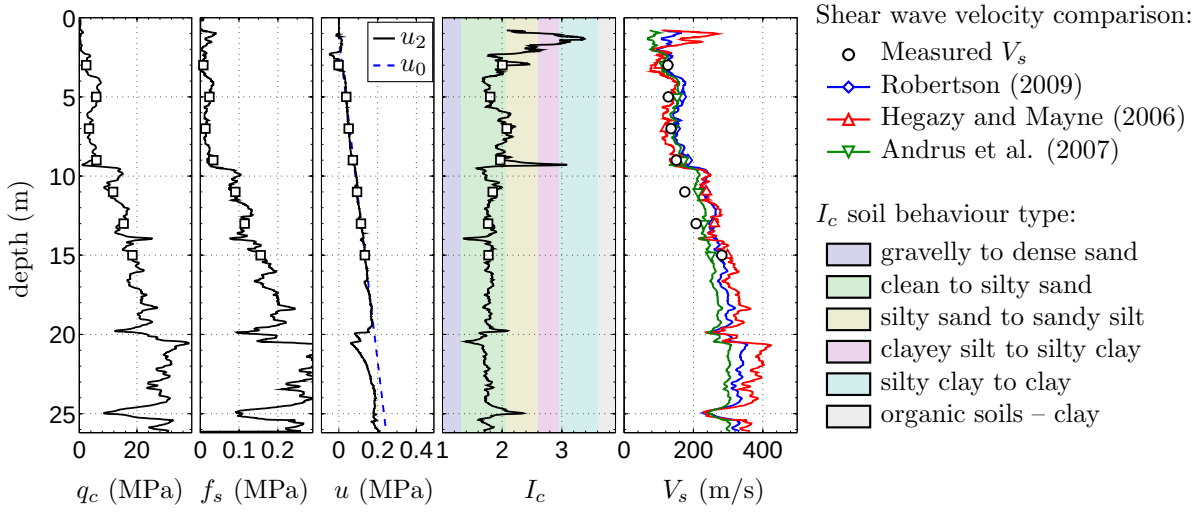

Figure A.26: SCPTu BUR45 (CPT-306) E2485779.75 N5745636.58.

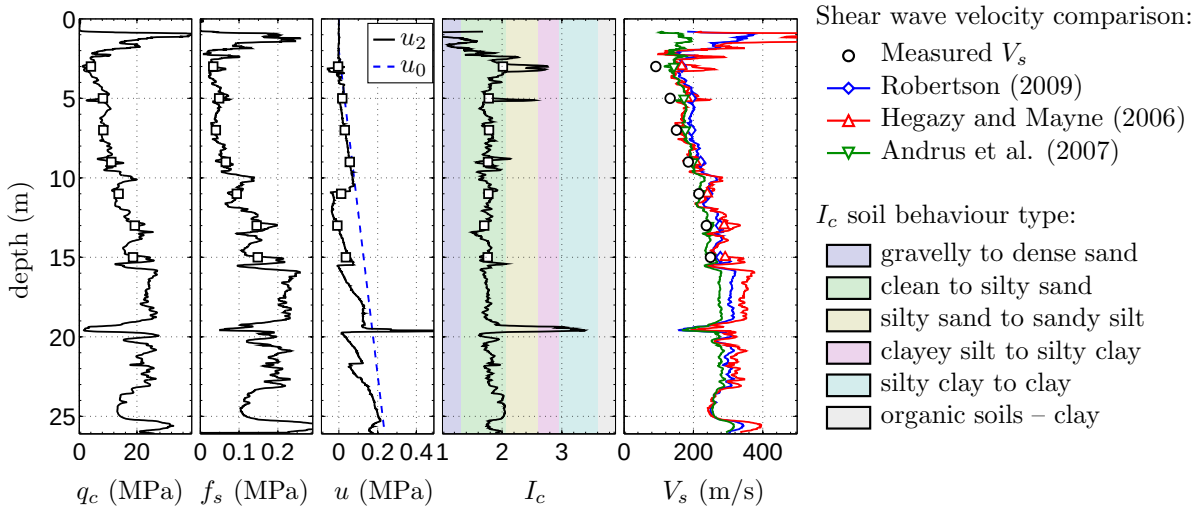

Figure A.27: SCPTu BUR48 (CPT-309) E2484876.17 N5746351.59.

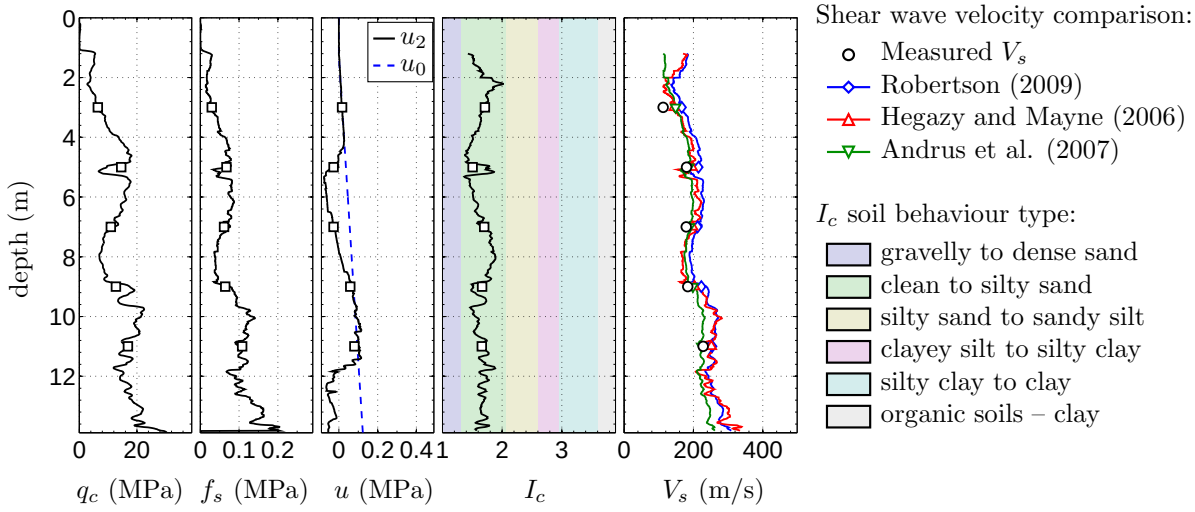

Figure A.28: SCPTu BUR96 (CPT-347) E2484563.50 N5746718.74.

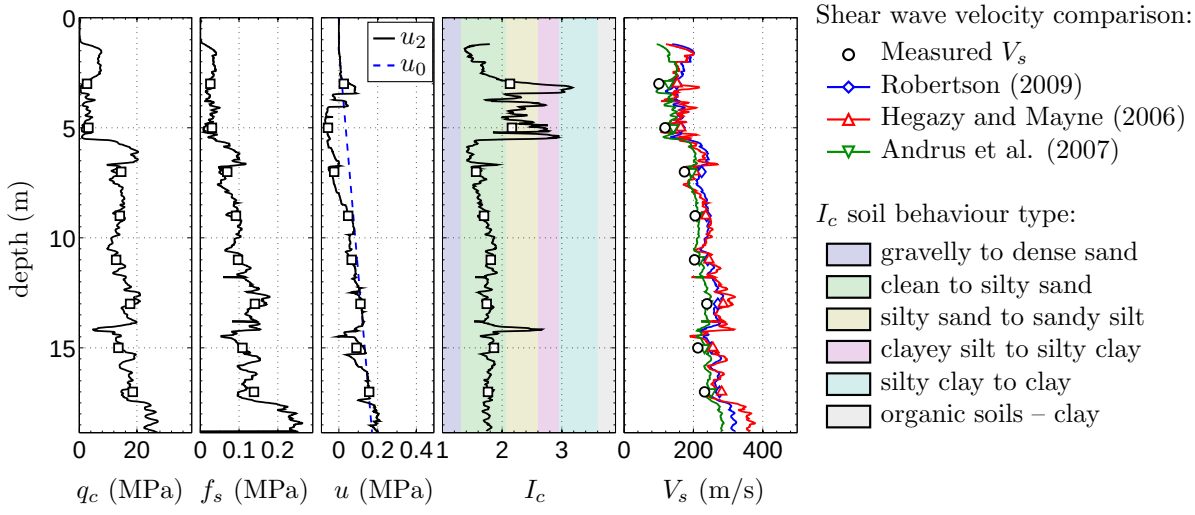

Figure A.29: SCPTu BUR102 (CPT-353) E2484302.27 N5746420.17.

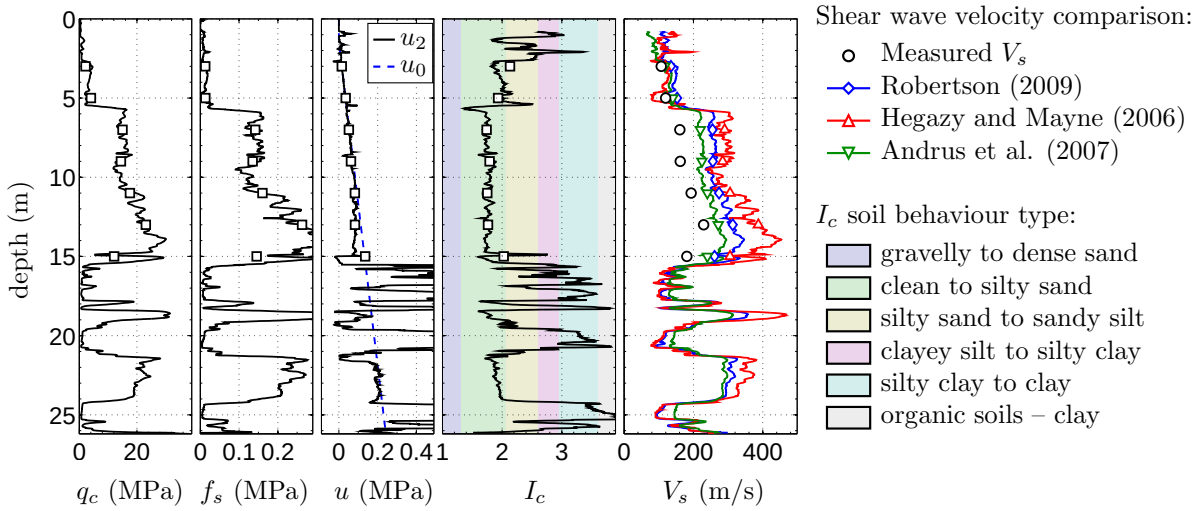

Figure A.30: SCPTu DAL09 (CPT-1086) E2483727.15 N5742924.35.

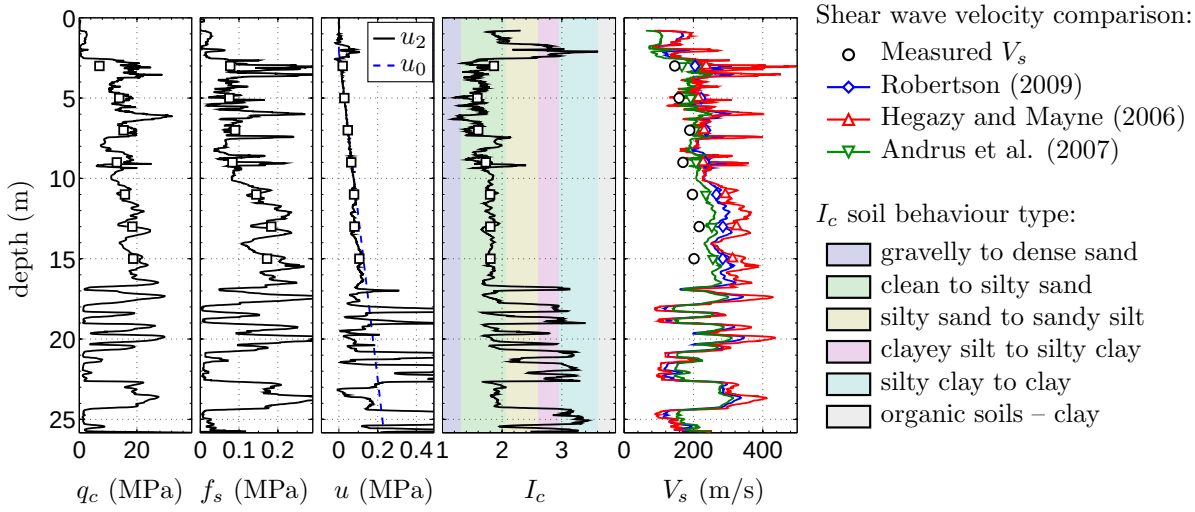

Figure A.31: SCPTu DAL11 (CPT-1088) E2483476.93 N5743226.02.

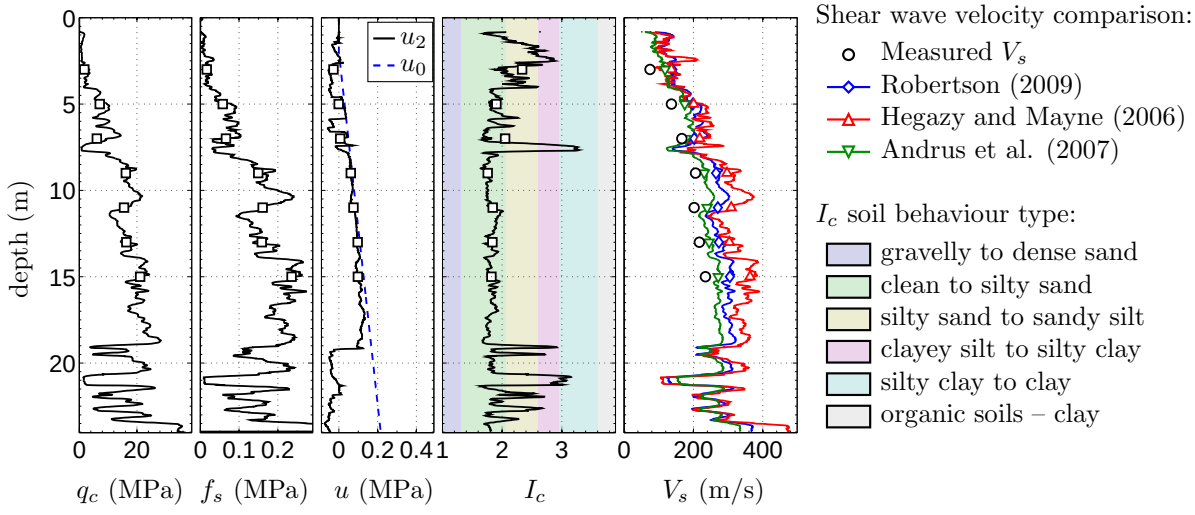

Figure A.32: SCPTu DAL18 (CPT-1095) E2483688.85 N5743389.65.

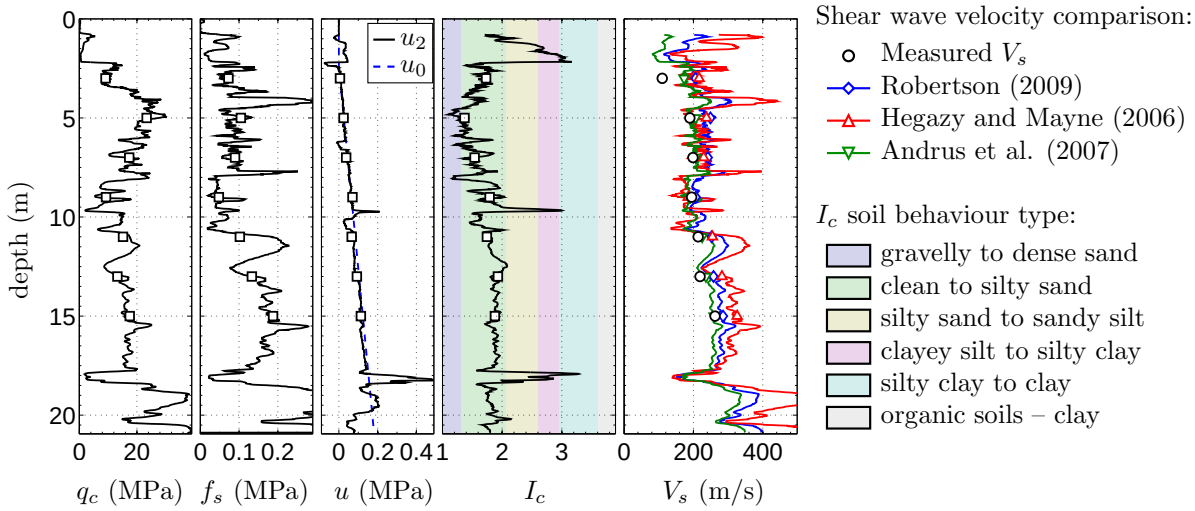

Figure A.33: SCPTu DAL21 (CPT-1098) E2484261.61 N5743602.67.

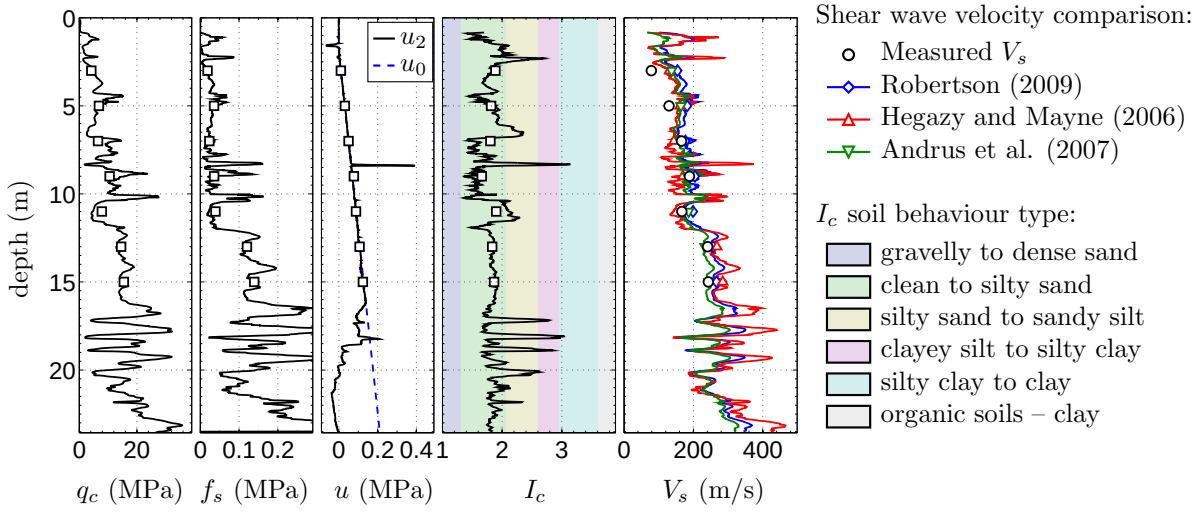

Figure A.34: SCPTu DAL27 (CPT-1104) E2484133.09 N5743960.71.

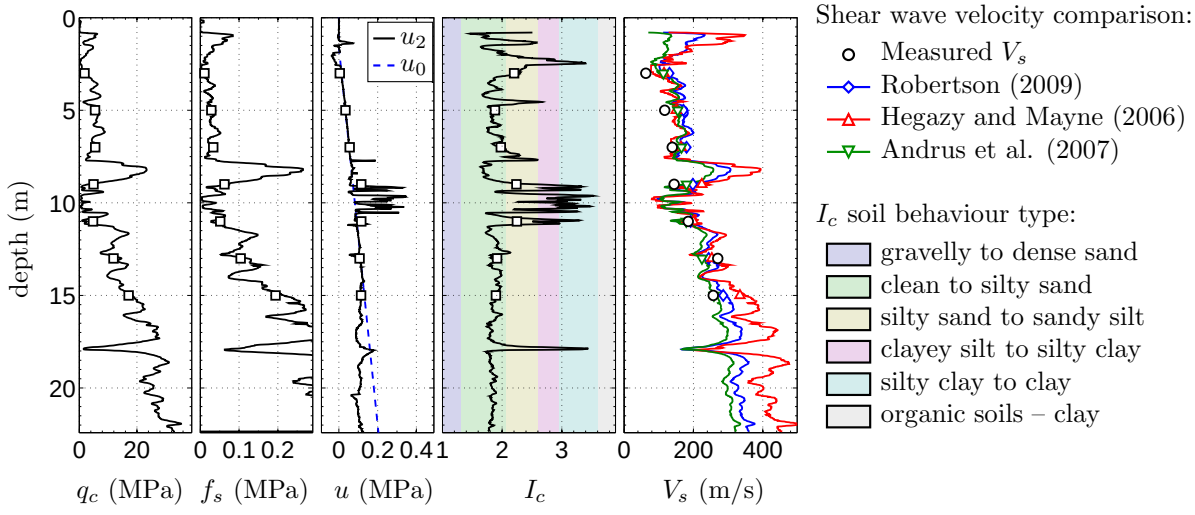

Figure A.35: SCPTu DAL34 (CPT-1111) E2484304.16 N5744359.38.

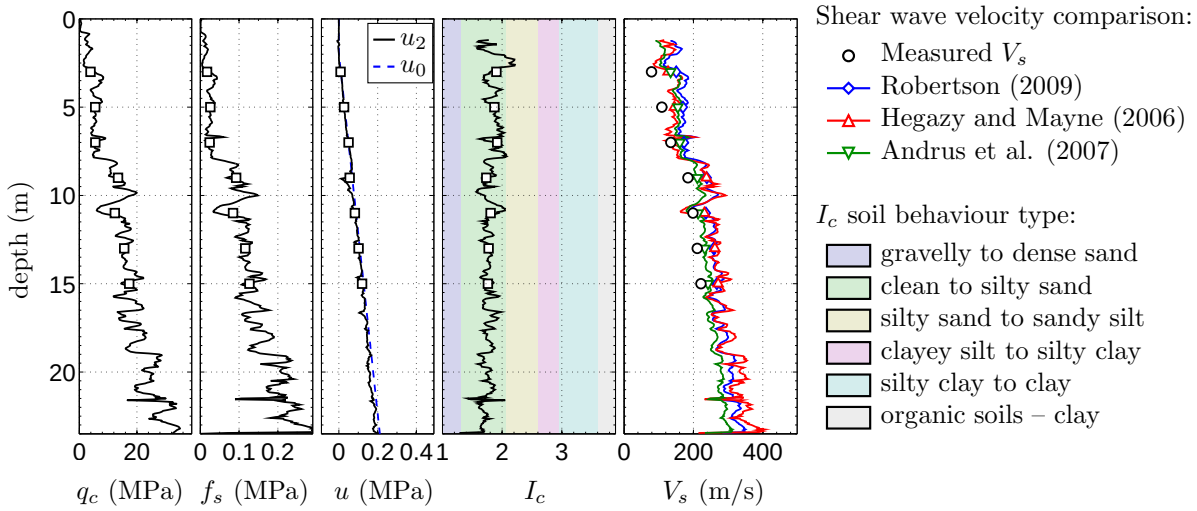

Figure A.36: SCPTu DAL35 (CPT-1112) E2483809.98 N5744535.74.

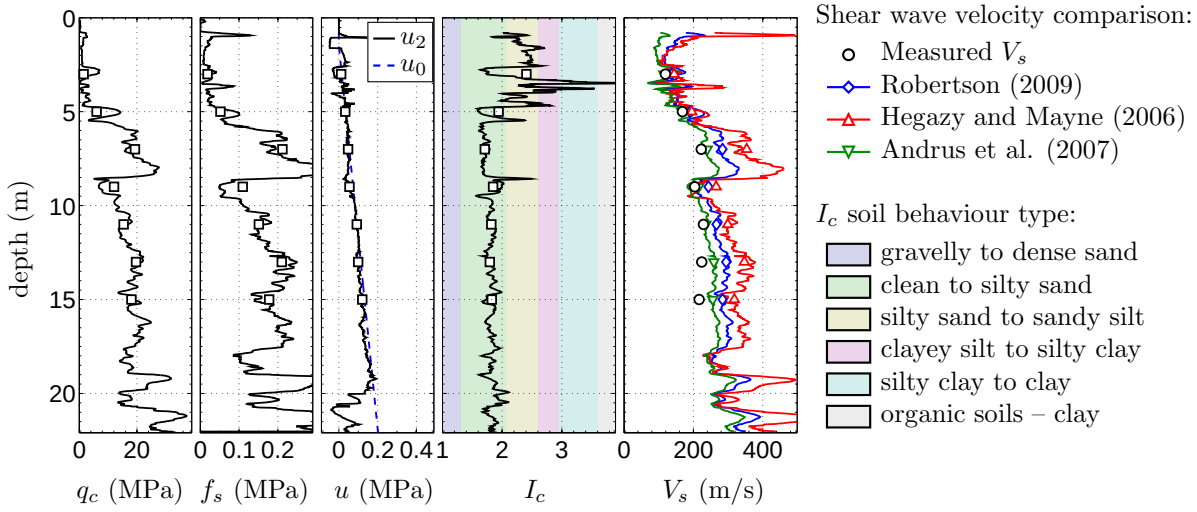

Figure A.37: SCPTu DAL40 (CPT-1117) E2483528.80 N5744091.00.

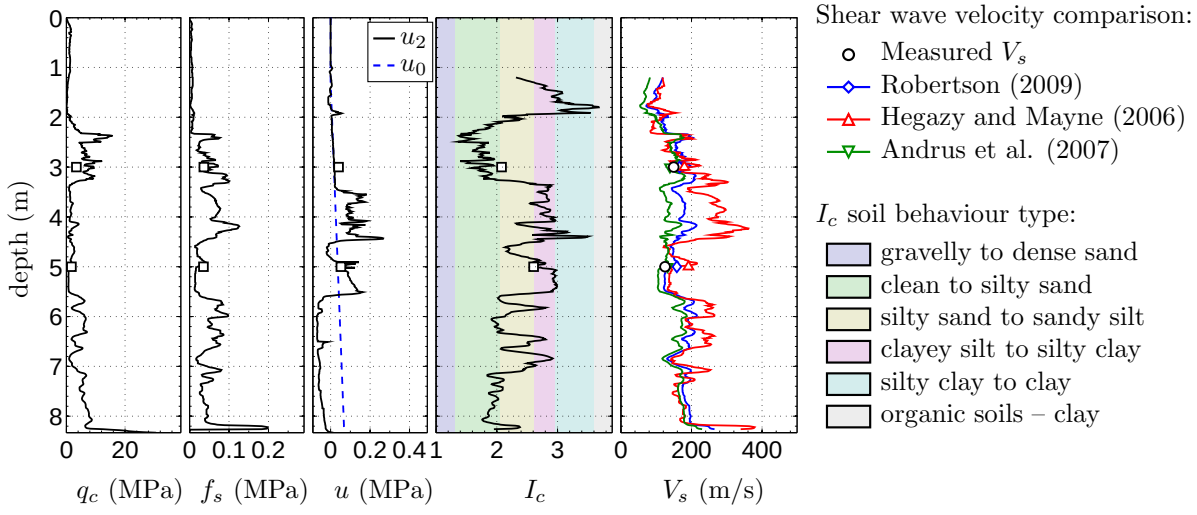

Figure A.38: SCPTu FND10 (CPT-1149) E2477471.51 N5743235.30.

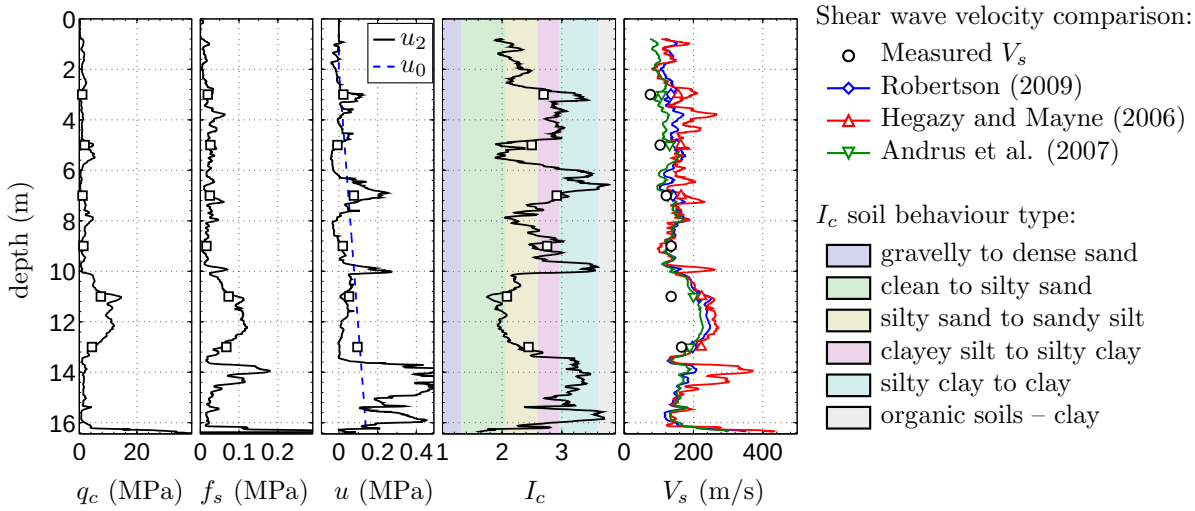

Figure A.39: SCPTu HAL27 (CPT-1192) E2474911.54 N5734791.92.

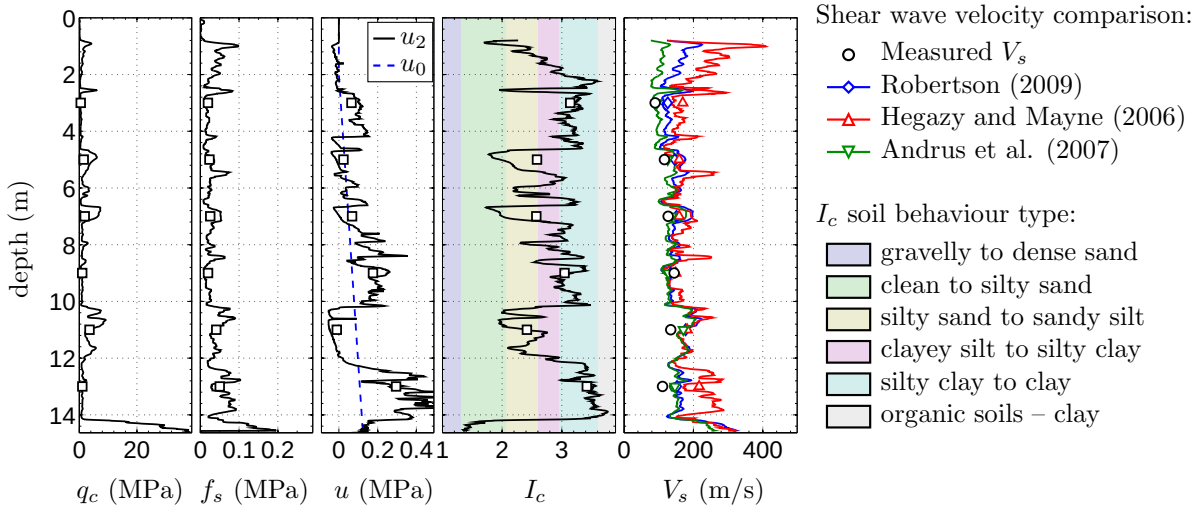

Figure A.40: SCPTu HAL35 (CPT-1200) E2475810.34 N5736625.93.

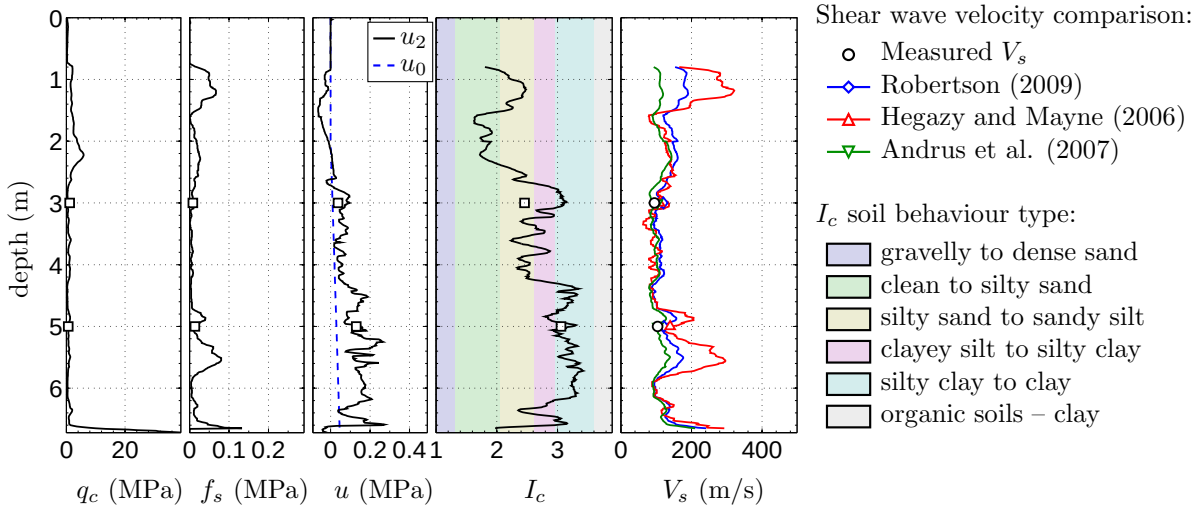

Figure A.41: SCPTu HAL45 (CPT-1210) E2474779.43 N5737377.85.

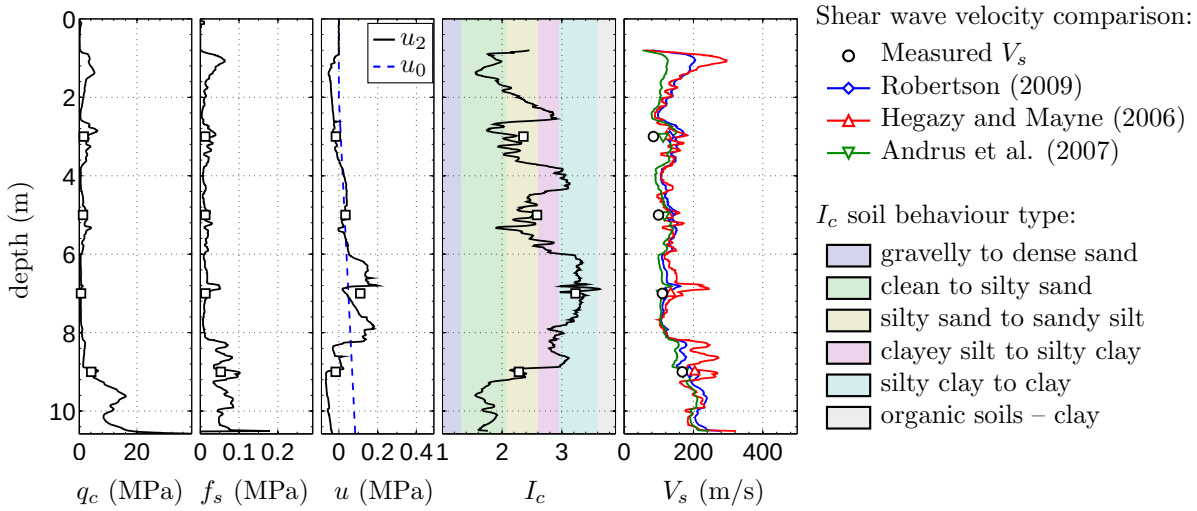

Figure A.42: SCPTu HNH02 (CPT-1200) E2478453.96 N5737651.34.

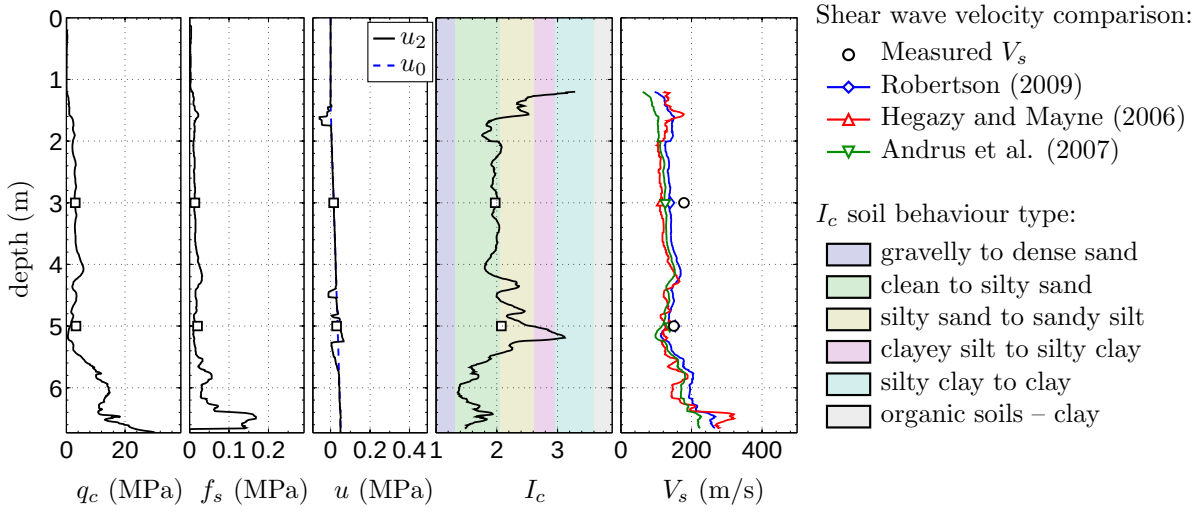

Figure A.43: SCPTu KAN36 (CPT-1295) E2482775.71 N5757888.13.

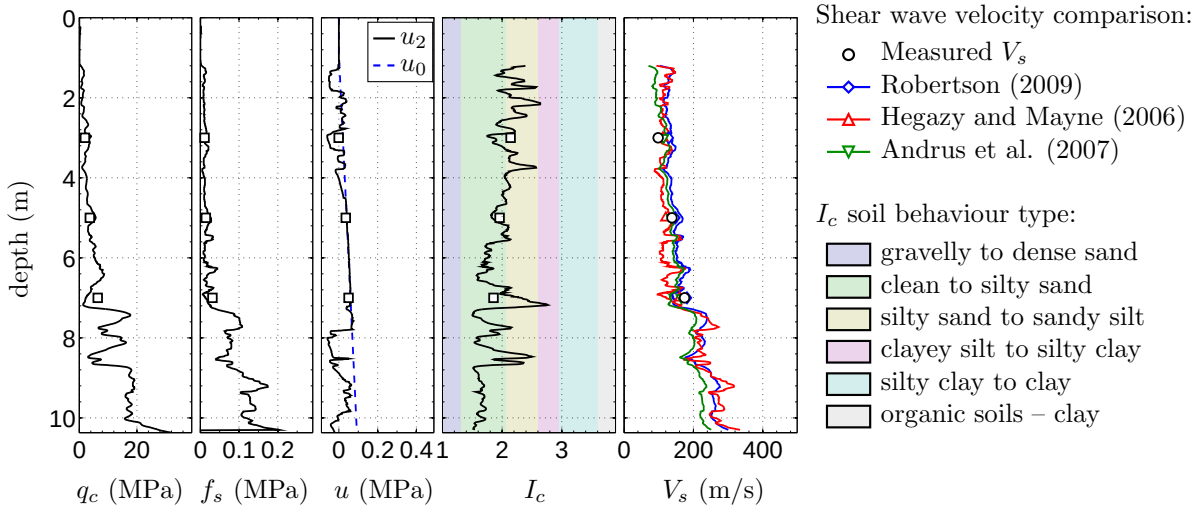

Figure A.44: SCPTu KAN38 (CPT-1297) E2483096.04 N5757798.19.

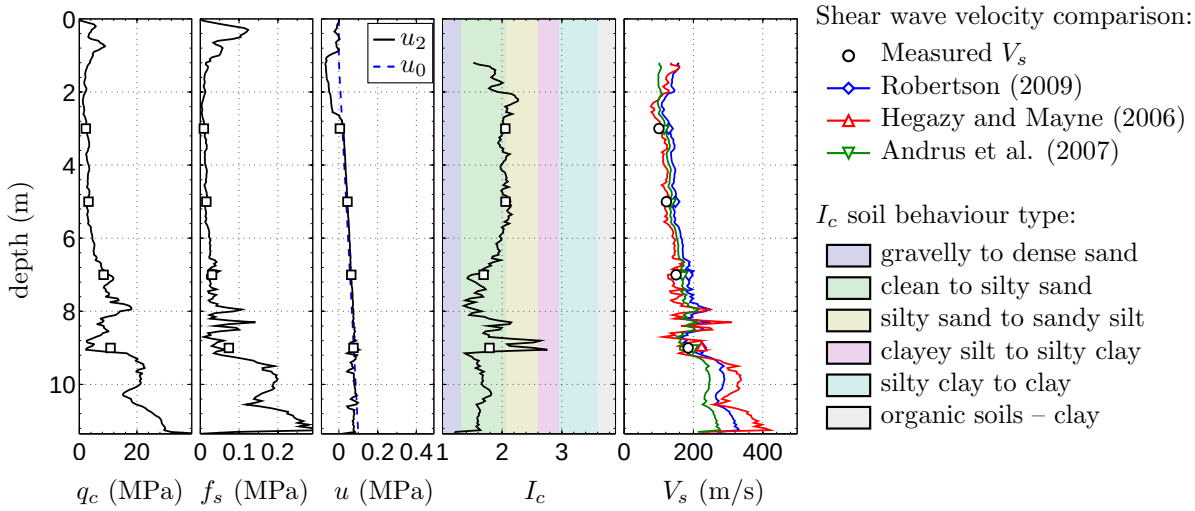

Figure A.45: SCPTu KAN41 (CPT-1300) E2483340.31 N5757874.66.

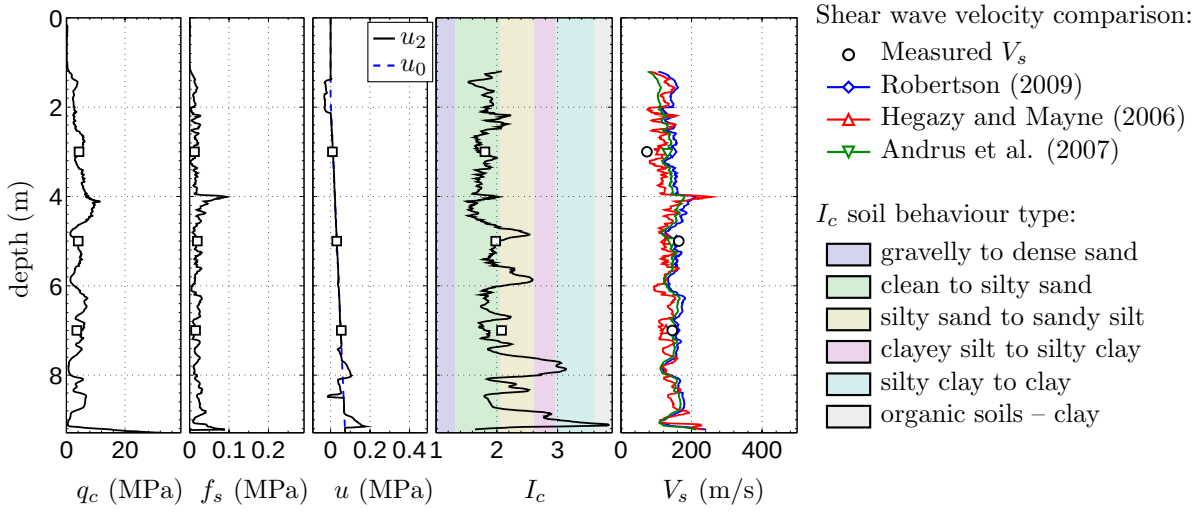

Figure A.46: SCPTu KAN42 (CPT-1301) E2482227.55 N5758443.61.

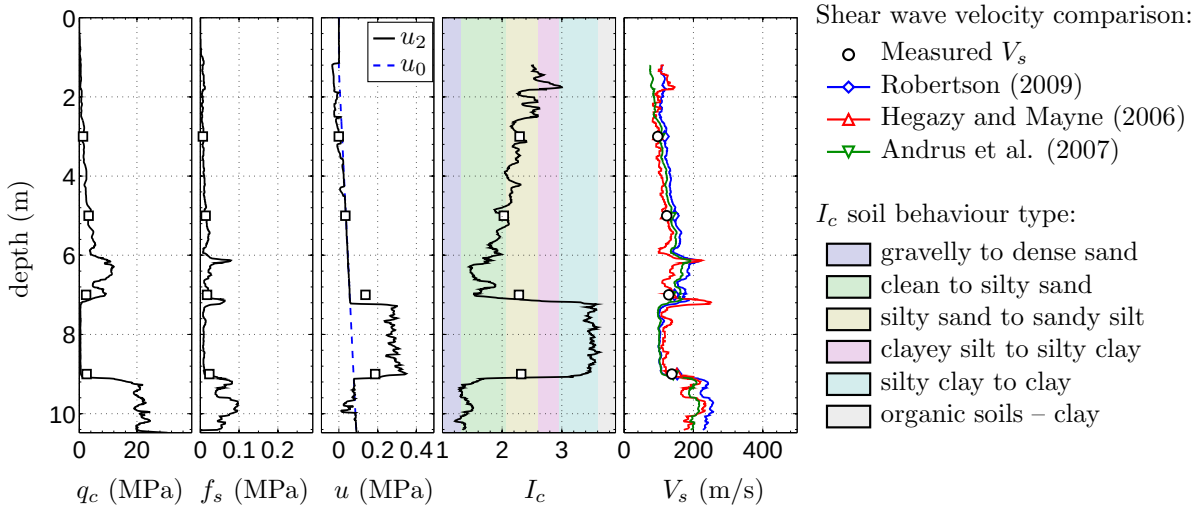

Figure A.47: SCPTu KAS41 (CPT-1342) E2482082.79 N5758520.38.

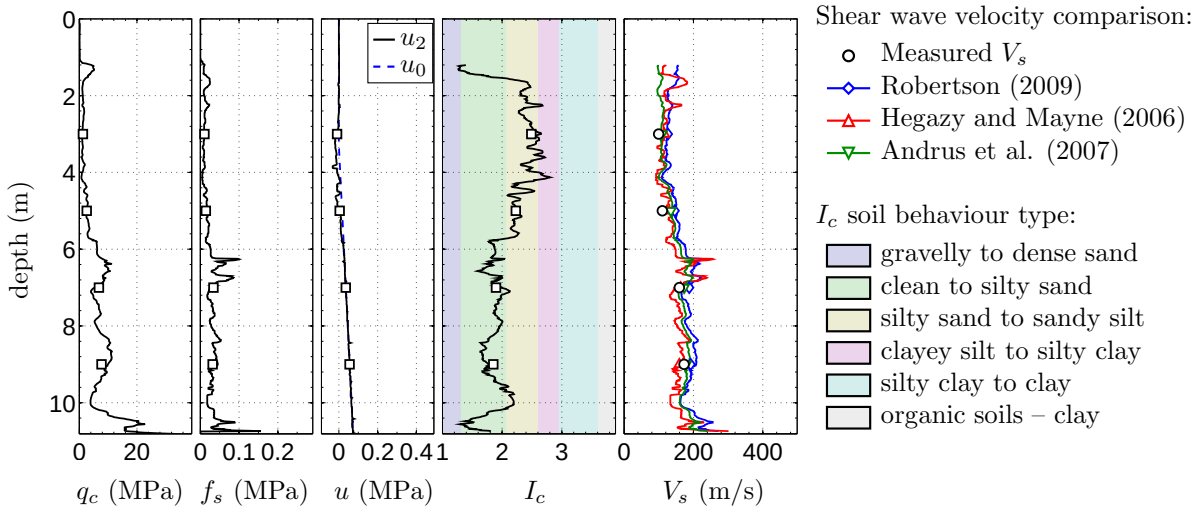

Figure A.48: SCPTu KAS44 (CPT-1344) E2482661.37 N5757791.10.

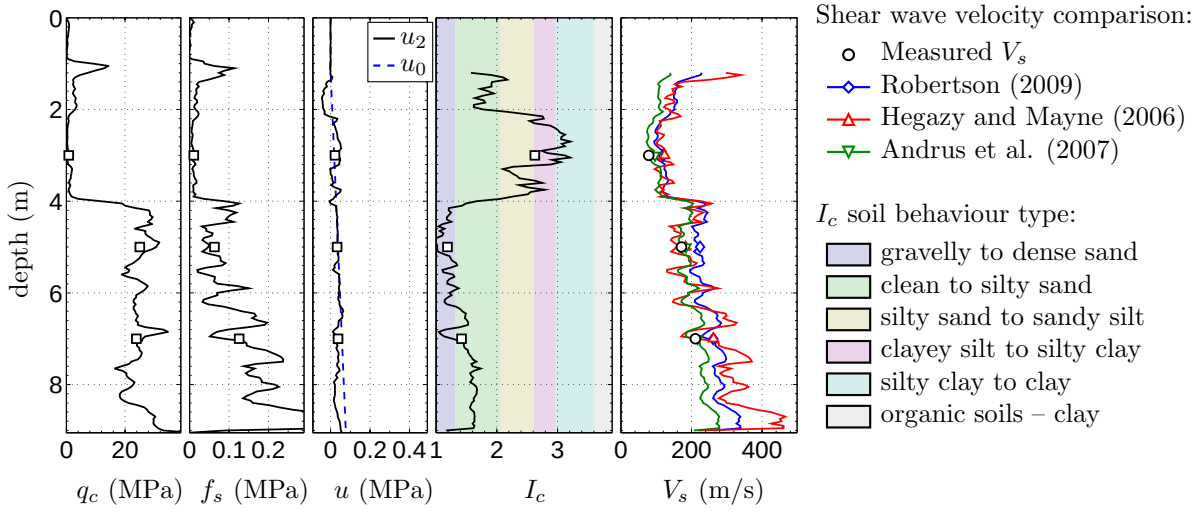

Figure A.49: SCPTu KAS46 (CPT-1346) E2482726.64 N5757598.05.

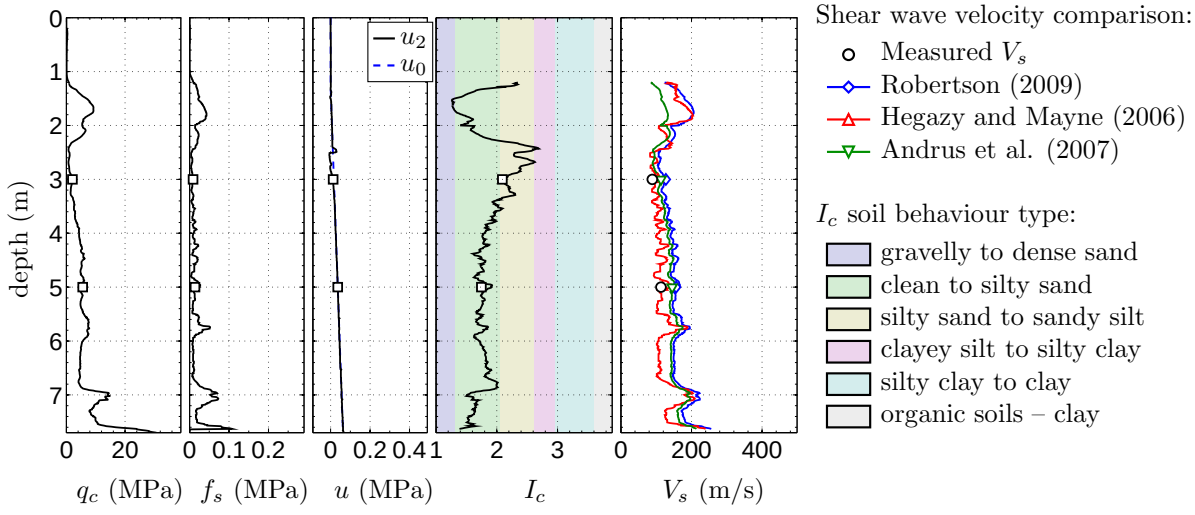

Figure A.50: SCPTu KAS52 (CPT-1351) E2482466.96 N5756996.86.

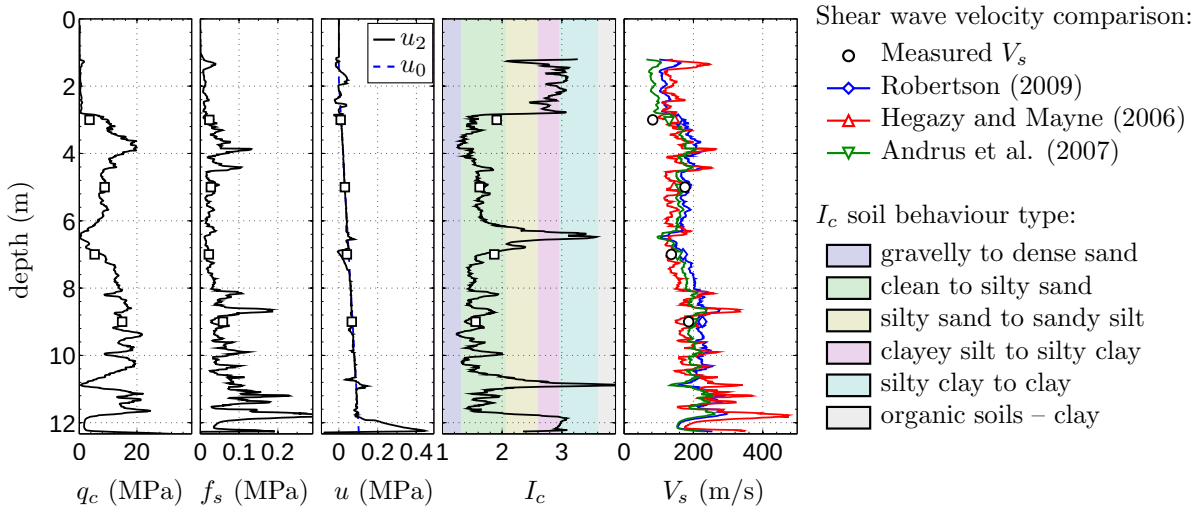

Figure A.51: SCPTu KAS54 (CPT-1353) E2482296.18 N5758180.17.

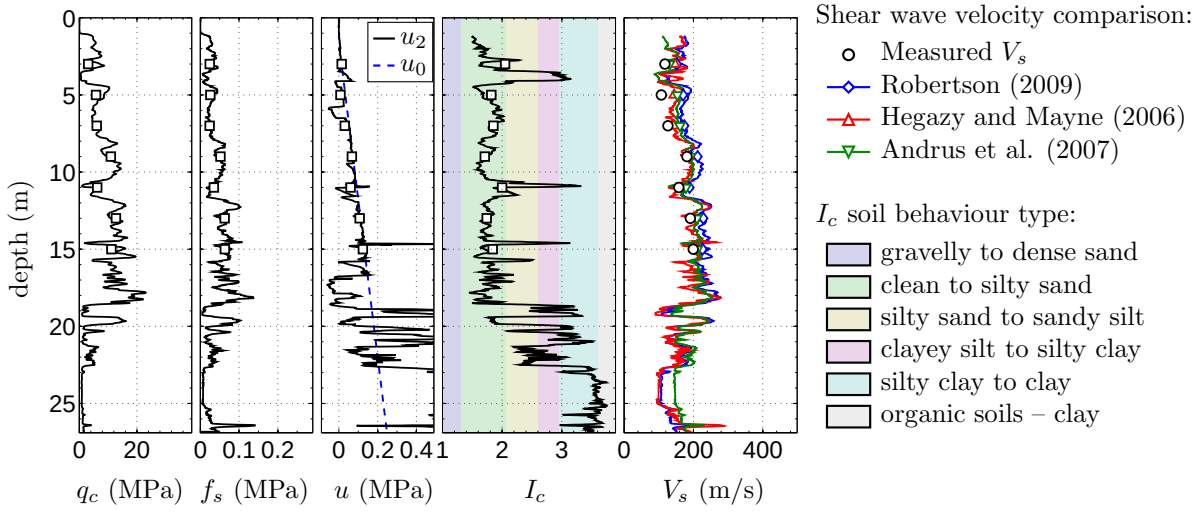

Figure A.52: SCPTu LWD27 (CPT-1384) E2483059.99 N5741014.31.

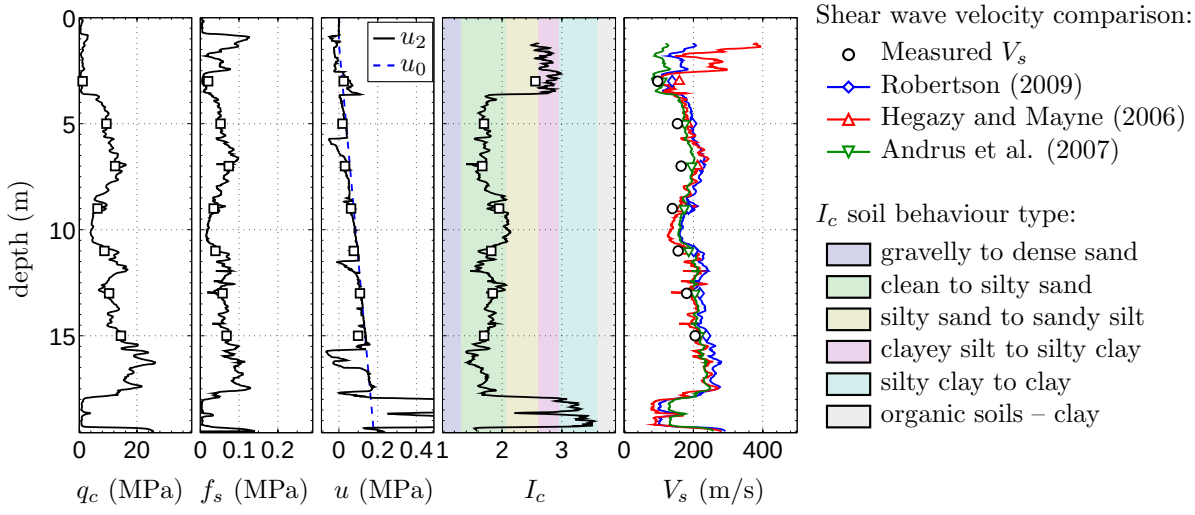

Figure A.53: SCPTu LWD29 (CPT-1386) E2483138.18 N5740801.36.

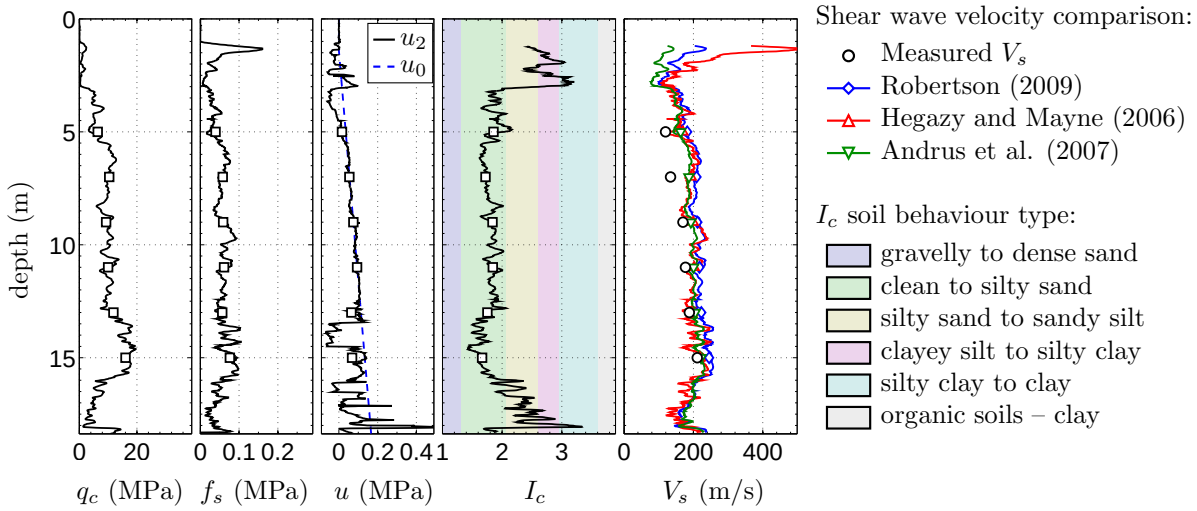

Figure A.54: SCPTu LWD32 (CPT-1389) E2483685.94 N5740188.69.

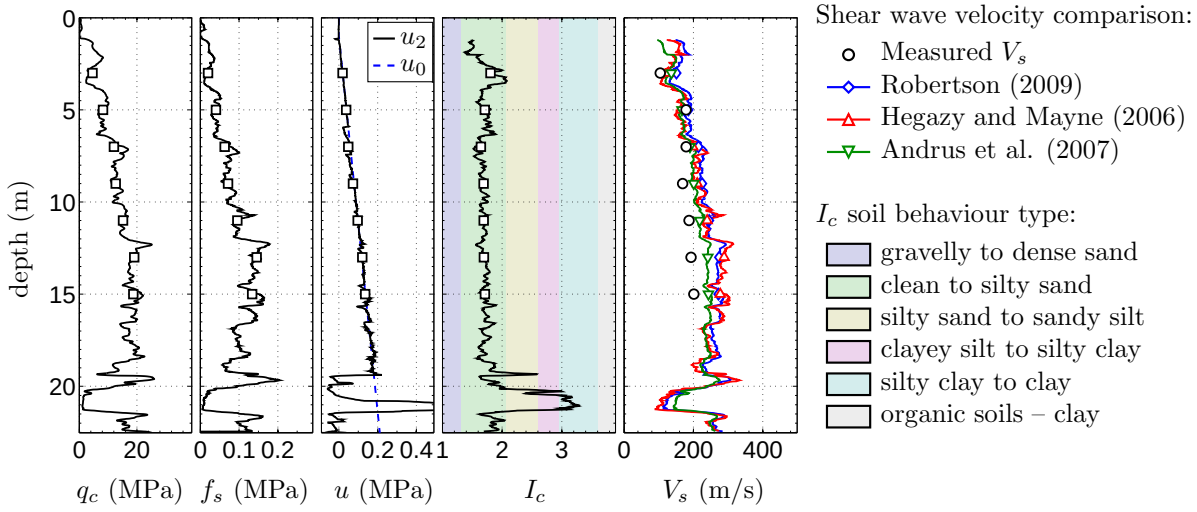

Figure A.55: SCPTu LWD37 (CPT-1394) E2483944.86 N5741865.03.

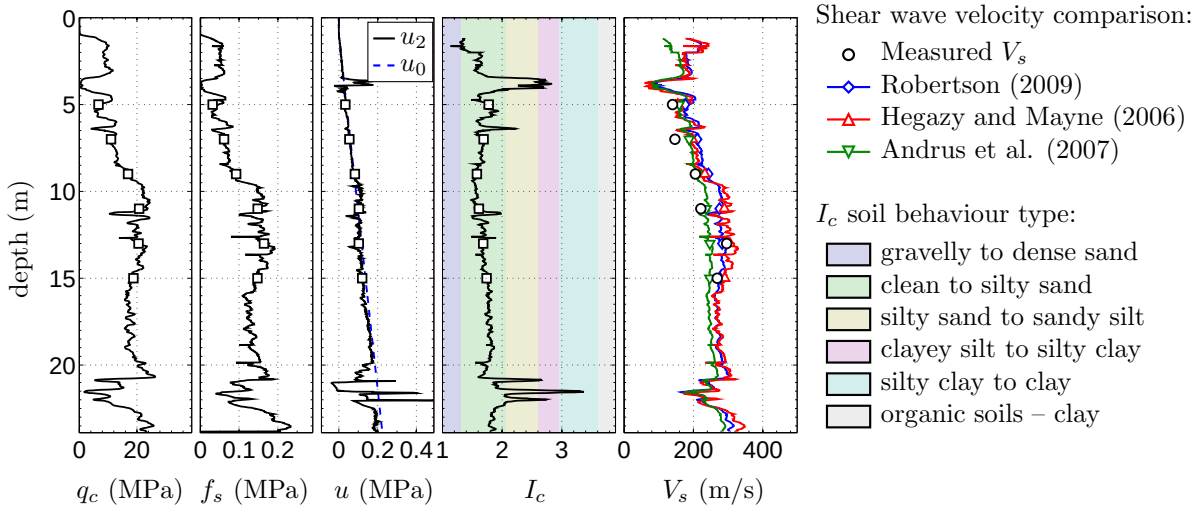

Figure A.56: SCPTu NNB05 (CPT-1458) E2486862.58 N5746424.54.

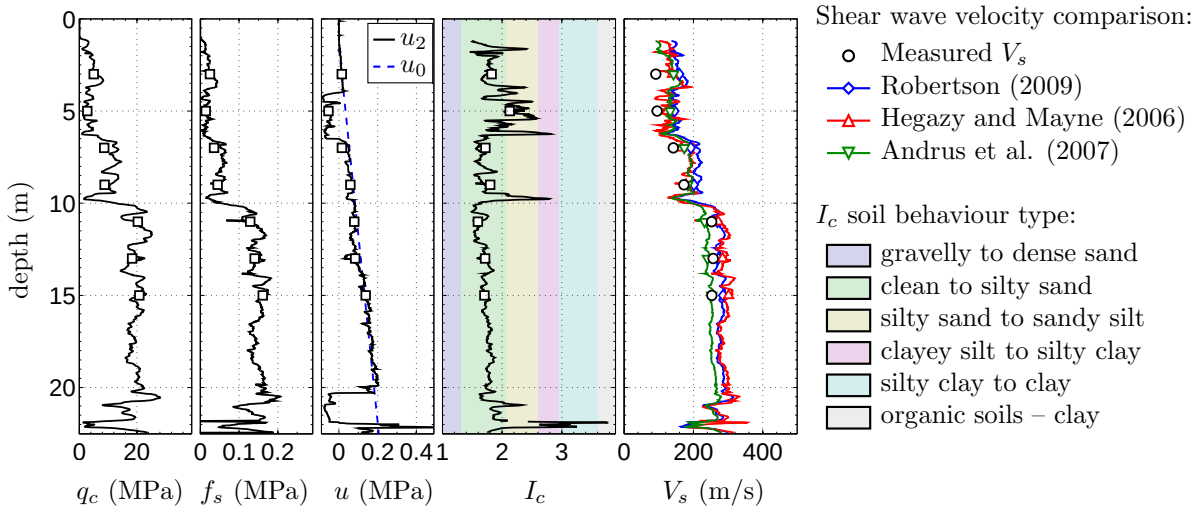

Figure A.57: SCPTu NNB08 (CPT-1460) E2486643.96 N5745803.75.

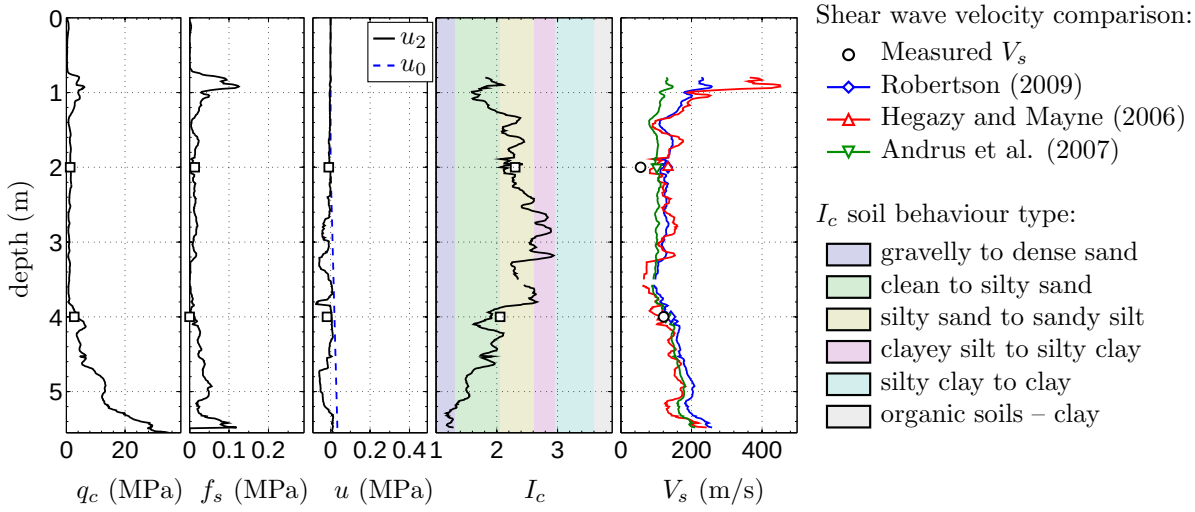

Figure A.58: SCPTu RCH16 (CPT-528) E2483299.42 N5743648.39.

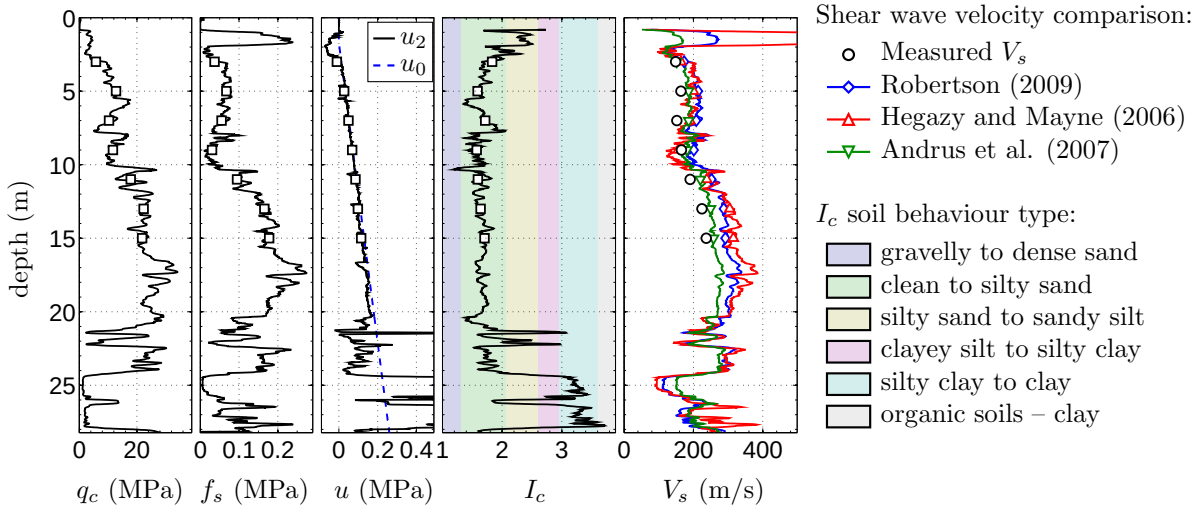

Figure A.59: SCPTu RCH17 (CPT-529) E2482768.36 N5743572.88.

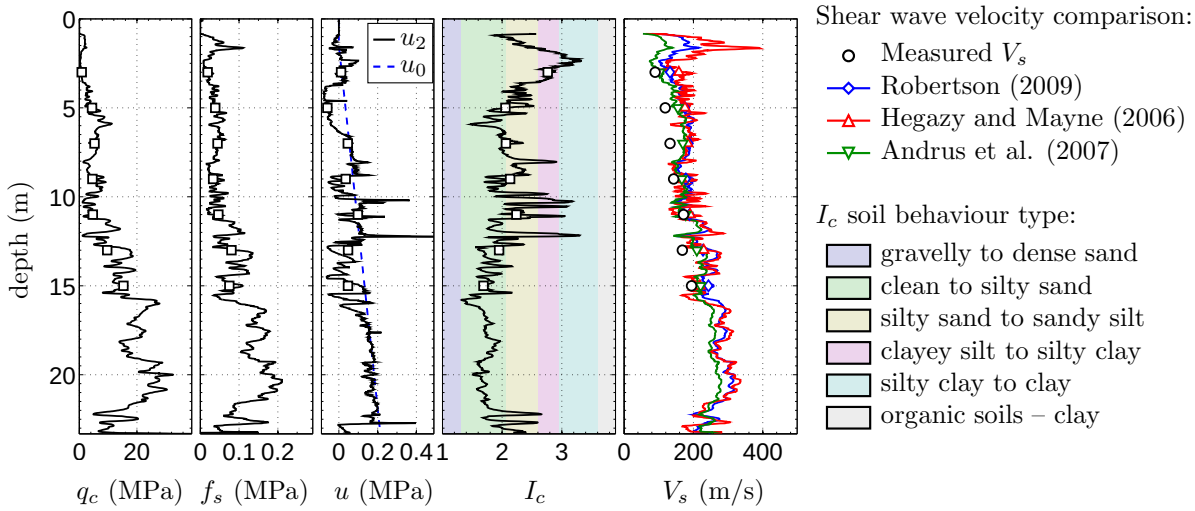

Figure A.60: SCPTu RCH25 (CPT-537) E2482078.57 N5743606.26.

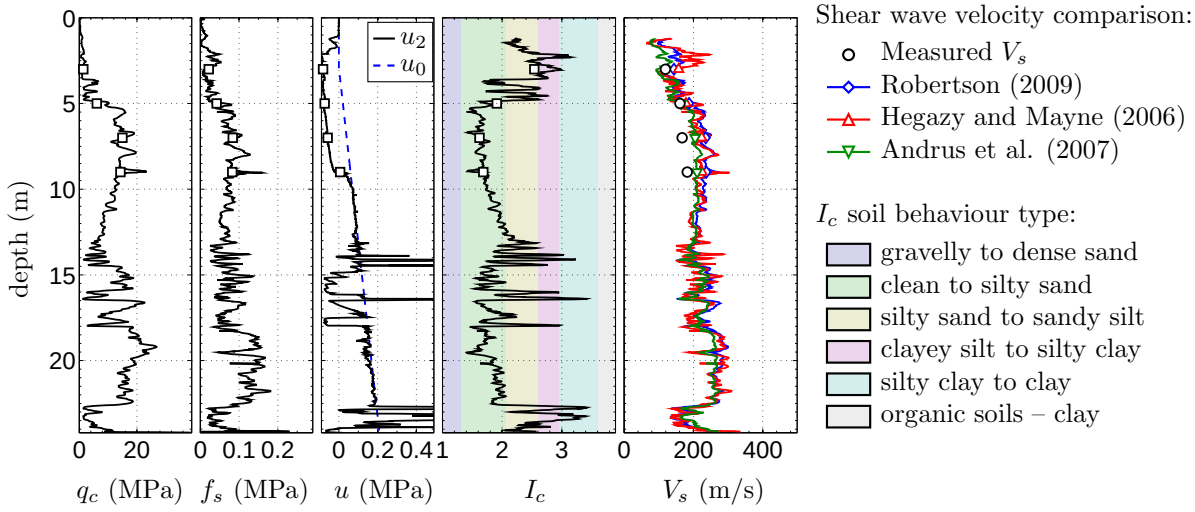

Figure A.61: SCPTu RCH59 (CPT-568) E2481978.45 N5742587.20.

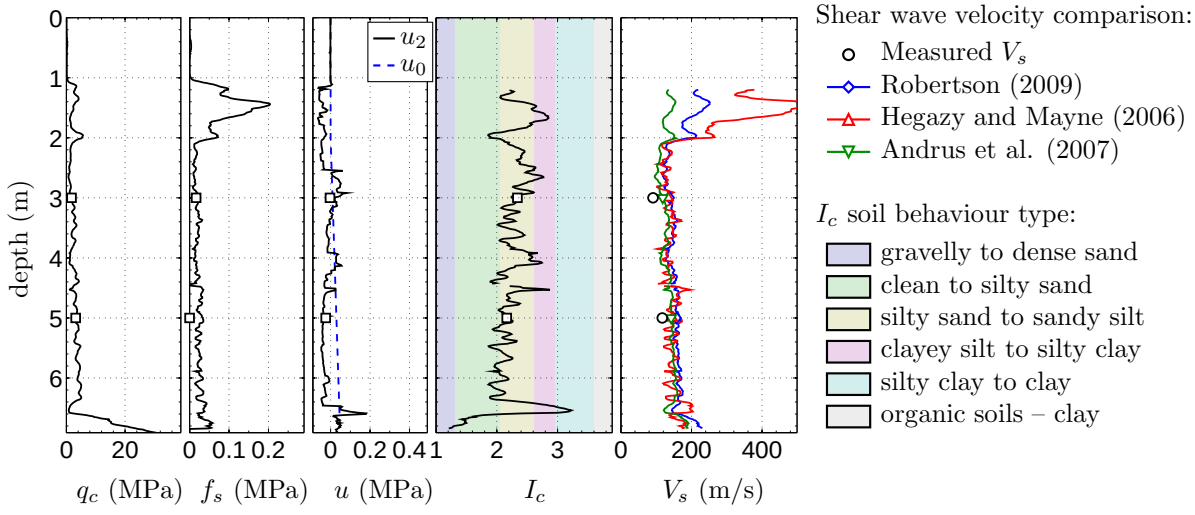

Figure A.62: SCPTu RCH64 (CPT-573) E2482076.47 N5744067.97.

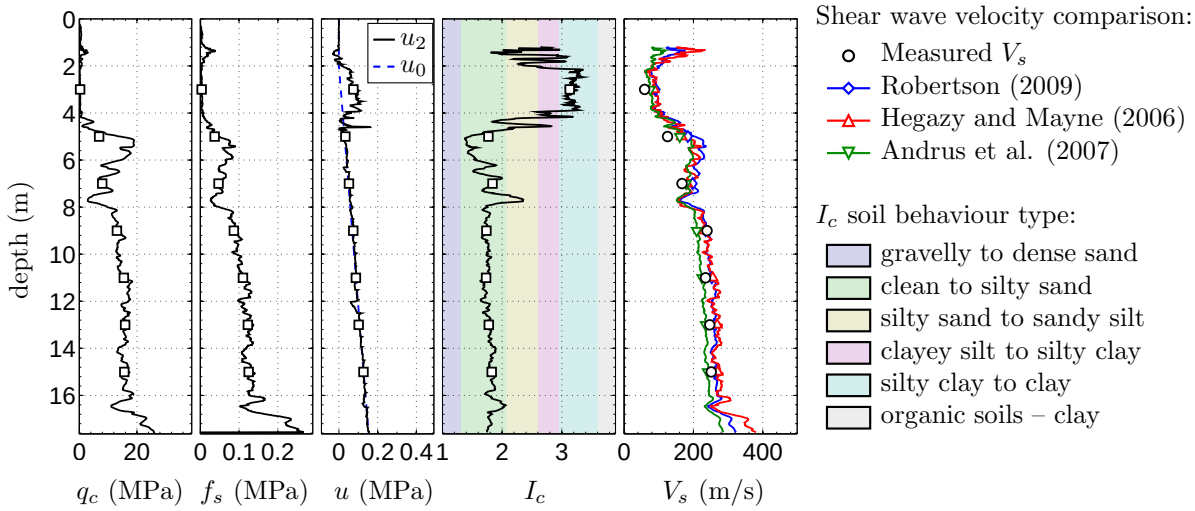

Figure A.63: SCPTu RCL03 (CPT-585) E2488906.91 N5738659.35.

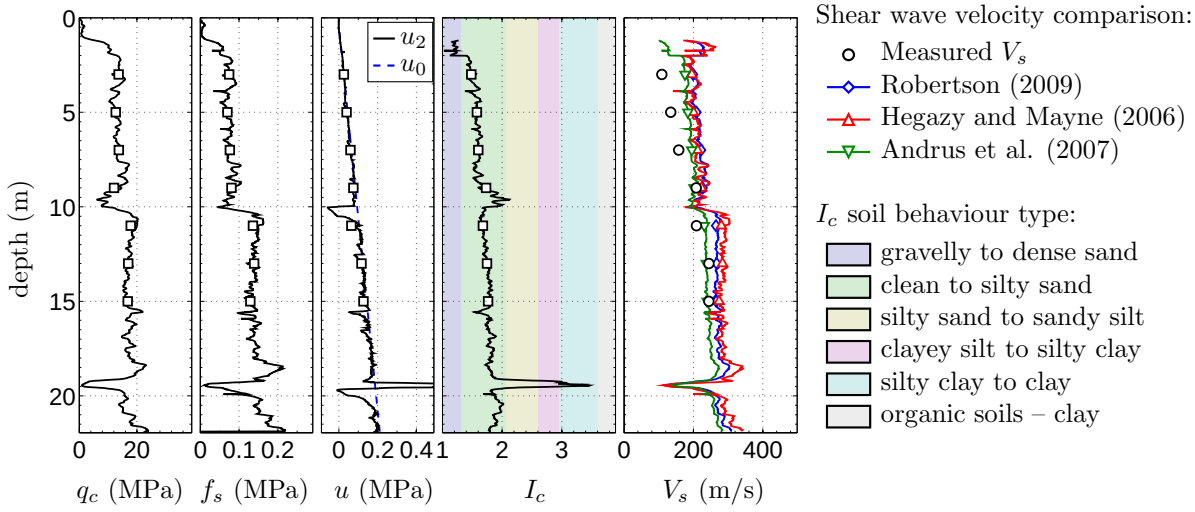

Figure A.64: SCPTu SNB10 (CPT-666) E2488245.87 N5742600.90.

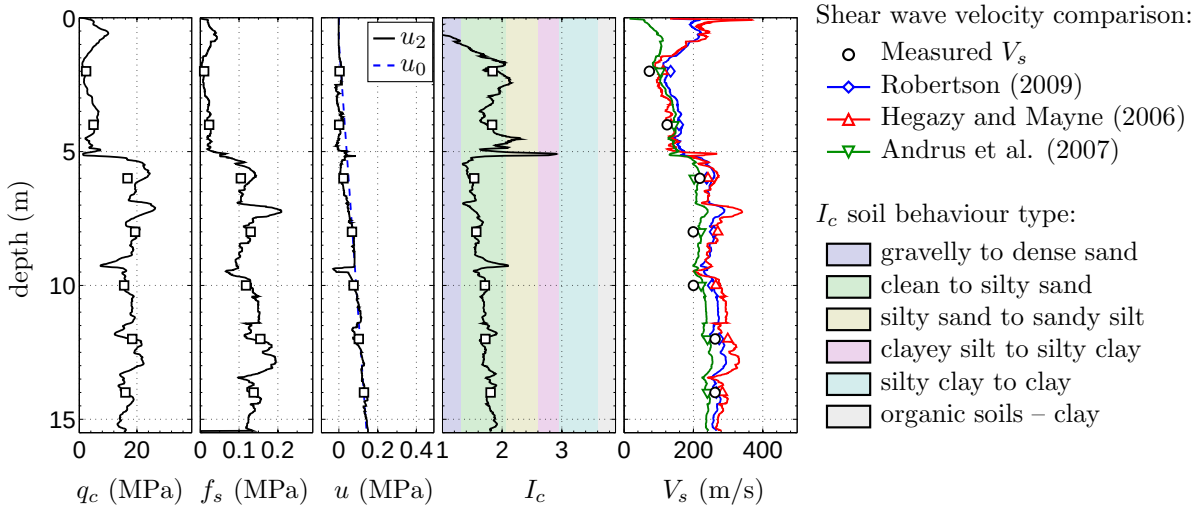

Figure A.65: SCPTu SPE01 (CPT-667) E2485129.50 N5752949.68.

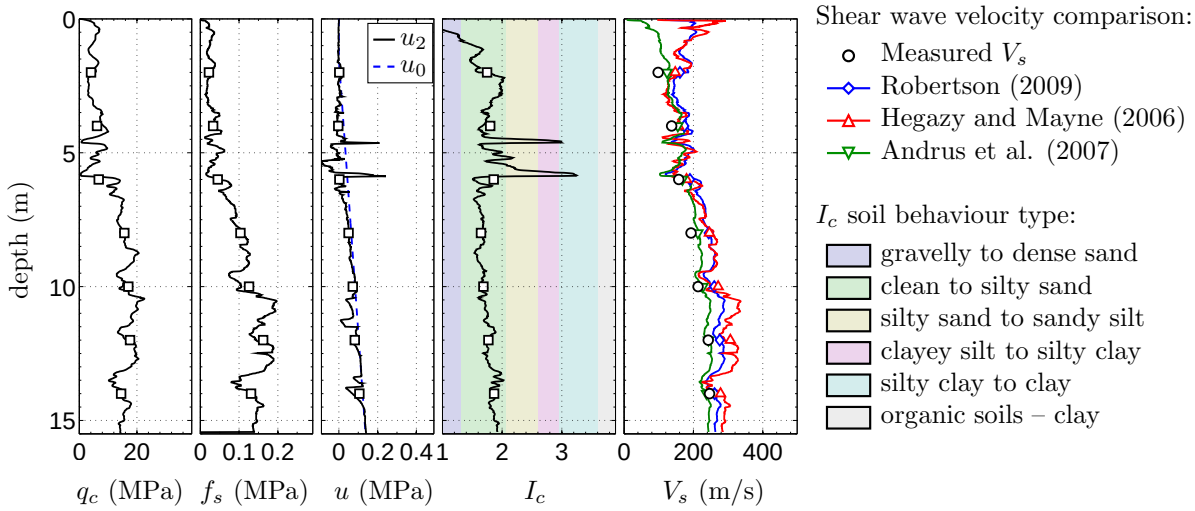

Figure A.66: SCPTu SPE03 (CPT-669) E2485150.05 N5752895.96.

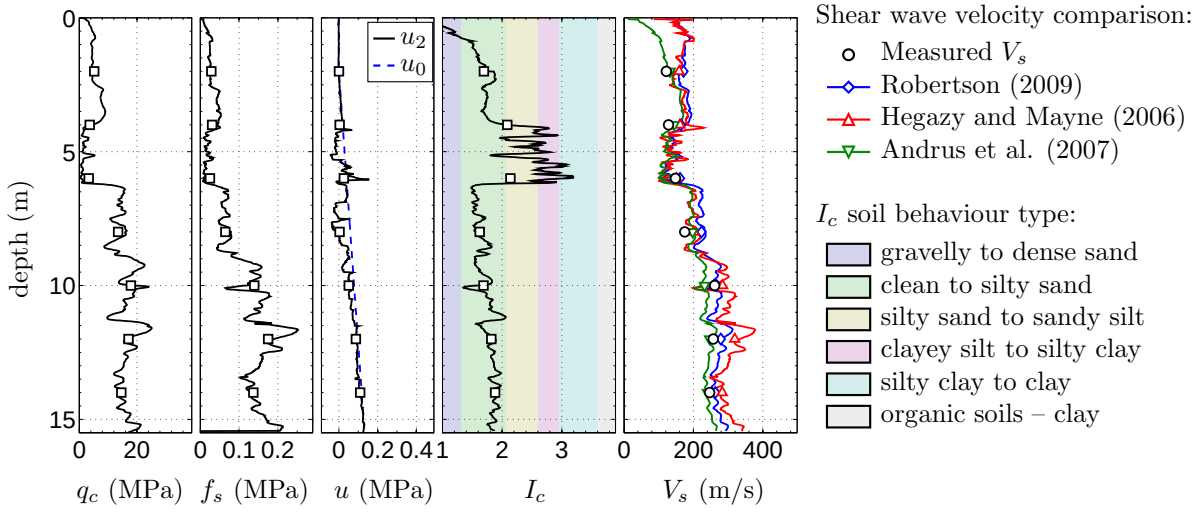

Figure A.67: SCPTu SPE05 (CPT-671) E2485180.66 N5752823.66.

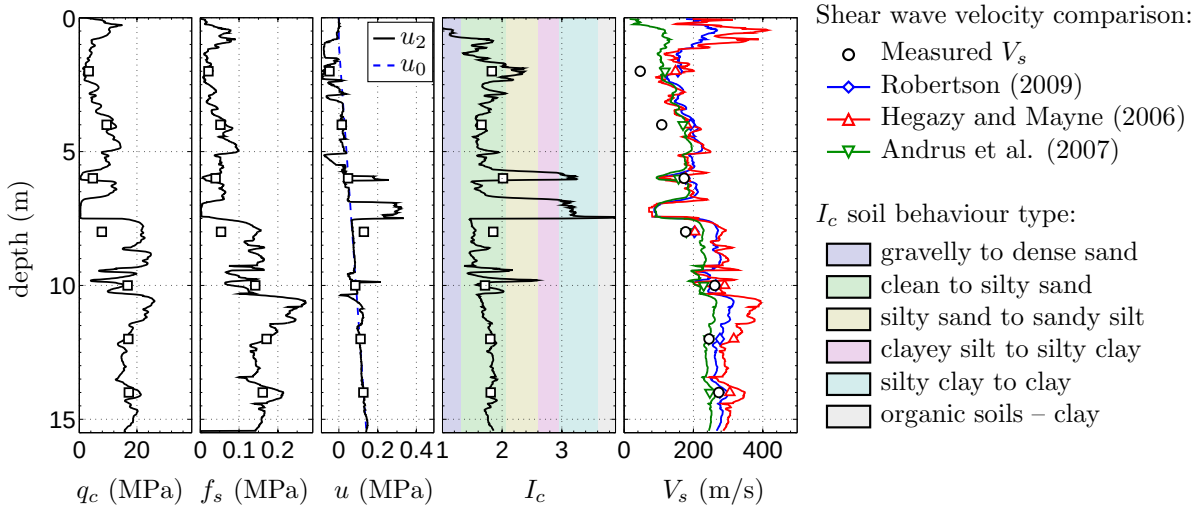

Figure A.68: SCPTu SPE07 (CPT-673) E2485216.86 N5752868.78.

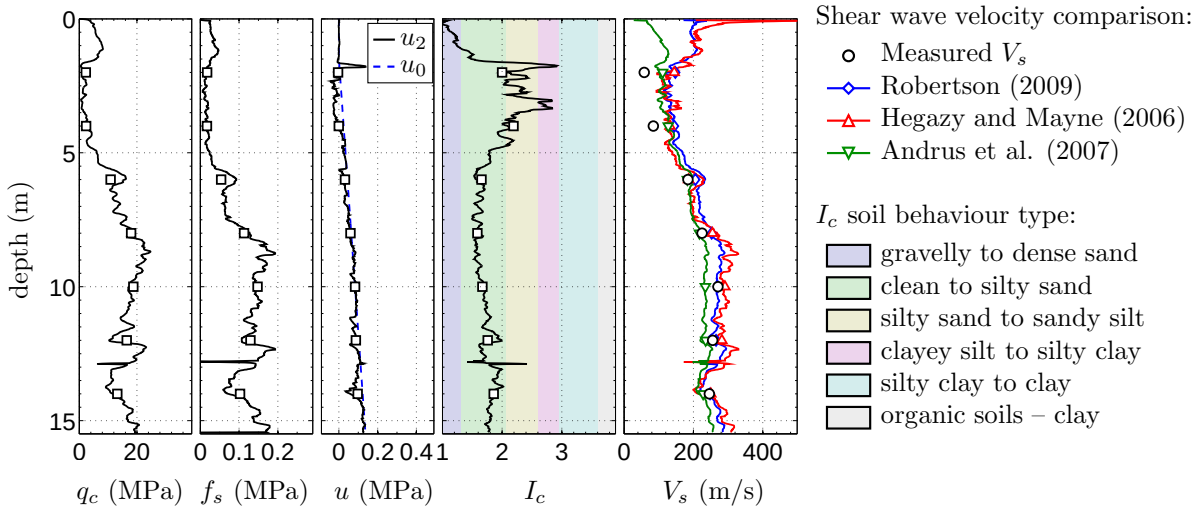

Figure A.69: SCPTu SPE11 (CPT-677) E2485290.67 N5752880.39.

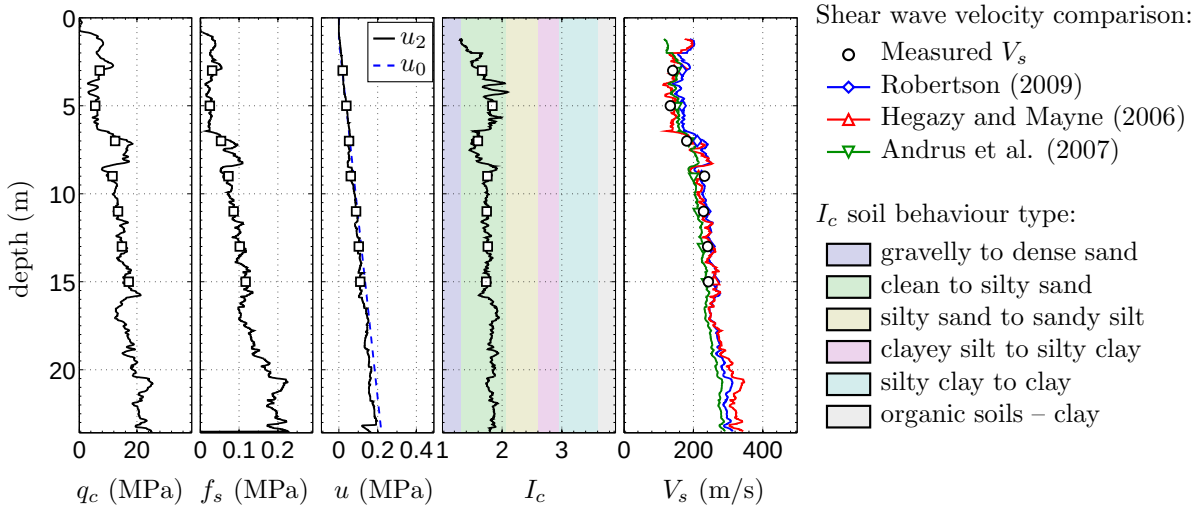

Figure A.70: SCPTu SSH04 (CPT-712) E2489797.82 N5739037.08.

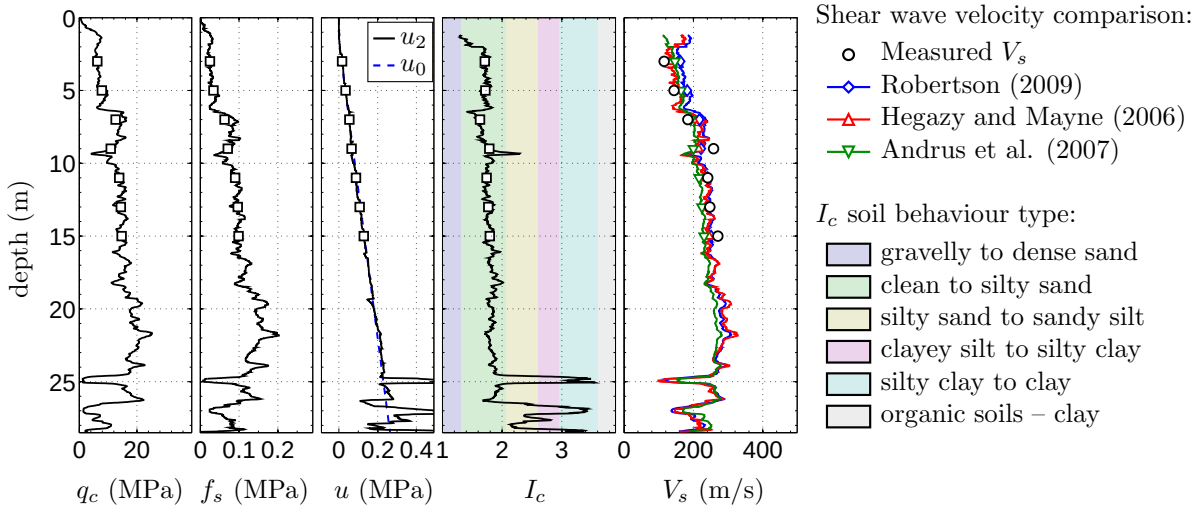

Figure A.71: SCPTu SSH07 (CPT-715) E2489492.49 N5739775.09.

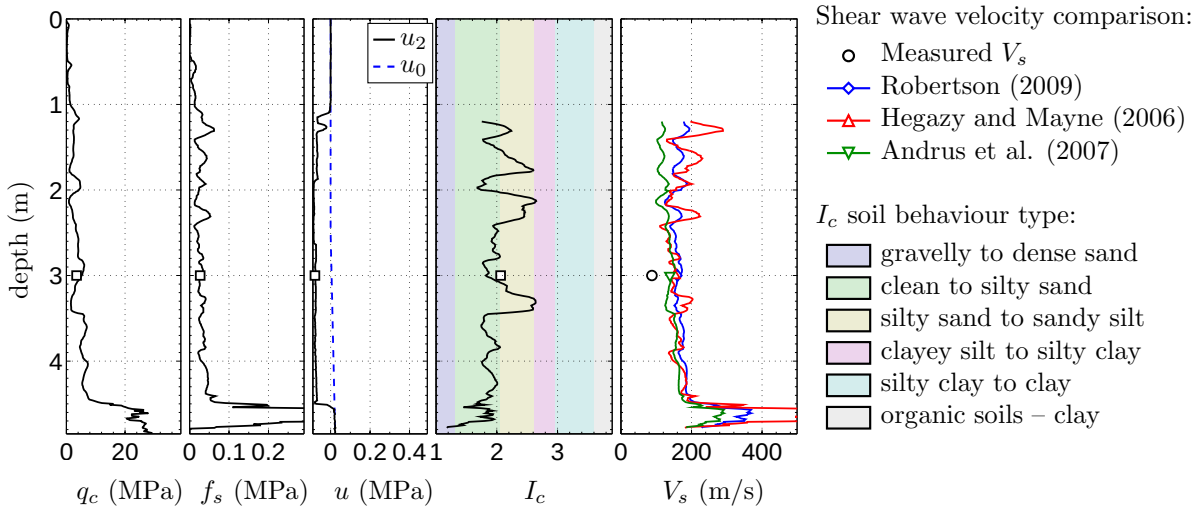

Figure A.72: SCPTu STA41 (CPT-735) E2480245.14 N5743944.19.

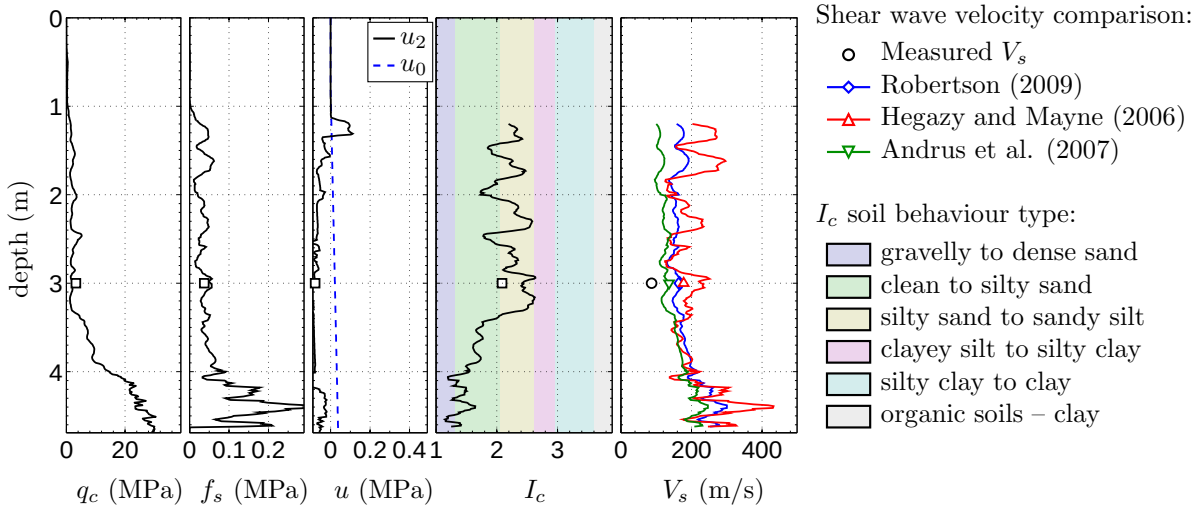

Figure A.73: SCPTu STA46 (CPT-762) E2480447.77 N5744447.99.

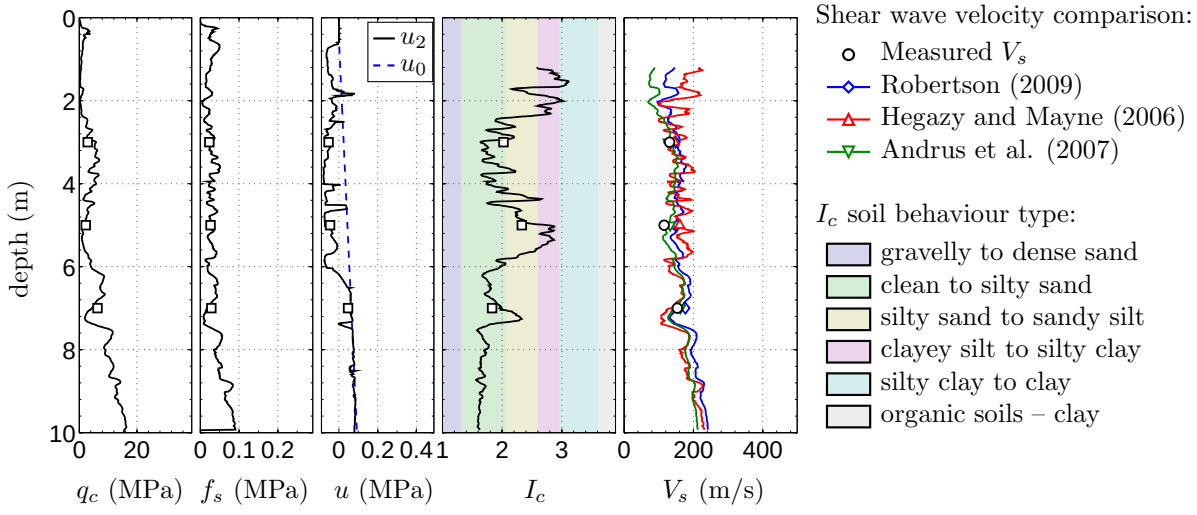

Figure A.74: SCPTu STA51 (CPT-767) E2481169.00 N5744525.63.

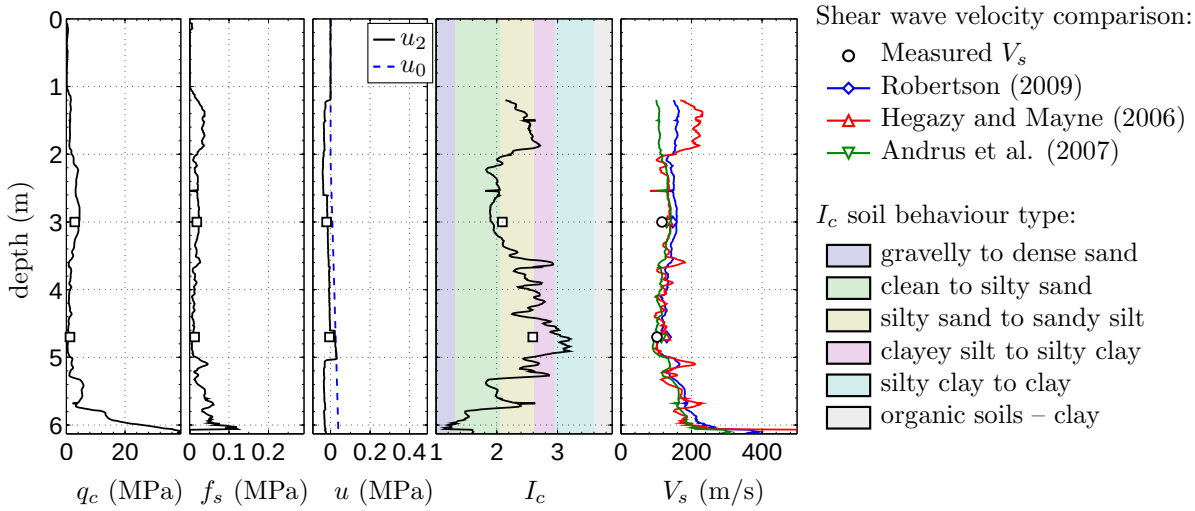

Figure A.75: SCPTu TTP04 (CPT-838) E2473503.45 N5727236.75.

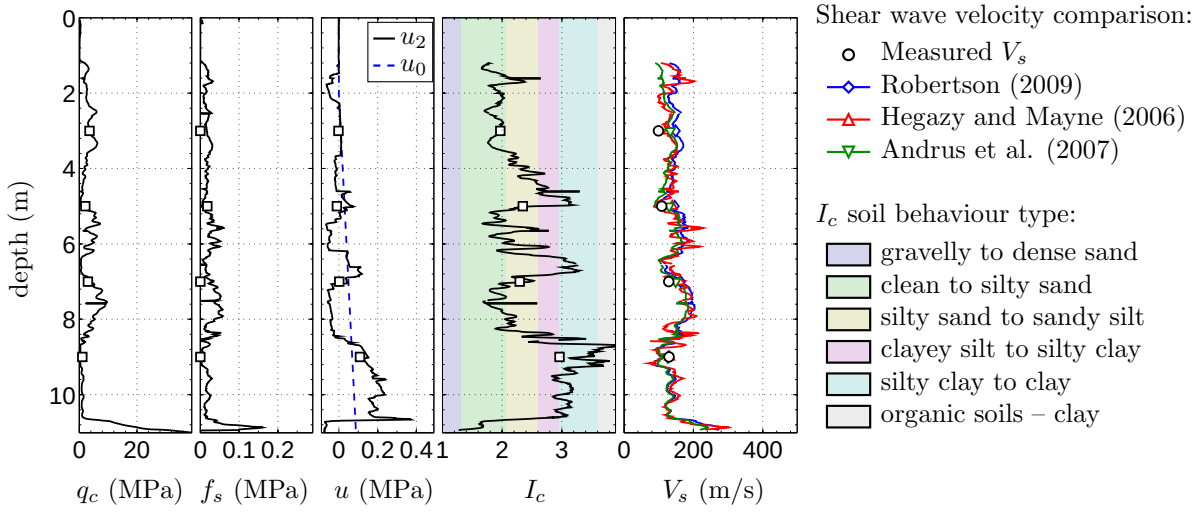

Figure A.76: SCPTu TTP05 (CPT-839) E2473819.80 N5726748.80.

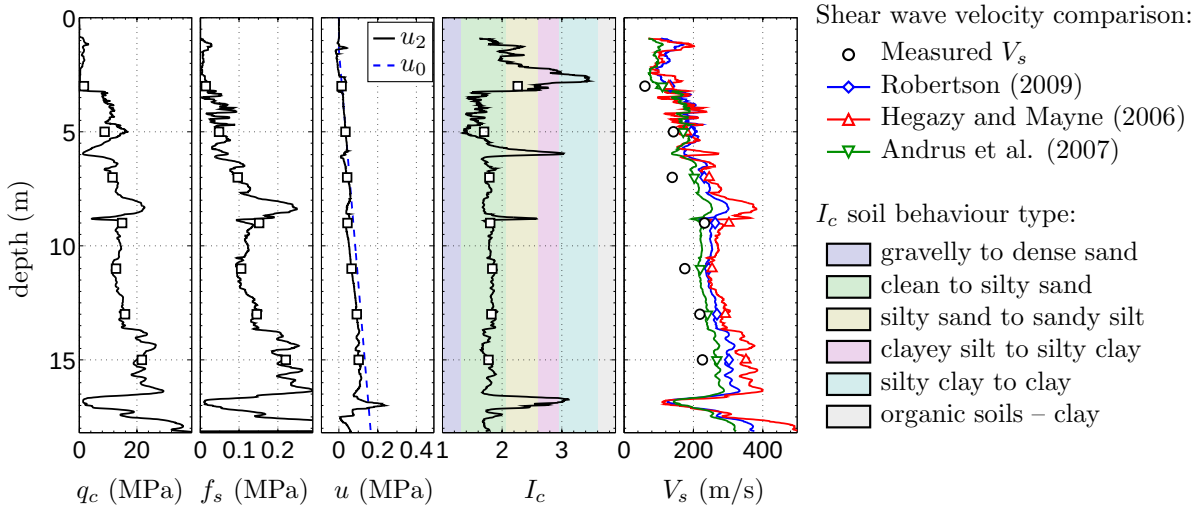

Figure A.77: SCPTu WAI10 (CPT-851) E2484234.38 N5743250.42.

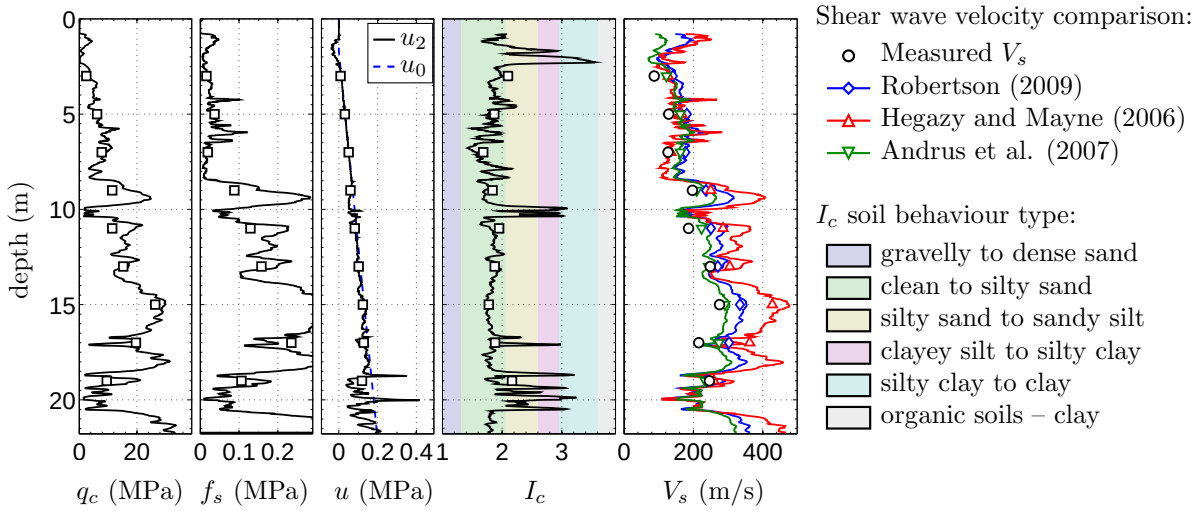

Figure A.78: SCPTu WAI14 (CPT-855) E2484399.86 N5743788.60.

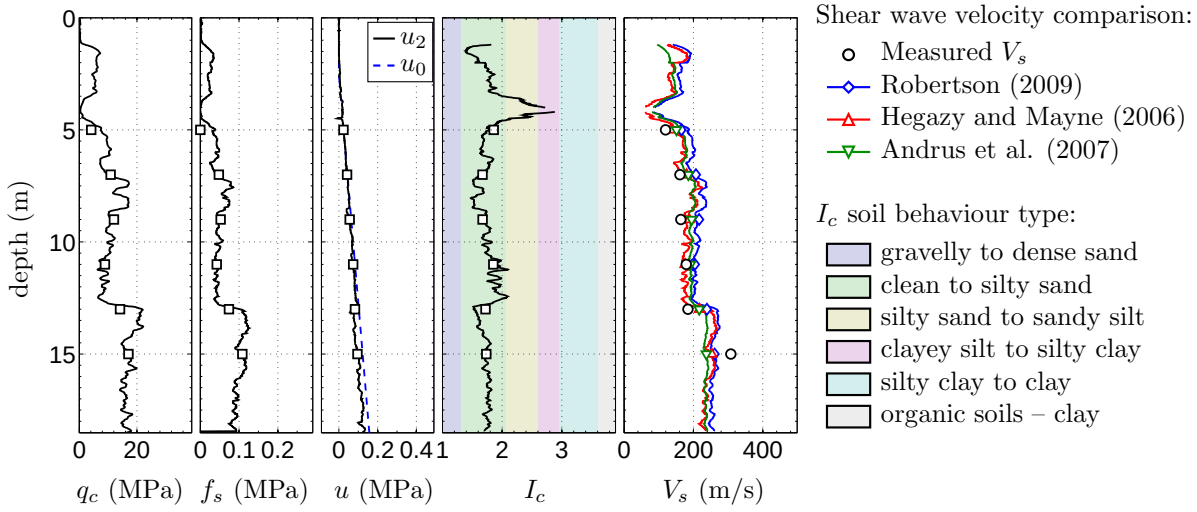

Figure A.79: SCPTu WQP01 (CPT-91) E2486711.35 N5746885.75.

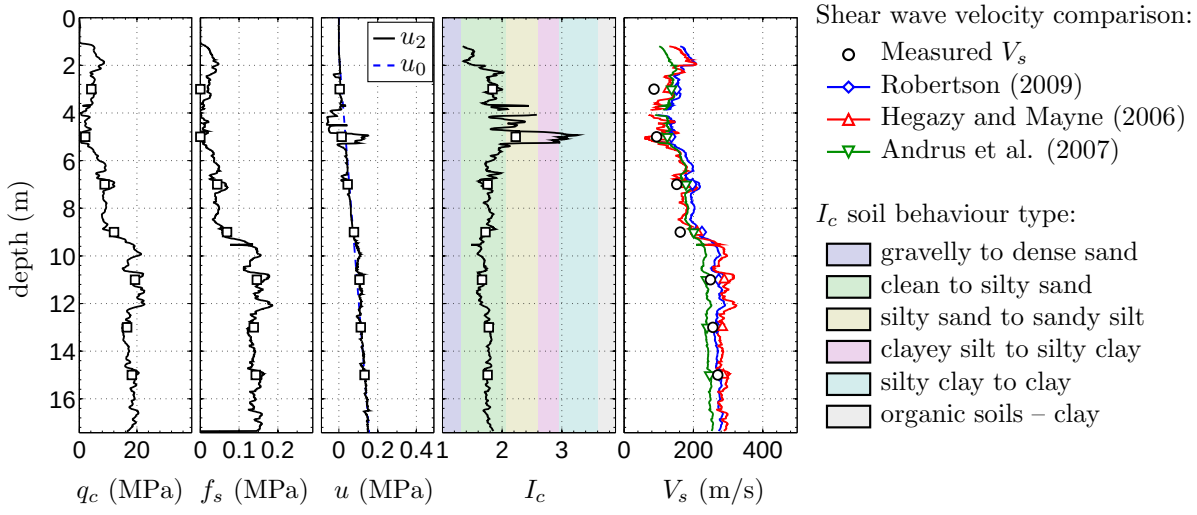

Figure A.80: SCPTu WQP22 (CPT-932) E2485938.33 N5747840.06.

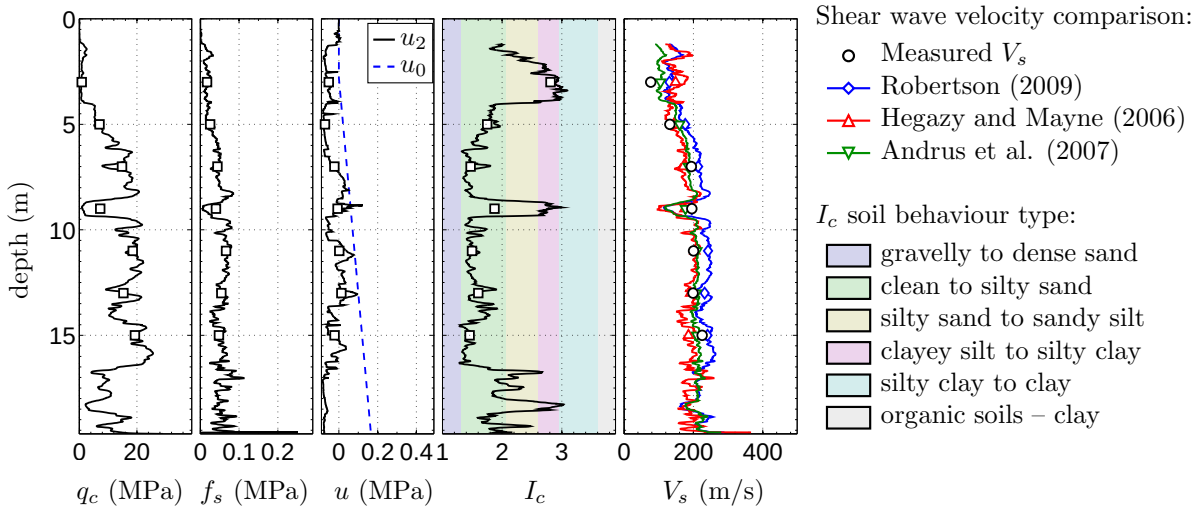

Figure A.81: SCPTu WSW01 (CPT-934) E2482804.56 N5739627.31.

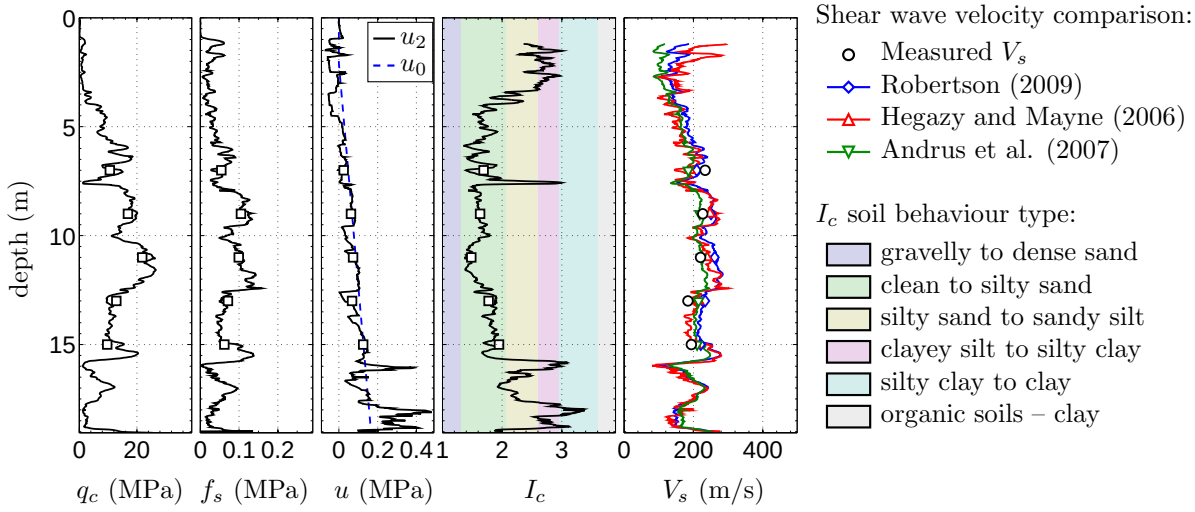

Figure A.82: SCPTu WSW06 (CPT-939) E2483143.44 N5739856.79.

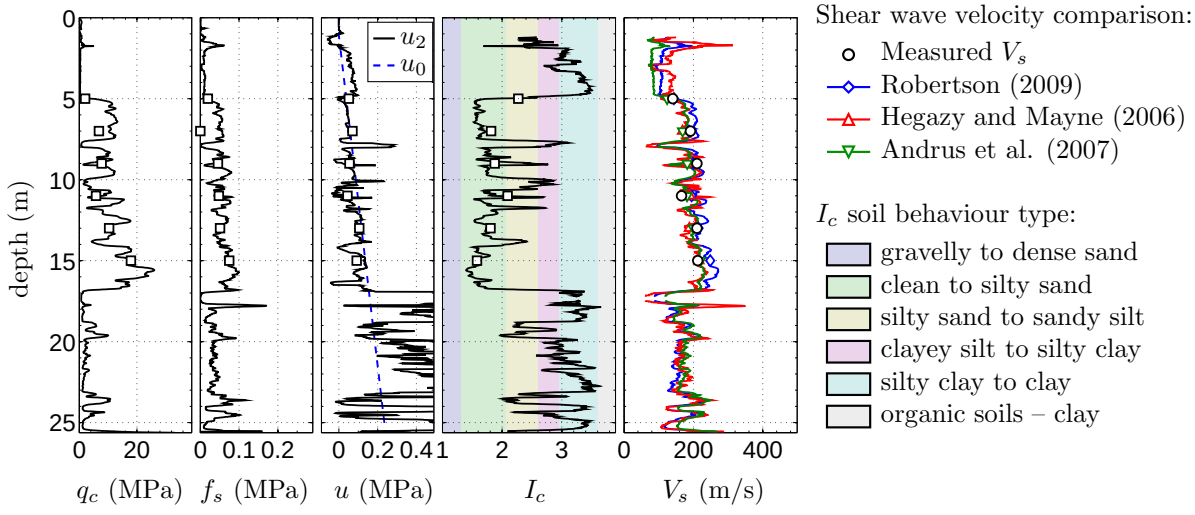

Figure A.83: SCPTu WSW12 (CPT-945) E2483192.00 N5739387.89.

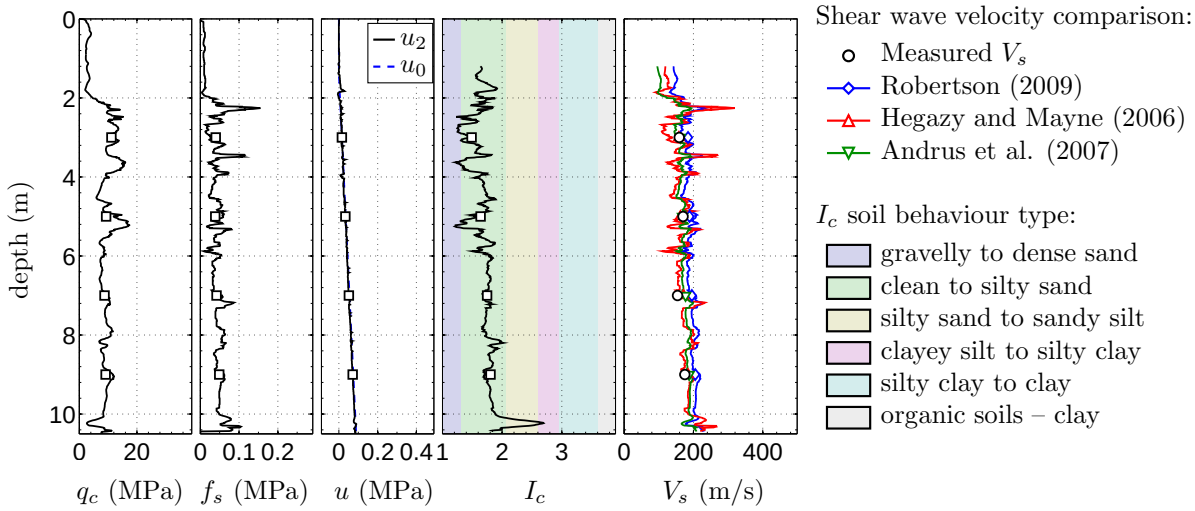

Figure A.84: SCPTu WSW35 (CPT-966) E2484277.52 N5739552.06.

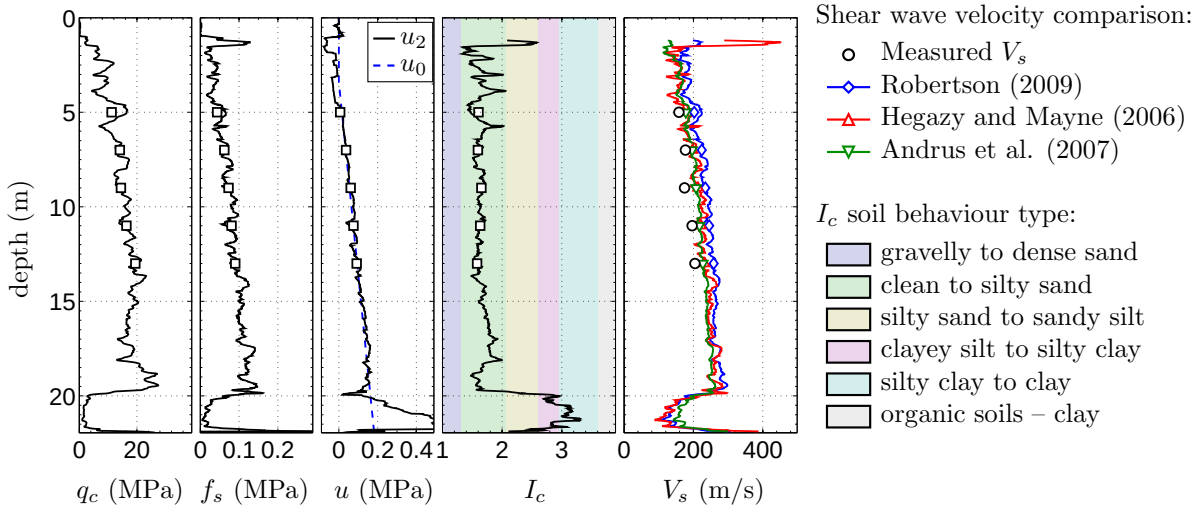

Figure A.85: SCPTu WSW43 (CPT-974) E2485398.25 N5739166.38.

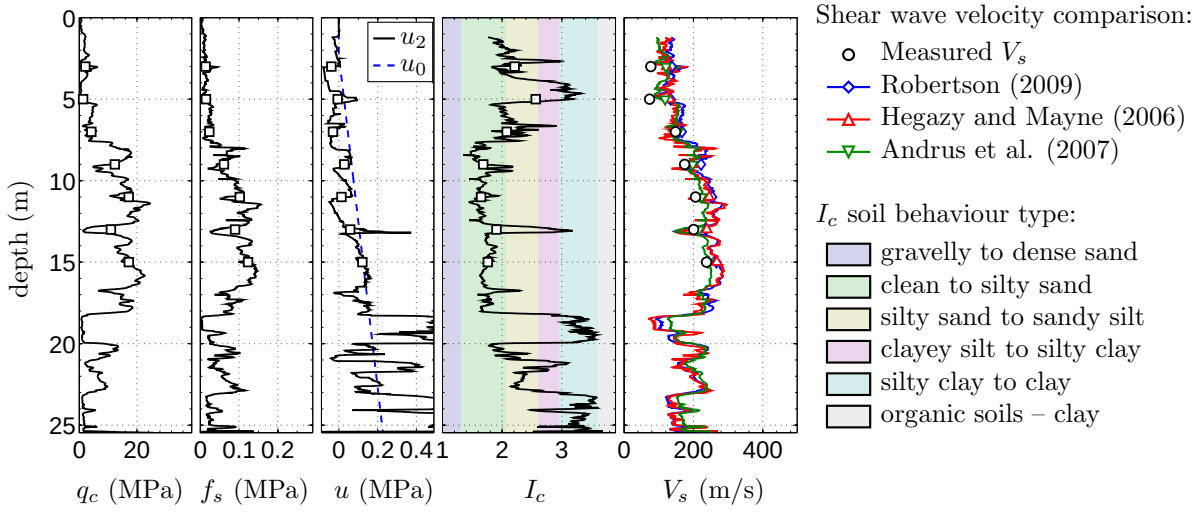

Figure A.86: SCPTu WTM09 (CPT-995) E2482532.30 N5740313.45.

Appendix B

RESIDUAL VARIATIONS FOR REGRESSION FUNCTIONAL FORMS

The residuals (see Equation 4.7) computed between the estimated regression lines and measured shear wave velocity data points are plotted against raw cone tip resistance, q_c, frictional resistance, f_s, depth, z, estimated V_s, and the I_c soil behaviour type index in Figures B.2–B.1. The marker colours correspond to the I_c value or depth of the data points as indicated on each figure or page. The black lines represent the moving averages (solid lines) with 95% confidence intervals (dashed lines) for each set of residuals. The regression functional forms are indicated by Equation number noted in Chapter 4, with Equation 4.1 corresponding to the form of Andrus et al. (2007), Equation 4.2 to the form of Hegazy and Mayne (2006), Equation 4.3 to the form of Robertson (2009), Equation 4.4 to the form of Wair et al. (2012), and Equations 4.5 and 4.6 to hybrid forms that combine different terms from the regression functions of Andrus et al. (2007) and Wair et al. (2012).

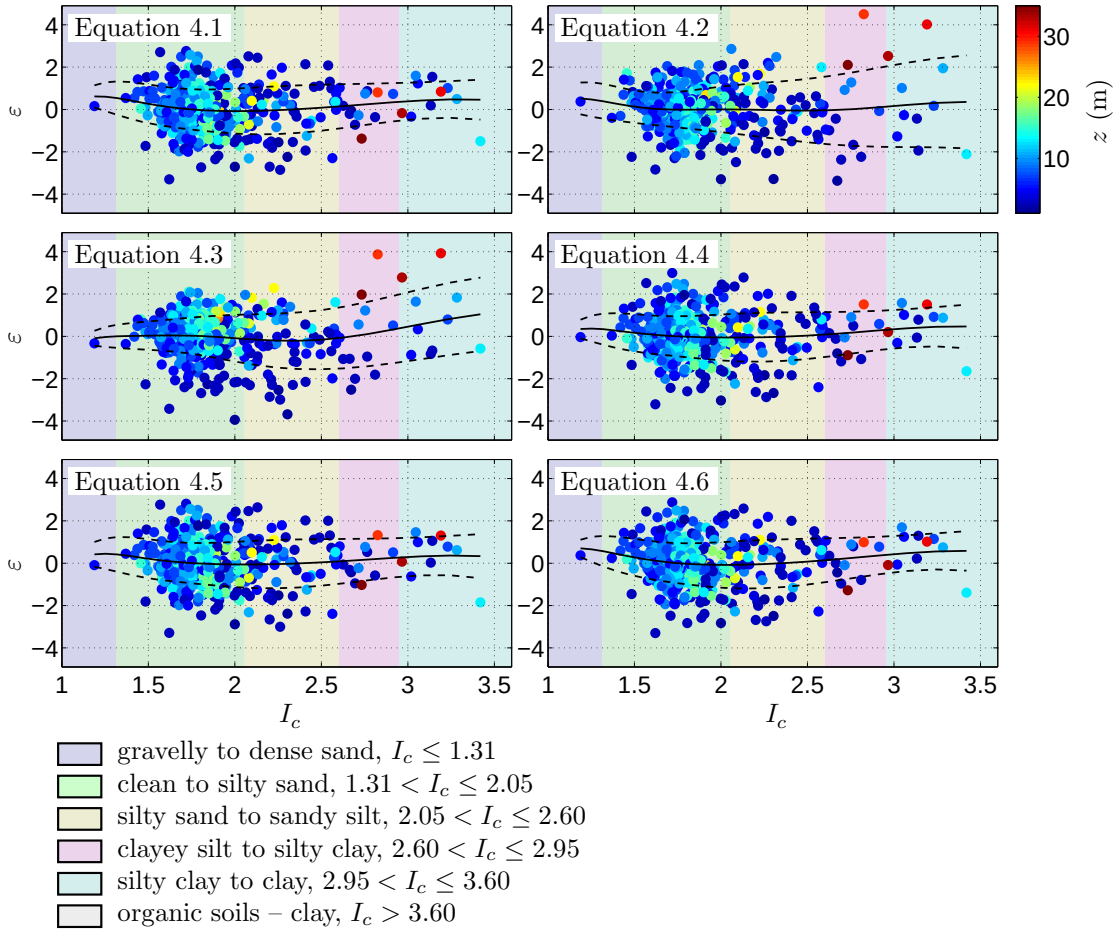

Figure B.1: Variation of residuals with I_c for indicated regression forms.

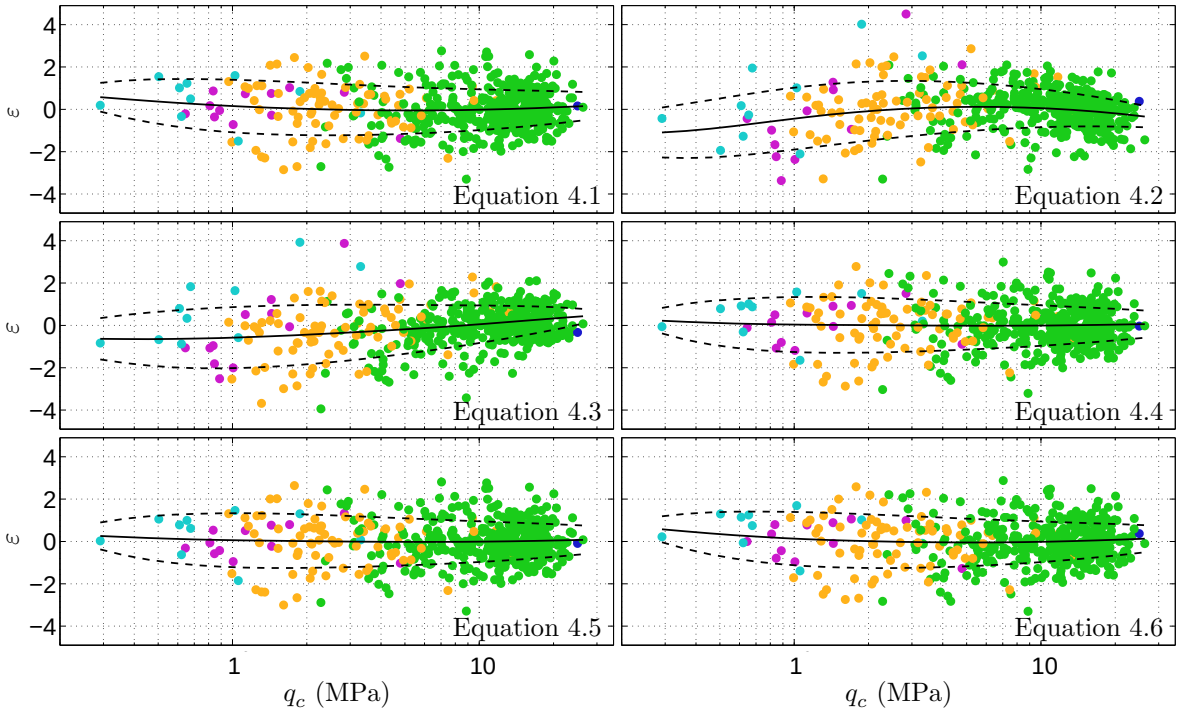

Figure B.2: Variation of residuals with cone tip resistance, q_c, for indicated regression forms.

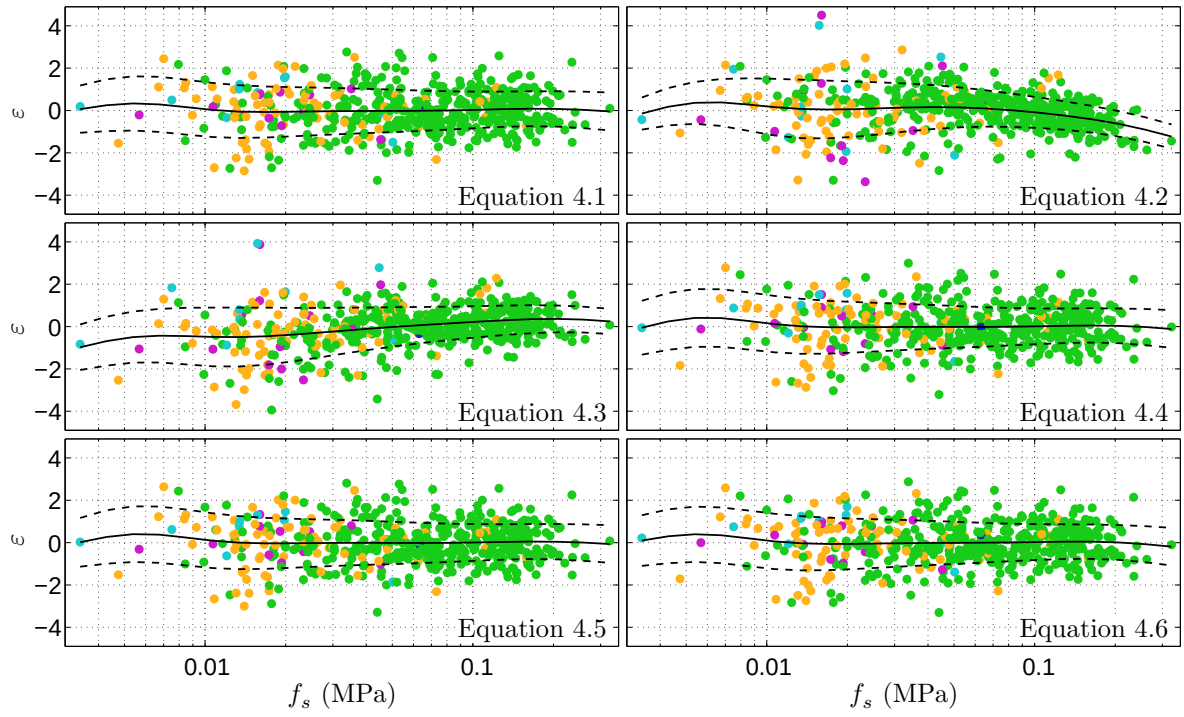

- gravelly to dense sand, $I_c \leq 1.31$
- clean to silty sand, $1.31 < I_c \leq 2.05$
- silty sand to sandy silt, $2.05 < I_c \leq 2.60$
- clayey silt to silty clay, $2.60 < I_c \leq 2.95$
- silty clay to clay, $2.95 < I_c \leq 3.60$
- organic soils – clay, $I_c > 3.60$

Figure B.3: Variation of residuals with friction resistance, f_s, for indicated regression forms.

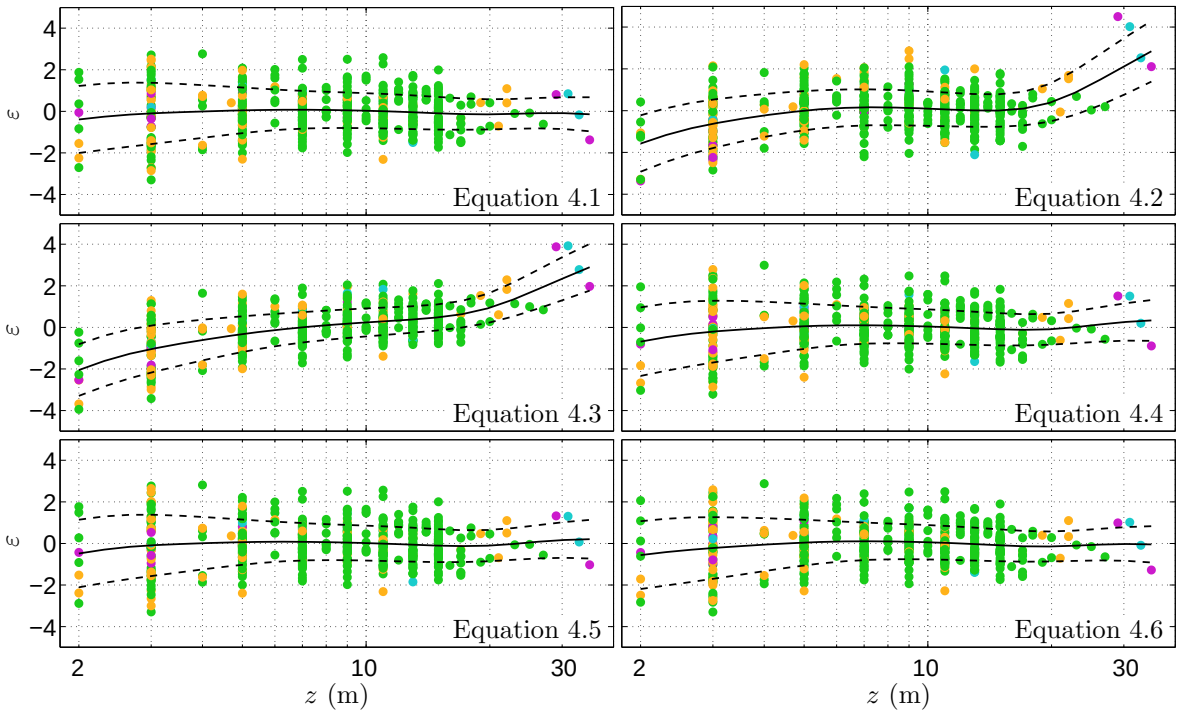

Figure B.4: Variation of residuals with depth, z, for indicated regression forms.

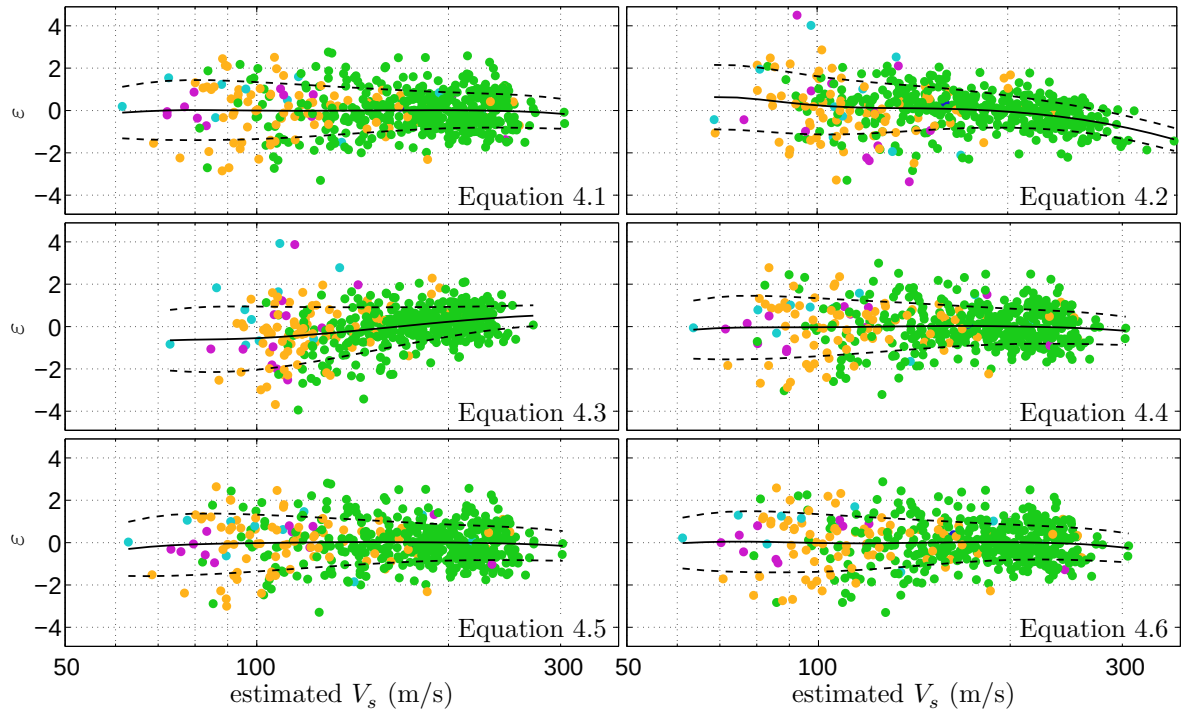

- gravelly to dense sand, $I_c \leq 1.31$
- clean to silty sand, $1.31 < I_c \leq 2.05$
- silty sand to sandy silt, $2.05 < I_c \leq 2.60$
- clayey silt to silty clay, $2.60 < I_c \leq 2.95$
- silty clay to clay, $2.95 < I_c \leq 3.60$
- organic soils – clay, $I_c > 3.60$

Figure B.5: Variation of residuals with estimated V_s for indicated regression forms.

Appendix C

MEASURED AND ESTIMATED V_s PROFILES FOR DATABASE SITES

The CPT tip resistance, q_c, frictional resistance, f_s, hydrostatic pore pressure, u_0, measured pore pressure, u_2, and computed I_c soil behaviour type index profiles for each site in the Canterbury SCPTu database are shown in Figures C.1–C.86. These plots include a comparison of the measured V_s profiles (white circular markers) with the median predicted V_s profiles (solid blue lines) estimated using the Canterbury-specific CPT-V_s correlation given in Equation 4.10. The shaded regions bounded by dashed lines represent the 16th and 84th percentile predictions computed using Equation 4.12 for each case. The SCPTu ID and associated Canterbury Geotechnical Database CPT number (in parentheses) are noted for each site along with the Easting-Northing site locations.

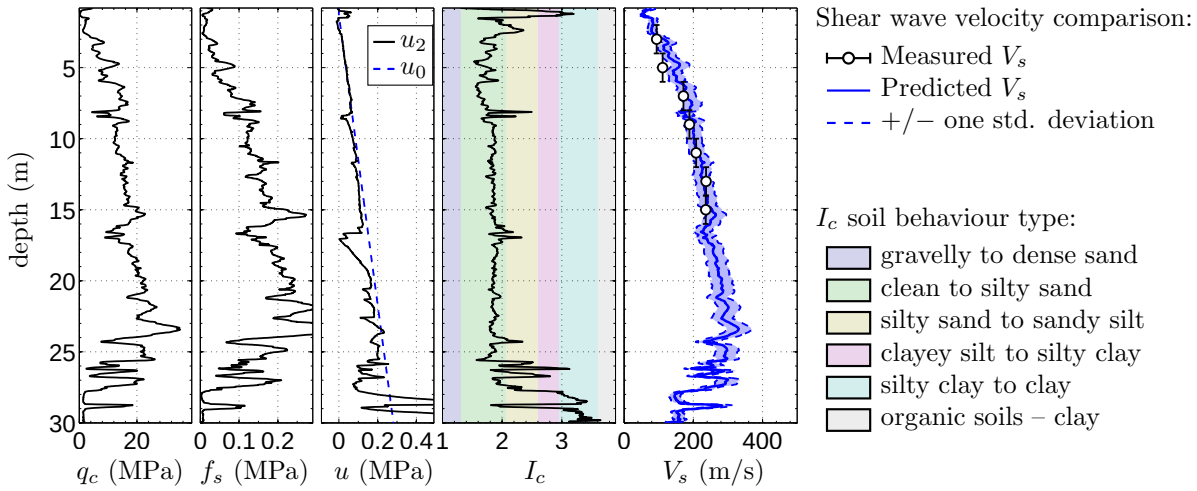

Figure C.1: SCPTu ARN03 (CPT-3) E2486512.58 N5743861.75.

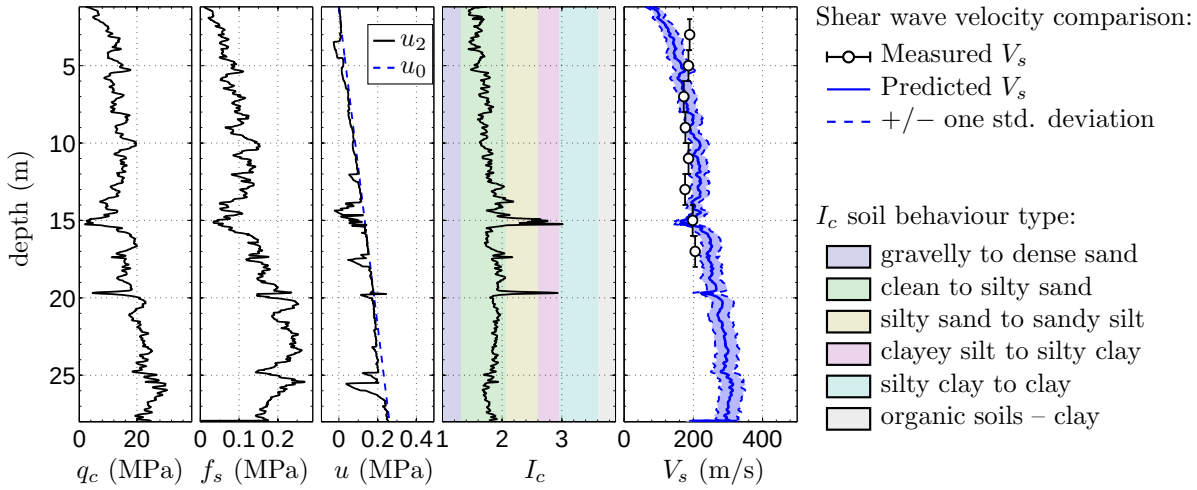

Figure C.2: SCPTu ARN09 (CPT-9) E2485920.04 N5743126.63.

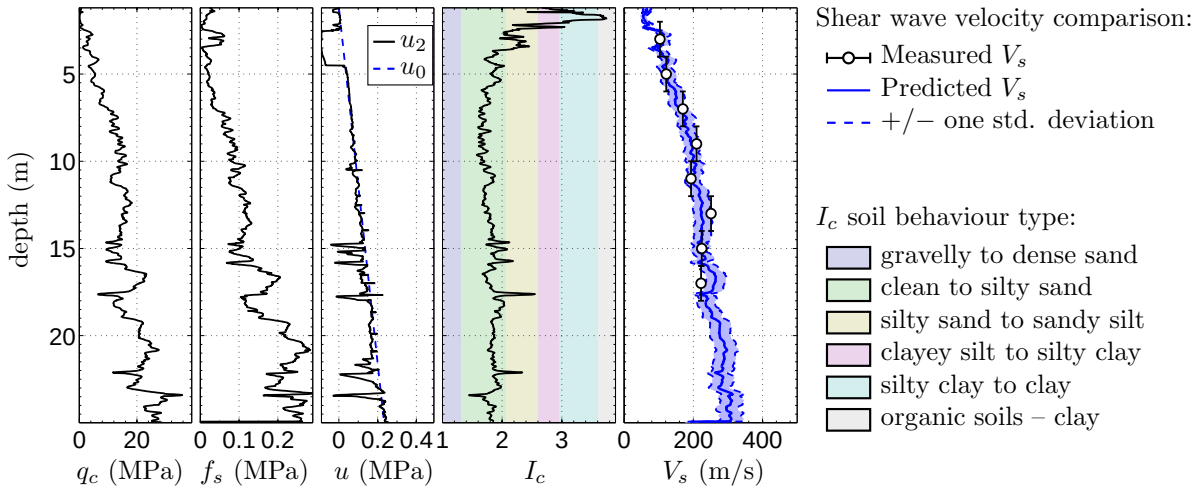

Figure C.3: SCPTu ARN19 (CPT-19) E2486449.96 N5743141.33.

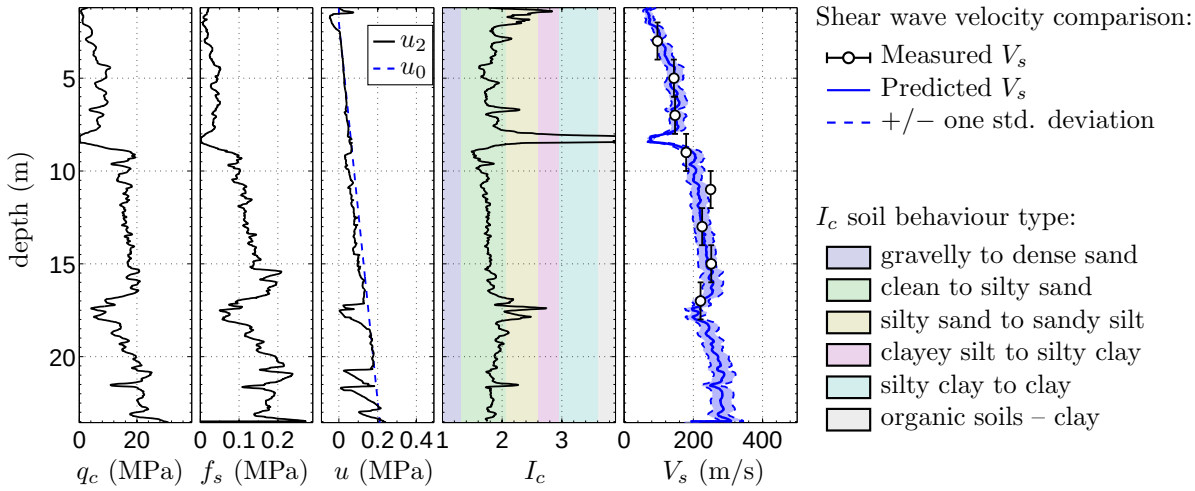

Figure C.4: SCPTu ARN25 (CPT-25) E2486613.15 N5743869.23.

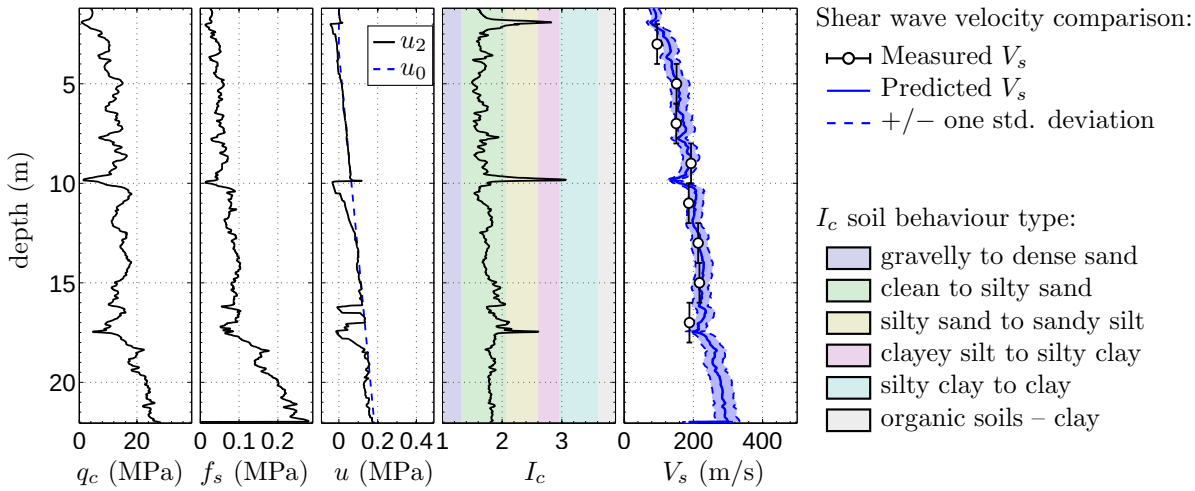

Figure C.5: SCPTu ARN27 (CPT-27) E2486130.57 N5743990.60.

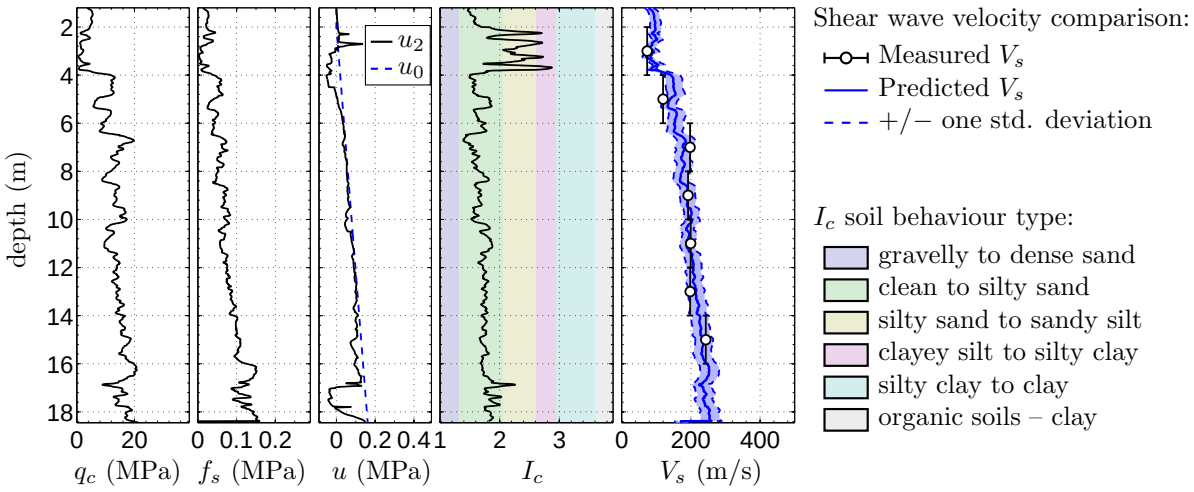

Figure C.6: SCPTu ARN28 (CPT-28) E2486352.61 N5744307.41.

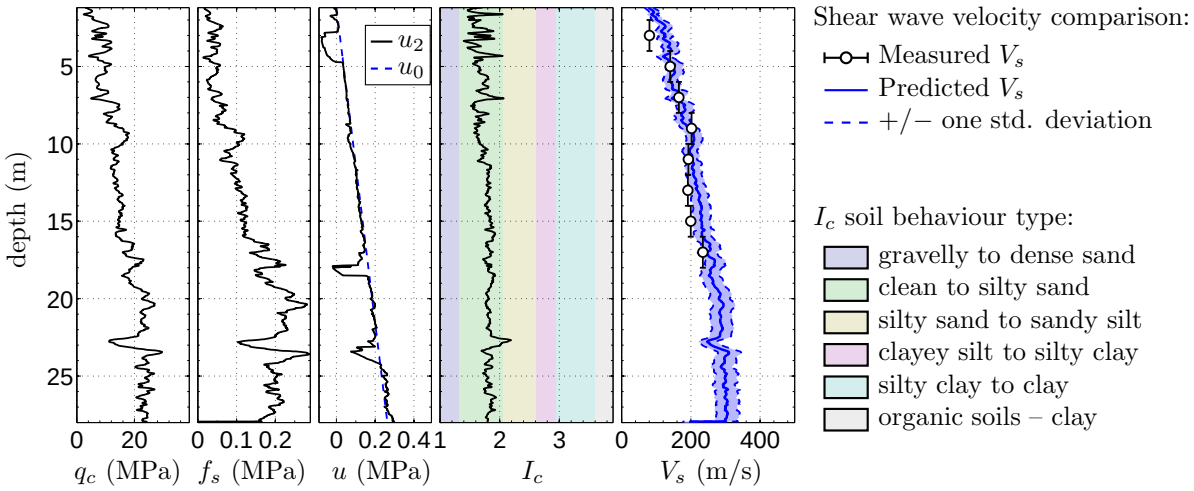

Figure C.7: SCPTu ARN29 (CPT-29) E2486571.38 N5744149.65.

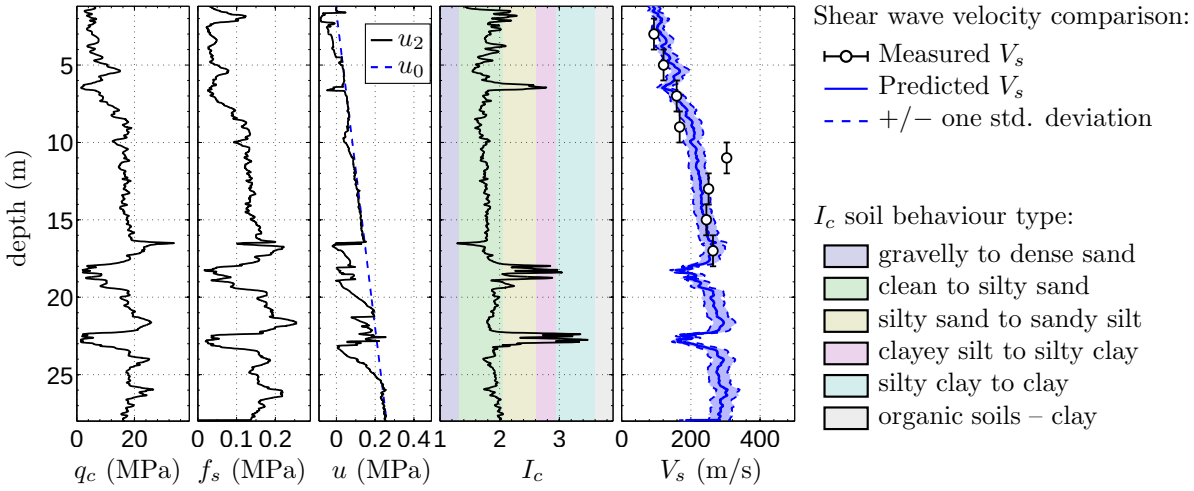

Figure C.8: SCPTu ARN34 (CPT-34) E2486810.77 N5744461.05.

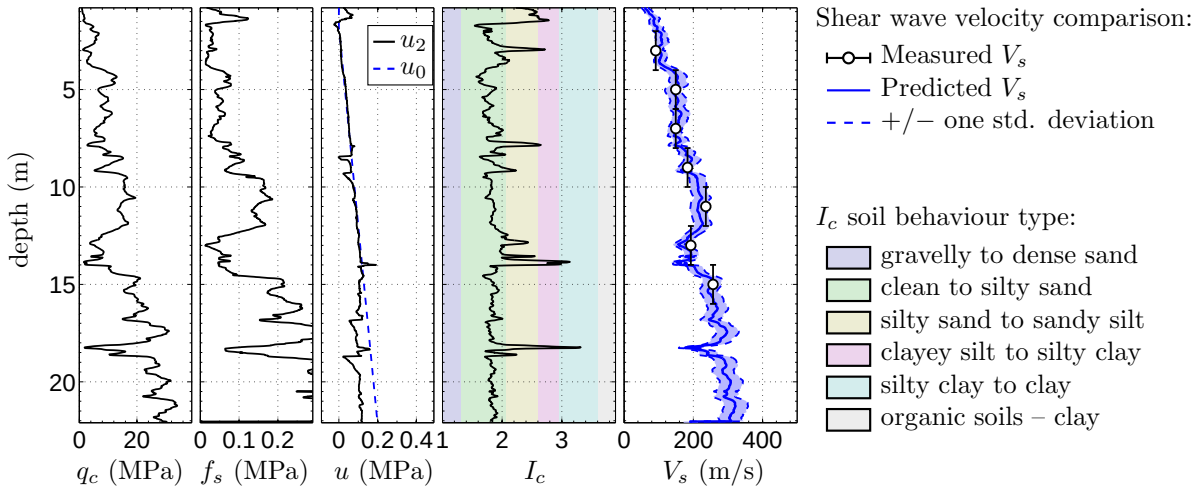

Figure C.9: SCPTu AVD02 (CPT-36) E2484604.59 N5744501.00.

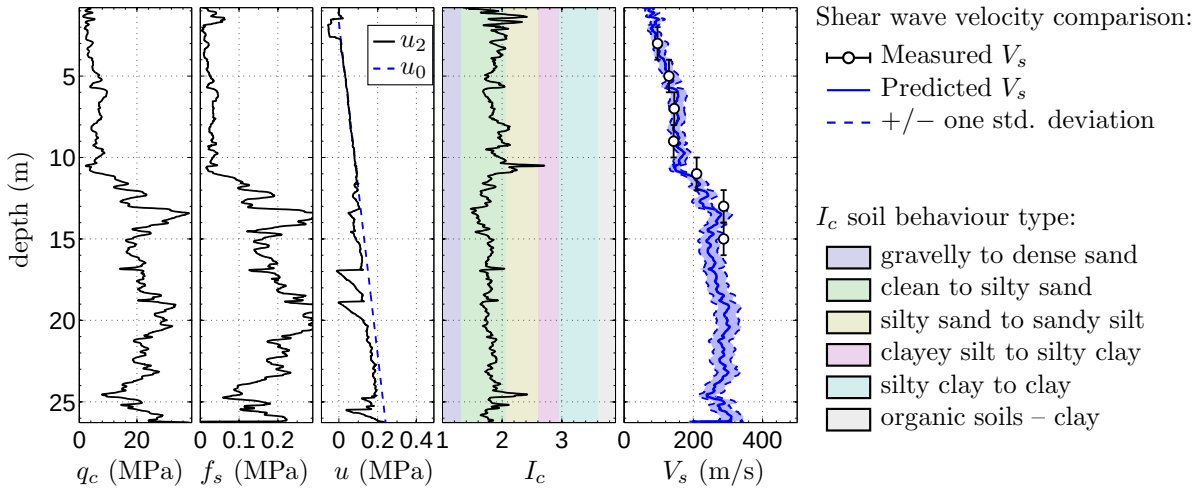

Figure C.10: SCPTu AVD09 (CPT-43) E2484547.92 N5745096.05.

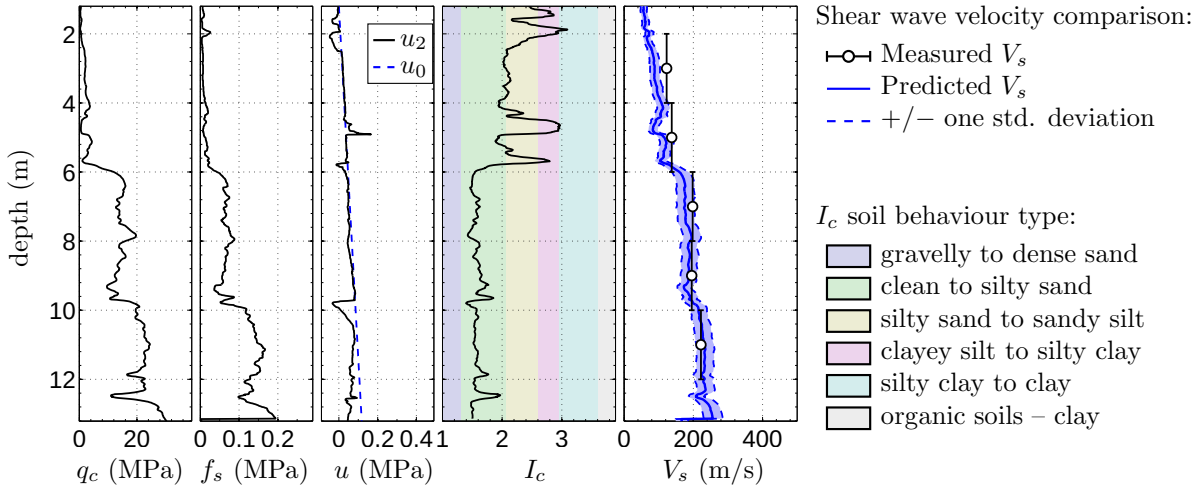

Figure C.11: SCPTu AVL03 (CPT-92) E2481679.63 N5742615.49.

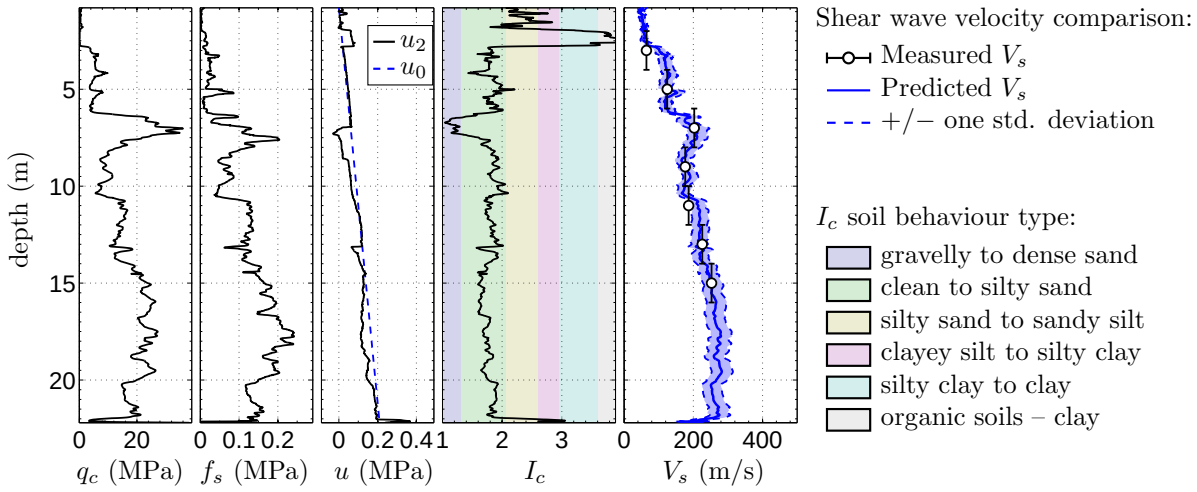

Figure C.12: SCPTu AVS14 (CPT-108) E2482869.70 N5743026.94.

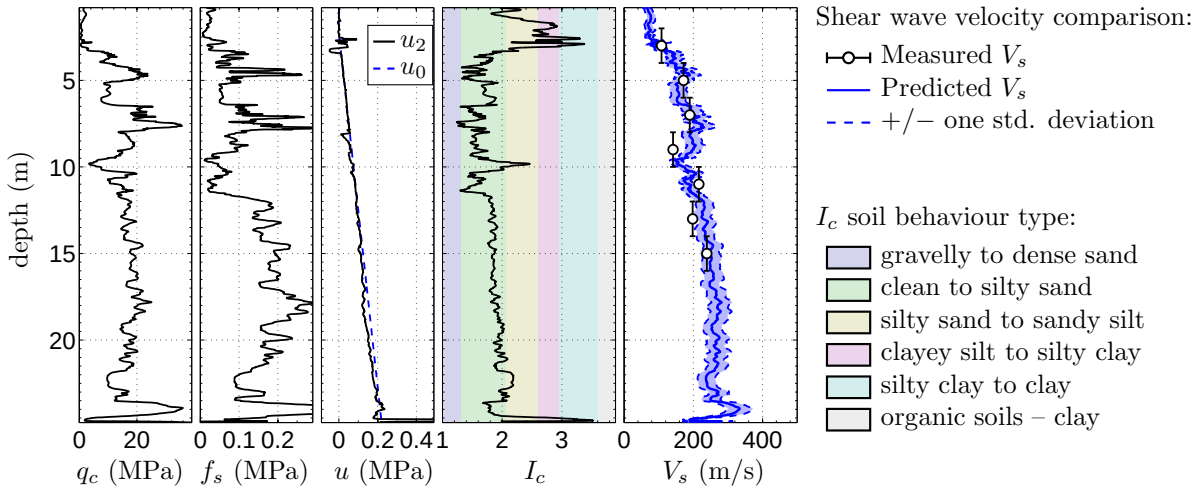

Figure C.13: SCPTu AVS16 (CPT-110) E2483172.56 N5743169.95.

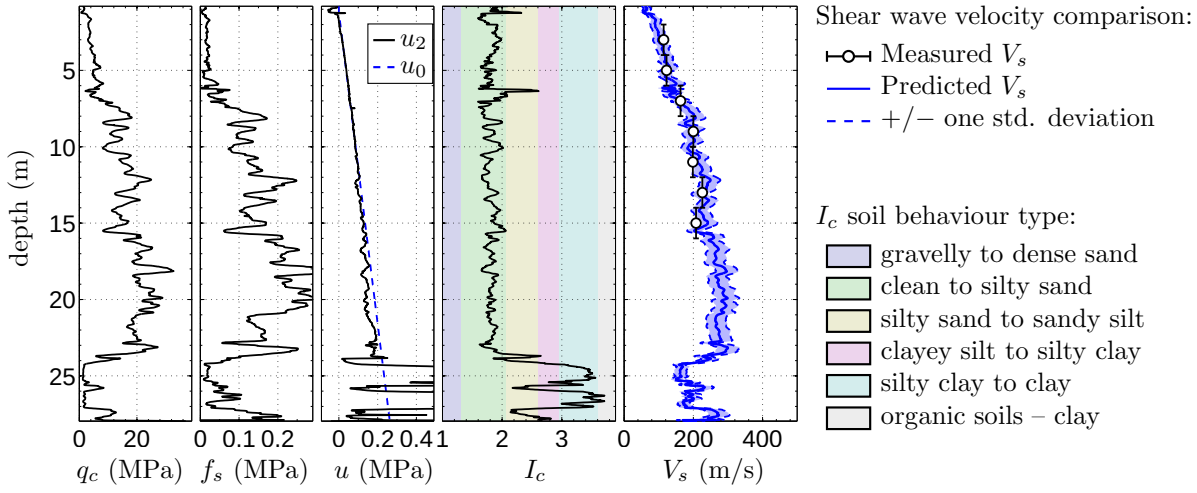

Figure C.14: SCPTu AVS21 (CPT-115) E2483488.92 N5743376.06.

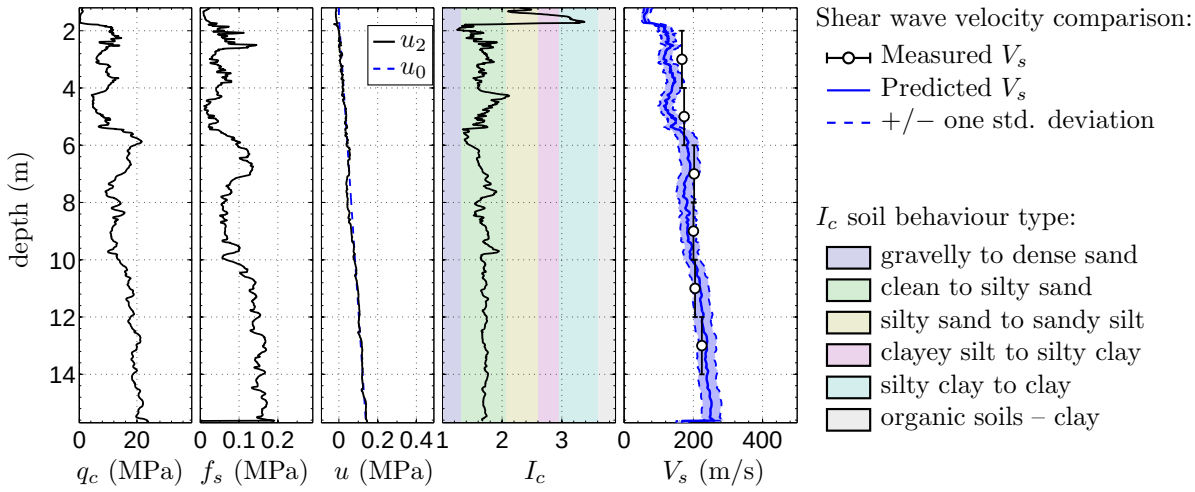

Figure C.15: SCPTu AVS22 (CPT-116) E2482981.25 N5743477.02.

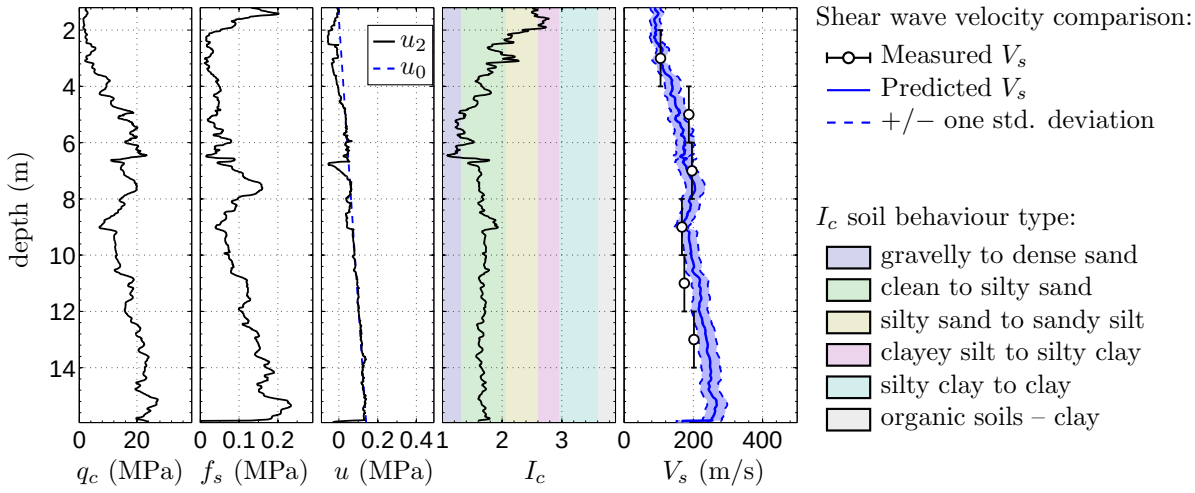

Figure C.16: SCPTu AVS49 (CPT-137) E2483716.42 N5742749.17.

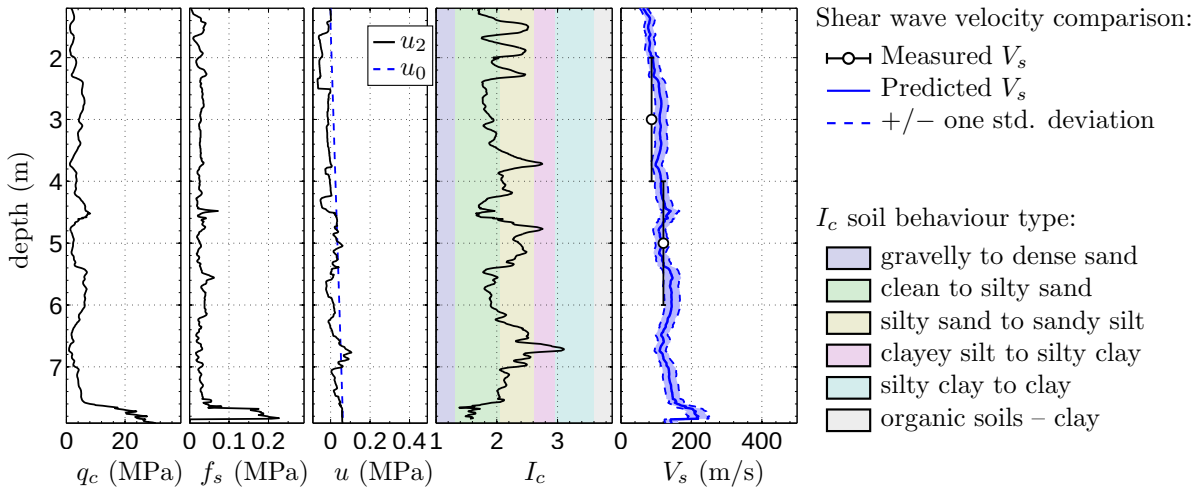

Figure C.17: SCPTu BDL03 (CPT-145) E2475526.77 N5747008.16.

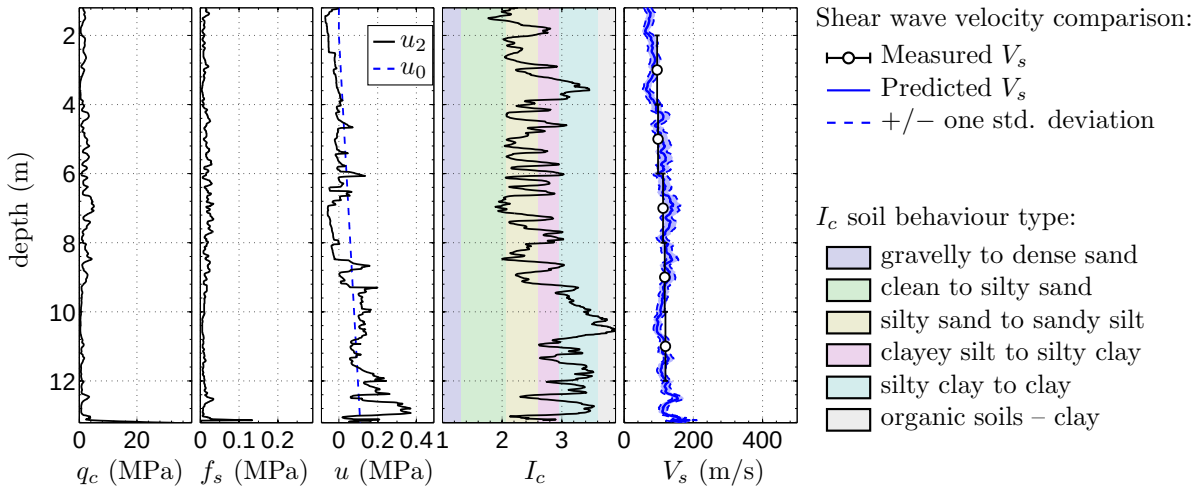

Figure C.18: SCPTu BDL08 (CPT-150) E2476410.74 N5747328.40.

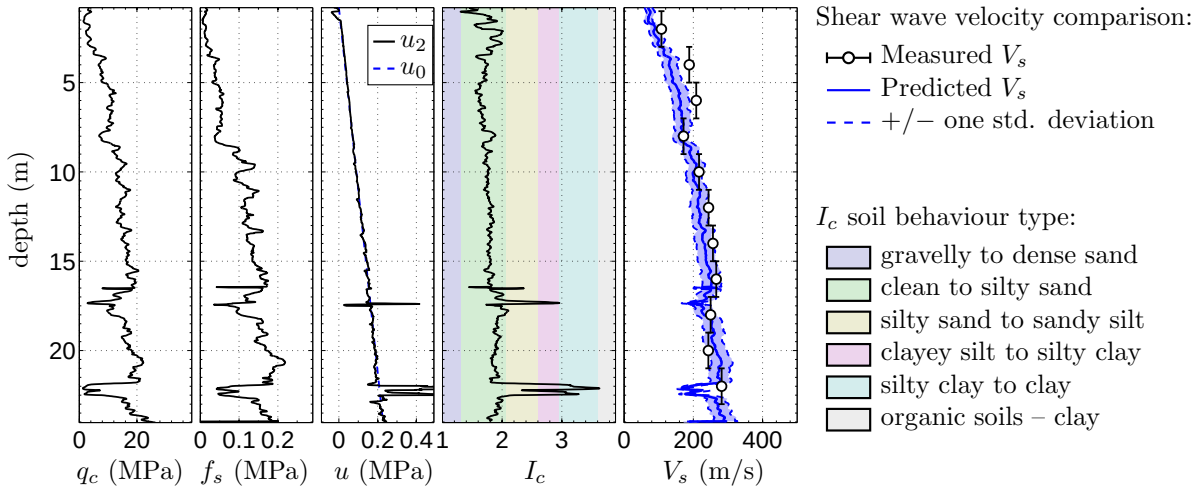

Figure C.19: SCPTu BEX15 (CPT-167) E2487522.33 N5744064.06.

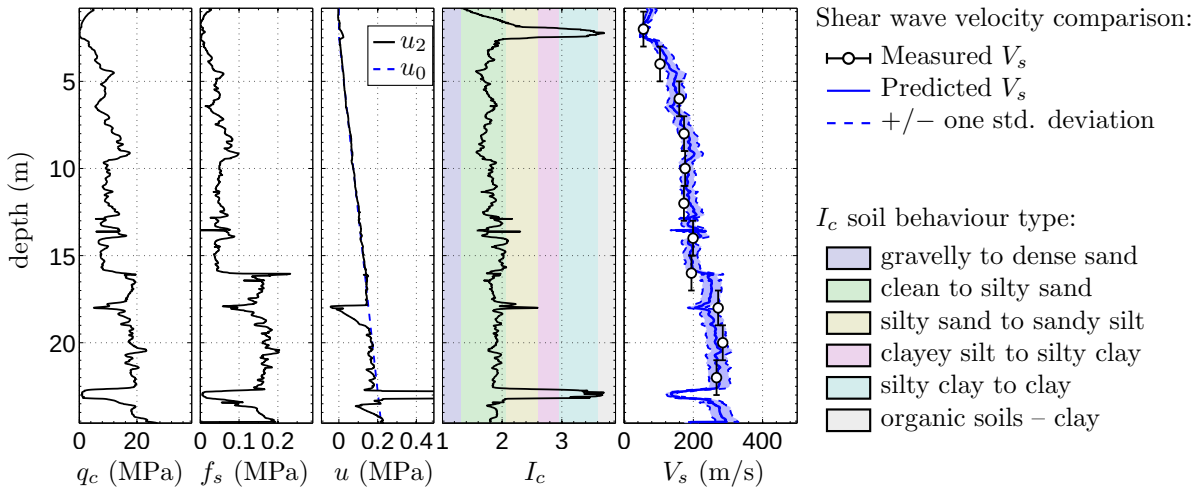

Figure C.20: SCPTu BEX17 (CPT-169) E2487273.26 N5744320.98.

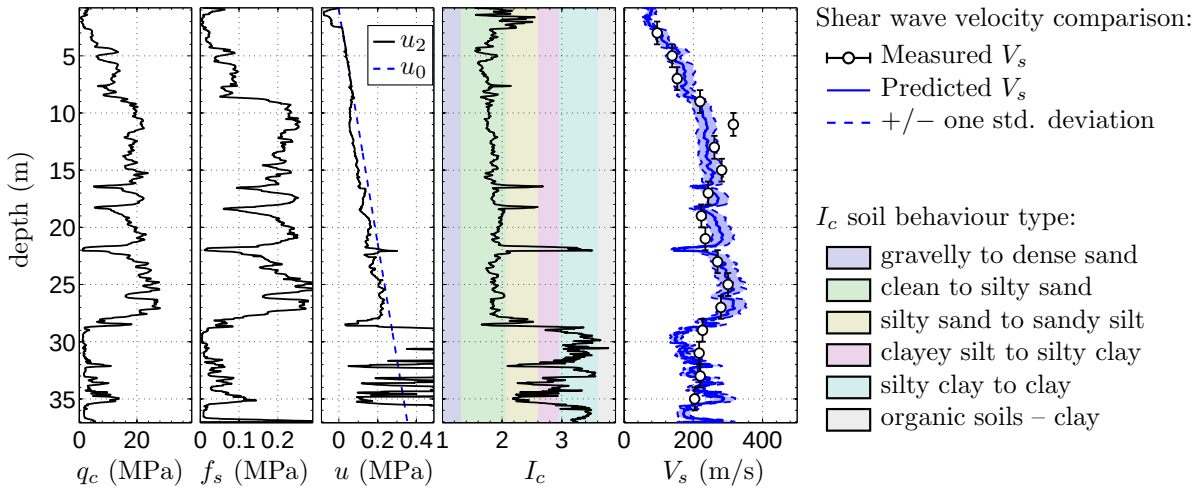

Figure C.21: SCPTu BEX19 (CPT-171) E2486919.80 N5744438.91.

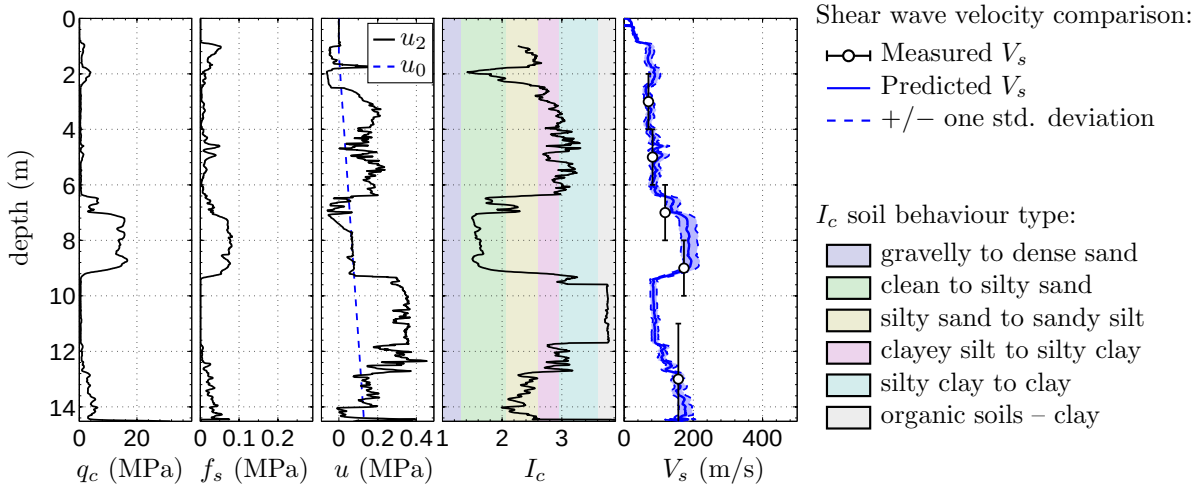

Figure C.22: SCPTu BKM12 (CPT-207) E2481292.89 N5738183.06.

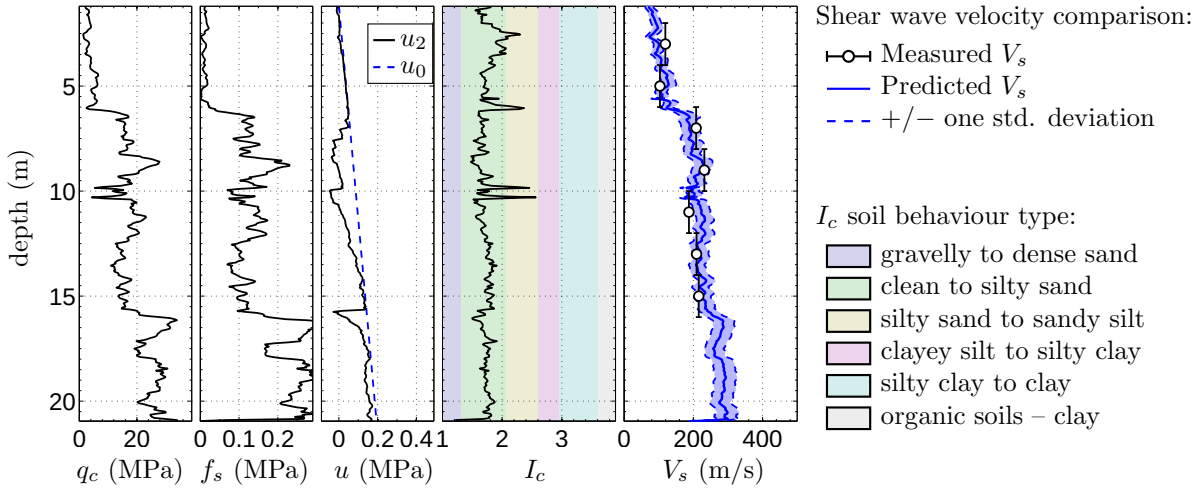

Figure C.23: SCPTu BUR30 (CPT-291) E2483884.34 N5745481.95.

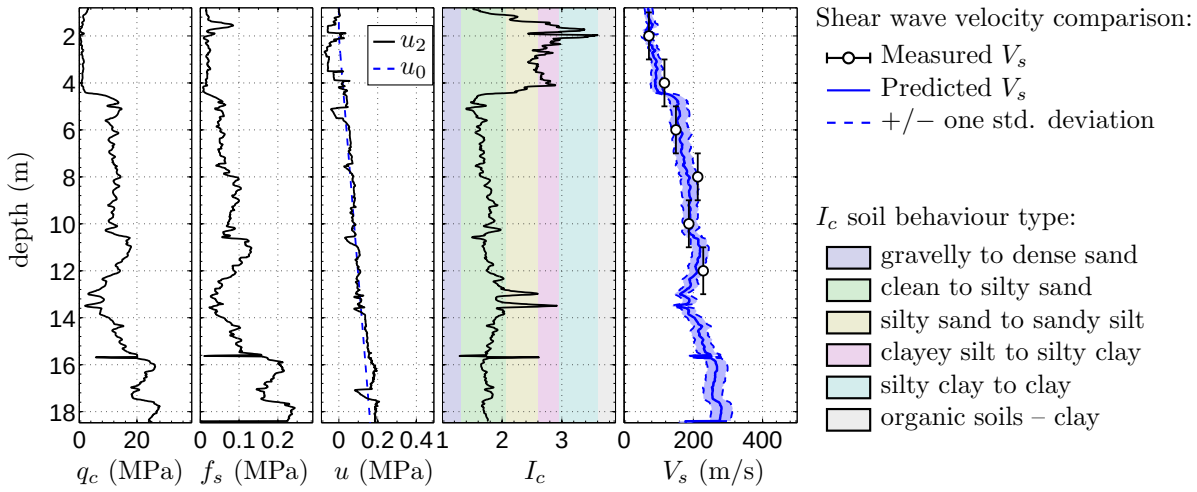

Figure C.24: SCPTu BUR36 (CPT-297) E2484228.47 N5746352.35.

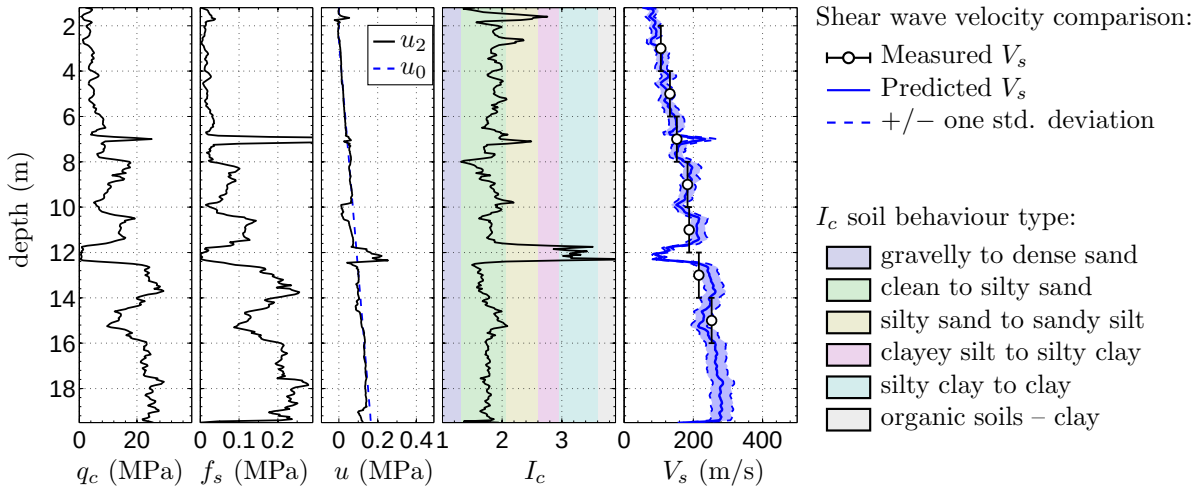

Figure C.25: SCPTu BUR40 (CPT-301) E2485244.01 N5745047.00.

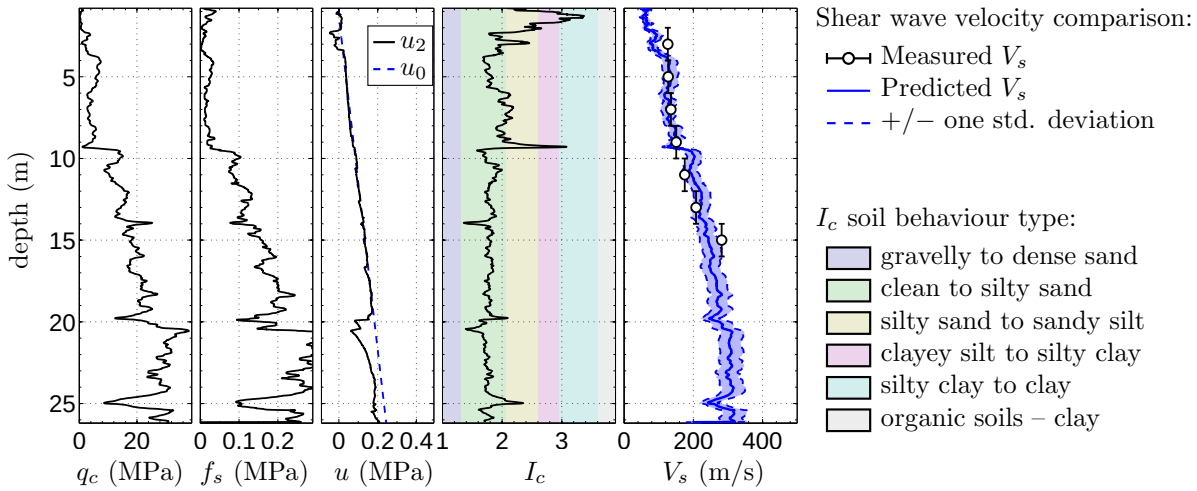

Figure C.26: SCPTu BUR45 (CPT-306) E2485779.75 N5745636.58.

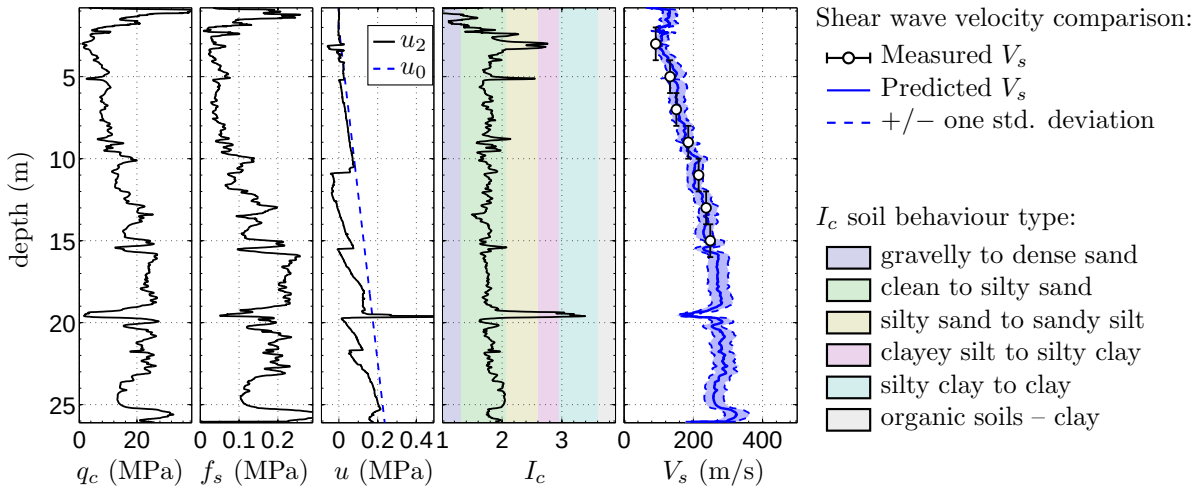

Figure C.27: SCPTu BUR48 (CPT-309) E2484876.17 N5746351.59.

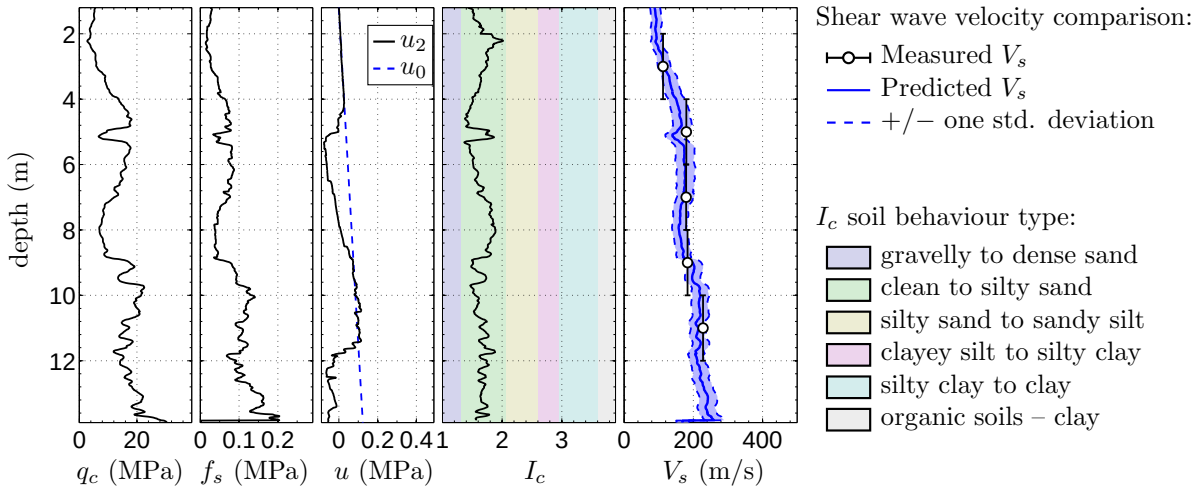

Figure C.28: SCPTu BUR96 (CPT-347) E2484563.50 N5746718.74.

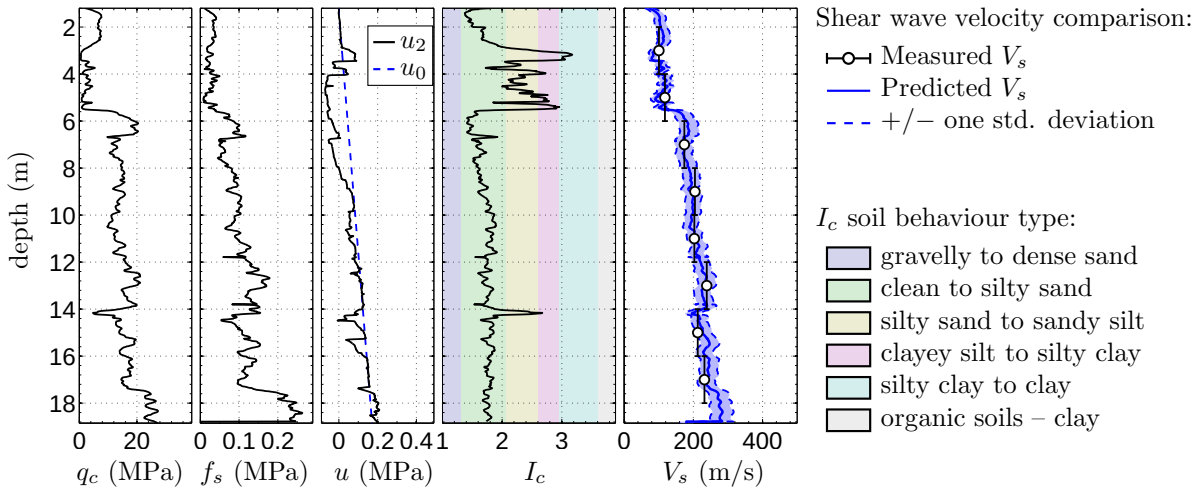

Figure C.29: SCPTu BUR102 (CPT-353) E2484302.27 N5746420.17.

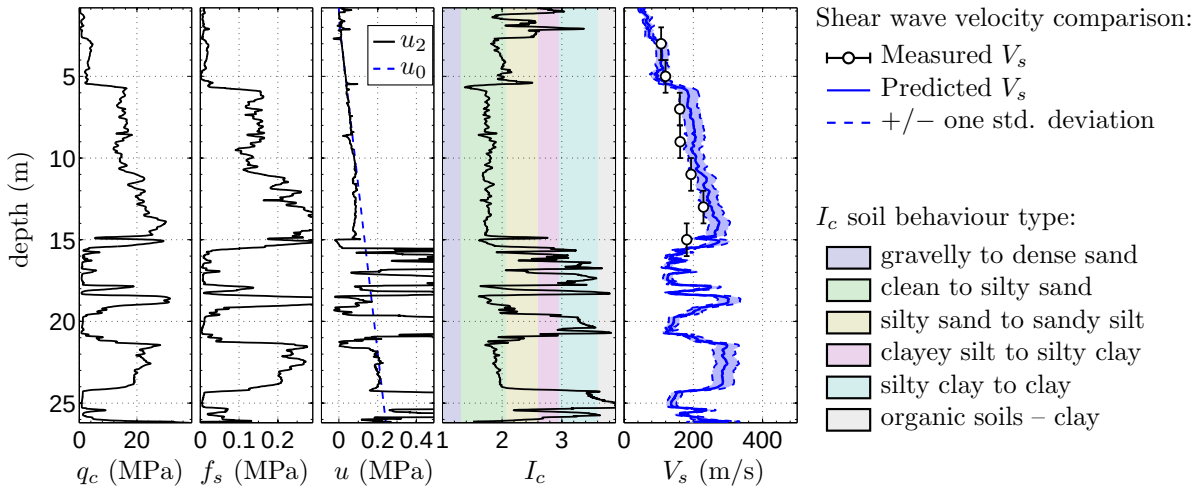

Figure C.30: SCPTu DAL09 (CPT-1086) E2483727.15 N5742924.35.

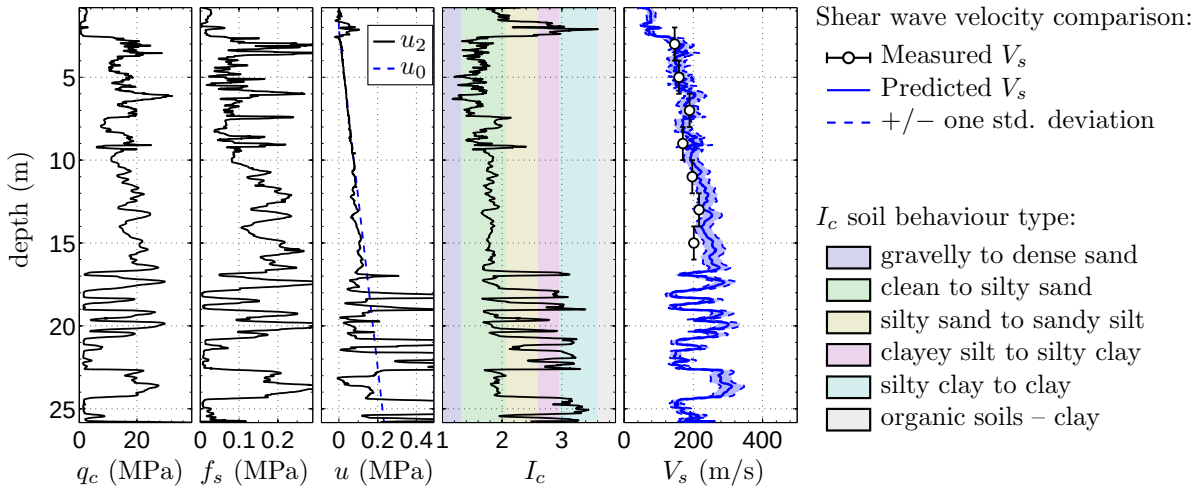

Figure C.31: SCPTu DAL11 (CPT-1088) E2483476.93 N5743226.02.

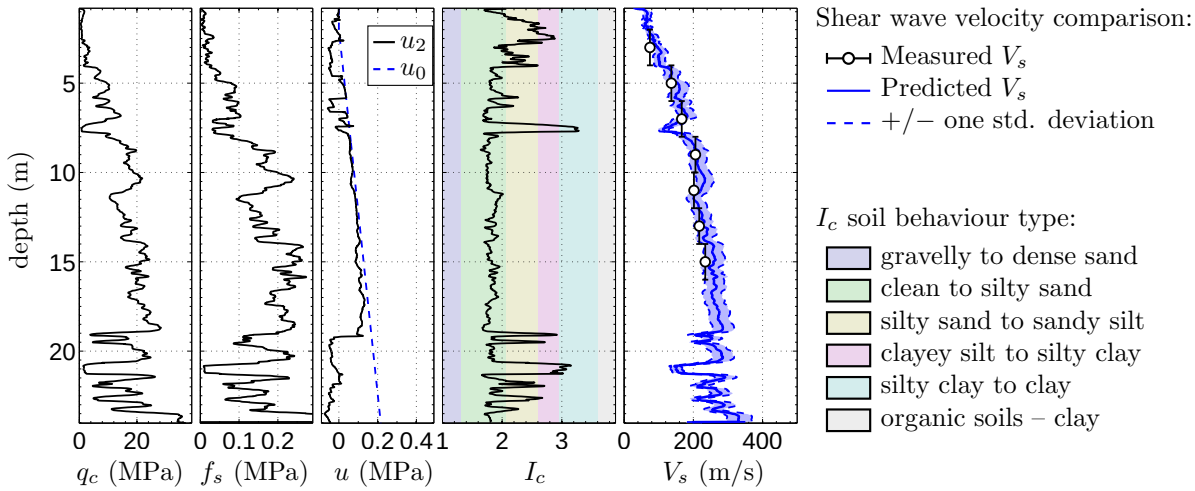

Figure C.32: SCPTu DAL18 (CPT-1095) E2483688.85 N5743389.65.

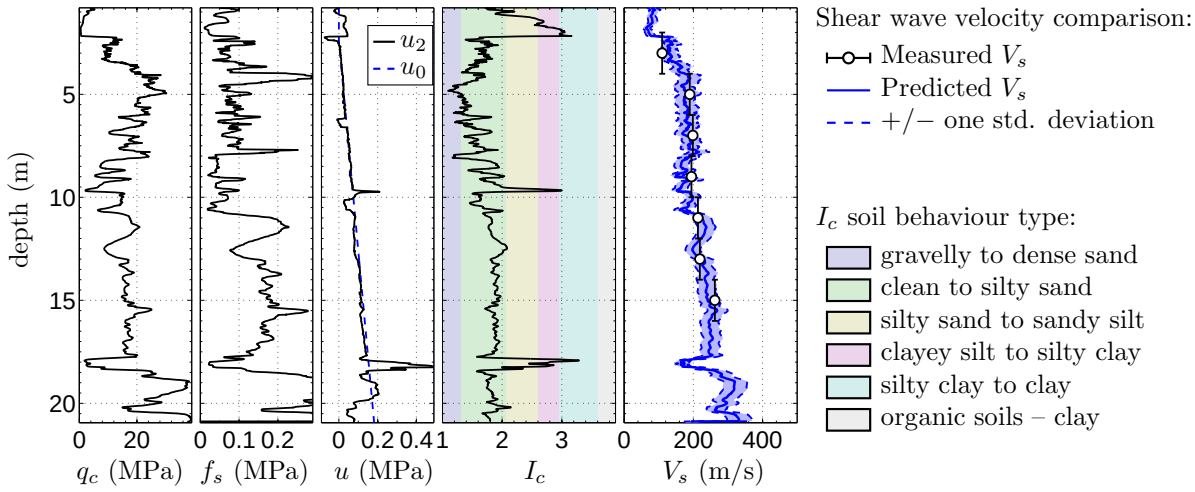

Figure C.33: SCPTu DAL21 (CPT-1098) E2484261.61 N5743602.67.

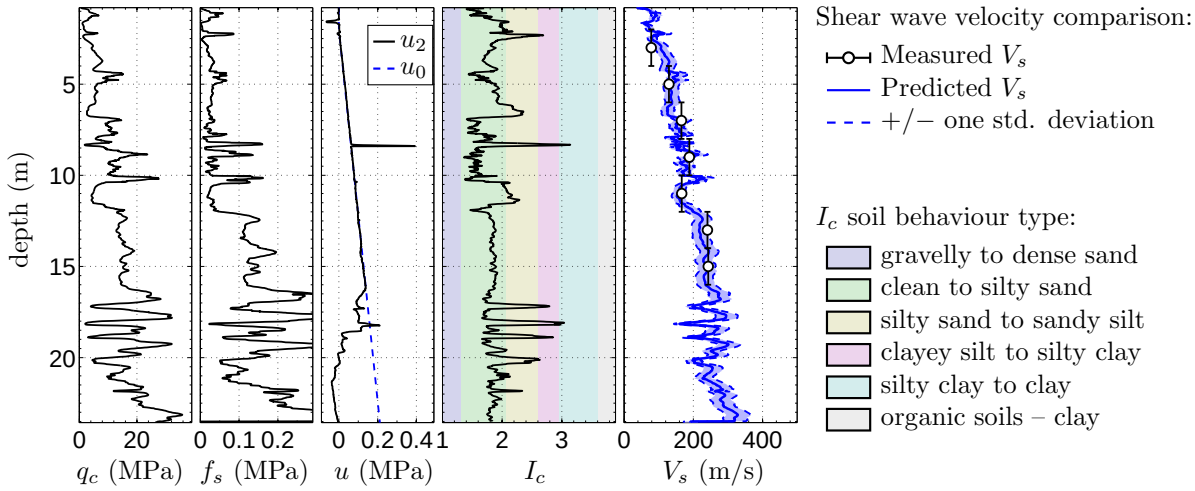

Figure C.34: SCPTu DAL27 (CPT-1104) E2484133.09 N5743960.71.

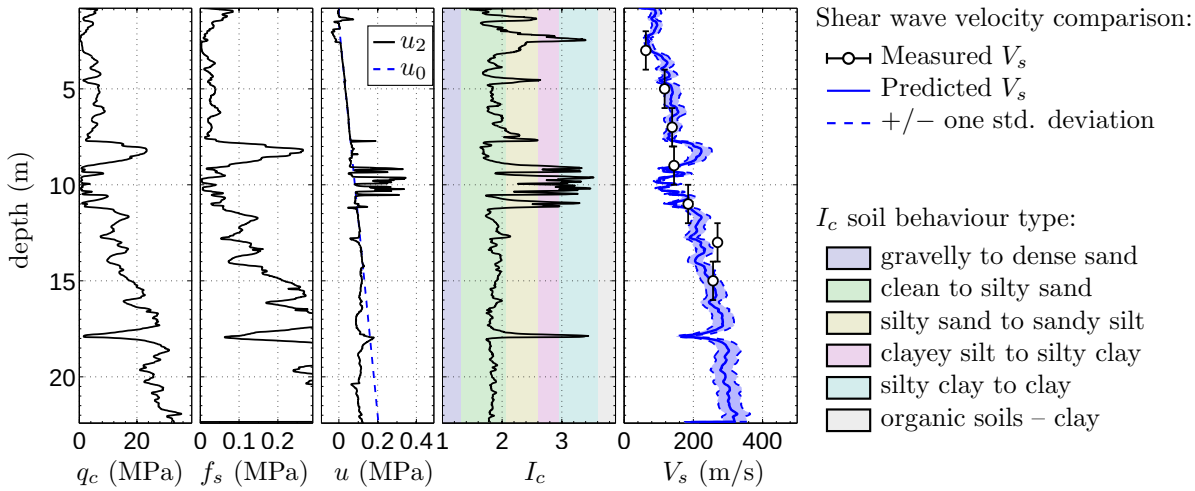

Figure C.35: SCPTu DAL34 (CPT-1111) E2484304.16 N5744359.38.

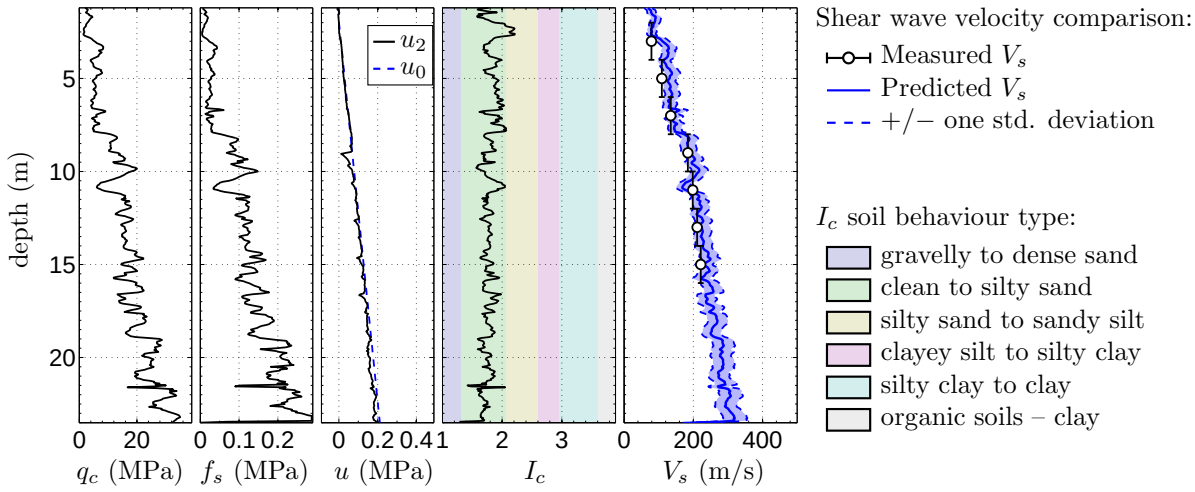

Figure C.36: SCPTu DAL35 (CPT-1112) E2483809.98 N5744535.74.

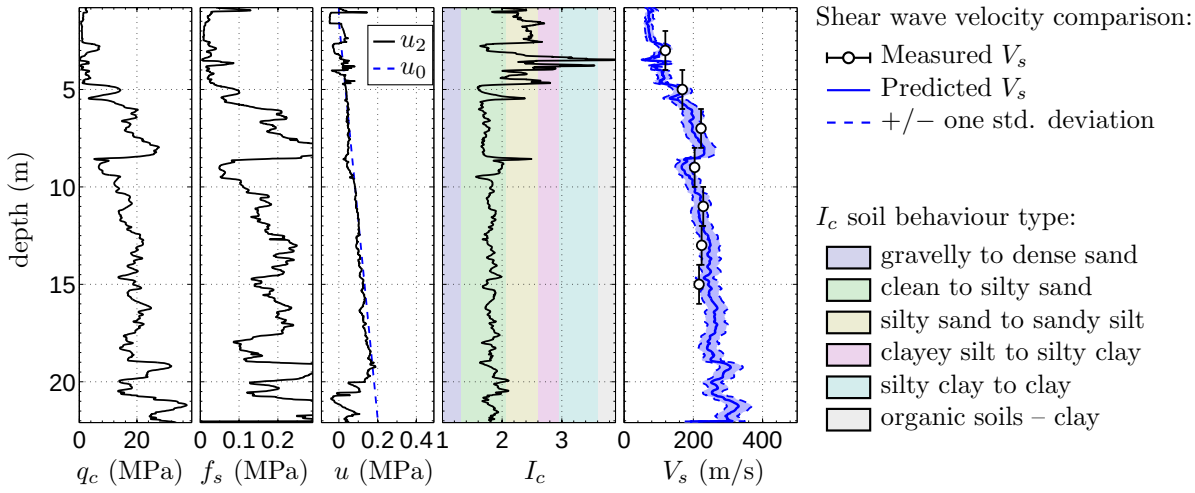

Figure C.37: SCPTu DAL40 (CPT-1117) E2483528.80 N5744091.00.

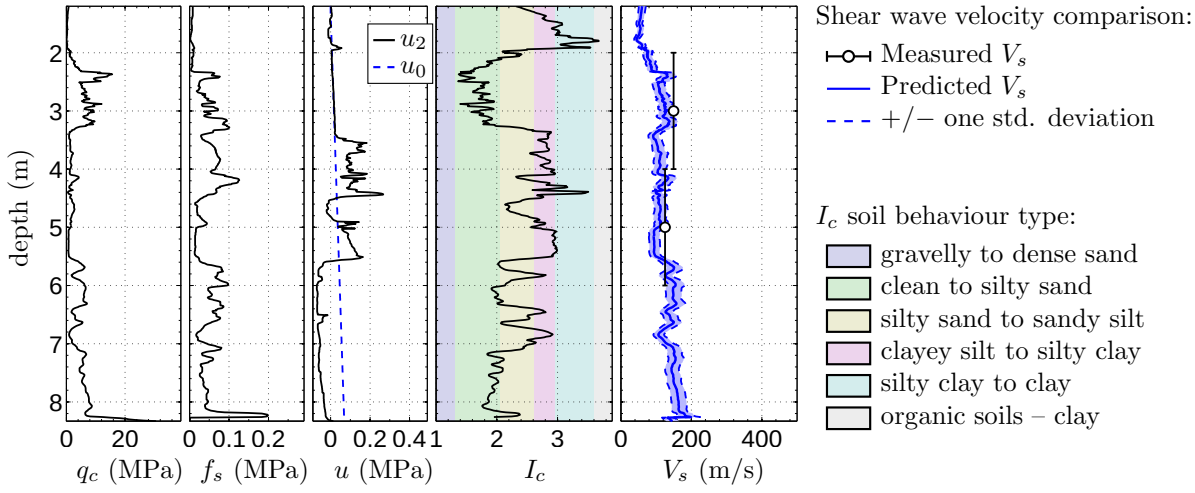

Figure C.38: SCPTu FND10 (CPT-1149) E2477471.51 N5743235.30.

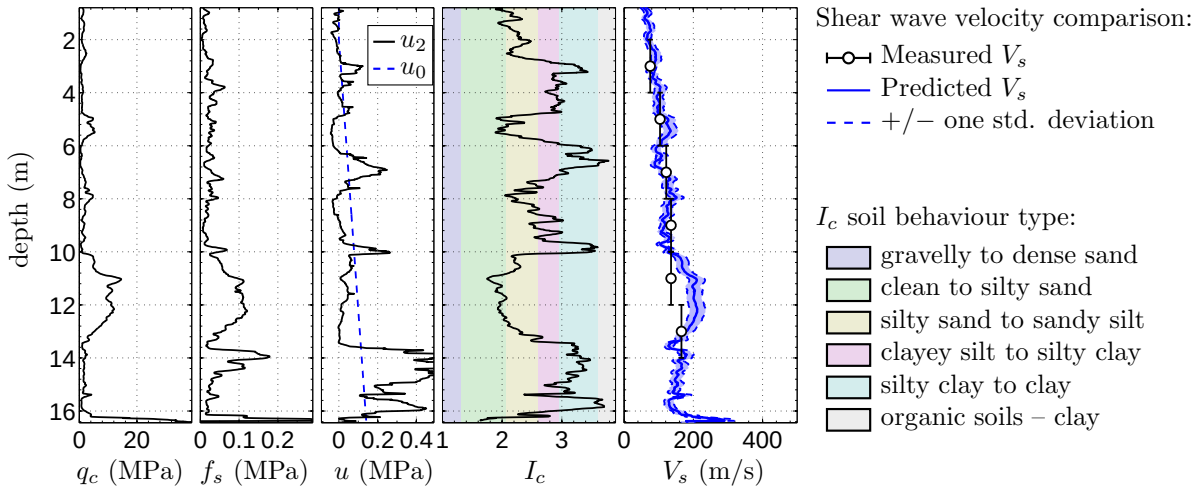

Figure C.39: SCPTu HAL27 (CPT-1192) E2474911.54 N5734791.92.

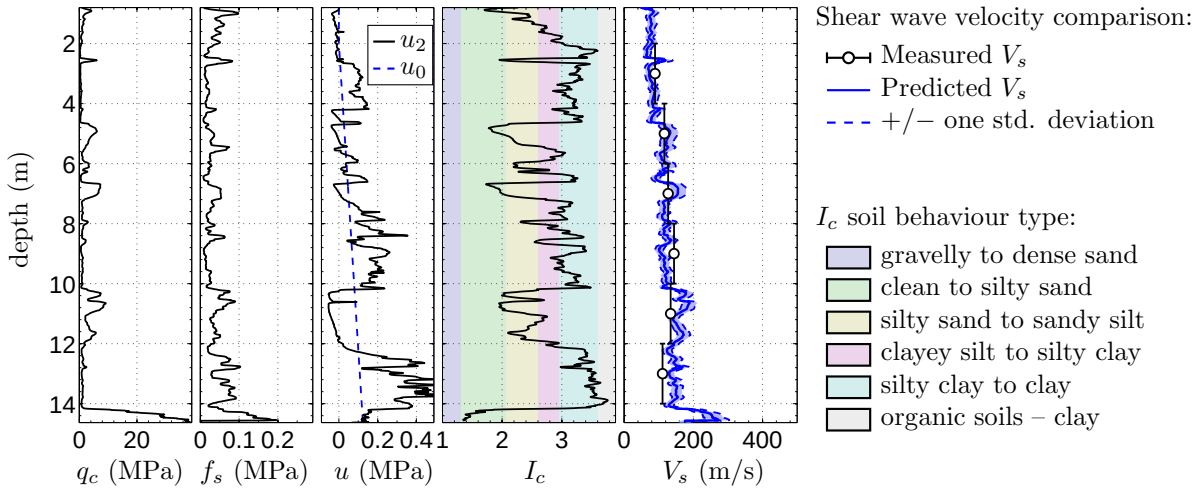

Figure C.40: SCPTu HAL35 (CPT-1200) E2475810.34 N5736625.93.

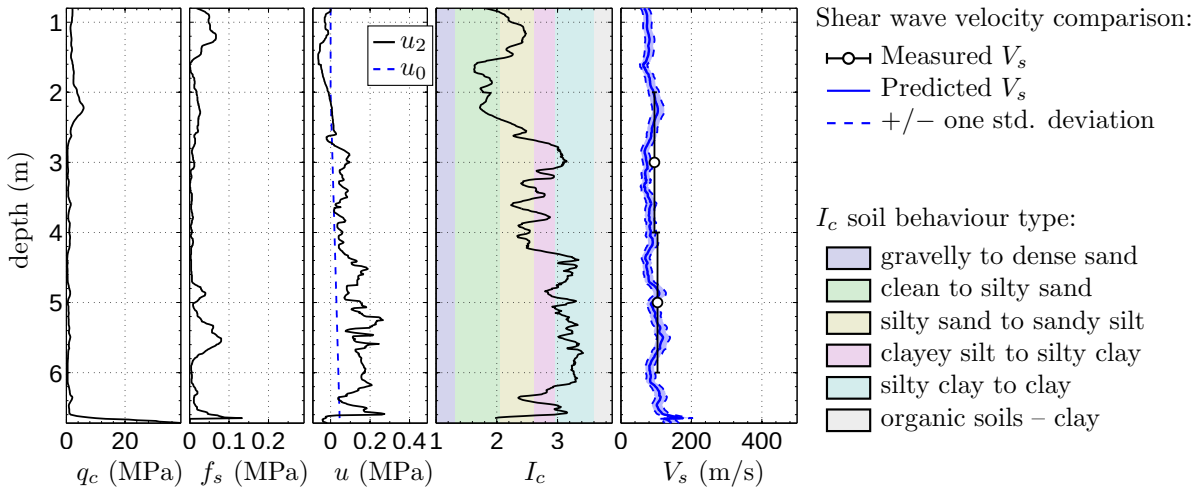

Figure C.41: SCPTu HAL45 (CPT-1210) E2474779.43 N5737377.85.

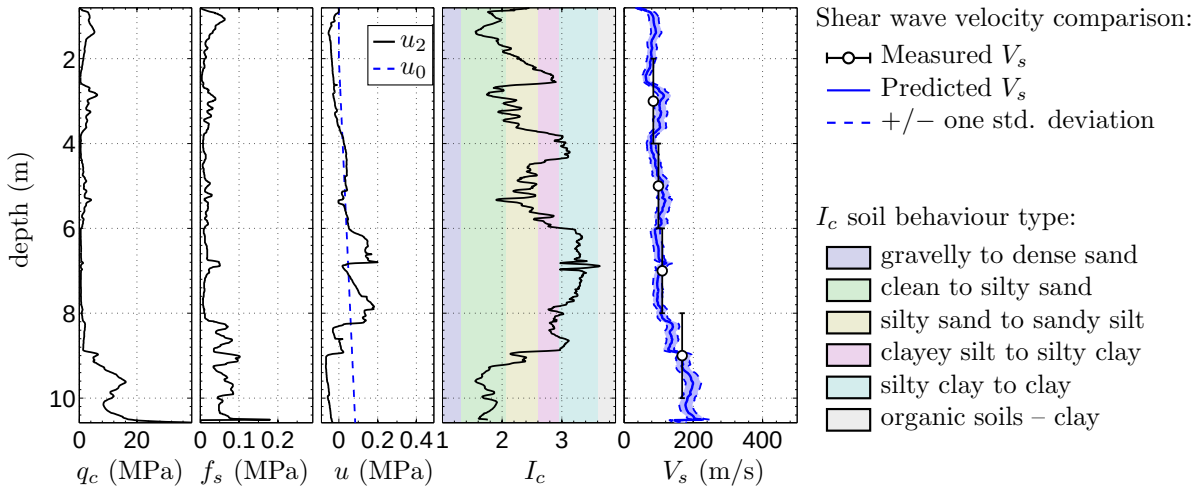

Figure C.42: SCPTu HNH02 (CPT-1200) E2478453.96 N5737651.34.

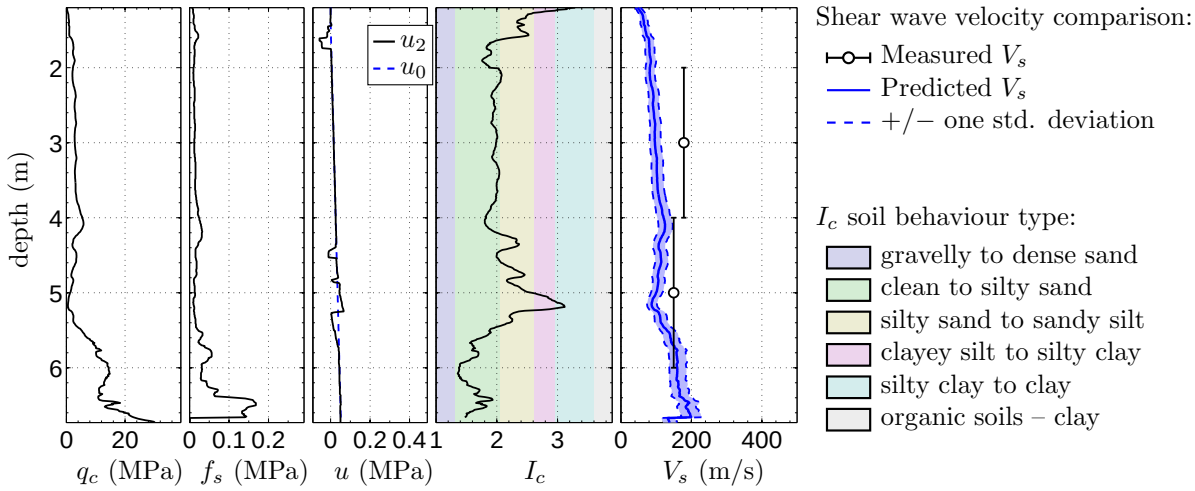

Figure C.43: SCPTu KAN36 (CPT-1295) E2482775.71 N5757888.13.

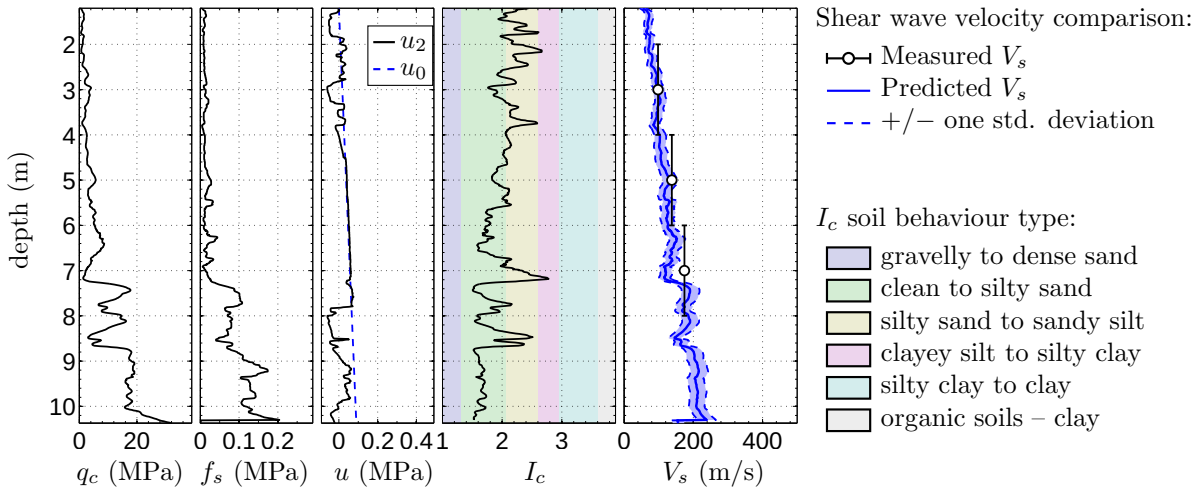

Figure C.44: SCPTu KAN38 (CPT-1297) E2483096.04 N5757798.19.

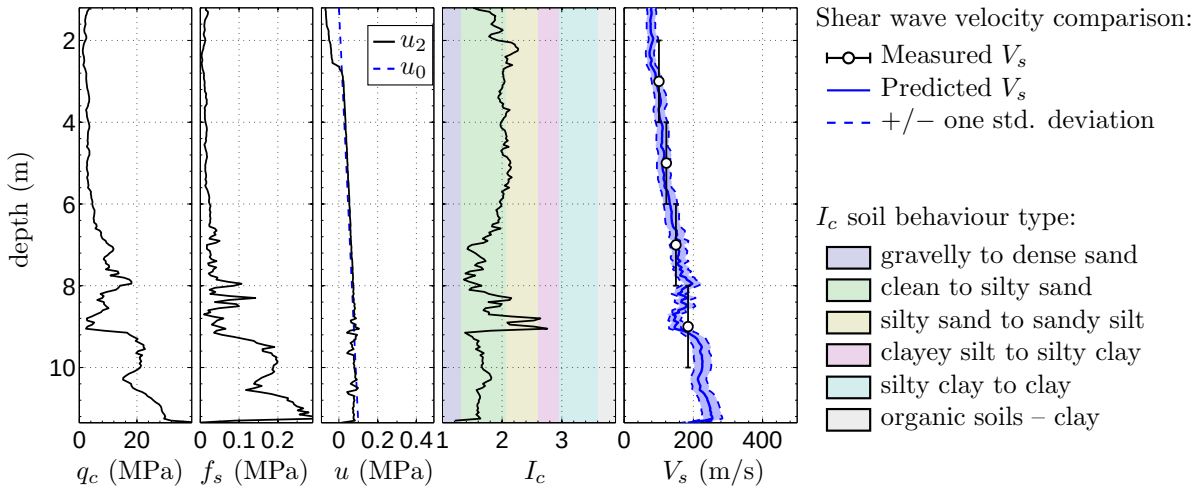

Figure C.45: SCPTu KAN41 (CPT-1300) E2483340.31 N5757874.66.

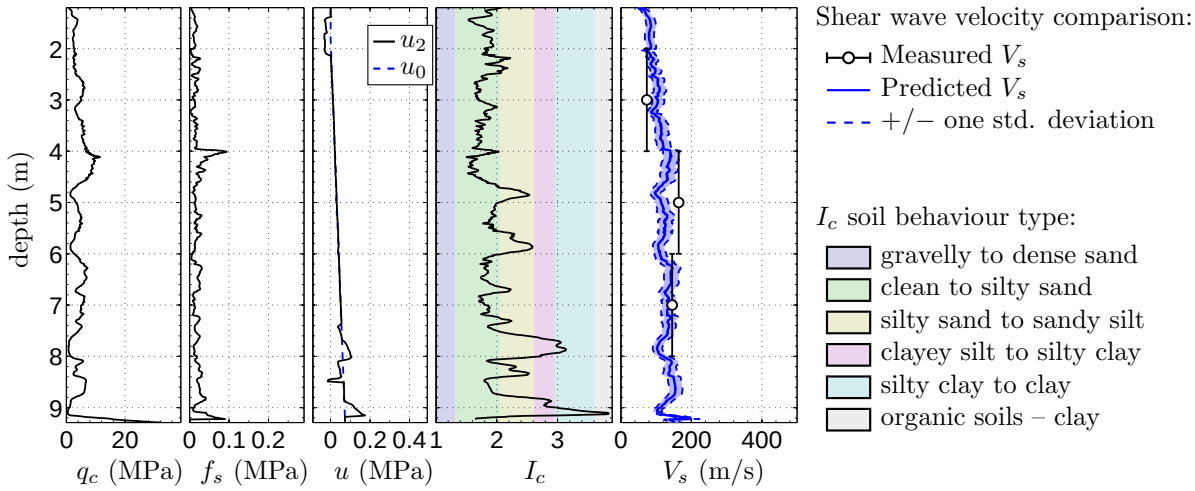

Figure C.46: SCPTu KAN42 (CPT-1301) E2482227.55 N5758443.61.

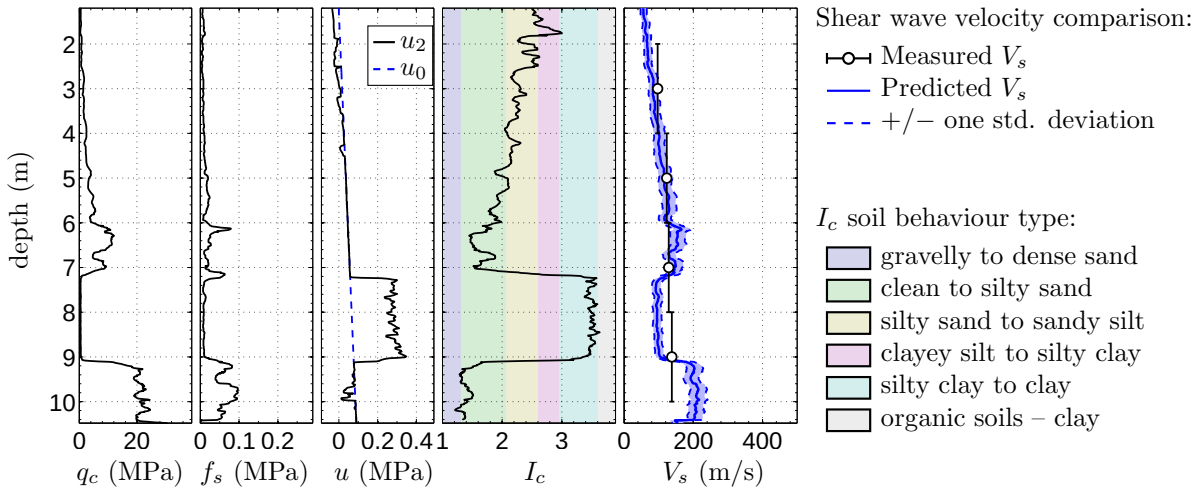

Figure C.47: SCPTu KAS41 (CPT-1342) E2482082.79 N5758520.38.

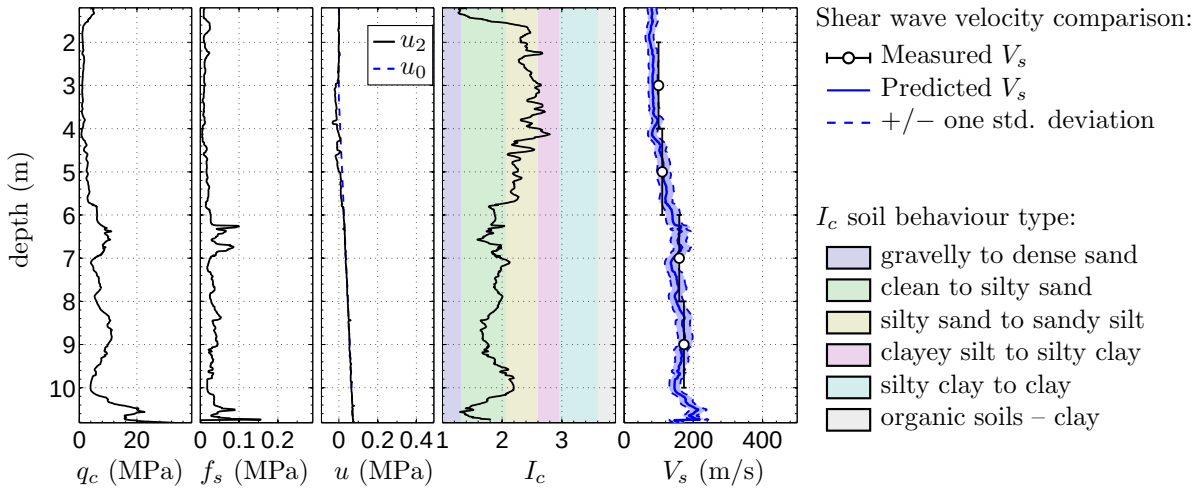

Figure C.48: SCPTu KAS44 (CPT-1344) E2482661.37 N5757791.10.

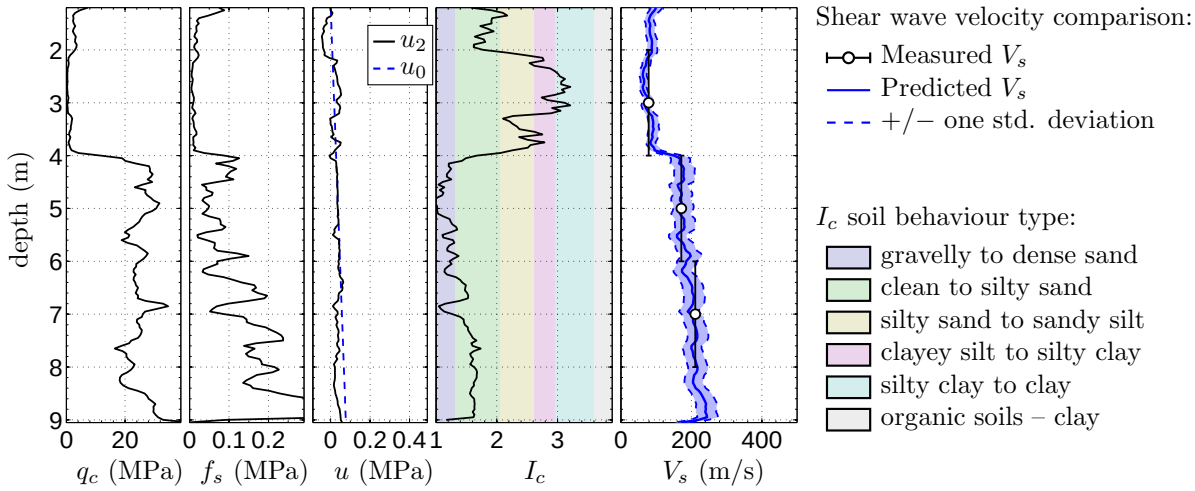

Figure C.49: SCPTu KAS46 (CPT-1346) E2482726.64 N5757598.05.

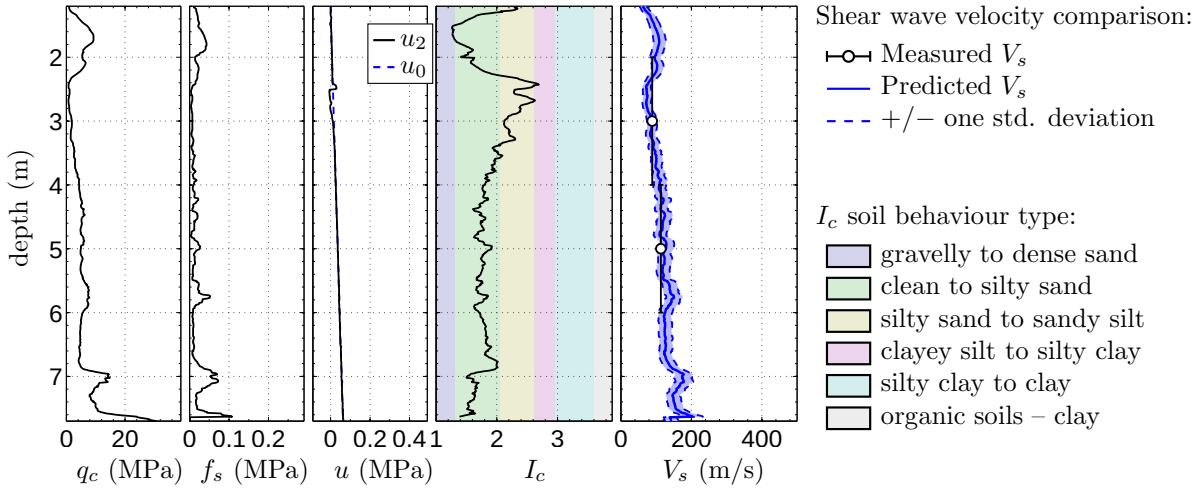

Figure C.50: SCPTu KAS52 (CPT-1351) E2482466.96 N5756996.86.

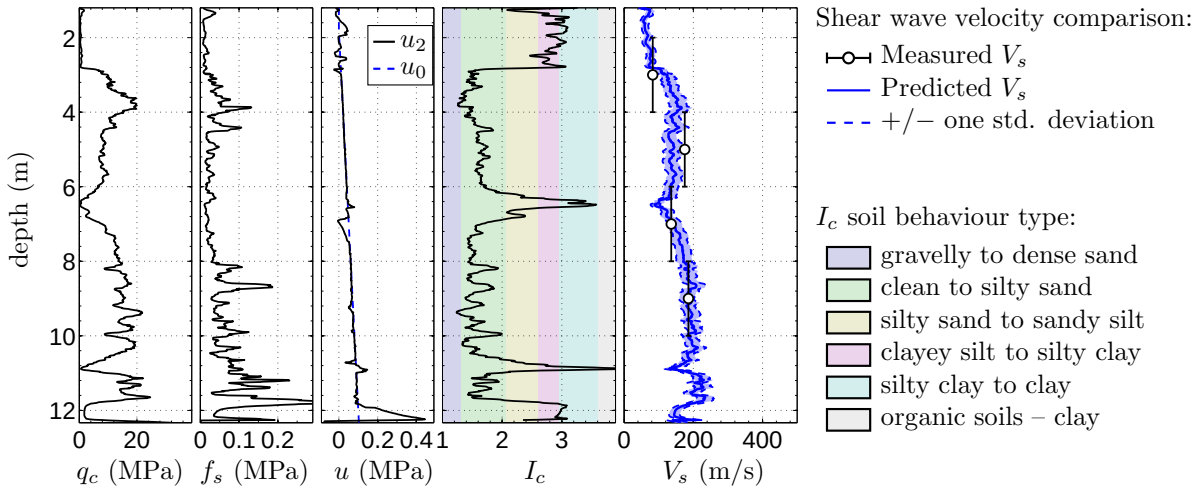

Figure C.51: SCPTu KAS54 (CPT-1353) E2482296.18 N5758180.17.

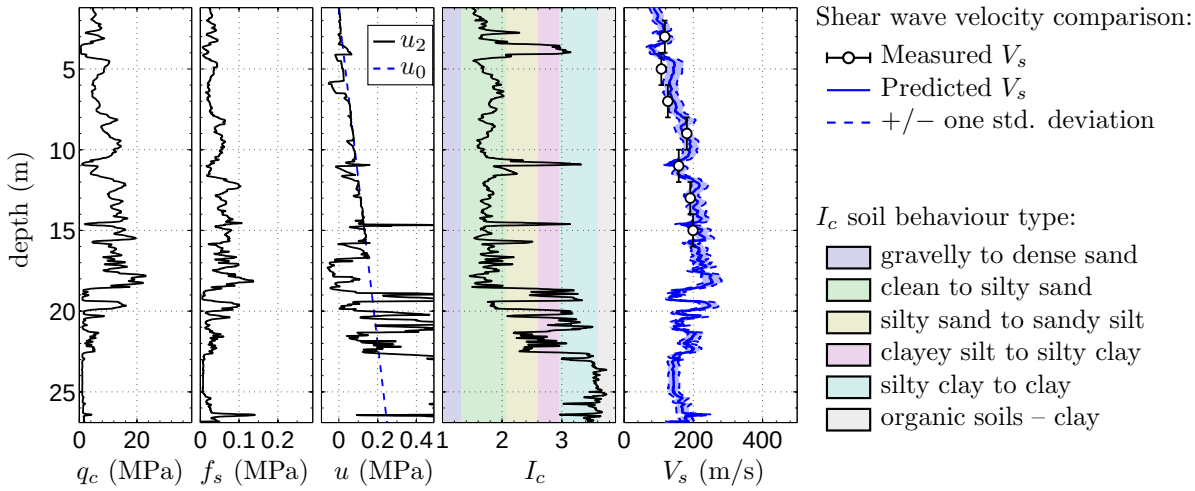

Figure C.52: SCPTu LWD27 (CPT-1384) E2483059.99 N5741014.31.

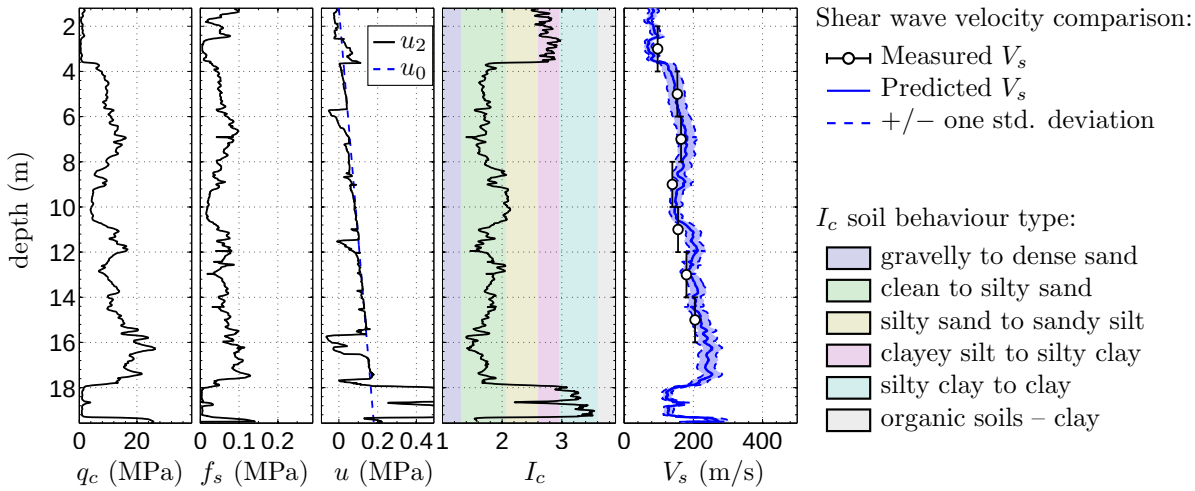

Figure C.53: SCPTu LWD29 (CPT-1386) E2483138.18 N5740801.36.

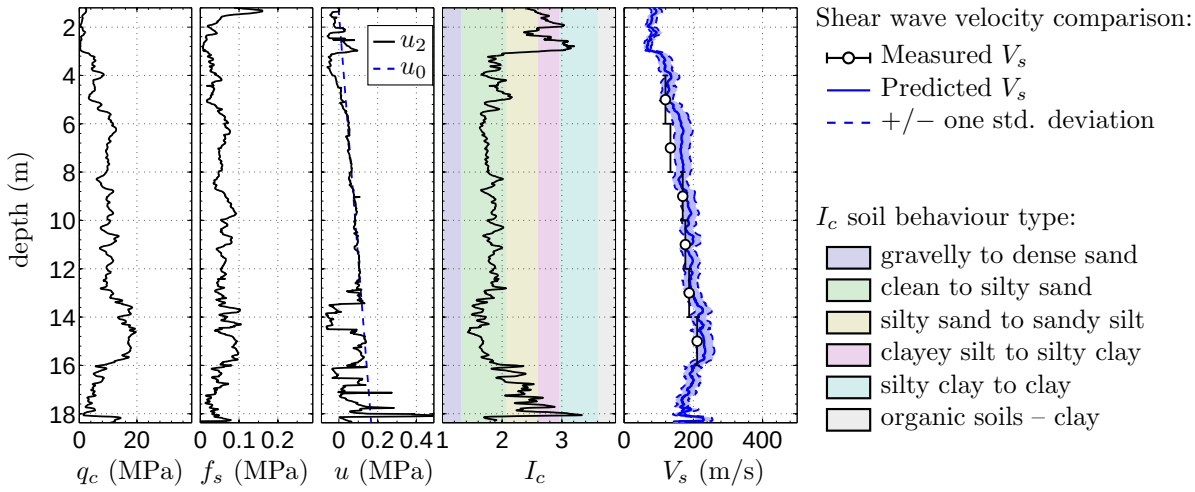

Figure C.54: SCPTu LWD32 (CPT-1389) E2483685.94 N5740188.69.

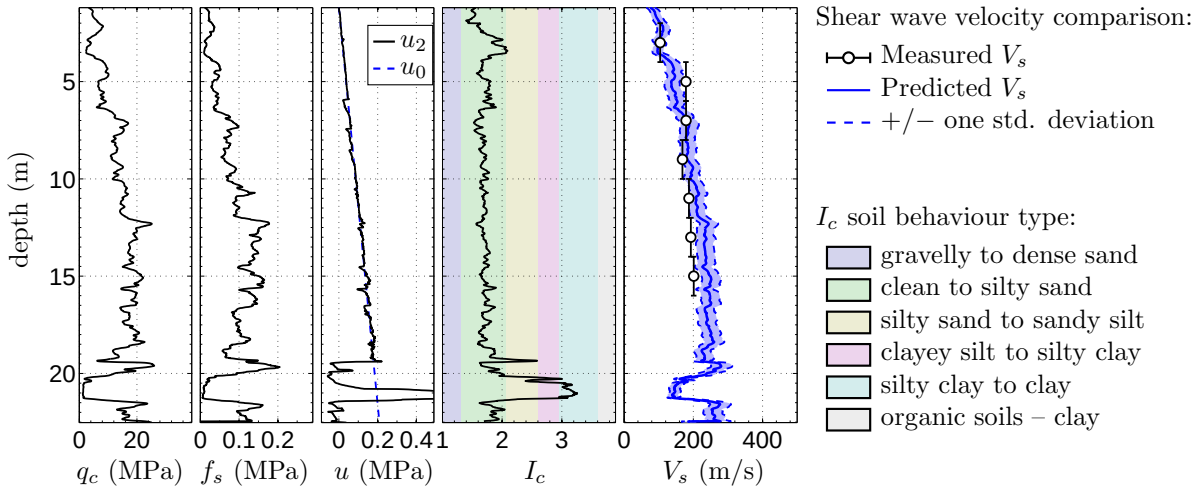

Figure C.55: SCPTu LWD37 (CPT-1394) E2483944.86 N5741865.03.

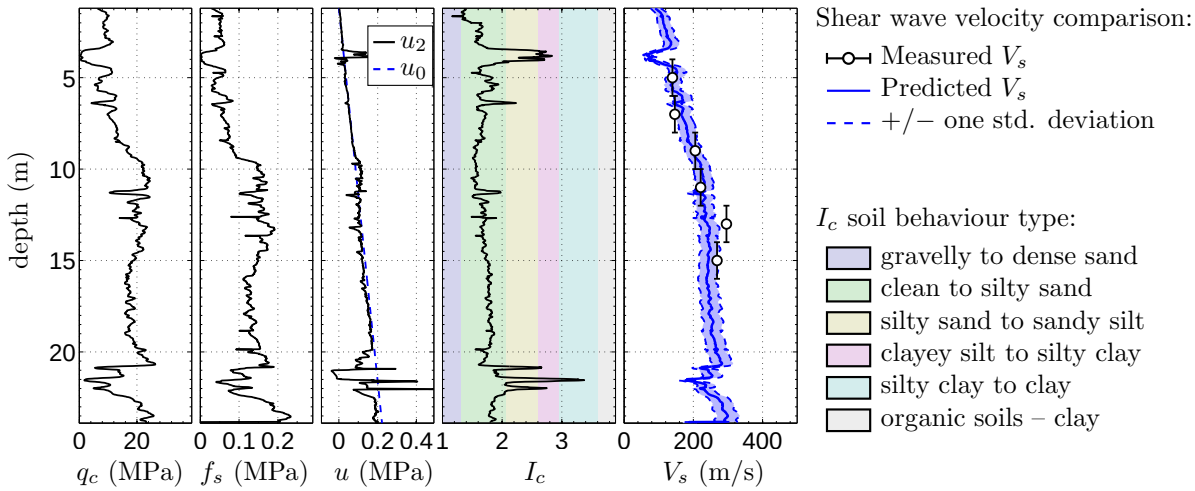

Figure C.56: SCPTu NNB05 (CPT-1458) E2486862.58 N5746424.54.

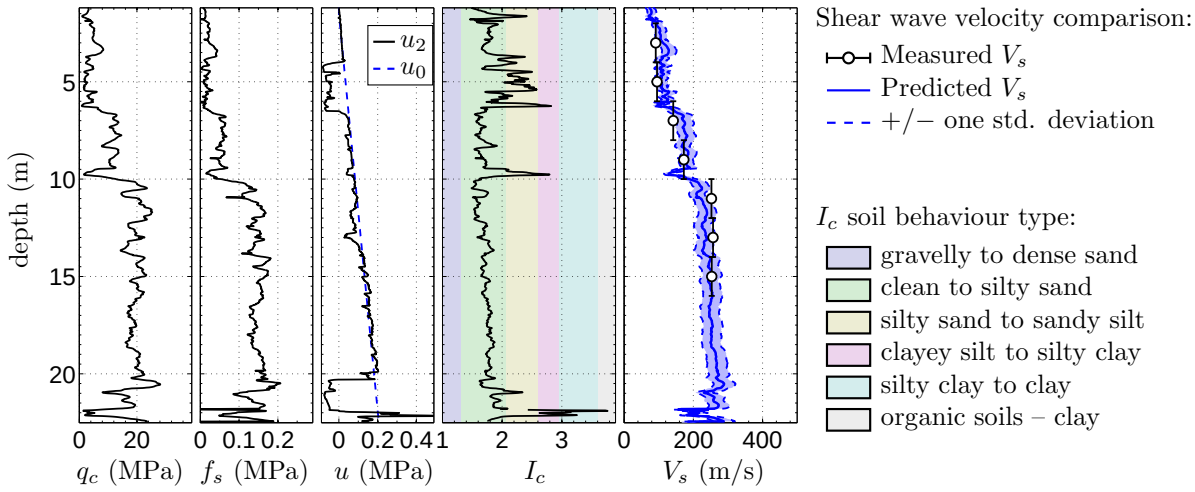

Figure C.57: SCPTu NNB08 (CPT-1460) E2486643.96 N5745803.75.

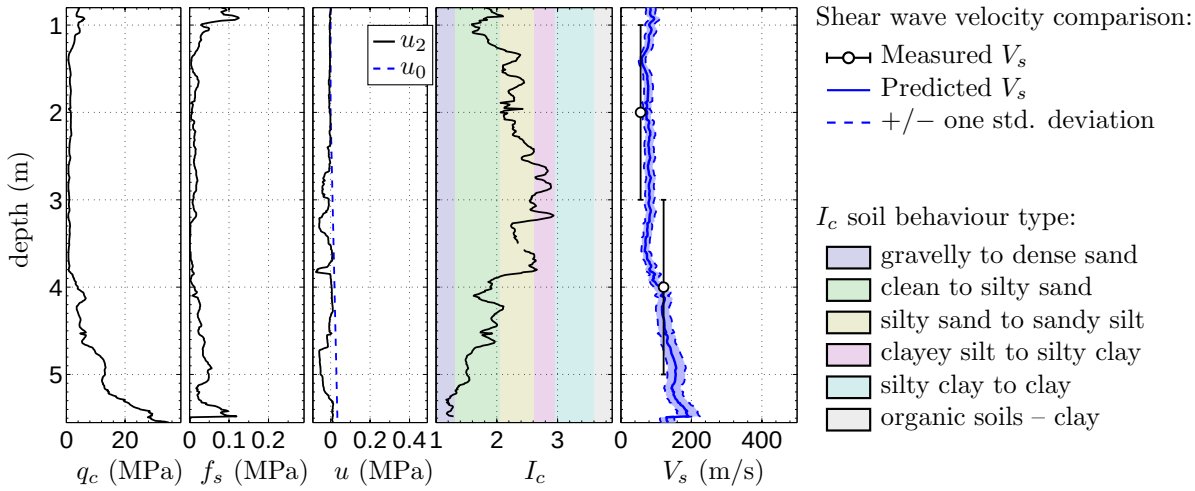

Figure C.58: SCPTu RCH16 (CPT-528) E2483299.42 N5743648.39.

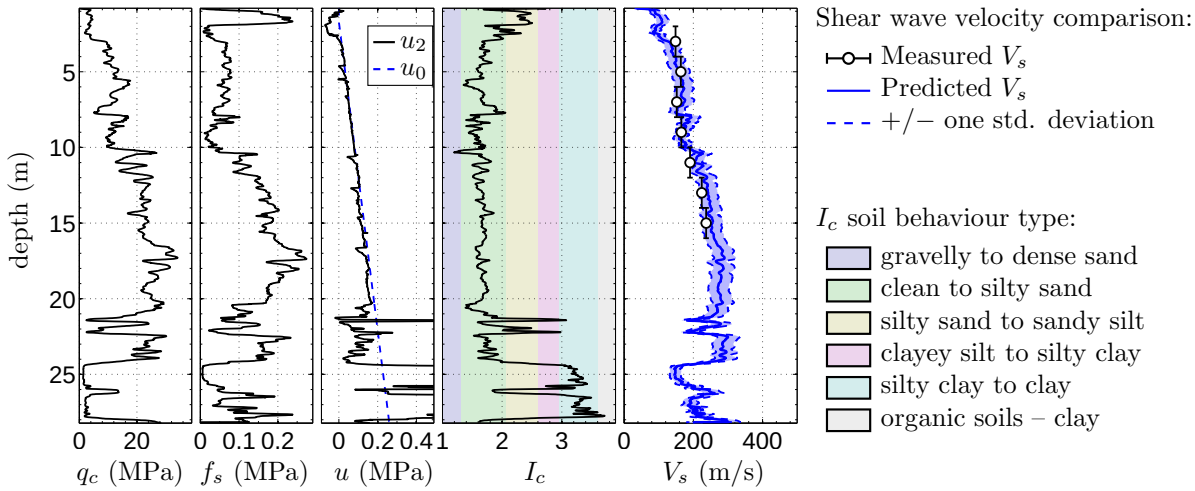

Figure C.59: SCPTu RCH17 (CPT-529) E2482768.36 N5743572.88.

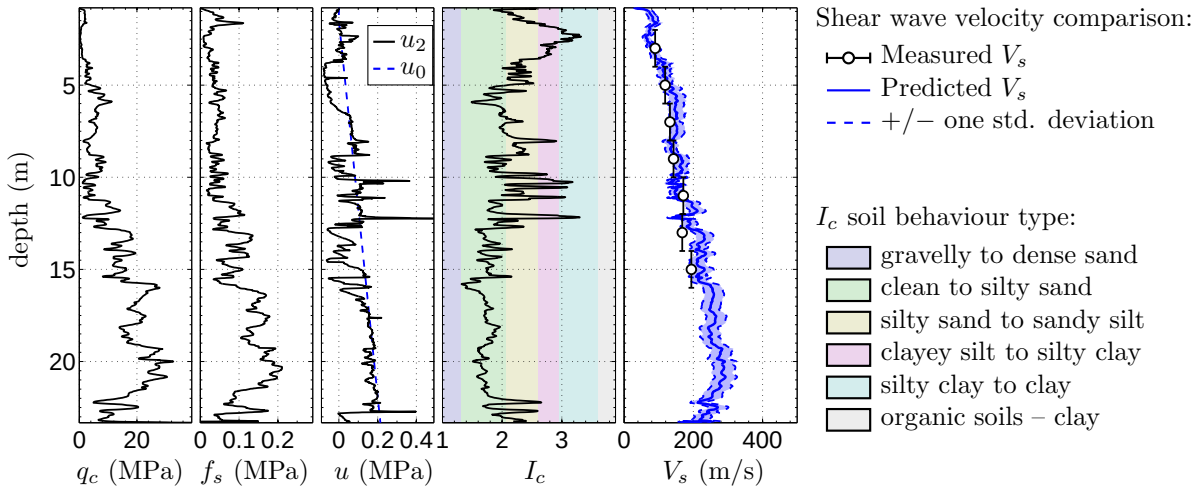

Figure C.60: SCPTu RCH25 (CPT-537) E2482078.57 N5743606.26.

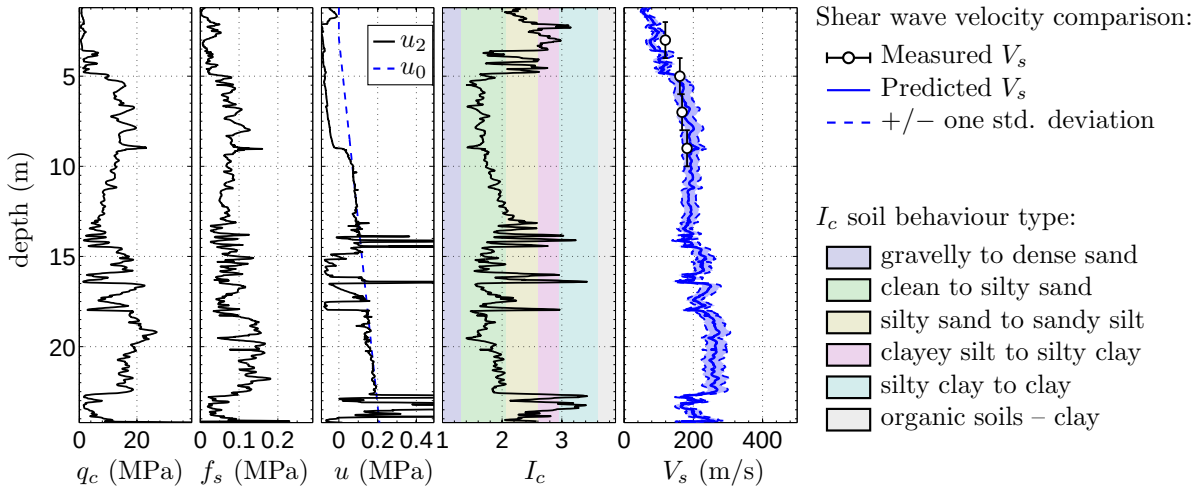

Figure C.61: SCPTu RCH59 (CPT-568) E2481978.45 N5742587.20.

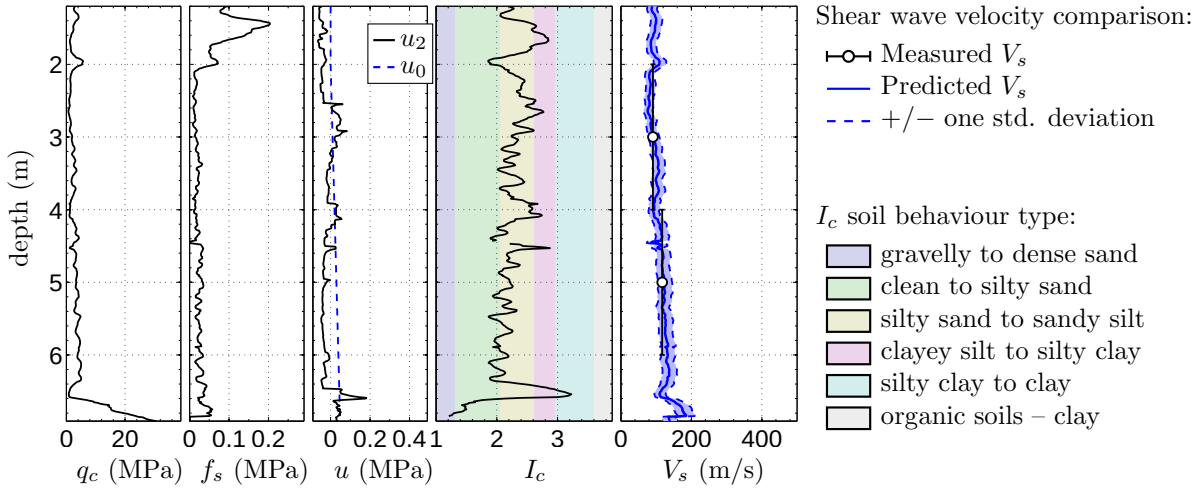

Figure C.62: SCPTu RCH64 (CPT-573) E2482076.47 N5744067.97.

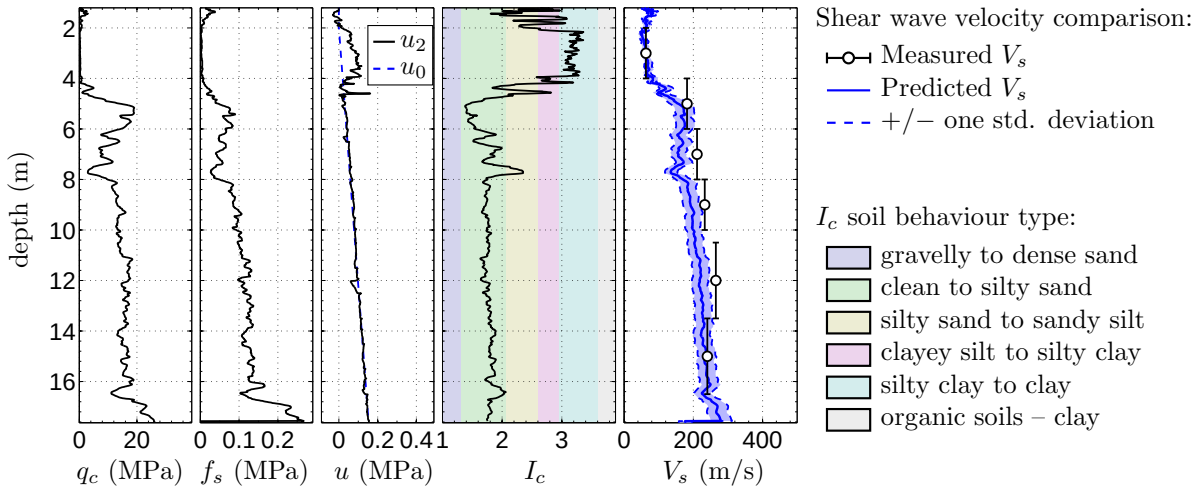

Figure C.63: SCPTu RCL03 (CPT-585) E2488906.91 N5738659.35.

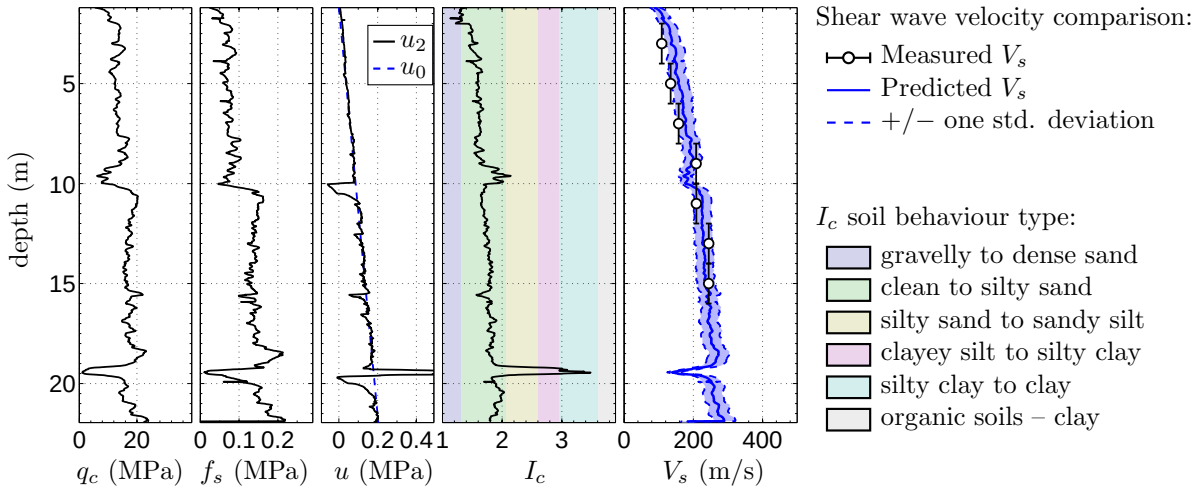

Figure C.64: SCPTu SNB10 (CPT-666) E2488245.87 N5742600.90.

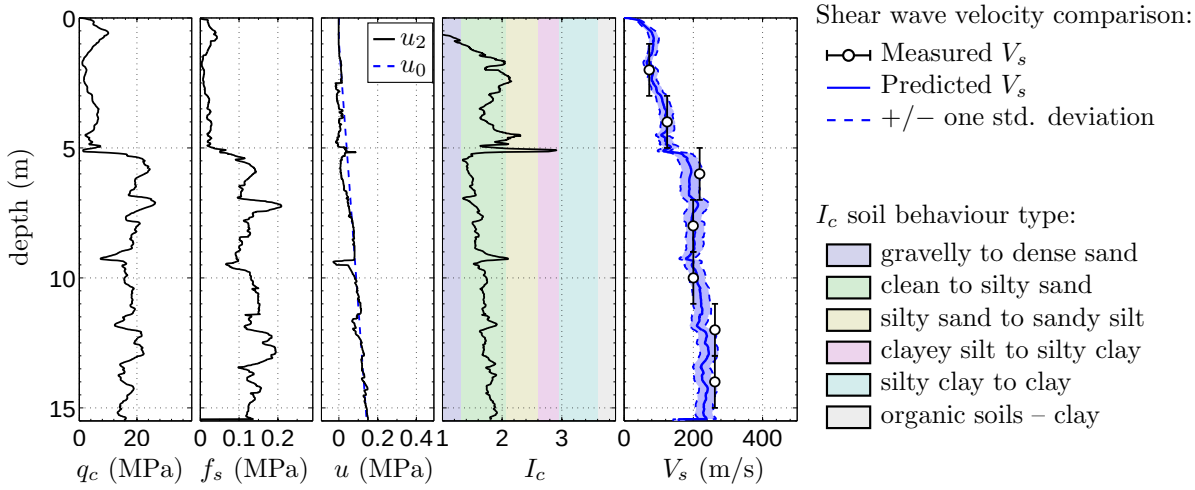

Figure C.65: SCPTu SPE01 (CPT-667) E2485129.50 N5752949.68.

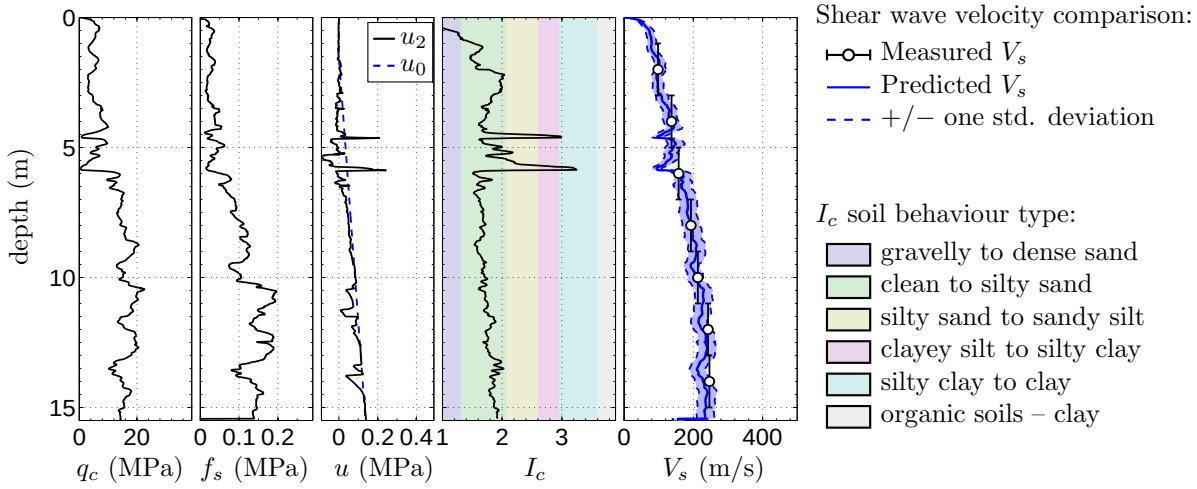

Figure C.66: SCPTu SPE03 (CPT-669) E2485150.05 N5752895.96.

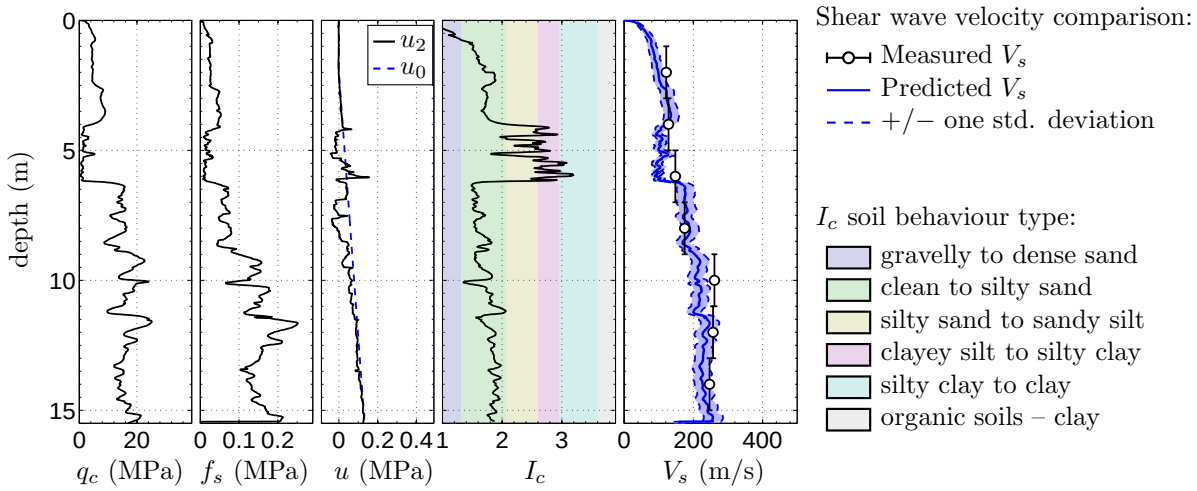

Figure C.67: SCPTu SPE05 (CPT-671) E2485180.66 N5752823.66.

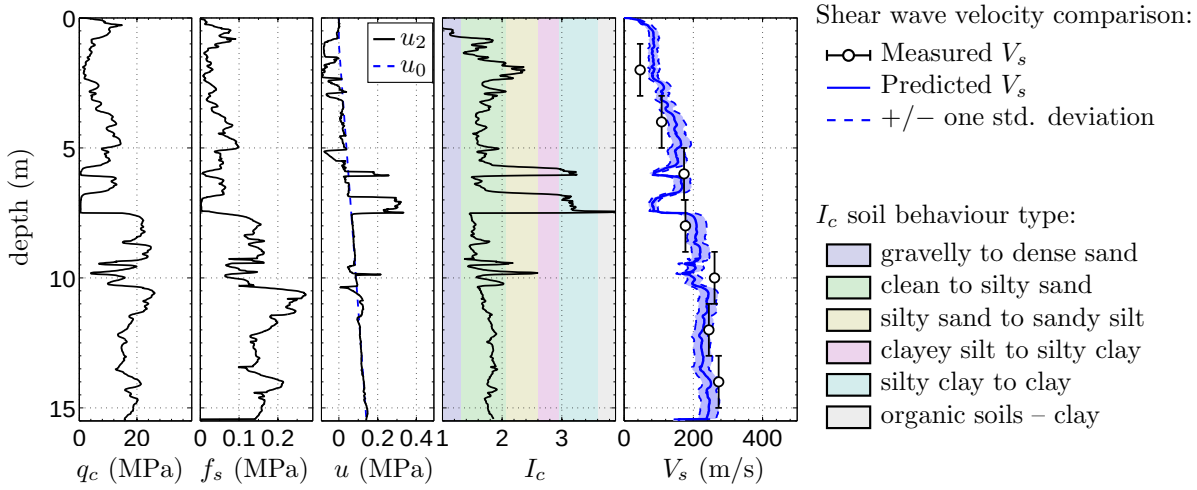

Figure C.68: SCPTu SPE07 (CPT-673) E2485216.86 N5752868.78.

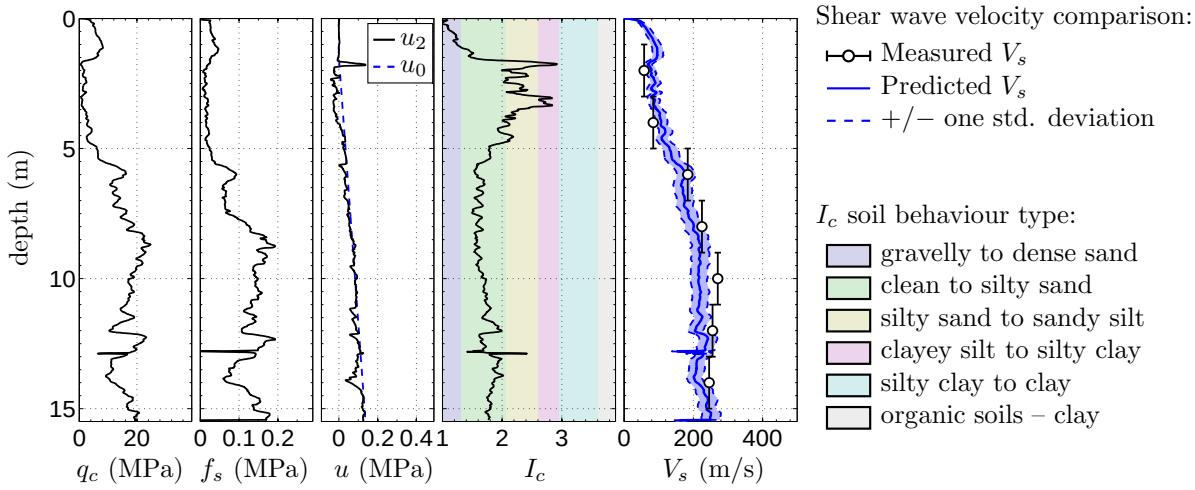

Figure C.69: SCPTu SPE11 (CPT-677) E2485290.67 N5752880.39.

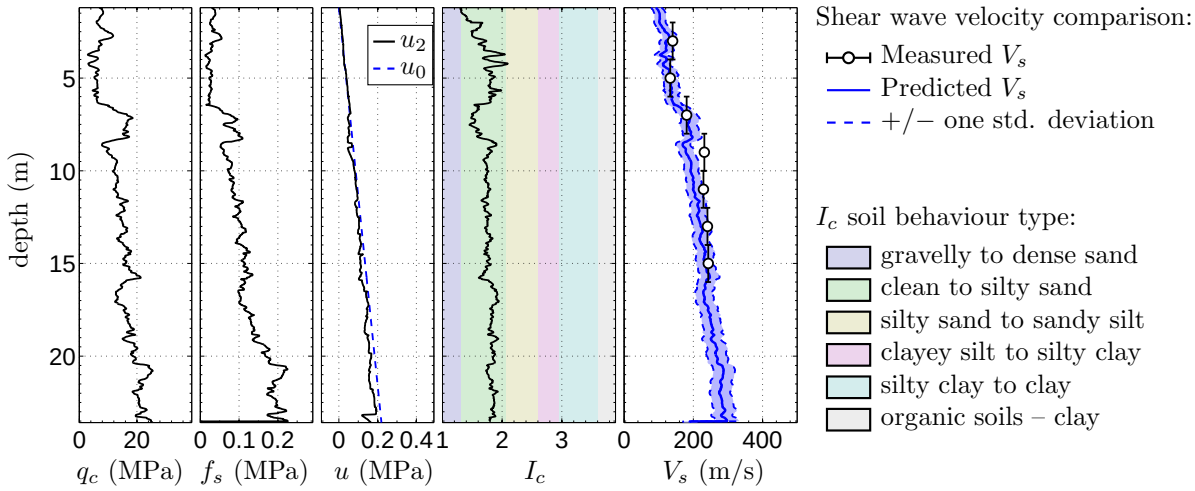

Figure C.70: SCPTu SSH04 (CPT-712) E2489797.82 N5739037.08.

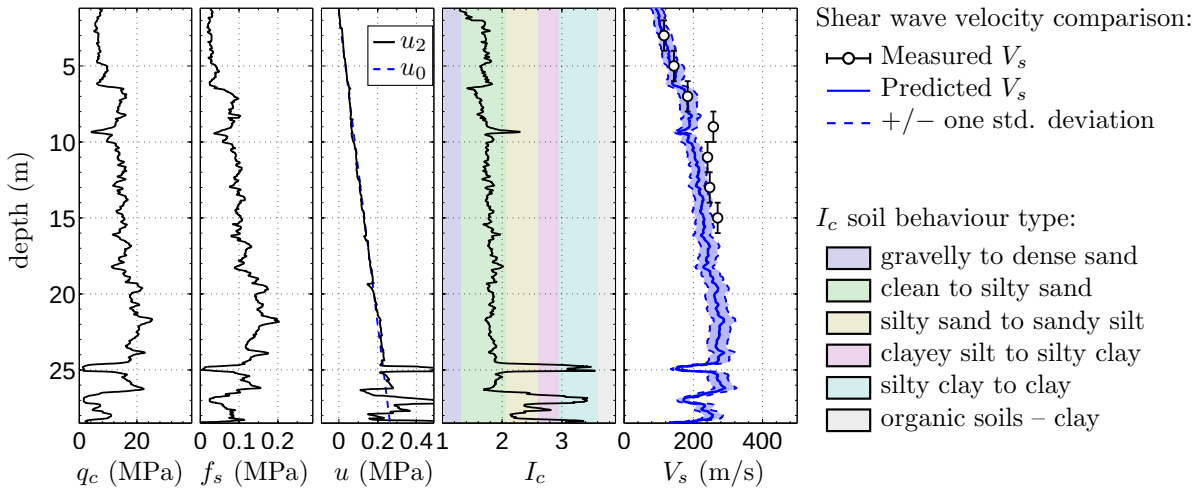

Figure C.71: SCPTu SSH07 (CPT-715) E2489492.49 N5739775.09.

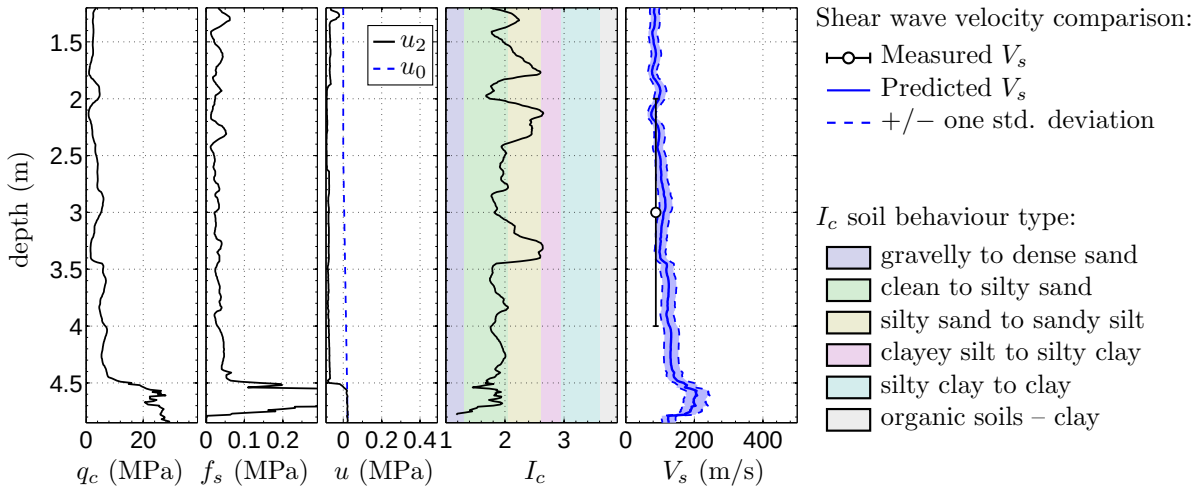

Figure C.72: SCPTu STA41 (CPT-735) E2480245.14 N5743944.19.

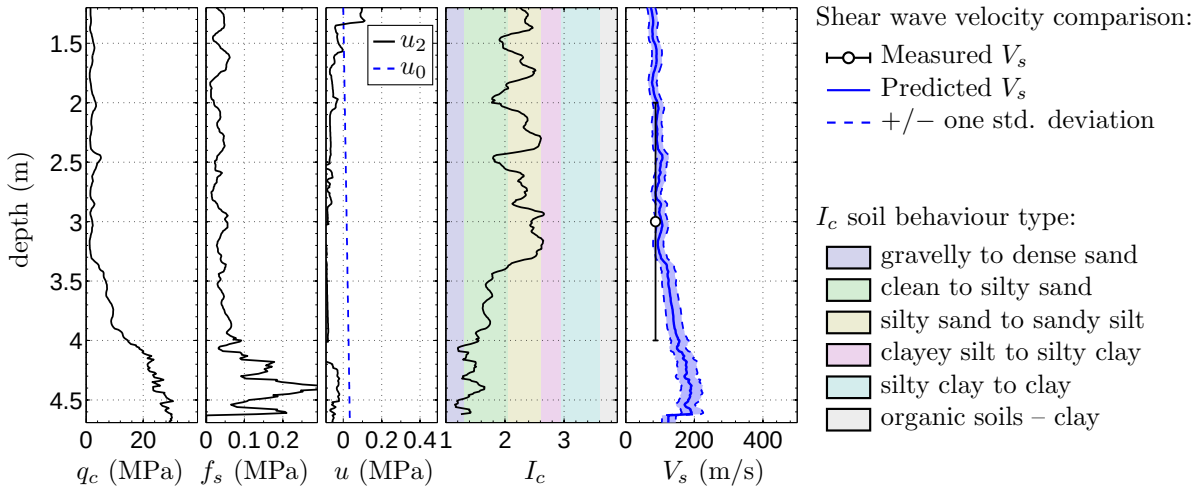

Figure C.73: SCPTu STA46 (CPT-762) E2480447.77 N5744447.99.

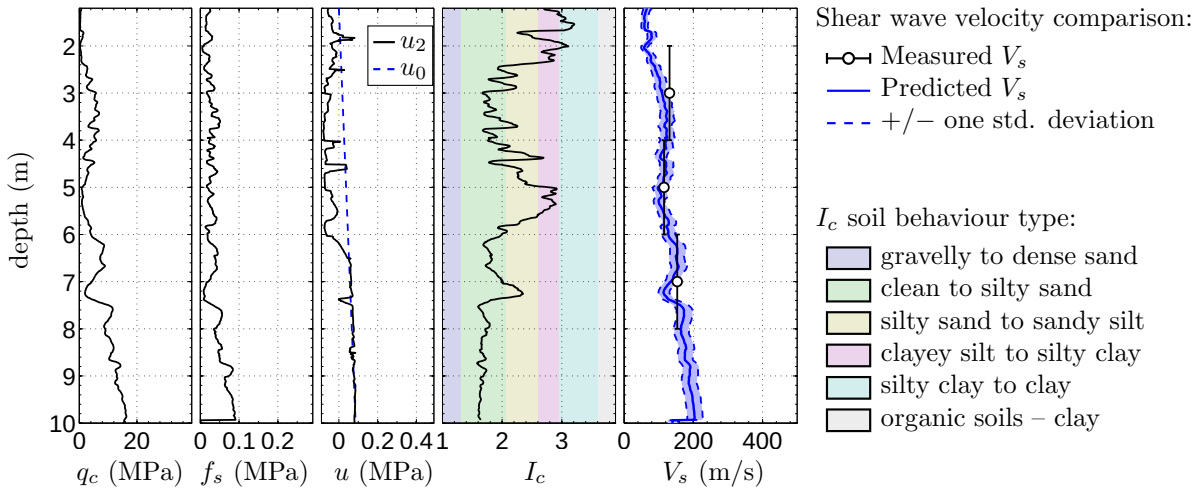

Figure C.74: SCPTu STA51 (CPT-767) E2481169.00 N5744525.63.

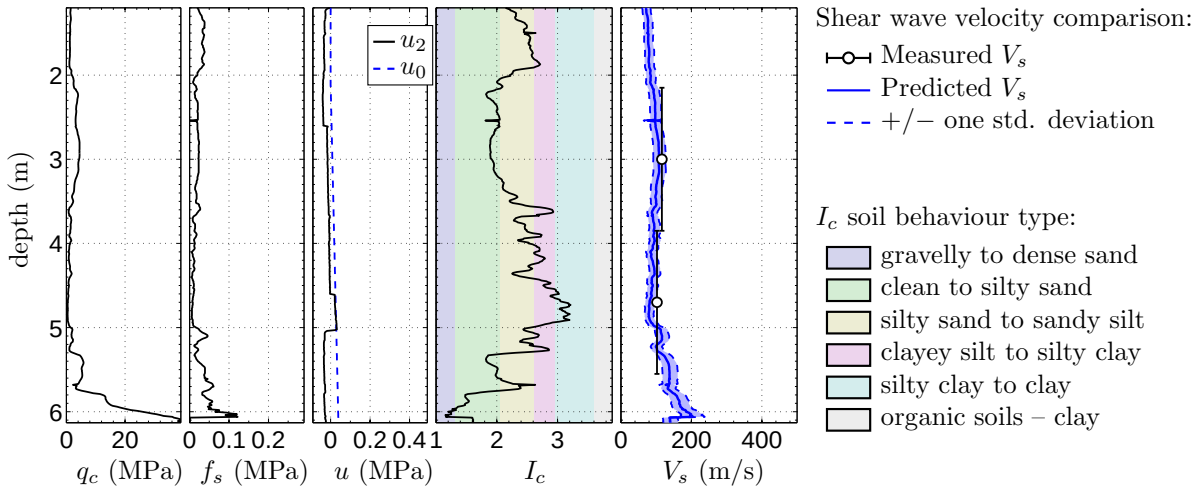

Figure C.75: SCPTu TTP04 (CPT-838) E2473503.45 N5727236.75.

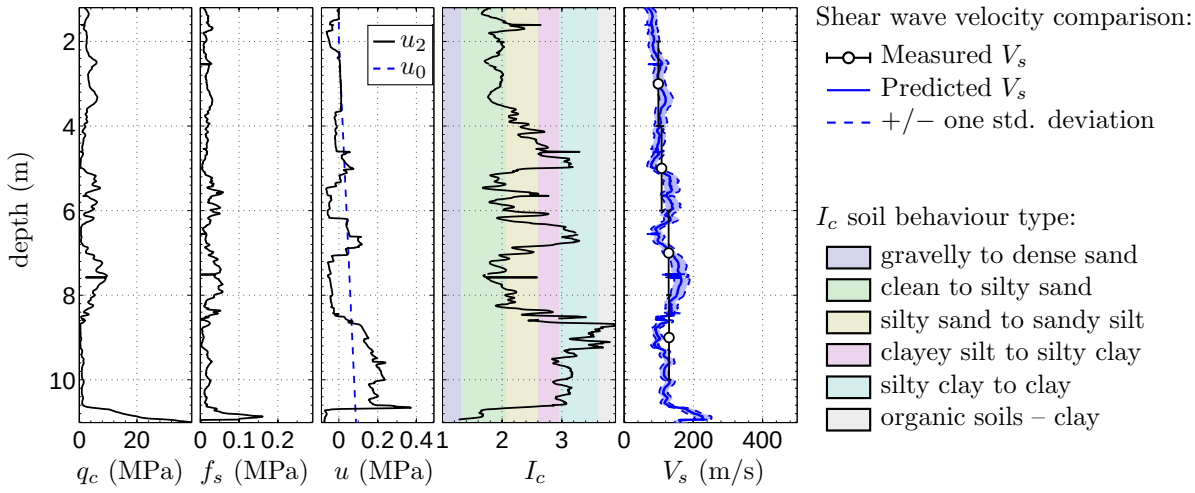

Figure C.76: SCPTu TTP05 (CPT-839) E2473819.80 N5726748.80.

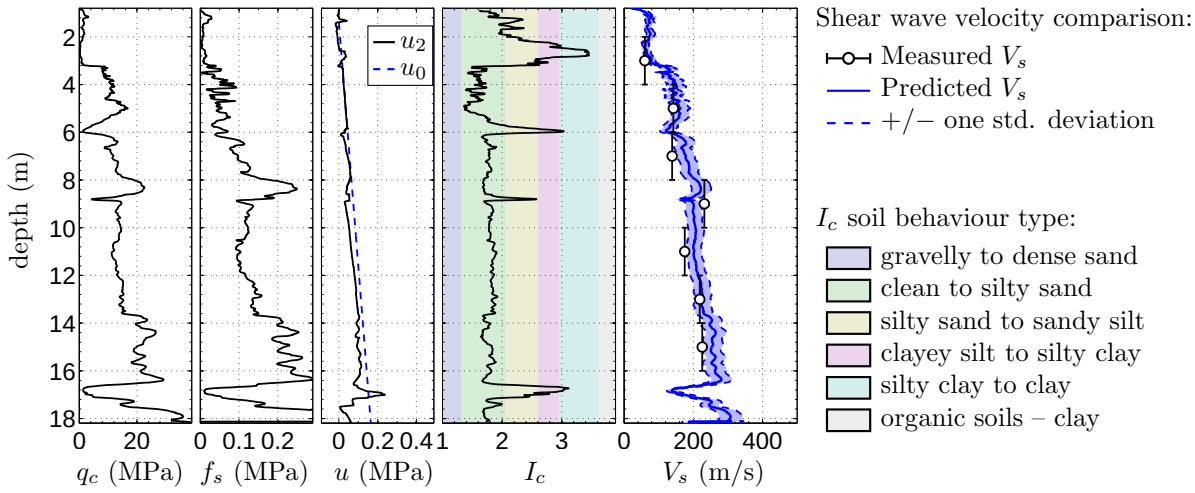

Figure C.77: SCPTu WAI10 (CPT-851) E2484234.38 N5743250.42.

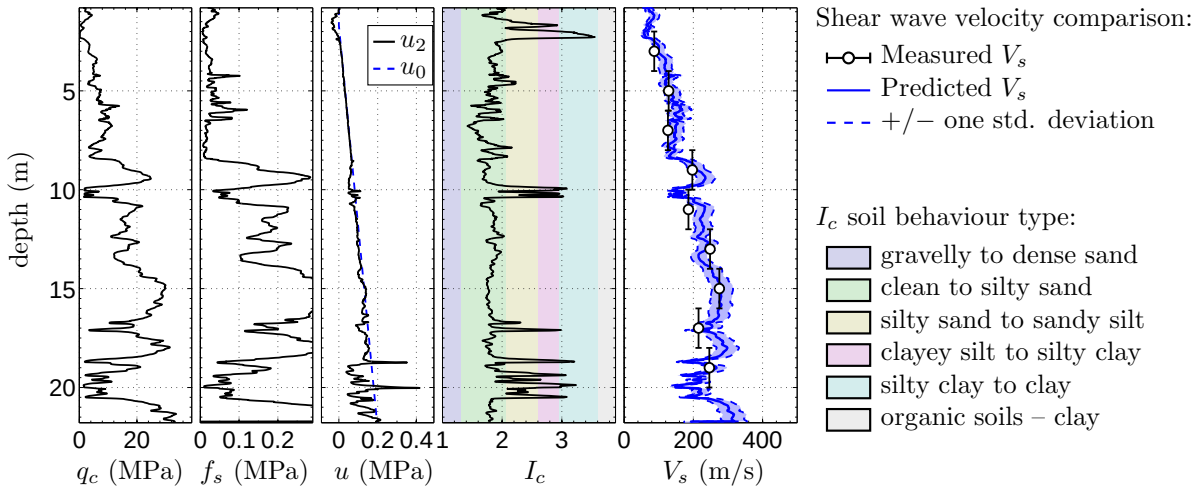

Figure C.78: SCPTu WAI14 (CPT-855) E2484399.86 N5743788.60.

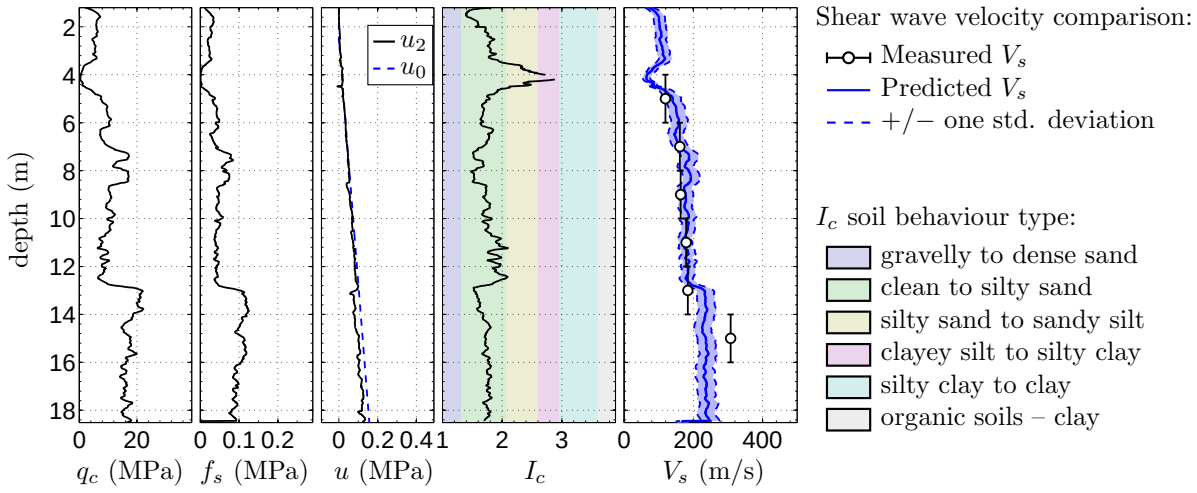

Figure C.79: SCPTu WQP01 (CPT-91) E2486711.35 N5746885.75.

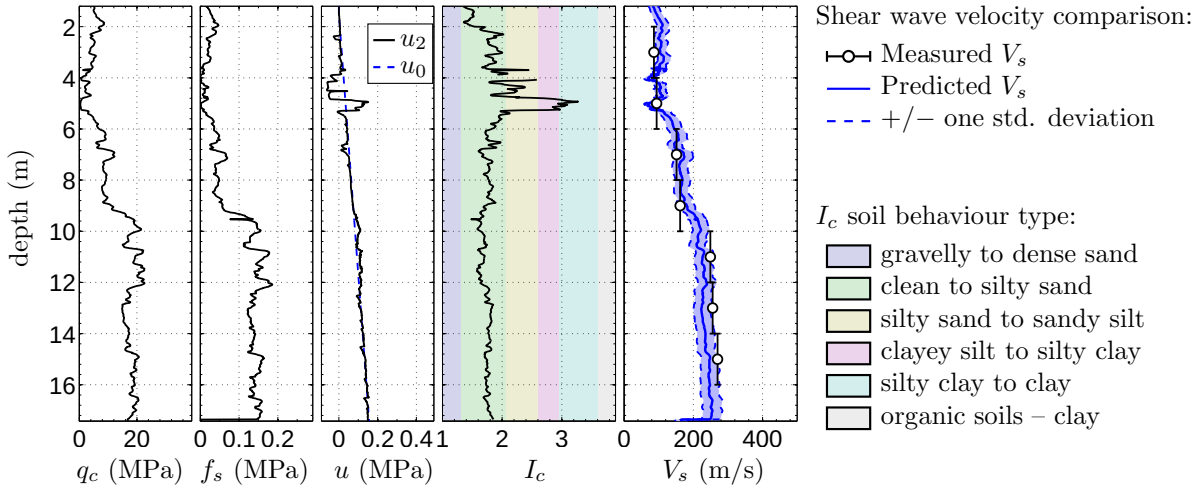

Figure C.80: SCPTu WQP22 (CPT-932) E2485938.33 N5747840.06.

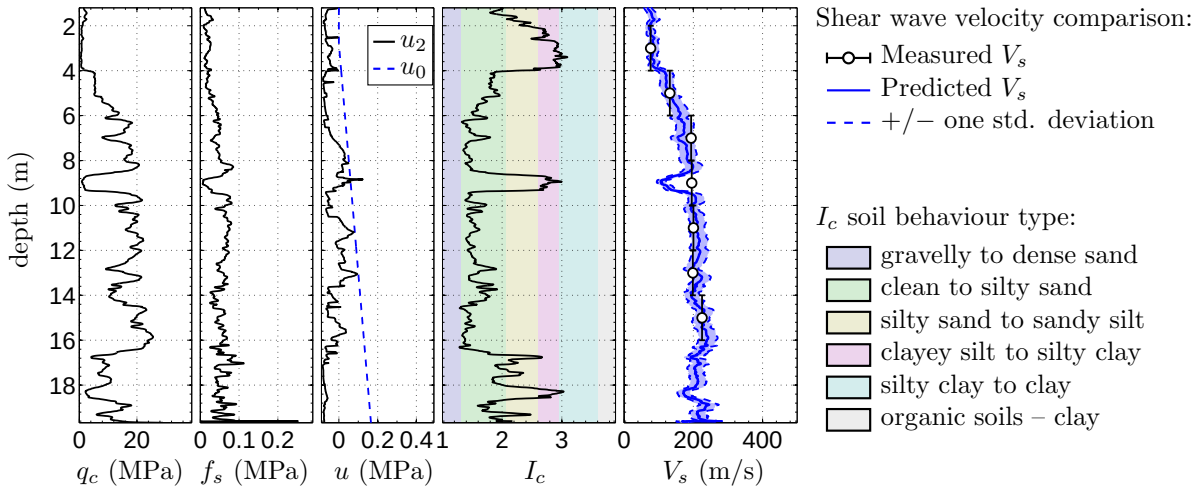

Figure C.81: SCPTu WSW01 (CPT-934) E2482804.56 N5739627.31.

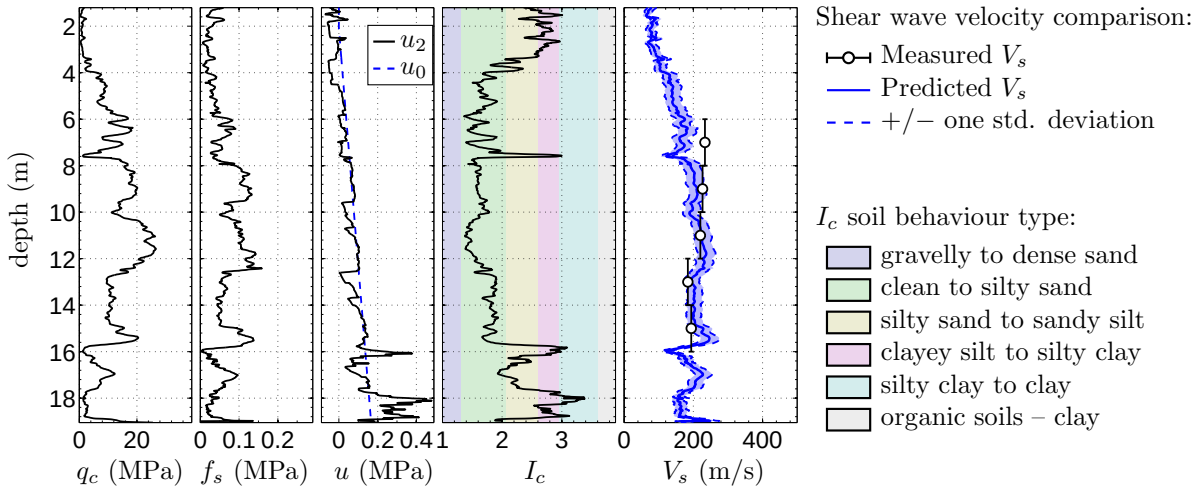

Figure C.82: SCPTu WSW06 (CPT-939) E2483143.44 N5739856.79.

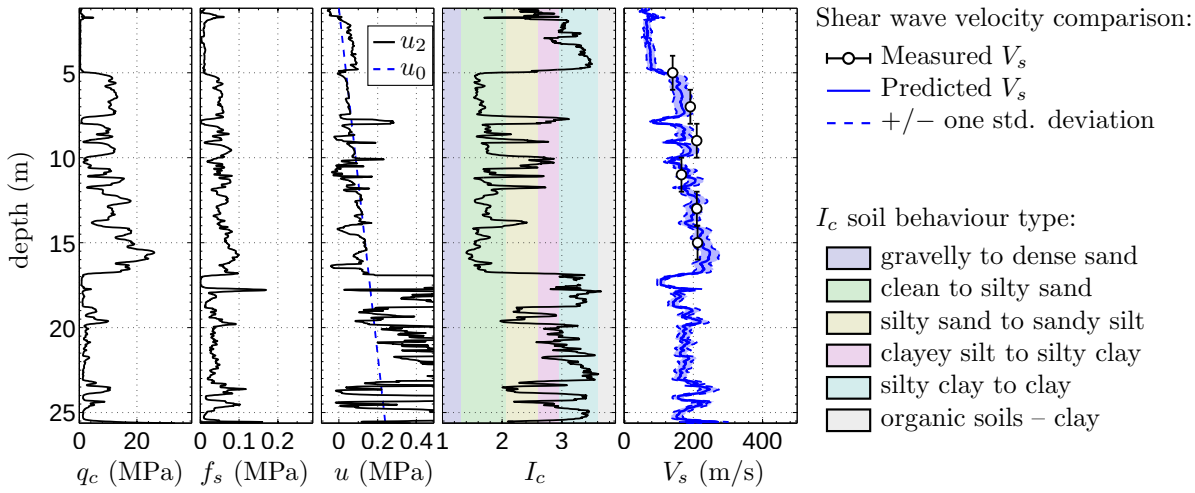

Figure C.83: SCPTu WSW12 (CPT-945) E2483192.00 N5739387.89.

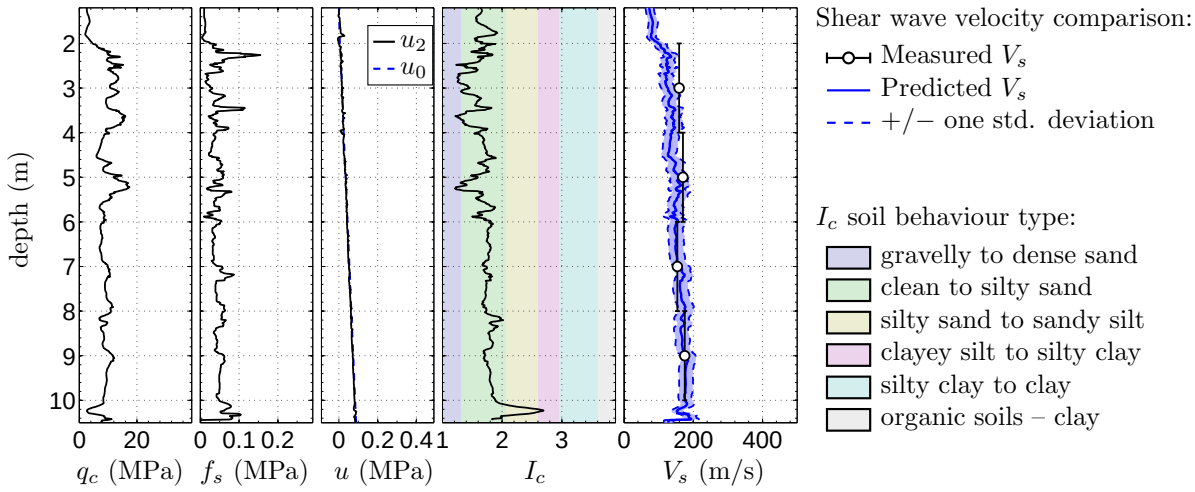

Figure C.84: SCPTu WSW35 (CPT-966) E2484277.52 N5739552.06.

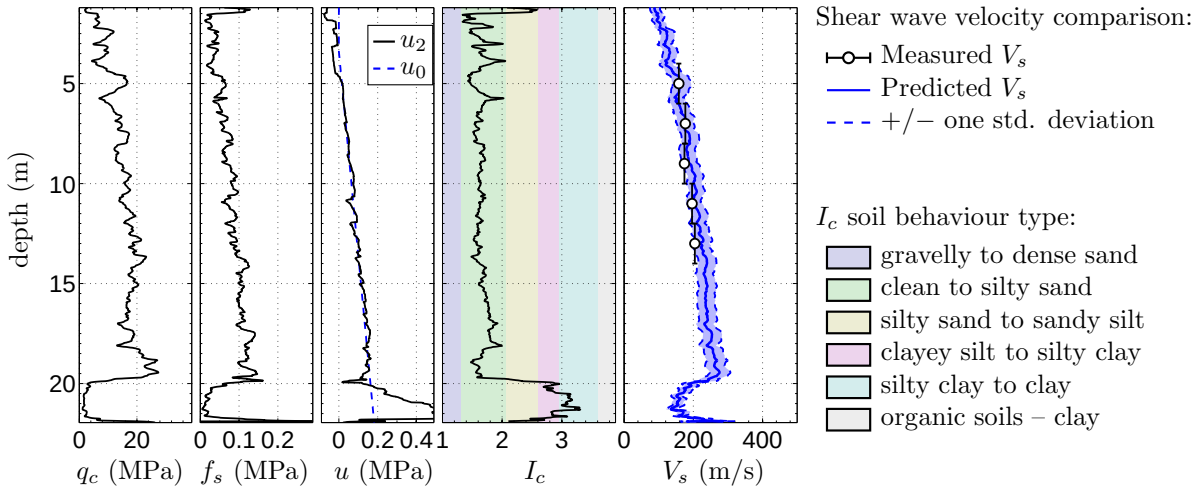

Figure C.85: SCPTu WSW43 (CPT-974) E2485398.25 N5739166.38.

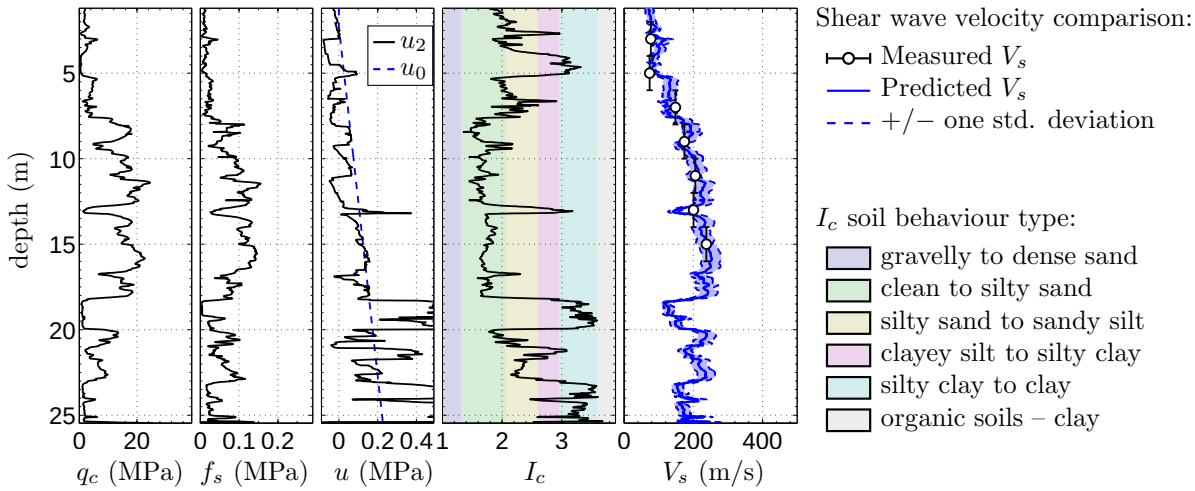

Figure C.86: SCPTu WTM09 (CPT-995) E2482532.30 N5740313.45.